frontiers | Research Topics

Plant molecular farming for the production of next-generation vaccines and biologics – prospects and challenges

Edited by
Balamurugan Shanmugaraj and Kathleen L. Hefferon

Published in
Frontiers in Plant Science

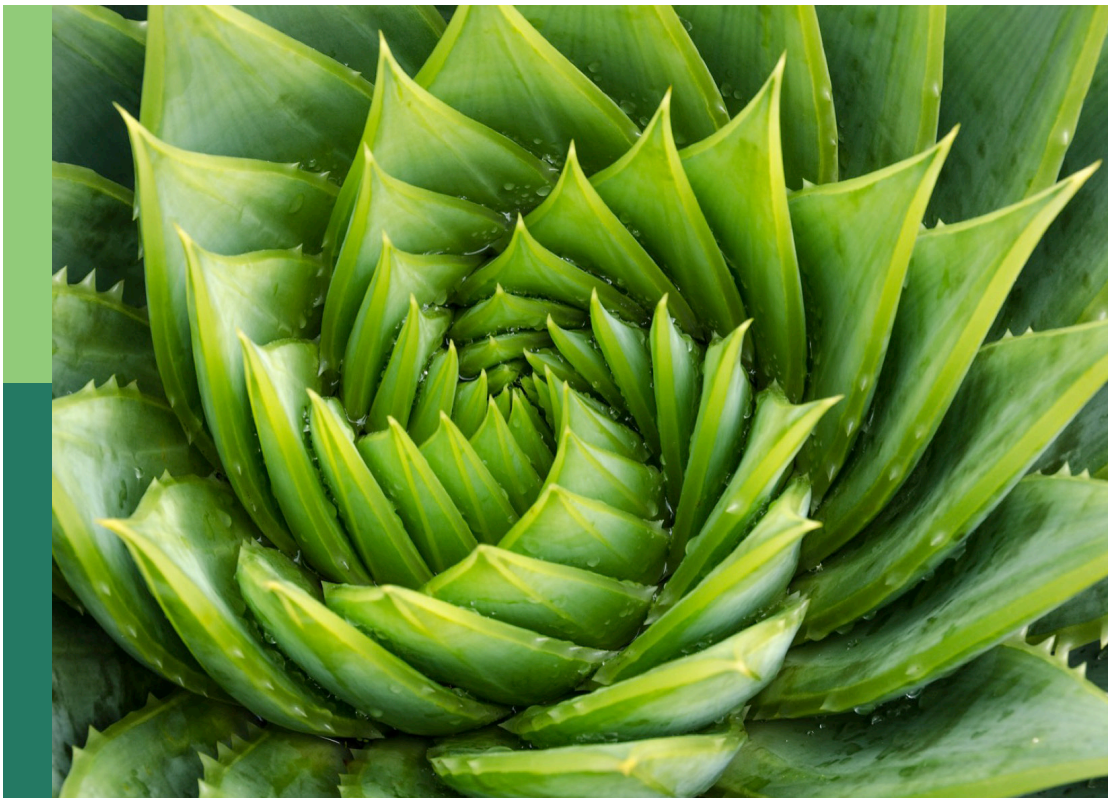

ISSN 1664-8714
ISBN 978-2-8325-4566-9
DOI 10.3389/978-2-8325-4566-9

About Frontiers

Frontiers is more than just an open access publisher of scholarly articles: it is a pioneering approach to the world of academia, radically improving the way scholarly research is managed. The grand vision of Frontiers is a world where all people have an equal opportunity to seek, share and generate knowledge. Frontiers provides immediate and permanent online open access to all its publications, but this alone is not enough to realize our grand goals.

Frontiers journal series

The Frontiers journal series is a multi-tier and interdisciplinary set of open-access, online journals, promising a paradigm shift from the current review, selection and dissemination processes in academic publishing. All Frontiers journals are driven by researchers for researchers; therefore, they constitute a service to the scholarly community. At the same time, the *Frontiers journal series* operates on a revolutionary invention, the tiered publishing system, initially addressing specific communities of scholars, and gradually climbing up to broader public understanding, thus serving the interests of the lay society, too.

Dedication to quality

Each Frontiers article is a landmark of the highest quality, thanks to genuinely collaborative interactions between authors and review editors, who include some of the world's best academicians. Research must be certified by peers before entering a stream of knowledge that may eventually reach the public - and shape society; therefore, Frontiers only applies the most rigorous and unbiased reviews. Frontiers revolutionizes research publishing by freely delivering the most outstanding research, evaluated with no bias from both the academic and social point of view. By applying the most advanced information technologies, Frontiers is catapulting scholarly publishing into a new generation.

What are Frontiers Research Topics?

Frontiers Research Topics are very popular trademarks of the *Frontiers journals series*: they are collections of at least ten articles, all centered on a particular subject. With their unique mix of varied contributions from Original Research to Review Articles, Frontiers Research Topics unify the most influential researchers, the latest key findings and historical advances in a hot research area.

Find out more on how to host your own Frontiers Research Topic or contribute to one as an author by contacting the Frontiers editorial office: frontiersin.org/about/contact

Plant molecular farming for the production of next-generation vaccines and biologics – prospects and challenges

Topic editors

Balamurugan Shanmugaraj — Chulalongkorn University, Thailand

Kathleen L. Hefferon — Cornell University, United States

Citation

Shanmugaraj, B., Hefferon, K. L., eds. (2024). *Plant molecular farming for the production of next-generation vaccines and biologics – prospects and challenges*. Lausanne: Frontiers Media SA. doi: 10.3389/978-2-8325-4566-9

Table of contents

frontiers | Frontiers in Plant Science

TYPE Editorial
PUBLISHED 27 February 2024
DOI 10.3389/fpls.2024.1381234

OPEN ACCESS

EDITED AND REVIEWED BY
James Lloyd,
Stellenbosch University, South Africa

*CORRESPONDENCE
Balamurugan Shanmugaraj
balagene3030@gmail.com
Kathleen Hefferon
klh22@cornell.edu

RECEIVED 03 February 2024
ACCEPTED 07 February 2024
PUBLISHED 27 February 2024

CITATION
Shanmugaraj B and Hefferon K (2024) Editorial: Plant molecular farming for the production of next-generation vaccines and biologics – prospects and challenges. *Front. Plant Sci.* 15:1381234. doi: 10.3389/fpls.2024.1381234

Editorial: Plant molecular farming for the production of next-generation vaccines and biologics – prospects and challenges

Balamurugan Shanmugaraj[1*] and Kathleen Hefferon[2*]

[1]Department of Pharmacognosy and Pharmaceutical Botany, Faculty of Pharmaceutical Sciences, Chulalongkorn University, Bangkok, Thailand, [2]Department of Microbiology, Cornell University, Ithaca, NY, United States

KEYWORDS

plant molecular farming, vaccines, nicotiana, biologics, plants

Editorial on the Research Topic
Plant molecular farming for the production of next-generation vaccines and biologics – prospects and challenges

Plant molecular farming, meaning the use of plants as production platforms for the generation of vaccines, monoclonal antibodies and other therapeutic agents, continues to expand and mature (Shanmugaraj et al., 2020). This multidisciplinary field draws knowledge from the researchers with expertise in plant science, medicine and the pharmaceutical sciences, and regularly engages with the academic, government and industrial sectors. Plants have been cultivated as sources of medicine for ages, and novel approaches based on synthetic biology have advanced the use of plants to generate biologics of all sorts, thus wedding modern medicine to its historical past. Vaccines produced in plants are efficacious, inexpensive and incorporates post translational modifications not found in bacterial systems, yet lack the risk of human pathogen contamination, unlike their mammalian production system counterparts. Plant systems can easily be scaled up, can be stored at ambient temperatures and their facile use makes them excellent candidates for low to middle income countries (He et al., 2021; Lobato Gómez et al., 2021).

This Research Topic covers a variety of subjects that are highly relevant for plant made pharmaceuticals at their current stage of development. One common theme that comes through is the production of monoclonal antibodies for a variety of medical purposes. For example, in Improving the efficacy of plant-made anti-HIV monoclonal antibodies for clinical use, Grandits et al. describe how *Nicotiana benthamiana* plants were utilized to produce three broadly neutralizing antibodies (mAbs which block virus attachment and entry) as an alternative to or combination with antiretroviral therapy. The authors engineered plant-made bNAbs which were greater in efficacy and exhibited an improved pharmacokinetic profile. Cocktails of these antibodies could mitigate the high cost and availability issues of anti-HIV therapies where HIV-1 is found in greatest abundance, low- to middle- income countries. The manuscript 'Anti-tumor effect of plant-produced anti-

CTLA-4 monoclonal antibody in a murine model of colon cancer,' by Bulaon et al. describes the production of an anti-CTLA-4 2C8 mAbs to cytotoxic T lymphocyte-associated protein 4 in *Nicotiana benthamiana* plants and examination of their use as a cancer immunotherapy in knocked-in mice with colon tumors. The results of this study indicate that plant-based versions of mAbs could overcome the exorbitant costs associated with cancer care, particularly in developing countries.

Advances in glycan engineering for plant production of biologics also predominate this Research Topic. In Production and N-glycan engineering of Varlilumab in *Nicotiana benthamiana*, by Nguyen et al., an N-glycan-engineered version of the CD27-targeting monoclonal antibody Varlilumab was expressed in *Nicotiana benthamina* plants. Similarly, Beihammer et al. incorporated a protozoan oligosaccharyltransferase to improve its ability to glycosylate the Fc of IgG1.

Contributions by Margolin et al., Mamedov et al. and Ruocco et al. address the SARS-CoV-2 pandemic in multiple ways. Margolin et al. used an integrated host and glyco-engineering approach, NXS/T Generation™, to produce SARS-CoV-2 prefusion spike trimers in *Nicotiana benthamiana*, and compared glycan profile as well as immunogenicity to mammalian counterparts, while Mamedov et al. produced an RBD variants cocktail in Nicotiana plants that worked effectively against both Omicron and Delta variants. Ruocco et al. describe the analysis of six different RBD variants produced in plants in terms of yield and N-glycan profiles.

This Research Topic also addresses other aspects of molecular farming, such as food-borne illness. In Accumulation of colicin M protein and its biological activity in transgenic lettuce and mizuna plants, by Shcherbak et al., antimicrobial protein Colicin M (ColM) was expressed in lettuce and mizuna plants. Extracts from these plants demonstrated effectiveness in blocking infection by two noteworthy strains of EHEC as well as several anti-biotic resistant strains of *E. coli*. A preliminary study of the immunogenic response of plant-derived multi-epitopic peptide vaccine candidate of *Mycoplasma gallisepticum* in chickens, Mugunthan et al. cover the response in poultry to a plant-made vaccine to *Mycoplasma gallisepticum* (MG), and avian respiratory infection. Finally, in Artificial intelligence-driven systems engineering for next-generation plant-derived biopharmaceuticals, Parthiban et al. explore the integration of recombinant protein engineering with AI-based machine learning and deep learning algorithms through the lens of plant made pharmaceutical production. Using this approach, the authors gather insight into protein folding and stability, glycan profiles, protein activity and organelle targeting.

The number of papers published in this Research Topic, coupled with the wide variety of applications described, illustrates the relevance of molecular farming today. As plant -made pharmaceuticals evolve, they will continue to address the many urgent issues that we face in global health for many years to come.

Author contributions

BS: Writing – original draft, Writing – review & editing. KH: Writing – original draft, Writing – review & editing.

Acknowledgments

We thank authors of the papers published in this Research Topic for their valuable contributions and the referees for their rigorous reviews. We also thank the editorial board, especially Berna Ustun, Rhiannon Jackson and Rebecca Carver, for their support.

Conflict of interest

The authors declare that the research was conducted in the absence of any commercial or financial relationships that could be construed as a potential conflict of interest.

The author(s) declared that they were an editorial board member of Frontiers, at the time of submission. This had no impact on the peer review process and the final decision.

Publisher's note

References

He, W., Baysal, C., Lobato Gómez, M., Huang, X., Alvarez, D., Zhu, C., et al. (2021). Contributions of the international plant science community to the fight against infectious diseases in humans—part 2: Affordable drugs in edible plants for endemic and re-emerging diseases. *Plant Biotechnol. J.* 19, 1921–1936. doi: 10.1111/pbi.13658

Lobato Gómez, M., Huang, X., Alvarez, D., He, W., Baysal, C., Zhu, C., et al. (2021). Contributions of the international plant science community to the fight against human infectious diseases – part 1: epidemic and pandemic diseases. *Plant Biotechnol. J.* 19, 1901–1920. doi: 10.1111/pbi.13657

Shanmugaraj, B., I. Bulaon, C. J., and Phoolcharoen, W. (2020). Plant molecular farming: A viable platform for recombinant biopharmaceutical production. *Plants* 9, 842. doi: 10.3390/plants9070842

frontiers | Frontiers in Plant Science

TYPE Original Research
PUBLISHED 27 February 2023
DOI 10.3389/fpls.2023.1126470

OPEN ACCESS

EDITED BY
Balamurugan Shanmugaraj,
Chulalongkorn University, Thailand

REVIEWED BY
Marcello Donini,
Italian National Agency for New Technologies, Energy and Sustainable Economic Development (ENEA), Italy
Andreas Schiermeyer,
Fraunhofer Society (FHG), Germany
Shiv Verma,
Case Western Reserve University, United States

*CORRESPONDENCE
Melanie Grandits
melanie.grandits@kcl.ac.uk

†These authors have contributed equally to this work and share senior authorship

SPECIALTY SECTION
This article was submitted to Plant Biotechnology, a section of the journal Frontiers in Plant Science

RECEIVED 17 December 2022
ACCEPTED 01 February 2023
PUBLISHED 27 February 2023

CITATION
Grandits M, Grünwald-Gruber C, Gastine S, Standing JF, Reljic R, Teh AY-H and Ma JK-C (2023) Improving the efficacy of plant-made anti-HIV monoclonal antibodies for clinical use.
Front. Plant Sci. 14:1126470.
doi: 10.3389/fpls.2023.1126470

Improving the efficacy of plant-made anti-HIV monoclonal antibodies for clinical use

Melanie Grandits[1]*, Clemens Grünwald-Gruber[2], Silke Gastine[3], Joseph F. Standing[3], Rajko Reljic[1], Audrey Y-H. Teh[1†] and Julian K-C. Ma[1†]

[1]Molecular Immunology Unit, Institute for Infection and Immunity, St. George's University of London, London, United Kingdom, [2]Core Facility Mass Spectrometry, University of Natural Resources and Life Sciences, Vienna, Austria, [3]Infection, Immunity and Inflammation Research and Teaching Department, University College London (UCL) Great Ormond Street Institute of Child Health, London, United Kingdom

Introduction: Broadly neutralising antibodies are promising candidates for preventing and treating Human Immunodeficiency Virus/Acquired Immunodeficiency Syndrome (HIV/AIDS), as an alternative to or in combination with antiretroviral therapy (ART). These mAbs bind to sites on the virus essential for virus attachment and entry, thereby inhibiting entry into the host cell. However, the cost and availability of monoclonal antibodies, especially combinations of antibodies, hampers implementation of anti-HIV bNAb therapies in low- to middle- income countries (LMICs) where HIV-1 prevalence is highest.

Methods: We have produced three HIV broadly neutralizing antibodies (bNAbs), 10-1074, VRC01 and 3BNC117 in the Nicotiana benthamiana transient expression system. The impact of specific modifications to enhance potency and efficacy were assessed. To prolong half-life and increase bioavailability, a M252Y/S254T/T256E (YTE) or M428L/N434S (LS) mutation was introduced. To increase antibody dependent cellular cytotoxicity (ADCC), we expressed an afucosylated version of each antibody using a glycoengineered plant line.

Results: The majority of bNAbs and their variants could be expressed at yields of up to 47 mg/kg. Neither the expression system nor the modifications impacted the neutralization potential of the bNAbs. Afucosylated bNAbs exhibit enhanced ability to bind to FcγRIIIa and trigger ADCC, regardless of the presence of Fc amino acid mutations. Lastly, we demonstrated that Fc-modified variants expressed in plants show enhanced binding to FcRn, which results in a favourable in vivo pharmacokinetic profile compared to their unmodified counterparts.

Conclusion: Tobacco plants are suitable expression hosts for anti-HIV bNAbs with increased efficacy and an improved pharmacokinetic profile.

KEYWORDS

bNAb, HIV, Half-Life, glycosylation, pharmacokinetics, antibody engineering, ADCC, plant molecular biopharming

Introduction

Around 38 million people are living with Human Immunodeficiency Virus/Acquired Immunodeficiency Syndrome (HIV/AIDS) globally, with the majority of patients in less developed regions (UNAIDS, 2019). Combination antiretroviral therapy (cART) offers HIV patients the prospect of almost normal life-expectancy and very low risk of transmission (Mills et al., 2011). Yet, there are approximately 1.5 million new infections each year and still a considerable number of deaths (approximately 650000 people worldwide in 2021)(UNAIDS, 2021). Moreover, a 2019 report published by the WHO revealed that in 12 out of 18 assessed countries, drug resistance to first line non-nucleoside reverse transcriptase inhibitors (NNRTI) had exceeded 10% (World Health Organization, 2019). This trend was further emphasised by a survey conducted in nine sub-Saharan African countries, which showed that over 50% of infants newly diagnosed with HIV carry a NNRTI resistant strain (World Health Organization, 2019). Therefore, there is an urgent need for alternative treatment approaches.

Broadly neutralising antibodies (bNAbs) are considered to be one of the most promising candidates. They naturally develop approximately 1 year post-infection in rare individuals known as elite neutralisers (Doria-Rose et al., 2009). A number of bNAbs have been isolated, but only a few have been considered as treatment candidates for HIV-1. bNAbs 10-1074 (Mouquet et al., 2012), VRC01 (Wu et al., 2010) and 3BNC117 (Scheid et al., 2012) are three of the most promising candidates currently in clinical trials. Co-development of multiple bNAbs is necessary, as any bNAb-based therapy is likely to require administration of two or more antibodies to provide adequate coverage and avoid development of viral resistance (Caskey et al., 2016).

10-1074 targets the V3 loop and glycan on gp120 (Mouquet et al., 2012), which is responsible for binding to the co-receptor CCR5 or CXCR4. 10-1074 has a neutralisation breadth of about 60% and a half-life of 24 days in healthy individuals (Mouquet et al., 2012; Caskey et al., 2017). On the other hand, VRC01 and 3BNC117 target the CD4 binding site of gp120 (Wu et al., 2010; Scheid et al., 2012), which is essential for HIV-1 to enter the host cell. VRC01 has a neutralisation breadth of about 91% and 3BNC117 of 82%, with half-lives of 15 and 17 days respectively, in uninfected individuals (Caskey et al., 2015; Gaudinski et al., 2018).

Several *in vivo* studies have demonstrated the ability of bNAbs to protect against HIV-1 infection upon repeated exposure (Pegu et al., 2014; Gautam et al., 2016, 2018). Furthermore, there is evidence that a single course of early bNAb combination therapy can induce long-lasting virus control, as shown in Simian-Human Immunodeficiency Virus (SHIV) infected non-human primates (NHPs) treated with 3BNC117 and 10-1074 (Nishimura et al., 2017). Human clinical studies have demonstrated that VRC01, 3BNC117 and 10-1074 are well-tolerated and safe (Caskey et al., 2015, 2017; Ledgerwood et al., 2015), and there are ongoing studies investigating whether these bNAbs alone or in combination can be used to treat patients with established infection (e.g. NCT03571204, NCT02591420).

An affordable manufacturing platform is key to successful delivery of mAb-based therapies. About 93% of mAb production sites are located in either Europe or the USA (Grilo and Mantalaris, 2019), as low-to-middle income countries (LMICs) usually lack the capital to invest in traditional pharmaceutical production sites (Murad et al., 2020). Plants may offer an attractive alternative to current manufacturing platforms, as initial investment for upstream processes would be greatly reduced compared to mammalian-cell expression systems (Nandi et al., 2016) and culture medium – soil and fertiliser – is inexpensive and can be sourced locally (Murad et al., 2020). Furthermore, the cultivation of plants does not require highly specialised personnel and production can be modularly upscaled by expanding greenhouse facilities or acreage (Pogue et al., 2010). Successful expression of several anti-HIV bNAbs has been demonstrated in *Nicotiana benthamiana* and *Nicotiana tabacum*, with yields up to 400 mg/kg (Teh et al., 2014; Rosenberg et al., 2015), and plant-produced anti-HIV bNAb 2G12 has been shown to be safe and well-tolerated in humans (Ma et al., 2015).

bNAbs also have some limitations. bNAbs have to be given intravenously, whereas cART can be conveniently self-administered orally (Caskey et al., 2016). This would complicate bNAb therapy, especially in areas with limited medical infrastructure. Furthermore, monoclonal antibody therapies are expensive (average annual cost: $96,731) (Hernandez et al., 2018), thus frequent interventions with mAbs would add to the economic burden. This makes the case for increasing the potency of bNAbs and prolonging their *in vivo* half-lives, to reduce treatment frequency, improve patient compliance and reduce cost.

While the potential to effectively neutralise the virus is considered to be the main attribute of anti-HIV bNAbs, several studies have shown that their ability to perform effector functions, such as antibody-dependent cellular cytotoxicity (ADCC), can contribute to their potency and efficacy (Hessell et al., 2007, 2009; Bournazos et al., 2014). Moreover, it is speculated that bNAbs with the propensity for enhanced ADCC may be able to contribute to clearance of latent virus reservoirs (Caskey et al., 2016). The removal of the core fucose residue on the N297 glycan of Immunoglobulin Gs (IgGs) is one way to improve binding of the IgG Fc-region to FcγRIIIa, the key receptor that participates in ADCC (Vidarsson et al., 2014). Afucosylation of the N297 glycan has been shown to improve ADCC in mAbs targeting various diseases (Zeitlin et al., 2011).

Here, we use an emerging plant based expression system building on earlier clinical trials using plant-derived mAbs (Ma et al., 2015). IgG mAbs produced in plants differ significantly only in *N*-glycosylation compared with those produced in mammalian (CHO/HEK) cell-based systems. For this reason we used a glycoengineered plant line (ΔXF) (Strasser et al., 2008) for antibody production, in which fucosylation is minimised and glycoforms that are not normally produced by mammalian cells are avoided.

A key player in extending the half-life of IgGs is the neonatal receptor (FcRn), which salvages IgG from degradation in the lysosome (Petkova et al., 2006). Improvement in half-life is linked to increased affinity of IgG to FcRn at pH 6, which can be achieved by introducing a modification, for example M252Y/S254T/T256E (YTE) (Dall'Acqua et al., 2002) or M428L/N434S (LS) (Zalevsky et al., 2010) into the Fc region of the target antibody. These modifications resulted in a 3-4 fold enhancement of half-life of mAbs in NHPs and this approach has been widely used to prolong half-life of various IgGs (Dall'Acqua et al., 2002; Zalevsky et al., 2010; Gaudinski et al., 2018; Gautam et al., 2018). Currently several clinical studies are investigating the safety and efficacy

of anti-HIV bNAbs carrying half-life extending mutations (e.g. NCT04250636, NCT05612178, NCT04173819).

We investigated the feasibility of using tobacco plants to express bNAbs, which have been modified to enhance half-life. These modifications include amino acid modifications (YTE or LS). We compared non-modified and modified versions of the anti-HIV bNAbs VRC01, 3BNC117 and 10-1074, with regard to their expression yield, *in vitro* functionality and *in vivo* half-life. We showed that neither the expression system nor the modifications impact neutralisation breadth and potency of the bNAbs. Furthermore, all plant-generated bNAbs exhibit higher affinity to FcγRIIIa, associated with removal of core-fucose, compared to their respective mammalian-cell made counterparts. This translated to higher ADCC activation *in vitro*. bNAbs with half-life extending modifications in their Fc-region showed improved binding to FcRn, which resulted in functional changes, demonstrated by *in vitro* transcytosis and most importantly up to 28% reduction in clearance in transgenic hFcRn mice when compared to the non-modified versions.

Results

Here, we present the detailed data for bNAb 10-1074 only. Similar approaches and analyses were performed for bNAbs VRC01 and 3BNC117 and these are presented as supplemental figures and summarised at the end of this results section. If not specified, modified bNAb refers to the mutation affecting FcRn binding affinity in the Fc region.

Expression of bNAbs in glycomodified *Nicotiana benthamiana* plants

YTE or LS mutations were introduced into the constant region of human γ-chain by site-directed mutagenesis. The respective variable regions of mAbs VRC01, 3BNC117 or 10-1074 were then introduced upstream of human light and heavy chain constant region genes. Three different versions of the heavy chain constant region were prepared: the non-modified (HC), YTE modified (YTE) or LS modified (LS) constant region. Heavy and light chain gene combinations were then assembled in MIDAS-p, a modular plant expression vector (Pinneh et al., 2021). All bNAbs were expressed transiently in ΔXF *Nicotiana benthamiana* (Strasser et al., 2008) using *Agrobacterium tumefaciens* harbouring the respective T-DNA constructs. The bNAb variants will be referred to as 10-1074 HC ΔXF, 10-1074 YTE ΔXF, 10-1074 LS ΔXF and compared with CHO-derived 10-1074 CHO.

N. benthamiana leaves were harvested 6 days post-infiltration (dpi). Average crude extract yields for 10-1074 HC ΔXF and 10-1074 YTE ΔXF were comparable (44.0 mg/kg ± 5.3 fresh weight (FW) vs 47.7 mg/kg ± 24.3 FW), whereas the average yield of 10-1074 LS was much lower (3.2 mg/kg 0.1 FW). The latter yields were considered below the threshold to generate reasonable purified amounts of this bNAb variant for further analysis, so this variant was abandoned.

A standard mAb purification protocol using Protein A affinity chromatography (Teh et al., 2014) resulted in recovery of 10-1074 HC ΔXF (13.3 ± 3.1 mg/kg FW) and of 10-1074 YTE ΔXF (9.2 ± 3.9 mg/kg FW), representing only 30% and 19% recovery respectively. Addition of 0.01% polysorbate 80 during affinity purification restored the recovery yield for 10-1074 HC ΔXF (47.0 ± 10.8 mg/kg FW) but had no impact on the yield of 10-1074 YTE ΔXF (12.6 ± 0.2 mg/kg FW).

Integrity and purity of bNAb variants

The quality and purity of 10-1074 HC ΔXF and YTE ΔXF were confirmed by SDS-PAGE (Figure 1A). Under non-reducing conditions, bands corresponding to the fully assembled antibody (150-180 kDa) and minor degradation products were observed. The pattern of bands was similar to that of a commercial myeloma-derived human IgG mAb control. Under reducing conditions, bands consistent with intact heavy and light chains were detected. This was confirmed by western blot, which showed specific immunoreactivity

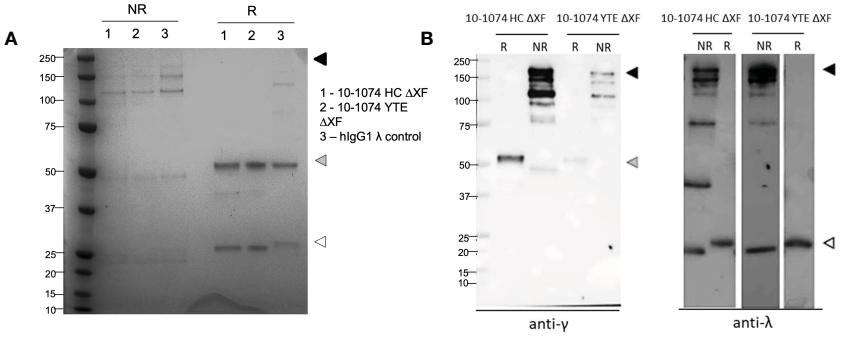

FIGURE 1
Yields and assembly of plant-expressed 10-1074 Fc variants. Representative SDS-PAGE **(A)** and anti-γ/Λ Western blots **(B)** of non-reduced (NR) and reduced (R) purified 10-1074 non-modified (HC) and YTE variant expressed in λXF *N. benthamiana* plants. Arrows indicate fully assembled bNAb (black), heavy chain (grey) or light chain (white). Commercial human IgG1λ from human myeloma plasma (Sigma, USA) was used as control.

for each band, with either anti-gamma or anti-lambda chain antisera (Figure 1B, right).

Glycosylation of bNAb variants

bNAbs produced in ΔXF *Nicotiana benthamiana* were expected to lack α1,3-fucose and β1,2-xylose. PNGase F is an enzyme that cleaves all *N*-linked oligosaccharides from proteins unless the core-GlcNAc carries α1,3-fucose. bNAbs were digested with PNGase F and resolved using SDS-PAGE alongside undigested bNAb controls. For all digested samples expressed in ΔXF *N. benthamiana*, a size shift in the heavy chain compared to the undigested control could be observed (Figure 2A – black triangle), supporting the absence of core fucose glycosylation.

This was confirmed by mass spectrometry (Figure 2B), which not only revealed GnGn as the prevalent glycoform (~80%) of 10-1074 HC ΔXF and YTE ΔXF, but also confirmed the absence of β1,2-xylose and only low-levels of α1,3-fucose (<2%). Up to 15% of bNAb were aglycoslyated (Figure 2C).

Binding kinetics to HIV-1 gp140

Surface plasmon resonance (SPR) was used to compare the HIV-1 UG37 gp140 binding affinity of the plant-produced bNAb variants and their mammalian-produced non-modified counterparts (Supplementary Table 4). No significant differences were observed ($p>0.05$, Tukey's multiple comparison test).

HIV-1 neutralisation

Viral neutralisation of bNAb variants was measured against a panel of HIV-1 pseudoviruses (Figure 3). First, we confirmed that the plant expressed 10-1074 HC ΔXF had equivalent neutralising activity compared to 10-1074 CHO, using a panel of seven HIV isolates (Figure 3A). A more extensive comparison was then performed, comparing 10-1074 HC ΔXF with 10-1074 YTE ΔXF, using a panel of 13 HIV isolates (Figure 3B). No differences were observed. Comparative neutralisation curves are also shown for the three antibodies against HIV BaL.26 (Figure 3C).

Binding kinetics to FcγRIIIa (CD16a) and ADCC

Binding kinetics of the plant-produced 10-1074 variants to soluble FcγRIIIa V158 were compared to their mammalian counterpart using SPR. Both bNAb variants produced in glycomodified ΔXF plants showed improved binding (9.4 and 6.3-fold respectively) when compared to their glycan unmodified, fucosylated mammalian counterpart (Figure 4A)

To determine whether increased affinity of the plant-made bNAbs to FcγRIIIa V158 results in a functional improvement in antibody-dependent cellular cytotoxicity (ADCC), a Reporter Assay was performed with effector cells carrying FcγRIIIa V158 (Figure 4B). For both ΔXF plant-made bNAbs, a concentration-dependent induction was observed. At 4 and 10μg/ml, 10-1074 HC ΔXF and YTE ΔXF induced significantly higher ADCC activation compared

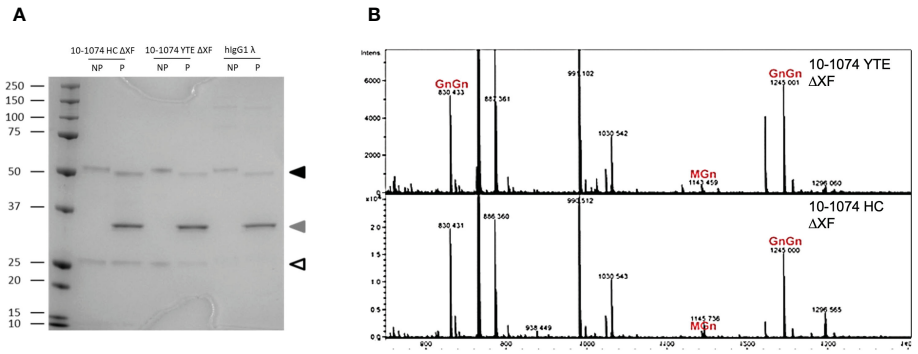

C

	10-1074 HC ΔXF	10-1074 YTE ΔXF
aglyc	15.42	11.63
Man5	ND	ND
Man7	ND	ND
Man8	ND	ND
Man9	ND	ND
GnM	4.75	4.89
GnGn	78.49	81.75
GnGnF	1.34	1.73
	% of glycoform present	

FIGURE 2
Glycosylation profiles of 10-1074 Fc variants. **(A)** Representative SDS-PAGE of untreated (NP) and PNGase F treated (P) 10-1074 HC ΔXF and YTE ΔXF variants, as well as mammalian cell-produced hIgG1λ. Arrows indicate enzymatically aglycosylated heavy chain (black), PNGase F (grey) and light chain (white). **(B, C)** Mass spectra showing dominant glycans present in purified 10-1074 YTE ΔXF (B; top) and 10-1074 HC ΔXF (B; bottom), as well as percentage of glycoforms present **(C)**. *N*-glycans are abbreviated according to the ProGlycAn system (www.proglycan.com).

10.3389/fpls.2023.1126470

A

HIV-1 Pseudovirus	Clade	IC_{50} (ng/mL) 10-1074 CHO	10-1074 HC ΔXF
BaL.26	C	81 ± 10	93 ± 15
CAAN5342	B	65	61
SC422-661.8	B	239	277
QH0692_42	B	536	967
6535	B	77	88
AC10.0	B	244	244
ZM135M.PL10a	C	675	652

B

HIV-1 Pseudovirus	Clade	IC_{50} (ng/mL) 10-1074 HC ΔXF	10-1074 YTE ΔXF
BaL.26	C	93 ± 15	74 ± 15
CAAN5342	B	61	62
SC422-661.8	B	277	224
ZM109F.PB4	C	>20000	>20000
pX1632	G	>20000	>20000
pCNE55	CRF01_AE	>20000	>20000
QH0692_42	B	469	373
REJO4541_67	B	>20000	>20000
6535	B	88	56
AC10.0	B	129	121
ZM135M.PL10a	C	333	386
CAP45_G3	C	>20000	>20000
ZM53M.PB12	C	>20000	>20000

C

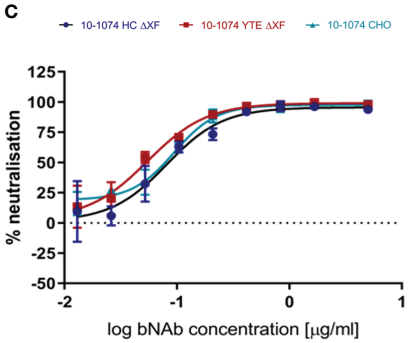

FIGURE 3
HIV-1 pseudovirus neutralisation comparison. **(A)** IC_{50}s of 10-1074 HC ΔXF and 10-1074 CHO against seven HIV-1 pseudovirus strains susceptible to 10-1074. BaL.26 (n=3 biological repeats), all other pseudovirus strains (n=1). **(B)** IC_{50}s of 10-1074 HC ΔXF and YTE ΔXF against 13 HIV-1 pseudovirus strains from different clades. Mean ± SD for BaL.26 (n=3 biological repeats) are shown. For all other pseudovirus strains n=1. **(C)** BaL.26 neutralisation curves of ΔXF *N. benthamiana* plant-made 10-1074 HC (blue), YTE (red), and 10-1074 CHO (light blue). Data points indicate average ± SD of 3 technical repeats.

A

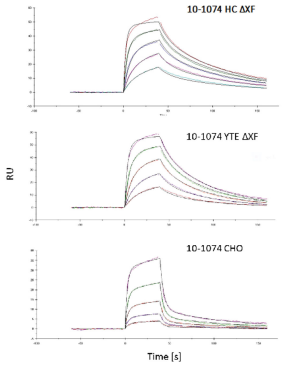

Sample	K_D [M]
10-1074 CHO	$78.0*10^{-8}$
10-1074 HC ΔXF	$8.32*10^{-8} \pm 2.0*10^{-8}$
10-1074 YTE ΔXF	$12.4*10^{-8} \pm 0.92*10^{-8}$

B

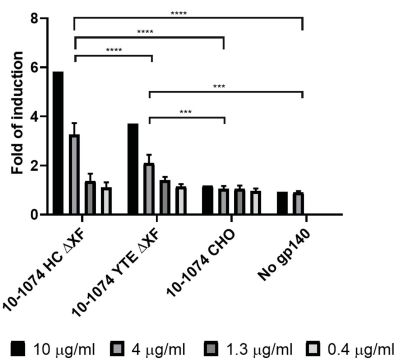

FIGURE 4
FcγRIIIa binding and ADCC activation comparison. **(A)** Representative SPR sensorgram showing binding of ΔXF *N. benthamiana*-produced 10-1074 HC ΔXF (top), 10-1074 YTE ΔXF (middle) and mammalian cell-produced 10-1074 CHO (bottom) to FcγRIIIa V158 at five different concentrations (0.0625, 0.125, 0.25, 0.5 and 1 μM) along with equilibrium dissociation constants (K_Ds; bottom table). KDs of 10-1074 HC ΔXF and YTE ΔXF were averages ± SD of three biological repeats. **(B)** FcγRIIIa activation by 10-1074 HC ΔXF, YTE ΔXF and CHO in the presence of HIV-1 UG37 gp140. Activation was measured by fold-induction of luciferase expression controlled by NFAT pathway. Values represent average fold-induction ± SD of 3 biological repeats (except for 10 μg/mL, where n=1). A two-way ANOVA with Tukey's multiple comparison test was performed to determine significant differences. 10-1074 HC ΔXF without HIV-1 UG37 gp140 was used as negative control. Significant differences could only be observed at 4 μg/ml (ns $p > 0.05$, ***$p \leq 0.001$, ****$p \leq 0.0001$).

with the CHO produced 10-1074 mAb ($p<0.05$). At these concentrations, 10-1074 HC ΔXF was also significantly more potent than 10-1074 YTE ΔXF ($p<0.05$).

Binding kinetics to FcRn and *in vitro* transcytosis

Binding of bNAbs bearing the YTE mutation to human neonatal Fc receptor (hFcRn) was determined by SPR. CM5 chips were coated directly with the 10-1074 bNAb variants and a series of concentrations of recombinant hFcRn were flowed over the chip. The sensorgrams show much higher binding of recombinant hFcRn to 10-1074 YTE ΔXF when compared to the HC ΔXF non-modified control (Figure 5A). Whilst an affinity of 1.021 x 10^{-7} M could be calculated for 10-1074 YTE ΔXF, the unusual nature of the dissociation curve for HC ΔXF made it impossible to calculate a comparative value.

To demonstrate that this change in binding affinity to FcRn had a functional consequence, a transcytosis assay was performed using transgenic MDCK.2 cells constitutively expressing hFcRn/hβ_2m. MDCK.2 hβ_2m-expressing cells served as control. Transepithelial resistance was measured to verify the formation of tight junctions and ranged between 250-350 Ω*cm^2. bNAbs were added to the apical side (pH 6.0) and the basolateral supernatant was removed after 2 hours of incubation to determine the amount of transcytosed bNAb by ELISA. Increased transcytosis was observed at all concentrations for 10-1074 YTE ΔXF. Minimal or no antibody was detected in the basolateral supernatant when 10-1074 HC ΔXF or 10-1074 CHO was tested. (Figure 5B).

In vivo pharmacokinetic studies

In vivo pharmacokinetic studies were performed using B6.Cg-*Fcgrt*^{tm1Dcr} Tg(CAG-FCGRT)276Dcr/DcrJ mice transgenic for hFcRn, that were given a single intravenous 2 mg/kg dose of bNAb. Results from four replicate experiments are shown (Figure 6). 10-1074 CHO and 10-1074 HC ΔXF followed first-order pharmacokinetics (Figure 6, Expt. 4 and Expts. 1-3 top graphs, Supplementary Figure 7). 10-1074 YTE ΔXF antibody depletion was delayed, following a nonlinear pattern most likely attributed to target mediated drug disposition kinetics (Dua et al., 2015). In Expts 1-3, 5/12 mice retained an average of 84.4% of the bNAb at 144 hours Figure 6

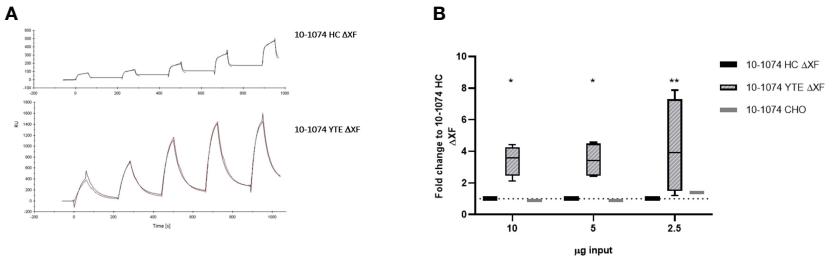

FIGURE 5
hFcRn binding and *in vitro* transcytosis comparison. **(A)** SPR sensorgrams showing binding of 10-1074 HC ΔXF (top) and 10-1074 YTE ΔXF plant-produced 10-1074 (bottom) to hFcRn at five different concentrations (75, 100,150, 200 and 250 nM). **(B)** Transcytosis of 10-1074 HC ΔXF, YTE ΔXF and CHO across MDCK.2 cell layer constitutively expressing hFcRn/hβ_2m. Values indicate average fold-change ± SD of bNAbs in output wells (pH 7.4) compared to 10-1074 HC ΔXF when 2.5, 5 or 10 μg of bNAbs were introduced into the input wells (pH 6.0). hβ_2m expressing MDCK.2 cell layers were used as negative controls. 4 biological repeats were performed for plant-made 10-1074 HC ΔXF and YTE ΔXF and one for 10-1074 CHO. A two-way ANOVA with Tukey's multiple comparison test with 10-1074 HC ΔXF as control was performed to determine significant differences (*p≤ 0.05, **p≤ 0.01).

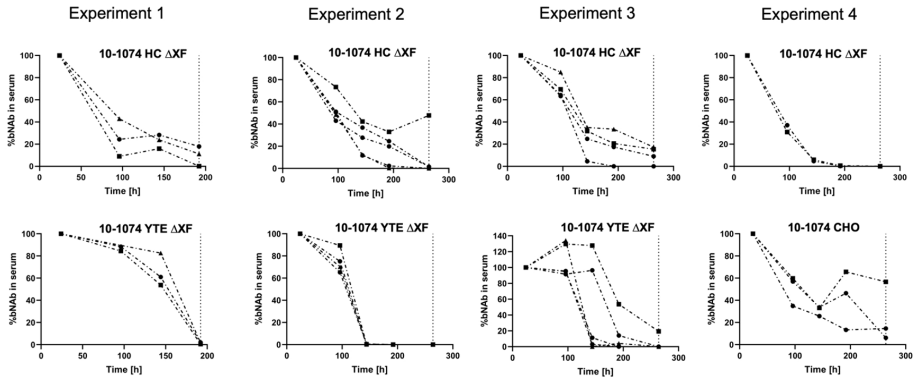

FIGURE 6
In vivo pharmacokinetics of 10-1074 Fc variants. Serum concentration (%) of 10-1074 HC ΔXF, YTE ΔXF and CHO in hFcRn transgenic mice across four separate experiments measured using ELISA. Serum concentration at day one was set to 100%. Each line represents a separate animal. The dashed vertical line demonstrates timepoint of sacrifice.

lower graphs), compared with an average of 24.7% in the 10-1074 HC ΔXF inoculated mice.

The area-under-the-curve (AUC, %*h) was calculated (Supplementary Table 5), as basic determination of half-life cannot be performed due to the mixed linear and nonlinear kinetics of 10-1074 YTE. The AUC showed that the introduction of the YTE mutation led to a 39% increase in AUC and therefore a reduction in clearance of 10-1074.

bNAbs VRC01 and 3BNC117

The average post-purification yield for VRC01 and 3BNC117 was in both cases highest for the non-modified (HC) version of the bNAb at 65 ± 8 mg/kg FW and 51 ± 21 mg/kg FW, respectively (Supplementary Figure 1A). The post-purification yield of VRC01 YTE ΔXF was 39mg/Kg, VRC01 LS ΔXF was 33mg/Kg, 3BNC117 YTE ΔXF was 31mg/Kg and 3BNC117 LS ΔXF was 38mg/Kg. Batch-to-batch variability was higher in plants infiltrated with YTE or LS constructs.

All bNAbs were assembled correctly (Supplementary Figures 1B–D) and PNGase digest verified the absence of α1,3-fucose in all variants of both bNAbs (Supplementary Figures 2A and B). As both VRC01 and 3BNC117 contain a glycosylation site in the light chain, a size shift in the light chain could also be observed for these samples (Supplementary Figures 2A and B).

A slight reduction in HIV gp140 binding affinity was determined for plant produced VRC01 but not for 3BNC117 mAb (Supplementary Table 2). This was not however, supported by decreased neutralisation potency of the plant-produced bNAbs (Supplementary Table 3), as observed in previous studies (Rosenberg et al., 2013; Teh et al., 2014). As seen with 10-1074, modified variants of both bNAbs performed equally in neutralisation assay when compared to the respective non-modified version (Supplementary Table 3).

Binding kinetics of all variants to FcγRIIIa V158 showed a 2.7 – 15-fold increase in affinity of the glycomodified plant-produced bNAbs compared to the non-modified, fucosylated mammalian versions. Like 10-1074, this increase is highest for the HC (Fc-unmodified) version of both bNAbs (1.6-4.9x) when compared to the Fc-modified bNAbs (Supplementary Figure 3A), but all variants demonstrated increased ADCC pathway activation (Supplementary Figures 3B and C).

Binding kinetics of VRC01 and 3BNC117 bNAbs to hFcRn was measured using CM5 chips coated with an anti-Human IgG Fab reagent. Equilibrium dissociation constants (K_Ds) were in the 10^{-8}M range (Supplementary Figure 4A). The YTE and LS versions of VRC01 and 3BNC117 had the highest affinities to hFcRn (Supplementary Figure 4A). Transcytosis assays showed that YTE and LS versions of the bNAbs was more efficiently transcytosed through hFcRn expressing cells (Supplementary Figures 4B and C).

In vivo, the decline in antibody after intravenous administration followed first-order kinetics (Supplementary Figure 5A). As with 10-1074, the modified versions demonstrated a favourable pharmacokinetic profile when compared to the non-modified versions. However, for VRC01 the mammalian produced version showed a more favourable profile than any of the plant-produced versions in the initial experiment. The AUC of VRC01 YTE ΔXF and VRC01 LS ΔXF was 35% and 28% higher respectively than VRC1 HC ΔXF. It was not possible to determine pharmacokinetics for 3BNC117 in the Tg276 mouse model, as bNAb levels were almost depleted after 96 h (Supplementary Figure 5B).

Discussion

bNAbs are of increasing interest as adjuncts or alternatives to cART for prevention or treatment of HIV-1 infection (Caskey et al., 2016), and are being assessed in a number of clinical trials. This is driven by the lack of a vaccine and the emergence of resistance to first line NNRTI which has been observed in up to 26% of ART initiators (World Health Organization, 2019). Additionally, passive immunisation with bNAbs may help with the reduction of the latent reservoir and trigger the immune system to effectively fight the virus (Caskey et al., 2016; Nishimura et al., 2017; Desikan et al., 2019). However, while the concept of bNAbs as sole treatment or in combination with cART seems promising, the need for intravenous administration and cost are major disadvantages (Caskey et al., 2016).

Improving efficacy by prolonging half-life and enhancing effector functions would be an important step to making bNAbs more accessible and affordable, particularly in countries with limited infrastructure. We also propose that a plant-based mAb expression platform may facilitate this goal. Here we investigated whether anti-HIV bNAbs with enhanced properties can be generated in glyco-engineered tobacco plants without compromising their potency. To improve efficacy, we introduced an YTE or LS mutation into the Fc-region, both known to prolong half-life *in vivo*. bNAbs with these improved properties may eventually allow for implementation of bNAbs for the treatment of chronically infected patients, and potentially be useful as pre- and post-exposure prophylaxis by offering immediate and effective long-term protection with less side-effects than current treatments. Furthermore, treatments with bNAbs may be beneficial in HIV-positive pregnant women, where standard Mother-to-Child Prevention therapy is either ineffective or initiated too late. As well as providing direct anti-viral treatment to the mother, placental transport of IgG *via* FcRn is a route for infants to obtain protective maternal IgGs *in utero* (Simister, 2003).

Three anti-HIV-1 bNAbs were successfully expressed in ΔXF *N. benthamiana* plants at high yields. Engineered versions of these antibodies were also produced, targeting the Fc region to alter binding to FcRn. Although there appears to be some yield penalty, variant bNAbs were still expressed at relatively high levels, with the exception of the LS mutant of bNAb 10-1074. For 10-1074 there was also a reduction in antibody recovery after Protein A affinity purification. This could be mitigated in the non-mutated heavy chain antibody version by the addition of Tween 80, but not in the YTE mutant. While Tween 80 is commercially used to protect mAbs from interface-induced aggregation, it is possible that the polysorbate may not be able to fully 'protect' mAbs carrying a YTE mutation, which has shown to lead to an around 11% loss in thermodynamic stability (Edgeworth et al., 2015). All plant-produced bNAb variants retained specificity and affinity to their antigen and displayed similar neutralisation potency compared with the same antibodies expressed conventionally in CHO cells. This is in accordance with previous

reports showing that potency was not affected by whether the bNAb was produced in a mammalian-cell or plant platform (Teh et al., 2014; Rosenberg et al., 2015; Gautam et al., 2018). Furthermore, our data confirmed that neither afucosylation nor the introduction of the YTE or LS mutation had any effect on the neutralisation potential of the bNAbs. This result was to be expected, as all alterations were limited to the Fc-region, even though some studies have suggested that changes in the Fc-region can influence the functionality of the Fab domain and vice versa (Cooper et al., 1994; Igawa et al., 2010; Tudor et al., 2012; Schoch et al., 2015; Jensen et al., 2017).

Afucosylation of the core-GlcNAc of mAbs has previously been shown to result in increased affinity to FcγRIIIa, which translated into enhanced ADCC activity (Shields et al., 2002; Okazaki et al., 2004; Ferrara et al., 2011; Luo et al., 2017; Marusic et al., 2018; Pereira et al., 2018; Stelter et al., 2020). We corroborated these findings and demonstrated that an increase in affinity to FcγRIIIa, and the subsequent improved induction of ADCC, can be obtained by removal of the N297 fucose in the presence of a YTE or LS mutation. The capability to perform ADCC may be important for maximising the potency of anti-HIV bNAbs – a number of studies have demonstrated a reduction in protection against HIV-1 conferred by bNAbs upon abrogation of effector functions (Hessell et al., 2007, 2009; Bournazos et al., 2014). Furthermore, several studies have shown a correlation between slow disease progression and high ADCC activity of antibodies (Baum et al., 1996; Banks et al., 2002; Gómez-Román et al., 2005; Lambotte et al., 2013; Madhavi et al., 2017), suggesting that bNAbs with enhanced ADCC may be beneficial for virus control.

The magnitude of improvement in ADCC varied between the three tested bNAbs, even though they had identical Fc-regions with differences only in the variable region. This supports findings of a recent study investigating the interaction of FcγRIIIa and mAbs, which revealed that several positions in the Fab-region, including the variable region, may be involved in the interaction with FcγRIIIa (Yogo et al., 2019). Interestingly, our results suggest that the Fab region could determine whether mutations introduced in the Fc region negatively affect the bNAb's potential to induce ADCC. There was no change in ADCC pathway activation between the different variants of 3BNC117 and VRC01, whereas 10-1074 YTE ΔXF showed a statistically significant reduced induction. Reduced ADCC ability of mAbs with YTE mutations has been previously reported (Dall"Acqua et al., 2006; Ko et al., 2014).

Introduction of the YTE or LS mutation led in all cases to improved binding to the neonatal receptor at pH 6 without impacting release at pH 7.4, consistent with previous reports for other mAbs (Dall'Acqua et al., 2002; Zalevsky et al., 2010). The higher affinity to the FcRn translated functionally to enhanced *in vitro* transcytosis. Transcytosis potential has been used as an indicator of *in vivo* clearance for mAbs engineered for altered binding to the neonatal receptor (Jaramillo et al., 2017).

Higher affinity for the FcRn resulted in a favourable pharmacokinetic profile, as has been established before for several mammalian-cell produced mAbs (Dall'Acqua et al., 2002; Zalevsky et al., 2010; Ko et al., 2014; Gautam et al., 2018). For 10-1074 and VRC01, we showed that the plant-produced bNAbs carrying the YTE and LS mutation result in a 26-28% and 22% reduction in *in vivo* clearance, respectively, in hFcRn Tg276 mice compared to the plant-produced non-modified version. These improvements are comparable to data from previous studies investigating half-life extension in the Tg276 hFcRn mouse model (Kang et al., 2018; Valente et al., 2020). Unfortunately, pharmacokinetics could not be determined for 3BNC117 with the employed sampling protocol, as the antibody was rapidly depleted after 96 h. While the pharmacokinetic data of hFcRn mice correlates with profiles seen in NHPs and humans (Tam et al., 2013; Avery et al., 2016), the half-lives of the same mAbs in Tg276 hFcRn transgenic mice may be up to 4.5 times shorter than in NHPs (Valente et al., 2020). In the case of 10-1074 YTE ΔXF a sudden, rapid decline in serum bNAb levels between 96 and 144 h was observed in half of the mice. Rosenberg et al. (2019) reported a similar drop in NHPs, when PGT121 – also a V3 glycan dependent bNAb – was modified with YTE. The authors established that the observed rapid decline correlated with the development of anti-drug antibodies against the bNAb (Rosenberg et al., 2019). However, in our study, IgM levels at 196 h and 264 h did not differ between those showing a rapid decline and those that did not (Supplementary Figure 6, Methods S1). Another reason for these differences in pharmacokinetics may have been the poor condition of the Tg276 offspring after several breeding rounds, leading to breeding difficulties which have been reported before (Tam et al., 2013). The offspring showed failure to thrive and could only be partially improved by a specialised diet. It is possible that hFcRn expression levels may vary in mice with impacted health, though it was not possible to confirm this hypothesis retrospectively. Thus the results from Experiment 2 and 3, which were performed with mice with impacted health, may be less reliable than the results obtained from Experiment 1. For future studies of pharmacokinetics of human mAbs it would be preferable to use the well-established Tg32 (B6.Cg-*Fcgrt*^{tm1Dcr} Tg(FCGRT)32Dcr/DcrJ) strain or potentially the newly established SYNB-h*FCRN* strain (Conner et al., 2022).

In conclusion, we have demonstrated that tobacco plants are suitable expression hosts for anti-HIV bNAbs modified by glycoengineering to provide enhanced efficacy in terms of binding to FcγRIIIa (for ADCC); and by YTE or LS mutations to enhance binding to FcRn, translating to enhanced transcytosis, *in vivo* half-life and slower clearance from the circulation (Supplementary Table 6). Importantly, we identified 10-1074 YTE and VRC01 LS in ΔXF *N. benthamiana* as lead candidates for further development. The production of these antibodies in plants would broaden the potential applications of bNAbs used as a one-time treatment in specific circumstances, such as prevention of mother-to-child-transmission late in pregnancy, post-exposure prophylaxis, and other emergency procedures where rapid control of reduction of viral load is necessary. Further work to assess the production of anti-HIV bNAbs in plants at scale is now warranted, to follow up on recent regulatory approvals and successful clinical trials for plant derived biologics (Ma et al., 2015; Ward et al., 2021).

Materials and methods

Control antibodies produced in mammalian cell expression systems

Mammalian cell-produced 10-1074 (ARP12477), 3BNC117 (ARP12474) and VRC01 (ARP3291) were obtained from the AIDS

Reagent Programme through the Centre for AIDS Reagents, NIBSC, UK.

Cloning of antibody heavy and light chain genes into plant expression (MIDAS-P) vectors

Site-directed mutagenesis was performed using QuikChange II site-directed mutagenesis kit (Agilent, USA) along with primers (Supplementary Table 1) designed to introduce the M252Y/S254T/T256E (YTE) or M428L/N434S (LS) mutations into human IgG1 Fc region with BsaI sites to insert variable regions. 10-1074 (Mouquet et al., 2012), VRC01 (Wu et al., 2010) and 3BNC117 (Scheid et al., 2011) light and heavy chain variable regions (V_L and V_H) were synthesised with BsaI sites and cloned into vectors containing modified or non-modified constant regions of human IgG1 heavy chain (C_H), human IgG lambda chain (C_L; for 10-1074), or human IgG kappa chain (C_L; for VRC01, 3BNC117). The MIDAS-P system (Pinneh et al., 2021) was used for tandem expression of the heavy and light chain genes in a single binary vector. Briefly, the heavy and light chain genes were cloned into the MIDAS-p entry vectors pWhite and pBlue (Pinneh et al., 2021) respectively. Then, pWhite or pBlue vectors containing the genes of interests were assembled into the destination vector pMIDAS using Golden Gate Assembly with BsaI (for pWhite) and then BsmBI (for pBlue). All plant expression vectors were then electroporated into *Agrobacterium tumefaciens* strain GV3101 PMP90/RK.

Agrobacterium transformation of *N. benthamiana* plants using vacuum infiltration

Vacuum infiltration of glycomodified ΔXF line (Strasser et al., 2008) or wild-type (WT) *N. benthamiana* was performed as described by Kapila et al. (1997). *Agrobacterium tumefaciens* GV3101/PMPRK carrying the heavy and light chain in MIDAS-p for each bNAb was grown for 24 h in Luria-Bertani broth supplemented with 50 μg/mL rifampicin, kanamycin and carbenicillin. After centrifugation the bacterial pellet was resuspended in infiltration solution containing 0.1 mM acetosyringone, 0.01 mM MES and 0.01 mM $MgCl_2$. The final OD_{600} of the suspension was adjusted to 0.2. 7-week-old ΔXF *Nicotiana benthamiana* plants were immersed into the bacterial suspension in a desiccator attached to a vacuum pump, a vacuum was applied for 2 minutes at 150 mbar before releasing, allowing the bacterial solution into the interstitial spaces of the plant leaves. The plants were then further grown in a controlled environment at 26°C for 6 days with a 18/6 hr light/dark cycle.

Extraction and purification of bNAbs from plant leaves

Antibodies were extracted from infiltrated leaves 6 days post infiltration (dpi) in 3 volumes (w/v) of PBS pH 7.4 with or without addition of 0.01% of polysorbate 80. Plant debris was removed by filtration through miracloth and centrifugation at 15008 x *g* for 50 minutes at 4°C. The crude extract was passed through a 0.45 μm filter, followed by a 0.22 μm filter.

mAbs were purified using Protein A-agarose (Sigma Aldrich, USA). The column was calibrated with 5 column volumes (CVs) of Binding Buffer (Sodium phosphate pH 7.0), before the introduction of the clarified plant crude extract. Washing steps were performed using 10 CVs of Binding Buffer and elution was performed using 0.1 M Glycine-HCl (pH 2.7). The eluate was neutralised using 1 in 10 dilution of 1 M Tris-HCl (pH 9.0) with or without addition of 0.1% polysorbate 80. Buffer-exchange to PBS (pH 7.4) was carried out using a Slide-A-Lyzer Dialysis Cassette (3500 MWCO). An Amicon Ultra-15 Centrifugal filter was used to concentrate the sample approximately 10-fold. Purified antibody concentrations were determined using Surface Plasmon Resonance.

The purity and assembly of antibodies was verified using SDS-PAGE and Western blot respectively. Samples were separated using NuPAGE 4-12% Bis-Tris gels (Novex, Invitrogen, USA) with 1% MOPS buffer (Novex, Invitrogen, USA). Gels were stained with Instant Blue (Expedeon, UK). For Western blotting, the separated proteins were blotted onto a nitrocellulose membrane (Amersham, GE Healthcare, UK) by semi-dry transfer. Blocking was performed with 5% (w/v) non-fat dried milk (NFDM) powder (Marvel) in TBST [1% (v/v) TBS + 0.1% (v/v) Tween 20]. Anti-hIgG-γ or anti-hIgG-κ/λ (both from The Binding Site, UK) antiserum was used for detection of heavy and light chains, respectively. The blots were developed using Pierce ECL Plus Western Blotting detection system following the manufacture's protocol.

PNGase F digest

PNGase F digest was carried out following the manufacturer's instructions (New England Biolabs, USA). Digested and non-digested glycoproteins were then separated *via* SDS-PAGE using a NuPAGE 10% Bis-Tris gel (Novex, Invitrogen, USA).

HIV-1 neutralisation assay

Neutralisation potency of the generated bNAbs was determined using a TZM-bl assay and HIV-1 pseudovirus as previously described (Wei et al., 2003; Montefiori, 2004; Sarzotti-Kelsoe et al., 2014). All cells were grown in and dilutions performed using Growth Medium [DMEM with 10% Fetal Calf Serum (FCS), Penicillin-Streptomycin (100 units/mL and 100μg/mL respectively)]. Pseudoviruses were generated by transfecting HEK 293T cells with an *Env*-deficient backbone plasmid and the relevant *Env*-plasmid.

For neutralisation assays, bNAbs were used at a starting concentration of 5 μg/ml and titrated threefold in triplicate in clear flat-bottom 96-well plates. Pseudoviruses at a dilution 20x above the background was added to each well, excluding the cells-only control, and incubated for 1 h. $1x10^4$ TZM-bl cells (Centre for AIDS Reagents, NIBSC, UK), in media supplemented with DEAE dextran, were added to each well and plates were incubated for 48 h at 37°C, 5% CO_2. The supernatant was removed, cells were washed with PBS and lysis buffer (Promega, USA) was added and plates were kept at -80°C overnight.

The thawed cell lysate was mixed 1:1 with Bright-Glo luciferase substrate (Promega Luciferase Assay System, USA) in a black flat bottom 96 well plate. Luminescence was measured using a GloMax plate reader (96 Microplate Luminometer, Promega, USA). Percentage of reduction in relative light units (RLU) was calculated relative to the RLU of the positive (virus plus cells) control. GraphPad Prism was used to plot the resulting curve and calculate IC_{50}s.

Surface plasmon resonance (SPR)

Antibody concentration was determined by capturing the purified antibodies and titrations of known concentration of human IgG kappa (Sigma, UK) on the Protein A-CM5 chip. The response units (RUs) were used to calculate antibody concentration from a standard curve using the BIAcore Evaluation software.

The binding kinetics of all variants of 10-1074, 3BNC117 and VRC01 to gp140, FcγRIIIa and FcRn were determined using SPR on a BIAcore X-100 instrument (Cytiva, USA) at 25°C. Measurements for gp140 and FcγRIIIa were performed using a Protein A capture approach. Protein A (Sigma Aldrich, USA) was immobilised onto a CM5 chip aiming for 5000 response units (RU) with standard amine coupling. HBS-EP+ (10 mM HEPES, pH7.4, 150 mM NaCl, 3 mM EDTA and 0.05% surfactant P-20) was used as running buffer. Each bNAb was captured to a R_{max} of 50. For gp140 measurements, UG37 gp140 (HIV Reagent Programme, USA) was applied at a concentration of 80 µg/ml and a flow rate of 40 µL/min. A contact time of 135s and a dissociation time of 3600s were used. Binding kinetics to FcγRIIIa were determined by applying a range of FcγRIIIa (R&D Systems, USA) concentrations (1, 0.5, 0.25, 0.125 and 0.0625 µM). A contact time of 40s and a flow rate of 50 µL/min were used. Chips were regenerated with 10 mM glycine-HCl, pH 1.5 for both experiments.

The binding kinetics of hFcRn to 10-1074 variants was determined by coating CM5 chips with the respective bNAb to a RU of 10000 and applying multiple concentrations (75,100,150,200,250 nM) of rhFcRn (R&D Systems, USA) at a flow rate of 30 µL/min, a contact time of 60s and dissociation time of 90s. Binding of VRC01 and 3BNC117 to FcRn was determined by using a Human Fab Capture kit (Cytiva, UK). The bNAbs were captured to the Rmax of 100RU and rhFcRn at concentrations of 10, 25, 50,75,100 nM were flowed over the chip with contact time of 60s and dissociation time of 90s, at a flow rate of 30 µL/min. In both experiments, PBS-T (PBS with 0.05% Tween-20), pH 6.0 was used as running buffer. Chips were regenerated with 10 mM glycine-HCl, pH 2.1.

All sensorgrams were corrected with appropriate blank references and fit globally with BIAcore Evaluation software using a 1:1 Langmuir model of binding or a two-state reaction model.

Transcytosis assay

Human neonatal Fc receptor (hFcRn) transcytosis assay was performed as previously described (Claypool et al., 2002). Briefly, 0.75 x 10^6 MDCK hβ_2m (vector only control) or MDCK hFcRn/hβ_2m (supplied by Professor Richard Blumberg of Harvard Medical School) cells were grown on 12mm transwell plates with a pore size of 0.4µm (CoStar, USA) in Growth Medium [DMEM with 10% Fetal Calf Serum (FCS), Penicillin-Streptomycin (100 units/mL and 100µg/mL respectively) and 2mM L-glutamine] at 37°C, 5% CO_2 for 4 days. 12 hours before the experiments, the medium was changed to serum-free medium without antibiotics. Trans-epithelial resistance was measured on the day of the experiment. The cells in the transwell were washed with Hanks' Balanced Salt Solution (HBSS), pH 7.4. Then, the input (apical) and output (basal) wells were equilibrated with HBBS, pH 6.0 and HBBS, pH 7.4 respectively, for 20 minutes, at 37°C, 5% CO_2. 10, 5 or 2.5 µg of respective bNAbs were added to apical side (pH 6). Basolateral supernatant was collected after a 2 hour further incubation. Antibody concentration was quantified using ELISA.

Enzyme-linked immunosorbent assay (ELISA)

ELISA was used to detect mAbs in transcytosis assays and for serum half-life experiments. 96-well flat-bottom immunosorbent plates were coated overnight at 4°C with 5 µg/ml of sheep α-hIgG γ-chain antibody (The Binding Site, UK). Wells were blocked with 5% NFDM (w/v) in PBS with 0.1% (v/v) Tween 20 for 1 hour at 37°C.

Serum samples were applied at 1:50 (Bleed 1) and 1:15 (all remaining bleeds) dilution in duplicate. Basolateral supernatants from transcytosis assays were applied without dilution. A threefold serial dilution row in blocking buffer was performed. Plates were incubated overnight at 4°C. Peroxidase-conjugated anti-IgG κ or IgG λ (Sigma Aldrich, USA) at 1 in 1000 in blocking buffer was applied and plates incubated for 1 h at 37°C. Plates were washed with wash buffer (water with 0.01% Tween 20) after each incubation step. Bound antibodies were detected using TMB substrate solution (Invitrogen, USA). The colour reaction was stopped using 2M sulphuric acid and absorbance was measured at 450nm using a Sunrise plate reader (Tecan). Antibody concentrations were determined using titration curves of known human IgG κ or IgG λ as standards.

Antibody-dependent cellular cytotoxicity (ADCC) activation assay

To determine the ability of the bNAbs to activate ADCC, ADCC Bioreporter Assay, V Variant (Promega, USA) was used. bNAbs were diluted to an appropriate starting concentration and 3-fold dilution series performed in sterile white flat bottom 96 well plates. An equal volume of HIV-1 UG37 gp140 was added to each well and plates incubated for 1 hour at 37 (5% CO_2). ADCC effector cells (Jurkat T cells constitutively expressing surface FcγRIIIa-V158) were added to each well. Plates were incubated for 6 hours at 37°C, 5% CO_2, then, left at room temperature for 20 minutes before adding Bio-Glo Luciferase Substrate (Promega, USA). After 5 minutes, luminescence was measured using a GloMax. ADCC pathway activation was calculated as fold induction [Fold of induction= RLU (sample-substrate)/RLU(cells only-substrate)].

In vivo pharmacokinetic studies in human neonatal Fc receptor (hFcRn) transgenic mice

C57BL/6 mice with the mouse neonatal Fc receptor (FcRn) knocked out and transgenic for human FcRn [mFcRn KO hFcRn (276) $^{Tg/Tg}$; stock number 004919, The Jackson Laboratories, USA], were housed and bred in the Biological Research Facilities (BRF) at St. George's University of London (SGUL) under Home Office Regulations. All animal experiments were reviewed and approved by the Animal Welfare and Ethical Review Body (AWERB) of SGUL.

7- to 9-week-old male and female mice were randomised based on age and weight. Animal number per group (3-5) was chosen in accordance with previously published papers (Petkova et al., 2006; Zalevsky et al., 2010). Mice were weighed two days prior to injection. bNAbs were injected intravenously *via* the tail vein at 2mg/kg (~30-60 μg/mouse). PBS was injected as negative control. 50 μL blood samples were taken from the tail or saphenous vein after 24, 96, 144, 192 hours post-infusion. Mice were sacrificed after 192 or 264 h and a final blood sample *via* cardiac puncture was taken.

Blood samples were allowed to clot for 1 hour at 37°C followed by 4°C overnight, before centrifugation at 13,000rpm for 10 minutes and collection of serum. Serum was kept at -20°C. Analysis of bNAb present in serum was performed *via* an α-hIgG ELISA. The percentage of antibodies remaining in the serum was calculated against that from day 1 (set as 100%). The AUC was calculated using GraphPad Prism.

Statistics

All graphs were drawn and analysed using the GraphPad prism 8 software (GraphPad, USA). A One-way or two-way ANOVA with Tukey's multiple comparison test was carried out for statistical analysis as indicated in the text and/or figure legends.

Data availability statement

The raw data supporting the conclusions of this article will be made available by the authors, without undue reservation.

Ethics statement

The animal study was reviewed and approved by St George's Animal Welfare and Ethical Review Body (AWERB) and conducted at Biological Research Facility, under the project licence P1A7411AD.

Author contributions

Conceptualisation and design of study: AY-HT and JK-CM. Experimental investigation: MG, CG-G, and AY-HT. Data analysis: MG, SG, JS, JK-CM, and AY-HT. Writing (original draft): MG. Animal licence: RR. Funding acquisition: JK-CM. All authors contributed to the article and approved the submitted version.

Funding

The study was supported by Sir Joseph Hotung Charitable Settlement and Future-Pharma Advanced Grant Award (European Research Council).

Acknowledgments

We would like to thank the generous financial support of the Sir Joseph Hotung Charitable Settlement, the European Research Council through its Future-Pharma Advanced Grant Award and the Biotechnology and Biological Sciences Research Council (BBSRC) 21EBTA funding for the Celfacto project. We thank the Biological Research Facility (BRF) at St. George's University of London for help in performing the animal experiments. Special thanks to Mrs. Thais Guerra for the horticulture help, to Professor Herta Steinkellner from The University of Natural Resources and Life Sciences, Vienna for kindly providing the ΔXF *N. benthamiana* plant line, and to Professor Richard Blumberg of Harvard Medical School for MDCK.2 cells expressing hFcRn/β2m. Mammalian cells-produced 10-1074 (ARP12477), 3BNC117 (ARP12474) and VRC01 (ARP3291), UG37 gp140 (ARP0698) and plasmids for HIV-1 pseudovirus were obtained from the AIDS Reagent Programme through the Centre for AIDS Reagents, NIBSC, UK, supported by EURIPRED (EC FP7 Grant number 31266).

Conflict of interest

The authors declare that the research was conducted in the absence of any commercial or financial relationships that could be construed as a potential conflict of interest.

Publisher's note

Supplementary material

The Supplementary Material for this article can be found online at: https://www.frontiersin.org/articles/10.3389/fpls.2023.1126470/full#supplementary-material

SUPPLEMENTARY TABLE 1
Primers used in site-directed mutagenesis to introduce M252Y/S254T/T256E (YTE) or M428L/N434S (LS) mutation in heavy (γ) chain Fc regions of VRC01 or 3BNC117/10-1074. Nucleotides in bold indicate changes in the sequence. A different primer pair was chosen for VRC01 as a plasmid was already available and the nucleotide sequence of the Fc region -while maintaining the same amino acid composition- differed slightly to the one used for 3BNC117 and 10-1074.

SUPPLEMENTARY TABLE 2
Equilibrium dissociation constant (K_D), association constant (K_a) and dissociation constant (K_d) of VRC01 and 3BNC117 with unmodified (HC) or modified Fc regions (YTE or LS) to HIV-1 UG37 gp140. Values were from one biological repeat. VRC01 or 3BNC117 produced in HEK cells were used as positive control.

SUPPLEMENTARY TABLE 3
IC_{50}s of HC ΔXF, YTE ΔXF and LS ΔXF versions of VRC01 or 3BCN117 against 5 HIV-1 pseudovirus strains from different clades. Mean ± SD for BaL.26 (n=3 biological repeats) are shown. VRC01 or 3BNC117 produced in HEK cells were used as positive control.

SUPPLEMENTARY TABLE 4
Equilibrium dissociation constant (K_D), association constant (K_a) and dissociation constant (K_d) of 10-1074 Fc variants, as well as CHO-produced 10-1074 to HIV-1 UG37 gp140. Values for plant-made 10-1074 were the averages ± SD of 3 biological repeats, while values for 10-1074 CHO were from one measurement.

SUPPLEMENTARY TABLE 5
Mean ± SD of area under the curve (AUC) (%*h) calculated for 10-1074 HC ΔXF, YTE ΔXF and CHO (n= number per group).

SUPPLEMENTARY TABLE 6
Summary table of results for all variants of the 3 bNAbs 10-1074, VRC01 and 3BNC117. Highest average achieved yield is shown (with addition of 0.01% polysorbate 80 for 10-1074 HC and YTE ΔXF). For transcytosis fold change (compared the matching HC ΔXF) is only shown for the highest input (10 µg) of the respective bNAb.

SUPPLEMENTARY FIGURE 1
(A) Post-purification yields (expressed as mg/kg leaf fresh weight) of the unmodified **(HC)**, M252Y/S254T/T256E **(YTE)** or M428L/N434S **(LS)** variant of anti-HIV-1 bNAb VRC01 and 3BNC117. All bNAbs were expressed in glycomodified *Nicotinana benthamiana* plants lacking core β1,2-xylose and α1,3-fucose (ΔXF). Values are the average ± SD of 3 biological repeats. **(B)** Representative SDS-PAGE **(B)** of non-reduced **(NR)** and reduced **(R)** purified VRC01 HC, YTE or LS expressed in ΔXF *N. benthamiana* plants. Arrows indicate fully assembled bNAb (black), heavy chain (white) or light chain (grey). VRC01 from HEK cells was used as positive control. **(C and D)** Representative Western blot of non-reduced **(NR; C)** or SDS-PAGE of reduced **(R; D)** purified 3BNC117 HC, YTE or LS expressed in ΔXF *N. benthamiana* plants. Arrows indicate fully assembled bNAb (black), heavy chain (white) or light chain (grey). 3BCN117 from HEK cells was used as positive control for Western blot.

SUPPLEMENTARY FIGURE 2
Representative SDS-PAGE showing deglycosylation of ΔXF VRC01 **(A)** and 3BNC117 **(B)** Fc variants after PNGase treatment. NP indicate untreated and P indicated PNGase F treated samples. Arrows indicated enzymatically aglycosylated heavy chain (black), PNGase F (grey) and light chain (white).

SUPPLEMENTARY FIGURE 3
(A) Equilibrium dissociation constants (K_Ds) of ΔXF *N. benthamiana*-produced HC, YTE, LS Fc variants and mammalian cell-produced HEK HC variant of anti-HIV bNAbs VRC01 and 3BNC117 to FcγRIIIa. B and C) FcγRIIIa activation by ΔXF HC, ΔXF YTE, ΔXF LS variants, as well as wild type *N. benthamiana* **(WT)**-made HC and HEK HC variants of VRC01 **(B)** and 3BCN117 **(C)** in the presence of HIV-1 UG37 gp140. Activation was measured by fold-induction of luciferase expression controlled by NFAT pathway. Values represent average fold-induction ± SD of 2 biological repeats. A two-way ANOVA with Tukey's multiple comparison test was performed to determine significant differences.

SUPPLEMENTARY FIGURE 4
(A) Equilibrium dissociation constants (K_Ds) of ΔXF *N. benthamiana*-produced HC, YTE, LS Fc variants and mammalian cell-produced HC HEK variant of VRC01 and 3BNC117 to human neonatal Fc receptor (hFcRn). **(B and C)** Transcytosis of ΔXF *N. benthamiana*-made HC, YTE, LS, as well as HC HEK variants of VRC01 **(B)** and 3BCN117 **(C)** across MDCK.2 cell layer constitutively expressing hFcRn/$h\beta_2$m. $h\beta_2$m-expressing MDCK.2 cell layers were used as negative controls. pH of input wells and output wells were pH6 and 7.4 respectively. Values represent average ± SD of 2 biological repeats.

SUPPLEMENTARY FIGURE 5
(A) Serum concentration of VRC01 ΔXF HC, ΔXF YTE, ΔXF LS and HEK HC in hFcRn transgenic mice measured using ELISA. Each line represents a separate animal. Mean ± SD of area under the curve (AUC) (%*h) calculated for VRC01 ΔXF HC, ΔXF YTE, ΔXF LS and HEK HC (n= number per group) are shown. **(B)** Serum concentration of 3BNC117 ΔXF HC, ΔXF YTE, ΔXF LS and HEK HC in hFcRn transgenic mice using ELISA. Each value represents average ± SD of 3-4 animals.

SUPPLEMENTARY FIGURE 6
Individual values, mean ± SD of relative standardised serum anti-hIgG murine IgM levels for all experiments. IgM level differences were not statistically significant ($p \geq 0.05$) between 10-1074 variants.

SUPPLEMENTARY FIGURE 7
Log10 serum concentration (%) of 10-1074 HC ΔXF, YTE ΔXF and CHO in hFcRn transgenic mice across four separate experiments highlighting the linear elimination pattern of 10-1074 HC ΔXF and 10-1074 CHO and mixed-mode of 10-1074 YTE ΔXF. Data points for zero percent values cannot be transformed into log10 and are consequently missing in the graph.

References

Avery, L. B., Wang, M., Kavosi, M. S., Joyce, A., Kurz, J. C., Fan, Y. Y., et al. (2016). Utility of a human FcRn transgenic mouse model in drug discovery for early assessment and prediction of human pharmacokinetics of monoclonal antibodies. *MAbs* 8 (6), 1064–78. doi: 10.1080/19420862.2016.1193660

Banks, N. D., Kinsey, N., Clements, J., and Hildreth, J. E. (2002). Sustained antibody-dependent cell-mediated cytotoxicity (ADCC) in SIV-infected macaques correlates with delayed progression to AIDS. *AIDS Res Hum Retroviruses* 18 (16), 1197–1205. doi: 10.1089/08892220260387940

Baum, L. L., Cassutt, K. J., Knigge, K., Khattri, R., Margolick, J., Rinaldo, C., et al. (1996). HIV-1 gp120-specific antibody-dependent cell-mediated cytotoxicity correlates with rate of disease progression. *J. Immunol.* 157 (5), 2168–2173.

Bournazos, S., Klein, F., Pietzsch, J., Seaman, M. S., Nussenzweig, M. C., and Ravetch, J. V. (2014). Broadly neutralizing anti-HIV-1 antibodies require fc effector functions for *In vivo* activity. *Cell* 158 (6), 1243–1253. doi: 10.1016/j.cell.2014.08.023

Caskey, M., Klein, F., Lorenzi, J. C., Seaman, M. S., West, A. P. Jr, Buckley, N., et al. (2015). Viraemia suppressed in HIV-1-infected humans by broadly neutralizing antibody 3BNC117. *Nature* 522 (7557), 487–491. doi: 10.1038/nature14411

Caskey, M., Schoofs, T., Gruell, H., Settler, A., Karagounis, T., Kreider, E. F., et al. (2017). Antibody 10-1074 suppresses viremia in HIV-1-infected individuals. *Nat. Med.* 23 (2), 185–191. doi: 10.1038/nm.4268

Caskey, M., Klein, F., and Nussenzweig, M. C. (2016). Broadly neutralizing antibodies for HIV-1 prevention or immunotherapy. *N. Engl. J. Med.* 375 (21), 2019–2021. doi: 10.1056/NEJMp1613362

Claypool, S. M., Dickinson, B. L., Yoshida, M., Lencer, W. I., and Blumberg, R. S.. (2002). Functional reconstitution of human FcRn in madin-Darby canine kidney cells requires co-expressed human β2-microglobulin. *J. Biol. Chem.* 277 (31), 28038–28050. doi: 10.1074/jbc.M202367200

Conner, C. M., van Fossan, D., Read, K., Cowley, D. O., Alvarez, O., Xu, S., et al. (2022). A humanized fcrn transgenic mouse for preclinical pharmacokinetics studies. *BioRxiv*, 2022.10.24.513622. doi: 10.1101/2022.10.24.513622

Cooper, L. J., Robertson, D., Granzow, R., and Greenspan, N. S. (1994). Variable domain-identical antibodies exhibit IgG subclass-related differences in affinity and kinetic constants as determined by surface plasmon resonance. *Mol. Immunol. Engl.* 31 (8), 577–584. doi: 10.1016/0161-5890(94)90165-1

Dall'Acqua, W. F., Woods, R. M., Ward, E. S., Palaszynski, S. R., Patel, N. K., Brewah, Y. A., et al. (2002). Increasing the affinity of a human IgG1 for the neonatal fc receptor: biological consequences. *J. Immunol.* 169 (9), 5171–5180. doi: 10.4049/jimmunol.169.9.5171. United States.

Dall'Acqua, W. F., Kiener, P. A., and Wu, H. (2006). Properties of human IgG1s engineered for enhanced binding to the neonatal fc receptor (FcRn). *J. Biol. Chem.* 281 (33), 23514–23524. doi: 10.1074/jbc.M604292200

Desikan, R., Raja, R., and Dixit, N. M. (2019). Early exposure to broadly neutralizing antibodies triggers a switch from progressive disease to lasting control of SHIV infection. *bioRxiv* p, 548727. doi: 10.1101/548727

Doria-Rose, N. A., Klein, R. M., Manion, M. M., O'Dell, S., Phogat, A., Chakrabarti, B., et al. (2009). Frequency and phenotype of human immunodeficiency virus envelope-specific b cells from patients with broadly cross-neutralizing antibodies. *J. Virol.* 83 (1), 188–199. doi: 10.1128/jvi.01583-08

Dua, P., Hawkins, E., and van der Graaf, P. H. (2015). A tutorial on target-mediated drug disposition (TMDD) models. *CPT: Pharmacometrics Syst. Pharmacol.* 4 (6), 324–337. doi: 10.1002/psp4.41

Edgeworth, M. J., Phillips, J. J., Lowe, D. C., Kippen, A. D., Higazi, D. R., and Scrivens, J. H. (2015). Global and local conformation of human IgG antibody variants rationalizes loss of thermodynamic stability. *Angew Chem Int Ed Engl* 54 (50), 15156–15159. doi: 10.1002/anie.201507223

Ferrara, C., Grau, S., Jäger, C., Sondermann, P., Brünker, P., Waldhauer, I., et al. (2011). Unique carbohydrate-carbohydrate interactions are required for high affinity binding between FcγRIII and antibodies lacking core fucose. *Proc Natl Acad Sci USA*. 108 (31), 12669–12674. doi: 10.1073/pnas.1108455108

Gaudinski, M. R., Coates, E. E., Houser, K. V., Chen, G. L., Yamshchikov, G., Saunders, J. G., et al. (2018). Safety and pharmacokinetics of the fc-modified HIV-1 human monoclonal antibody VRC01LS: A phase 1 open-label clinical trial in healthy adults. *PloS Med.* 15 (1), e1002493. doi: 10.1371/journal.pmed.1002493

Gautam, R., Nishimura, Y., Pegu, A., Nason, M. C., Klein, F., Gazumyan, A., et al. (2016). A single injection of anti-HIV-1 antibodies protects against repeated SHIV challenges. *Nature* 533 (7601), 105–109. doi: 10.1038/nature17677

Gautam, R., Nishimura, Y., Gaughan, N., Gazumyan, A., Schoofs, T., Buckler-White, A., et al. (2018). A single injection of crystallizable fragment domain-modified antibodies elicits durable protection from SHIV infection. *Nat Med.* 24 (5), 610–616. doi: 10.1038/s41591-018-0001-2

Gómez-Román, V. R., Patterson, L. J., Venzon, D., Liewehr, D., Aldrich, K., Florese, R., et al. (2005). Vaccine-elicited antibodies mediate antibody-dependent cellular cytotoxicity correlated with significantly reduced acute viremia in rhesus macaques challenged with SIV mac251. *J. Immunol.* 174 (4), 2185–2189. doi: 10.4049/jimmunol.174.4.2185

Grilo, A. L., and Mantalaris, A. (2019). The increasingly human and profitable monoclonal antibody market. *Trends Biotechnol. Elsevier Ltd* 37 (1), 9–16. doi: 10.1016/j.tibtech.2018.05.014

Hernandez, I., Bott, S. W., Patel, A. S., Wolf, C. G., Hospodar, A. R., Sampathkumar, S., et al. (2018). Pricing of monoclonal antibody therapies: higher if used for cancer? *Am J Manag Care*. 24(2), 109–112.

Hessell, A. J., Hangartner, L., Hunter, M., Havenith, C. E., Beurskens, F. J., Bakker, J. M., et al. (2007). Fc receptor but not complement binding is important in antibody protection against HIV. *Nature* 449 (7158), 101–104. doi: 10.1038/nature06106

Hessell, A. J., Poignard, P., Hunter, M., Hangartner, L., Tehrani, D. M., Bleeker, W. K., et al. (2009). Effective, low-titer antibody protection against low-dose repeated mucosal SHIV challenge in macaques. *Nat. Med. Nat. Publishing Group* 15 (8), 951–954. doi: 10.1038/nm.1974

Igawa, T., Tsunoda, H., Tachibana, T., Maeda, A., Mimoto, F., Moriyama, C., et al. (2010). Reduced elimination of IgG antibodies by engineering the variable region. *Protein Engineering Design Selection* 23 (5), 385–392. doi: 10.1093/protein/gzq009

Jaramillo, C. A. C., Belli, S., Cascais, A. C., Dudal, S., Edelmann, M. R., Haak, M., et al. (2017). Toward in vitro-to-in vivo translation of monoclonal antibody pharmacokinetics: Application of a neonatal Fc receptor-mediated transcytosis assay to understand the interplaying clearance mechanisms. *MAbs* 9 (5), 781–791. doi: 10.1080/19420862.2017.1320008

Jensen, P. F., Schoch, A., Larraillet, V., Hilger, M., Schlothauer, T., Emrich, T., et al. (2017). A two-pronged binding mechanism of IgG to the neonatal fc receptor controls complex stability and IgG serum half-life. *Mol. Cell. Proteomics* 16 (3), 451–456. doi: 10.1074/mcp.M116.064675

Kang, C., Xia, L., Chen, Y., Zhang, T., Wang, Y., Zhou, B., et al. (2018). A novel therapeutic anti-HBV antibody with increased binding to human FcRn improves *in vivo* PK in mice and monkeys. *Protein Cell* 9 (1), 130–134. doi: 10.1007/s13238-017-0438-y

Kapila, J., Rycke, R. D., Montagu, M. V., and Angenon, G.. (1997). An agrobacterium-mediated transient gene expression system for intact leaves. *Plant Sci.* 122 (1), 101–108. doi: 10.1016/S0168-9452(96)04541-4

Ko, SY, Pegu, A, Rudicell, RS, Yang, ZY, Joyce, MG, Chen, X, et al. (2014). Enhanced neonatal Fc receptor function improves protection against primate SHIV infection. *Nature* 514 (7524), 642–5. doi: 10.1038/nature13612

Lambotte, O., Pollara, J., Boufassa, F., Moog, C., Venet, A., Haynes, B. F., et al. (2013). High antibody-dependent cellular cytotoxicity responses are correlated with strong CD8 T cell viral suppressive activity but not with B57 status in HIV-1 elite controllers. *PloS One* 8 (9), e74855. doi: 10.1371/journal.pone.0074855

Ledgerwood, J. E., Coates, E. E., Yamshchikov, G., Saunders, J. G., Holman, L., Enama, M. E., et al. (2015). Safety, pharmacokinetics and neutralization of the broadly neutralizing HIV-1 human monoclonal antibody VRC01 in healthy adults. *Clin. Exp. Immunol.* 182 (3), 289–301. doi: 10.1111/cei.12692

Luo, C., Chen, S., Xu, N., Wang, C., Sai, W. B., Zhao, W., et al. (2017). Glycoengineering of pertuzumab and its impact on the pharmacokinetic/pharmacodynamic properties. *Sci. Rep.* 7, 46347. doi: 10.1038/srep46347

Madhavi, V., Wines, B. D., Amin, J., Emery, S.ENCORE1 Study Group, , Lopez, E., et al. (2017). HIV-1 env- and vpu-specific antibody-dependent cellular cytotoxicity responses associated with elite control of HIV. *J. virology United States* 91 (18):e00700-17. doi: 10.1128/JVI.00700-17

Ma, JK, Drossard, J, Lewis, D, Altmann, F, Boyle, J, Christou, P, et al. (2015). Regulatory approval and a first-in-human phase I clinical trial of a monoclonal antibody produced in transgenic tobacco plants. *Plant Biotechnol. J.* 13 (8), 1106–1120. doi: 10.1111/pbi.12416

Marusic, C., Pioli, C., Stelter, S., Novelli, F., Lonoce, C., Morrocchi, E., et al. (2018). N-glycan engineering of a plant-produced anti-CD20-hIL-2 immunocytokine significantly enhances its effector functions. *Biotechnol Bioeng* 115 (3), 565–576. doi: 10.1002/bit.26503

Mills, E. J., Bakanda, C., Birungi, J., Chan, K., Ford, N., Cooper, C. L., et al. (2011). Life expectancy of persons receiving combination antiretroviral therapy in low-income countries: A cohort analysis from Uganda. *Ann. Internal Med.* 155 (4), 209–217. doi: 10.7326/0003-4819-155-4-201108160-00358

Montefiori, D. C. (2004). Evaluating neutralizing antibodies against HIV, SIV, and SHIV in luciferase reporter gene assays. *Curr Protoc Immunol* Chapter 12:12.11.1-12.11.17. doi: 10.1002/0471142735.im1211s64

Mouquet, H., Scharf, L., Euler, Z., Liu, Y., Eden, C., Scheid, J. F., et al. (2012). Complex-type n-glycan recognition by potent broadly neutralizing HIV antibodies. *Proc Natl Acad Sci U S A*. 109 (47), E3268–E3277. doi: 10.1073/pnas.1217207109

Murad, S., Fuller, S., Menary, J., Moore, C., Pinneh, E., Szeto, T., et al. (2020). Molecular pharming for low and middle income countries'. *Curr. Opin. Biotechnol.* Elsevier Ltd, 61 (November 2019), 53–59. doi: 10.1016/j.copbio.2019.10.005

Nandi, S., Kwong, A. T., Holtz, B. R., Erwin, R. L., Marcel, S., and McDonald, K. A. (2016). Techno-economic analysis of a transient plant-based platform for monoclonal antibody production. *MAbs* 8 (8), 1456–1466. doi: 10.1080/19420862.2016.1227901

Nishimura, Y., Gautam, R., Chun, T. W., Sadjadpour, R., Foulds, K. E., Shingai, M., et al. (2017). Early antibody therapy can induce long-lasting immunity to SHIV. *Nature* 543 (7646), 559–563. doi: 10.1038/nature21435

Okazaki, A., Shoji-Hosaka, E., Nakamura, K., Wakitani, M., Uchida, K., Kakita, S., et al. (2004). Fucose depletion from human IgG1 oligosaccharide enhances binding enthalpy and association rate between IgG1 and FcγRIIIa. *J. Mol. Biol.* 336 (5), 1239–1249. doi: 10.1016/j.jmb.2004.01.007

Pegu, A., Yang, Z. Y., Boyington, J. C., Wu, L., Ko, S. Y., Schmidt, S. D., et al. (2014). Neutralizing antibodies to HIV-1 envelope protect more effectively *in vivo* than those to the CD4 receptor. *Sci. Trans. Med.* 6 (243), 243ra88–243ra88. doi: 10.1126/scitranslmed.3008992

Pereira, N. A., Chan, K. F., Lin, P. C., and Song, Z.. (2018). The "less-is-more" in therapeutic antibodies: Afucosylated anti-cancer antibodies with enhanced antibody-dependent cellular cytotoxicity. *MAbs* 10 (5), 693–711.doi: 10.1080/19420862.2018.1466767

Petkova, S. B., Akilesh, S., Sproule, T. J., Christianson, G. J., Al Khabbaz, H., Brown, A. C., et al. (2006). Enhanced half-life of genetically engineered human IgG1 antibodies in a humanized FcRn mouse model: potential application in humorally mediated autoimmune disease. *Int. Immunol.* 18 (12), 1759–1769. doi: 10.1093/intimm/dxl110

Pinneh, E. C., van Dolleweerd, C. J., Göritzer, K., Drake, P. M. W., Ma, J. K., and Teh, A. Y. (2021). Multiple gene expression in plants using MIDAS-p, a versatile type II restriction-based modular expression vector. *Biotechnol. Bioengineering*. 119(6), 1660–1672. doi: 10.1002/bit.28073

Pogue, G. P., Vojdani, F., Palmer, K. E., Hiatt, E., Hume, S., Phelps, J., et al. (2010). Production of pharmaceutical-grade recombinant aprotinin and a monoclonal antibody product using plant-based transient expression systems. *Plant Biotechnol. J.* 8 (5), 638–654. doi: 10.1111/j.1467-7652.2009.00495.x

Rosenberg, Y., Sack, M., Montefiori, D., Forthal, D., Mao, L., Hernandez-Abanto, S., et al. (2013). Rapid high-level production of functional HIV broadly neutralizing monoclonal antibodies in transient plant expression systems. *PloS One* 8 (3):e58724. doi: 10.1371/journal.pone.0058724

Rosenberg, Y., Sack, M., Montefiori, D., Labranche, C., Lewis, M., Urban, L., et al. (2015). Pharmacokinetics and immunogenicity of broadly neutralizing HIV monoclonal antibodies in macaques. *PloS One* 10 (3), e0120451. doi: 10.1371/journal.pone.0120451

Rosenberg, Y. J., Lewis, G. K., Montefiori, D. C., LaBranche, C. C., Lewis, M. G., Urban, L. A., et al. (2019). Introduction of the YTE mutation into the non-immunogenic HIV bnAb PGT121 induces anti-drug antibodies in macaques. *PloS One* 14 (2), e0212649. doi: 10.1371/journal.pone.0212649

Sarzotti-Kelsoe, M., Bailer, R. T., Turk, E., Lin, C. L., Bilska, M., Greene, K. M., et al. (2014). Optimization and validation of the TZM-bl assay for standardized assessments of neutralizing antibodies against HIV-1. *J. Immunol. Methods* 409, 131–146. doi: 10.1016/j.jim.2013.11.022

Scheid, J. F., Mouquet, H., Ueberheide, B., Diskin, R., Klein, F., Oliveira, T. Y., et al. (2011). Sequence and structural convergence of broad and potent HIV antibodies that mimic CD4 binding. *Sci. (New York N.Y.)* 333 (6049), 1633–1637. doi: 10.1126/science.1207227

Schoch, A., Kettenberger, H., Mundigl, O., Winter, G., Engert, J., Heinrich, J., et al. (2015). Charge-mediated influence of the antibody variable domain on FcRn-dependent pharmacokinetics. *Proc. Natl. Acad. Sci.* 112 (19), 5997–6002. doi: 10.1073/pnas.1408766112

Shields, R. L., Lai, J., Keck, R., O'Connell, L. Y., Hong, K., Meng, Y. G., et al. (2002). Lack of fucose on human IgG1 n-linked oligosaccharide improves binding to human FcγRIII and antibody-dependent cellular toxicity. *J. Biol. Chem.* 277 (30), 26733–26740. doi: 10.1074/jbc.M202069200

Simister, N. E. (2003). Placental transport of immunoglobulin G. *Vaccine Netherlands* 21 (24), 3365–3369. doi: 10.1016/s0264-410x(03)00334-7

Stelter, S., Paul, M. J., Teh, A. Y., Grandits, M., Altmann, F., Vanier, J., et al. (2020). Engineering the interactions between a plant-produced HIV antibody and human fc receptors. *Plant Biotechnol. J.* 18 (2), 402–414. doi: 10.1111/pbi.13207

Strasser, R., Stadlmann, J., Schähs, M., Stiegler, G., Quendler, H., Mach, L., et al. (2008). Generation of glyco-engineered nicotiana benthamiana for the production of monoclonal antibodies with a homogeneous human-like n-glycan structure. *Plant Biotechnol. J.* 6 (4), 392–402. doi: 10.1111/j.1467-7652.2008.00330.x

Tam, S. H., McCarthy, S. G., Brosnan, K., Goldberg, K. M., and Scallon, B. J. (2013). Correlations between pharmacokinetics of IgG antibodies in primates vs. FcRn-transgenic mice reveal a rodent model with predictive capabilities. *mAbs* 5 (3), 397–405. doi: 10.4161/mabs.23836

Teh, A. Y., Maresch, D., Klein, K., and Ma, J. K. (2014). Characterization of VRC01, a potent and broadly neutralizing anti-HIV mAb, produced in transiently and stably transformed tobacco. *Plant Biotechnol. J.* 12 (3), 300–311. doi: 10.1111/pbi.12137

Tudor, D., Yu, H., Maupetit, J., Drillet, A. S., Bouceba, T., Schwartz-Cornil, I., et al. (2012). Isotype modulates epitope specificity, affinity, and antiviral activities of anti-HIV-1 human broadly neutralizing 2F5 antibody. *Proc Natl Acad Sci U S A*. 109 (31), 12680–12685. doi: 10.1073/pnas.1200024109

UNAIDS (2019). 2018 global hiv statistics'. *Unaids*, 1–6.

UNAIDS (2021). Global HIV statistics. *Fact Sheet*, 1–3.

Valente, D., Mauriac, C., Schmidt, T., Focken, I., Beninga, J., Mackness, B., et al. (2020). Pharmacokinetics of novel fc-engineered monoclonal and multispecific antibodies in cynomolgus monkeys and humanized FcRn transgenic mouse models. *MAbs* 12 (1), 1829337. doi: 10.1080/19420862.2020.1829337

Vidarsson, G., Dekkers, G., and Rispens, T. (2014). IgG subclasses and allotypes: From structure to effector functions. *Front. Immunol.* 5, 520. doi: 10.3389/fimmu.2014.00520

Ward, B. J., Séguin, A., Couillard, J., Trépanier, S., and Landry, N. (2021). Phase III: Randomized observer-blind trial to evaluate lot-to-lot consistency of a new plant-derived quadrivalent virus like particle influenza vaccine in adults 18-49 years of age. *Vaccine Netherlands* 39 (10), 1528–1533. doi: 10.1016/j.vaccine.2021.01.004

Wei, X., Decker, J. M., Wang, S., Hui, H., Kappes, J. C., Wu, X., et al. (2003). Antibody neutralization and escape by HIV-1. *Nature Engl.* 422 (6929), 307–312. doi: 10.1038/nature01470

World Health Organization (2019)HIV drug resistance report. Available at: http://scholar.google.com/scholar?hl=en&btnG=Search&q=intitle:Who+hiv+drug+resistance+report+2012#5.

Wu, X., Yang, Z. Y., Li, Y., Hogerkorp, C. M., Schief, W. R., Seaman, M. S., et al. (2010). Rational design of envelope identifies broadly neutralizing human monoclonal antibodies to HIV-1. *Science* 329 (5993), 856–861. doi: 10.1126/science.1187659.Rational

Yogo, R., Yamaguchi, Y., Watanabe, H., Yagi, H., Satoh, T., Nakanishi, M., et al. (2019). The Fab portion of immunoglobulin G contributes to its binding to Fcγ receptor III. *Sci Rep.* 9 (1), 11957. doi: 10.1038/s41598-019-48323-w

Zalevsky, J., Chamberlain, A. K., Horton, H. M., Karki, S., Leung, I. W., Sproule, T. J., et al. (2010). Enhanced antibody half-life improves *in vivo* activity. *Nat Biotechnol.* 28 (2), 157–9. doi: 10.1038/nbt.1601

Zeitlin, L., Pettitt, J., Scully, C., Bohorova, N., Kim, D., Pauly, M., et al. (2011). Enhanced potency of a fucose-free monoclonal antibody being developed as an Ebola virus immunoprotectant. *Proc Natl Acad Sci U S A*. 108 (51), 20690–20694. doi: 10.1073/pnas.1108360108

frontiers | Frontiers in Plant Science

TYPE Original Research
PUBLISHED 07 March 2023
DOI 10.3389/fpls.2023.1146234

OPEN ACCESS

EDITED BY
Qiang Chen,
Arizona State University, United States

REVIEWED BY
Michele Bellucci,
National Research Council (CNR), Italy
Hugh S. Mason,
Arizona State University, United States

*CORRESPONDENCE
Ros Chapman
ros.chapman@uct.ac.za
Emmanuel Margolin
emmanuel.margolin@gmail.com

SPECIALTY SECTION
This article was submitted to Plant Biotechnology, a section of the journal Frontiers in Plant Science

RECEIVED 17 January 2023
ACCEPTED 17 February 2023
PUBLISHED 07 March 2023

CITATION
Margolin E, Schäfer G, Allen JD, Gers S, Woodward J, Sutherland AD, Blumenthal M, Meyers A, Shaw ML, Preiser W, Strasser R, Crispin M, Williamson A-L, Rybicki EP and Chapman R (2023) A plant-produced SARS-CoV-2 spike protein elicits heterologous immunity in hamsters. *Front. Plant Sci.* 14:1146234. doi: 10.3389/fpls.2023.1146234

A plant-produced SARS-CoV-2 spike protein elicits heterologous immunity in hamsters

Emmanuel Margolin[1,2,3,4]*, Georgia Schäfer[2,3,5], Joel D. Allen[6], Sophette Gers[7], Jeremy Woodward[8], Andrew D. Sutherland[9], Melissa Blumenthal[3,5], Ann Meyers[4], Megan L. Shaw[10], Wolfgang Preiser[9], Richard Strasser[11], Max Crispin[6], Anna-Lise Williamson[1,3], Edward P. Rybicki[3,4] and Ros Chapman[1,3]*

[1]Division of Medical Virology, Department of Pathology, Faculty of Health Sciences, University of Cape Town, Cape Town, South Africa, [2]Wellcome Trust Centre for Infectious Disease Research in Africa, University of Cape Town, Cape Town, South Africa, [3]Institute of Infectious Disease and Molecular Medicine, Faculty of Health Sciences, University of Cape Town, Cape Town, South Africa, [4]Biopharming Research Unit, Department of Molecular and Cell Biology, University of Cape Town, Cape Town, South Africa, [5]International Centre for Genetic Engineering and Biotechnology, Observatory, Cape Town, Cape Town, South Africa, [6]School of Biological Sciences and Institute of Life Sciences, University of Southampton, Southampton, United Kingdom, [7]Pathcare VetLab, Cape Town, South Africa, [8]Electron Microscope Unit, University of Cape Town, Cape Town, South Africa, [9]Division of Medical Virology, Faculty of Medicine and Health Sciences, Stellenbosch University Tygerberg Campus, Cape Town, South Africa, [10]Department of Medical Biosciences, University of the Western Cape, Cape Town, South Africa, [11]Department of Applied Genetics and Cell Biology, University of Natural Resources and Life Sciences, Vienna, Austria

Molecular farming of vaccines has been heralded as a cheap, safe and scalable production platform. In reality, however, differences in the plant biosynthetic machinery, compared to mammalian cells, can complicate the production of viral glycoproteins. Remodelling the secretory pathway presents an opportunity to support key post-translational modifications, and to tailor aspects of glycosylation and glycosylation-directed folding. In this study, we applied an integrated host and glyco-engineering approach, NXS/T Generation™, to produce a SARS-CoV-2 prefusion spike trimer in *Nicotiana benthamiana* as a model antigen from an emerging virus. The size exclusion-purified protein exhibited a characteristic prefusion structure when viewed by transmission electron microscopy, and this was indistinguishable from the equivalent mammalian cell-produced antigen. The plant-produced protein was decorated with under-processed oligomannose N-glycans and exhibited a site occupancy that was comparable to the equivalent protein produced in mammalian cell culture. Complex-type glycans were almost entirely absent from the plant-derived material, which contrasted against the predominantly mature, complex glycans that were observed on the mammalian cell culture-derived protein. The plant-derived antigen elicited neutralizing antibodies against both the matched Wuhan and heterologous Delta SARS-CoV-2 variants in immunized hamsters, although titres were lower than those induced by the comparator mammalian antigen. Animals vaccinated with the plant-derived antigen exhibited reduced viral loads following challenge, as well as significant protection from SARS-CoV-2 disease as evidenced by reduced lung pathology, lower viral loads and

protection from weight loss. Nonetheless, animals immunized with the mammalian cell-culture-derived protein were better protected in this challenge model suggesting that more faithfully reproducing the native glycoprotein structure and associated glycosylation of the antigen may be desirable.

KEYWORDS

SARS-CoV-2, vaccine, glycoprotein, glycosylation, immunogenicity, challenge

1 Introduction

The increasing incidence of viral outbreaks highlights the need for pandemic preparedness and the importance of investing in infrastructure development for vaccine manufacturing (Krammer, 2020). This is particularly relevant in low-income countries, such as those in Africa, where the capacity for end-to-end vaccine manufacturing is limited and where vaccines are almost exclusively sourced from wealthier countries (Margolin et al., 2020a). Accordingly, there is a clear need to establish sustainable and self-sufficient manufacturing sites in these vulnerable regions. However, in most cases the costs remain prohibitive – especially where manufacturing processes are reliant on mammalian cell culture systems which are especially expensive.

Molecular farming, the production of proteins in plants, has risen to prominence in recent years following efficacy reports of plant-made vaccines against influenza (Ward et al., 2020) and SARS-CoV-2 (Hager et al., 2022), and the therapeutic treatment of Ebola virus infection with plant-produced antibodies (Group et al., 2016). The use of plants as pharmaceutical bioreactors offers several advantages that lend themselves towards implementation in developing countries, including most notably lower infrastructure requirements(Fischer and Buyel, 2020) and potentially lower production costs (Rybicki, 2009; Murad et al., 2020). Furthermore, large-scale transient protein production in plants can be completed within weeks without the need to generate stable cell lines, which is time consuming and comparatively slower (D'Aoust et al., 2010). This presents an obvious advantage for responding to pandemic outbreaks where speed and scale are critical. Lastly, protein-based drugs typically require a less stringent cold-chain than other vaccine modalities, such as mRNA, which is an important consideration for resource-limited countries (Pambudi et al., 2022).

Given these advantages it is unsurprising that several plant-made vaccines against SARS-CoV-2 are at various stages of clinical development. The most advanced candidate is Medicago Inc.'s virus-like particle (VLP) vaccine which was approved for use in Canada in February 2022, and which demonstrated 69.5% efficacy against symptomatic disease and 78.8% efficacy against moderate-to-severe disease (Hager et al., 2022). These VLPs are comprised of a chimaeric spike where the native transmembrane and cytoplasmic tail regions have been replaced with the equivalent domains from influenza H5 haemagglutinin (Ward et al., 2021). This modification improves the formation of VLPs presenting the spike, which bud from the host cell without the need for any additional accessory proteins (Ward et al., 2021). Other noteworthy plant-derived candidates in clinical testing include a recombinant SARS-CoV-2 receptor-binding domain (RBD) antigen from Baiya Phytopharm (Phase 1, NCT05197712) and a RBD protein conjugated to a tobacco mosaic virus scaffold (Royal et al., 2021) from Kentucky BioProcessing, Inc. (Phase 1/2, NCT04473690). Similar success has also been described in preclinical studies from academic groups who have reported expression and immunogenicity of RBD antigens (Maharjan et al., 2021; Mamedov et al., 2021; Mardanova et al., 2021; Shin et al., 2021; Siriwattananon et al., 2021a; Siriwattananon et al., 2021b) and a full-length spike ectodomain that was produced by co-expression of human calreticulin (Margolin et al., 2022b). More recently, A SARS-CoV-2 VLP composed exclusively of the native spike has also been described (Jung et al., 2022).

Historically the production of complex glycoproteins in their native conformations, and particularly envelope viral glycoproteins, has posed a considerable challenge for molecular farming (Margolin et al., 2018), as plant-derived glycosylation is distinct from that of mammalian cells (Strasser et al., 2014; Strasser, 2016), and the glycoproteins from enveloped viruses typically have extensive disulfide bonding and a consequent significant dependence on host chaperones (Alonzi et al., 2017). In many cases viral envelope glycoproteins only accumulate at low levels in plants (Kang et al., 2018) (Margolin et al., 2018), and the recombinant products may be poorly folded and aberrantly glycosylated (Strasser et al., 2014) (Margolin et al., 2021a; Margolin et al., 2022a). These observations can largely be attributed to inadequacies in the plant glycosylation-directed folding pathways, which do not always adequately support the high levels of glycosylation (Margolin et al., 2021a), chaperone-mediated folding and processing (Wilbers et al., 2016; Margolin et al., 2020c; Margolin et al., 2022b) that are required by many viral glycoproteins. Furthermore, plant-produced glycoproteins often display unique features in their glycosylation including lower glycan occupancy compared to mammalian hosts, elevated oligomannose-type N-glycans, plant-specific complex N-glycans and unwanted N-glycan processing events (Strasser, 2016; Shin et al., 2017; Castilho et al., 2018; Margolin et al., 2021a).

In order to address these challenges and exploit the advantages inherent in plant-based protein production, there has been an increasing drive to develop novel host engineering approaches to support the folding and glycosylation requirements of complex viral glycoproteins (Margolin et al., 2020b; Margolin et al., 2020d). Constraints in the host chaperone machinery can be addressed by over-expression of chaperones to support critical folding events (Margolin et al., 2020c; Margolin et al., 2021b; Rosenberg et al., 2022), and recent evidence suggests that a combinatorial approach may confer additional benefit (Rosenberg et al., 2022). This approach typically results in increased glycoprotein accumulation and reduced ER stress, as the toxicity associated with the accumulation of misfolded protein is alleviated. Impaired proteolytic maturation can similarly be addressed by transient host engineering, and the co-expression of the protease furin has been shown to support efficient maturation of prototype viral glycoproteins which would not otherwise be properly cleaved in plants (Margolin et al., 2020c; Margolin et al., 2022b). The plant glycosylation machinery also imposes a bottleneck for the production of many viral glycoproteins, and aberrant glycosylation has been implicated in protein misfolding and aggregation (Margolin et al., 2021a; Margolin et al., 2022a). Foreign glyco-epitopes have been associated with hypersensitive reactions and some plant glycoproteins are allergens (Altmann, 2007; Arnold and Misbah, 2008); however, plant-specific glycosylation has been shown to be safe in volunteers immunized with plant-derived VLPs (Ward et al., 2014; Ward et al., 2020; Ward et al., 2021). These can similarly be addressed by remodelling the cellular machinery for glycosylation in the plant host – by the *in situ* provision of heterologous machinery where the plant cell glycosylation machinery is limiting and by the elimination of plant enzymes which impart expression system-dependent modifications (Margolin et al., 2020b; Margolin et al., 2020d) (Shin et al., 2017).

We previously developed a combinatorial host engineering platform, NXS/T Generation™, to produce well-folded viral glycoproteins in *N. benthamiana* with improved glycosylation (Margolin et al., 2022a). The expression technology revolves around the transient expression of the lectin binding chaperones calnexin or calreticulin (Protein Origami™) to support protein folding (Margolin et al., 2020c), which is combined with a series of glyco-engineering strategies to remodel the plant glycosylation machinery. These involve the co-expression of a single subunit oligosaccharyltransferase from *Leishmania major* (LmSTT3D) to enhance glycan occupancy (Castilho et al., 2018), an RNA interference construct to ablate truncation of glycans by an endogenous β-N-acetylhexosaminidase (Shin et al., 2017), and the use of a mutant strain of *N. benthamiana* ΔXF where the activity of α1,3-fucosyltransferase and β1,2-xylosyltransferase have been suppressed to prevent the formation of plant-specific complex glycans (Strasser et al., 2008). The resulting antigens are referred to as "glycan-enhanced" (GE) as they represent a notable improvement over the glycosylation of the protein when produced in the absence of this integrated host and glyco-engineering approach. Specifically, the GE proteins comprise of increased glycan occupancy and negligible undesired plant-specific modifications, which are associated with a concomitant improvement in protein structure, folding and oligomerization (Margolin et al., 2022a).

The NXS/T Generation™ platform was recently used to produce a soluble trimeric HIV envelope gp140 vaccine and the resulting GE antigen elicited largely equivalent immune responses in rabbits compared to the same antigen produced in mammalian cells (Margolin et al., 2022a). Encouraged by these observations, we initiated studies to investigate the broad applicability of this host-engineering platform to other pandemic and emerging viruses, including SARS-CoV-2. Given that direct comparisons between plant-produced and mammalian cell-produced viral glycoproteins are generally lacking, we sought to establish how closely the GE antigens resemble the equivalent protein when produced in mammalian cells, both in terms of glycosylation and immunogenicity. Previous work by our group and others has demonstrated that the co-expression of human calreticulin substantially improved the yields of a soluble SARS-CoV-2 spike ectodomain (Song et al., 2022; Margolin et al., 2022b), warranting integration of this approach with the glyco-engineering strategies that comprise the NXS/T Generation™ Platform. Therefore, in the present study we have built on this work by producing an improved spike antigen (HexaPro) using the NXS/T Generation™ platform. The resulting GE spike was then compared to the equivalent material produced in mammalian cells with regard to its structure and glycosylation. Finally, the vaccines were evaluated for their ability to elicit immunity against both the homologous SARS-CoV-2 wildtype (Wuhan) strain and the heterologous Delta variant, and to protect against viral challenge with the heterologous Delta variant (B.1.617.2).

2 Materials and methods

2.1 Gene design and expression constructs for protein production

A human-codon optimized variant of the HexaPro spike antigen was synthesized by GenScript using the sequence reported by Hsieh et al., which contains the following mutations F817P, A892P, A899P, A942, K986P & V987P and the furin cleavage site was replaced with a short linker sequence GSAS from amino acid 682 to 685 (PDB 6XKL). The antigen also contains a synthetic C-terminal foldon trimerization motif, an HRV3C protease recognition sequence, a twin Strep-tag and an octa-histidine sequence as reflected in the original manuscript (Hsieh et al., 2020). Synthetic HindIII and AgeI sites were incorporated at the 5' end of the gene. EcoRI and XhoI sites were added to the 3' end of the gene coding sequence. A Kozak sequence (CCACC) was incorporated into the sequence immediately upstream of the start codon of the gene. The gene was cloned into pMEx for mammalian cell expression (van Diepen et al., 2018) and pEAQ-*HT* for plant expression (Sainsbury et al., 2009) using HindIII and EcoRI or AgeI and XhoI, respectively. The recombinant pEAQ-*HT* plasmid was transformed into *A. tumefaciens* AGL1 by electroporation. Recombinant *A.*

tumefaciens strains encoding LmSTT3D, human CRT and HEXO3RNAi have been described previously (Margolin et al., 2022a).

2.2 Production of SARS-CoV-2 HexaPro spike in plants

N. benthamiana ΔXF plants were propagated in flat trays at 25°C (55% humidity) under a controlled 16-hour light/8-hour dark photocycle, as described previously (Margolin et al., 2019). Recombinant spike was produced in *N. benthamiana* ΔXF by transient co-expression of the antigen with CRT, LmSTT3D and HEXO3RNAi, using *A. tumefaciens*-mediated infiltration to deliver the DNA coding sequences to the plant cells (Margolin et al., 2022a). The plant biomass was harvested 4 days post agroinfiltration and then homogenized in 2 buffer volumes of tris-buffered saline [pH 7.8], supplemented with 1% Depol 40 (Biocatalysts) and EDTA-free protease inhibitor (Roche). The resulting homogenate was incubated on an orbital shaker, at 4°C, for 1 hour and then filtered through Miracloth (Millipore Sigma) to remove insoluble plant debris. The pH was adjusted to 7.8 and the homogenate was clarified at 17000×g for 30 minutes. The sample was then filtered using a 0.45 µm Stericup-GP vacuum driven filter (Merck Millipore). The recombinant glycoprotein was captured using *Galanthus nivalis* lectin and trimeric spike was isolated by gel filtration, as described previously (Margolin et al., 2019).

2.3 Production of SARS-CoV-2 HexaPro in mammalian suspension cells

FreeStyle™ HEK293F cells (Invitrogen) were grown in sterile polycarbonate Erlenmeyer flasks on an orbital shaking platform set to 125 rpm. The cells were maintained at a density of 1-3×10^6 cells/ml at 37°C, with 8% CO_2. The cultures were passaged every 3-4 days, at a seeding density of 3×10^5 cells/ml, using fresh FreeStyle™ 293 Expression Medium (Invitrogen). Spike protein was transiently expressed by transfecting cells, at a density of 1×10^6 cells/ml, with 1 µg/ml of plasmid DNA. Polyethylenimine was used for transfections at a 3:1 ratio of transfection reagent:DNA. The culture media was harvested 5 days post-transfection and clarified by centrifugation at 2500×g, for 30 minutes. The clarified media was then filtered using a 0.45 µm Stericup-GP device (Merck Millipore). Spike trimers were purified as described for the plant-produced material.

2.4 Polyacrylamide gel electrophoresis and immunoblotting

Purified protein was resolved under denaturing conditions by SDS-PAGE as described previously (Margolin et al., 2019), and then immunoblotted using polyclonal mouse anti-His antibody (Serotech, MCA1396) at a 1:2000 dilution (Margolin et al., 2022b). Proteins were also resolved under native conditions using the BN-PAGE system followed by staining with BioSafe Coomassie G250 as previously reported (van Diepen et al., 2019).

2.5 Negative stain electron microscopy and image processing

Samples were pipetted onto glow-discharged (30 s in air) carbon-coated copper grids, washed three times in dH_2O and stained with 2% uranyl acetate. For each sample ~30 images were collected using SerialEM at 2.2 Å/pixel using a Tecnai F20 transmission electron microscope fitted with a DE16 camera (Direct Electron, San Diego, CA USA) operated at 200 kV at an electron dose of ~50 e/$Å^2$ and a defocus of −1.5 µm. Relion 3.1 (Scheres, 2012) was used for image processing and 3D reconstruction: briefly ~1 000 particles were manually picked and used to generate 2D class averages for reference-based picking yielding ~4000 particles. This particle set was refined using 2D classification and used to generate a *de novo* initial model using stochastic gradient descent (Punjani et al. 2017). Following refinement (final resolution: ~20 Å), UCSF Chimera (Pettersen et al., 2004) was used for three-dimensional visualization and rendering.

2.6 Site-specific N-glycan analysis of purified spike

Aliquots of spike protein were denatured for 1 h in 50 mM Tris/HCl, pH 8.0 containing 6 M of urea and 5 mM dithiothreitol (DTT). Next, spike proteins were alkylated by adding 20 mM iodoacetamide (IAA) and incubated for 1 h in the dark, followed by a 1 h incubation with 20 mM DTT to eliminate residual IAA. The alkylated spike proteins were buffer exchanged into 50 mM Tris/HCl, pH 8.0 using Vivaspin columns (3 kDa) and digested separately overnight using trypsin, chymotrypsin (Mass Spectrometry Grade, Promega), or alpha lytic protease (Sigma Aldrich) at a ratio of 1:30 (w/w). The next day, the peptides were dried and extracted using C18 Zip-tip (MerckMillipore). The peptides were dried again, resuspended in 0.1% formic acid and analyzed by nanoLC-ESI MS with an Ultimate 3000 HPLC (Thermo Fisher Scientific) system coupled to an Orbitrap Eclipse mass spectrometer (Thermo Fisher Scientific) using stepped higher energy collision-induced dissociation (HCD) fragmentation. Peptides were separated using an EasySpray PepMap RSLC C18 column (75 µm × 75 cm). A trapping column (PepMap 100 C18 3 µM, 75 µM × 2 cm) was used in line with the liquid chromatography (LC) before separation with the analytical column. The LC conditions were as follows: 275 min linear gradient consisting of 0%–32% acetonitrile in 0.1% formic acid over 240 min followed by 35 minutes of 80% acetonitrile in 0.1% formic acid. The flow rate was set to 300 nl/min. The spray voltage was set to 2.5 kV and the temperature of the heated capillary was set to 40°C. The ion transfer tube temperature was set to 275°C. The scan range was 375 – 1500 m/z. Stepped HCD collision energy was set to 15%, 25%, and 45%, and the MS2 for each energy was

combined. Precursor and fragment detection were performed using an Orbitrap at a resolution MS1= 120,000, MS2 = 30,000. The AGC target for MS1 was set to standard and injection time set to auto, which involves the system setting the two parameters to maximize sensitivity while maintaining cycle time. Full LC and mass spectrometry (MS) methodology can be extracted from the appropriate Raw file using XCalibur FreeStyle software or upon request.

Glycopeptide fragmentation data were extracted from the raw file using Byos (Version 3.5; Protein Metrics Inc.). The glycopeptide fragmentation data were evaluated manually for each glycopeptide; the peptide was scored as true-positive when the correct b and y fragment ions were observed along with oxonium ions corresponding to the glycan identified. The MS data was searched using the Protein Metrics 309 N-glycan library with sulfated glycans added manually combined with the Protein metrics 57 Plant N-linked glycan library. The relative amounts of each glycan at each site, as well as the unoccupied proportion were determined by comparing the extracted chromatographic areas for different glycotypes with an identical peptide sequence. All charge states for a single glycopeptide were summed. The precursor mass tolerance was set at 4 and 10 p.p.m. for fragments. A 1% false discovery rate was applied. The relative amounts of each glycan at each site as well as the unoccupied proportion were determined by comparing the extracted ion chromatographic areas for different glycopeptides with an identical peptide sequence. Glycans were categorized according to the composition detected. Chimera X v1.3 was used to visualize and represent the glycosylation of the S protein (Pettersen et al., 2021), using the .pdb file produced by (Zuzic et al., 2022), using S_full_domgly as the template.

HexNAc(2)Hex(10+) was defined as M9Glc, HexNAc(2)Hex (9–4) was classified as oligomannose-type. Any of these structures containing a fucose were categorized as FM (fucosylated mannose). HexNAc(3)Hex(5-6)X was classified as Hybrid with HexNAc(3) Hex(5-6)Fuc(1)X classified as Fhybrid. Complex-type N-glycans were classified according to the number of HexNAc subunits and the presence or absence of fucosylation. As this fragmentation method did not provide linkage information compositional isomers were grouped, so for example a triantennary glycan contained HexNAc 5 but so did a biantennary glycan with a bisect. Core glycans refer to truncated structures smaller than M3. Any compositions containing a monosaccharide corresponding to a pentose (e.g., Xylose) were classified in the pentose category. Likewise, any glycan composition detected containing at least one fucose or sialic acid were assigned as "Fucose" and "NeuAc," respectively.

2.7 Isolation, propagation and titration of SARS-CoV-2, delta variant

All work involving live SARS-CoV-2 was performed inside an accredited Biosafety Level 3 facility in accordance with the safety regulations regarding risk level 3 pathogens (WHO, 2021). SARS-CoV-2-positive patient samples were obtained from the National Health Laboratory Service (NHLS), Tygerberg, Cape Town, South Africa, and the lineage was confirmed to be SARS-CoV-2 Delta at Stellenbosch University (SU) as part of the Network for Genomic Surveillance in South Africa (NGS-SA) initiative (Msomi et al., 2020).

Vero E6 cells were maintained in Dulbecco's modified Eagle medium (DMEM) containing sodium pyruvate and L-glutamine (PAN Biotech, Aidenbach, Germany) with 10% foetal bovine serum (Gibco, Texas, USA) and 1% each of non-essential amino acids (Lonza, Basel, Switzerland), amphotericin B (Gibco, Texas, USA) and penicillin/streptomycin (PAN Biotech, Aidenbach, Germany). Vero E6 cells were grown at 37°C and 5% CO_2 and were passaged every 3-4 days.

For virus isolation, Vero E6 cells were seeded at $3.5x10^5$ cells/ml in a 6-well plate 18-24 hrs before infection. After one wash with 1xDPBS (PAN Biotech, Aidenbach, Germany) the cells were inoculated with patient sample that was diluted 1:5 in DMEM. The inoculum was removed after one hour incubation at room temperature, and the cells were washed once with 1xDPBS before the addition of post-infection media (DMEM, 2%FBS, 1% each of non-essential amino acids, amphotericin B, penicillin/streptomycin). The cells were incubated at 37°C with 5% CO_2 and monitored daily for 3-7 days or until >90% cytopathic effect (CPE) was observed. The cell culture supernatant was then harvested and used to infect freshly seeded Vero E6 cells to produce a second passage stock of the virus, and then a third passage stock. The third passage stock was sequence confirmed at SU using Oxford Nanopore Technology, as described previously (Maponga et al., 2022), to ensure no mutations had been introduced during passaging of the virus. The viral RNA load was quantified using a quantitative real time PCR assay specific for the E gene, as described by Corman et al. (Corman et al., 2020), and the infectious virus titer was determined using a standard plaque assay on Vero E6 cells.

2.8 Hamster vaccination and intranasal infection

Immunization and challenge experiments were carried out using 6–9-week-old male or female Syrian Golden Hamsters (*Mesocricetus auratus)*. All experimental procedures were conducted in the Research Animal Facility at the University of Cape Town, in accordance with AEC 021_005. Animal immunizations took place under BSL-2 conditions, whereas viral challenge experiments were confined to the BSL-3 laboratory using the IsoRAT900 Biocontainment system. Prior to challenge experiments, the Delta variant of SARS-CoV-2 was tested to determine the optimal inoculum for infection. Groups of 5 hamsters were inoculated intranasally with 10^4 PFU or 10^5 PFU virus or an equivalent volume of PBS. The body weights of the animals were monitored daily, and oropharyngeal swabs were collected prior to challenge and on days 3 and 6 post infection. The experiment was terminated on day 14 post-infection and organs were harvested for histological investigation.

The vaccine challenge study was conducted using 5 hamsters per experimental group. Animals were immunized intramuscularly

with 5 µg of protein, formulated 1:1 in Alhydrogel® adjuvant (van Diepen et al., 2018; Margolin et al., 2022b), on days 0 and 28. The experimental control group was immunized with an equivalent volume of PBS. Blood was drawn on day 0, 14 and 46. Vaccinated animals were transferred to the IsoRAT900 biocontainment system in the BSL3 laboratory on day 46 and were intranasally infected with 10^4 PFU of the Delta variant of SARS-CoV-2 on day 49. Oropharyngeal swabs were collected on days 46 (prior to infection), 52 (3 days post infection) and 55 (5 days post infection). The weight of the hamsters was recorded prior to both vaccination and infection, and then monitored daily following infection, until the experimental endpoint. The experiment was terminated on day 55. Lungs were collected in 10% buffered formalin.

2.9 Neutralization assay

Neutralizing antibodies against wild type/Wuhan and Delta viruses were quantified at weeks 0, 14 and 46 using a pseudovirus neutralization assay, as described previously (Margolin et al., 2022b). SARS-CoV-2 pseudovirions were generated in HEK-293T cells by co-transfection of plasmids pNL4-3.Luc.R-.E- (aidsreagent #3418) and pcDNA3.3-SARS-CoV-2-spike Δ18 (Wuhan strain) (Rogers et al., 2020) or pcDNA3.3-SARS-CoV-2-spike Δ18 – Delta (Delta variant), respectively. The latter was derived from plasmid pcDNA3.3-SARS-CoV-2-spike Δ18 (Wuhan strain) by side-directed mutagenesis using the QuikChange Lightning Multi Site-Directed Mutagenesis Kit (Agilent) together with the primers T19R (agccagtgtgtgaacctgaggaccaggaccc), R158G (aacaagtcctggatggagtctggggtctactcc), L452R (aggcaactacaactaccgctacagactgttcagga), T478K (atttaccaggctggcagcaaaccatgtaatggagt), D614G (gctgtgctctaccagggtgtgaactgtactgag), P681R (acccagaccaacagcagaaggagggcaaggtc), D950N (ccctgggcaaactccaaaatggtgtgaaccagaa), 156_157_del_F (acaacaagtcctggatggagtctagggtctactcc), and 156_157_del_R (ggagtagaccctagactccatccaggacttgttgt). Neutralization titres were reflected as the half maximal inhibitory dilution for each plasma sample.

2.10 Determination of SARS-CoV-2 viral loads

SARS-CoV-2 viral loads were determined from nasal swabs sampled in 500µl QVL Lysis Buffer containing 10µg/ml carrier RNA (Poly A) (Omega Bio-Tek). MS2 Phage Control (TaqMan™ 2019-nCoV Control Kit v2 (Applied Biosystems)) was added to each sample prior to RNA extraction as an internal positive control. RNA isolation was performed using the E.Z.N.A.® Viral RNA Kit (Omega Bio-Tek). This was followed by multiplex qRT-PCR of the isolated RNA on a QuantStudio™ 7 Flex Real-Time PCR System (Thermo Fisher) using the TaqMan™ 2019-nCoV Control Kit v2 (Applied Biosystems) including serial dilutions of known SARS-CoV-2 viral RNA ranging from $1x10^4$ copies/µl to 1x100 copies/µl. Viral loads were calculated based on the standard curve and expressed as copies/µl.

2.11 Histopathology

The lungs were sectioned and stained routinely with H&E for histopathology. Tissue was evaluated by light microscopy for evidence of necrosis/inflammation and/or repair/fibrosis. Lesions in the lung were graded as either absent (0), minimal (1), mild (2), moderate (3), marked (4) or severe (5). The severity of histopathology was graded based on observations of 1) lympho-plasmacytic infiltration, 2) bronchiolitis/peribronchiolitis, alveolitis and bullous emphysema, 3) vasculitis/perivasculitis and 4) atelectasis.

2.12 Statistical analyses

All statistical analyses were conducted using GraphPad Prism 9. Statistical comparisons between groups over time were analysed using a two-way Anova test whereas statistical comparisons between two groups at a single time point were made using a multiple unpaired t-test. A p value of <0.05 was considered as the threshold of significance for all statistical tests. The half maximal inhibitor dilution (ID_{50}) of sera samples was determined using a non-linear regression.

3 Results

3.1 Production of a glycan-enhanced SARS-CoV-2 spike in plants

The SARS-CoV-2 spike protein is a typical trimeric class 1 viral fusion protein which is initially synthesised as a single chain precursor of ~1300 amino acids that is cleaved by host proteases, such as furin, into two subunits, S1 and S2 (Duan et al., 2020; Zhang et al., 2021; Yan et al., 2022). The cleavage is essential for cell fusion and viral infectivity (Yan et al., 2022). The mature glycoprotein, on the viral surface, binds to the angiotensin-converting enzyme 2 (ACE2) receptor on the host cell membrane. This complex is then cleaved by the type 2 transmembrane protease TMPRSS2, triggering rearrangement of the protein from a metastable prefusion conformation to a stable postfusion conformation, activating the spike protein and enabling entry into the host cell (Duan et al., 2020; Zhang et al., 2021; Yan et al., 2022).

In order to produce the SARS-CoV-2 spike antigen in plants, we implemented an integrated suite of approaches that were previously developed to transiently remodel the plant secretory pathway to address host constraints in glycosylation and glycosylation-directed folding (NXS/T Generation™) (Margolin et al., 2022a). We applied this platform to produce a spike construct (HexaPro) that had been engineered to stabilize the antigen in the prefusion conformation by the incorporation of 6 proline mutations (Hsieh et al., 2020). Following affinity-chromatography and gel filtration (Figure 1A), aggregated material (fractions 31-35) was discarded (Figure 1B) and a homogenous population of well-ordered trimers (fractions 36-40) was recovered (Figure 1C). Coomassie-stained BN-PAGE gels verified the gel filtration peaks comprised of aggregates and

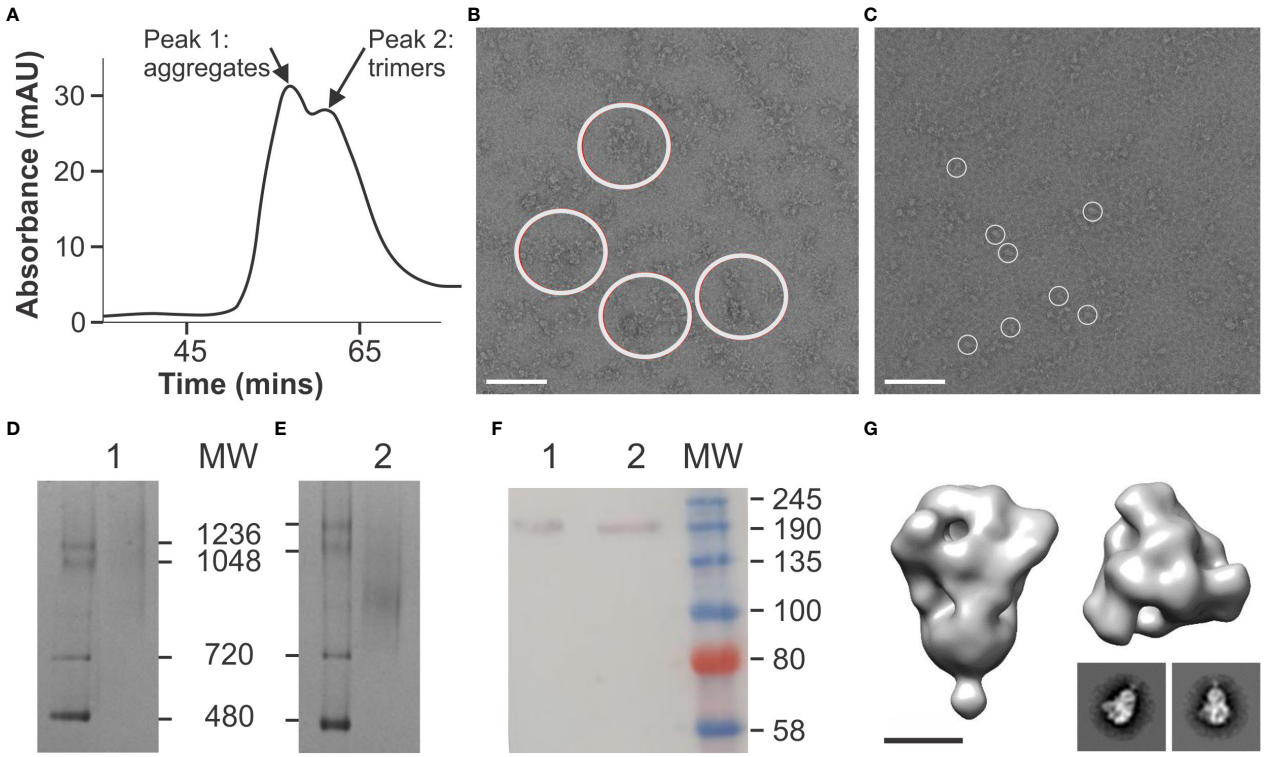

FIGURE 1
Production of a soluble, stabilized spike in plants. **(A)** Gel filtration profile of affinity-captured spike. Peak 1, fractions 31-35 = aggregates; Peak 2, fractions 36-40 = trimers. **(B)** Negative stain electron microscopy of fractions 31-35 derived from peak 1 (aggregates) in A. Large circles indicate large, clumps of aggregated spike protein. **(C)** Negative stain electron microscopy of fractions 36-40 derived from peak 2 (trimers) in A. Small circles indicate spike trimers. **(D)** Coomassie-stained BN-PAGE of fractions 31-35, peak 1 (aggregates) in A. **(E)** Coomassie-stained BN-PAGE of fractions 36-40, peak 2 (trimers) from A. **(F)** Western blotting of fractions 31-35 (lane 1) and 36-40 (lane 2) from peaks 1 and 2 respectively in A using polyclonal mouse anti-His antibody [Serotech, MCA1396]. **(G)** Three-dimensional reconstruction and class averages of purified trimeric spike protein (fractions 36-40) from electron micrographs shown in **(C)**.

trimers respectively (Figures 1D, E) and Western blotting confirmed the identity of the purified material with expected products observed at ~180 kDa (Figure 1F). Two-dimensional class averages and three-dimensional reconstruction of the purified spike trimers yielded a typical "kite-like" structure, which projected from a narrow base that would be proximal to the membrane in the context of the native virus (Figure 1G). When viewed from above the reconstruction depicted characteristic 3-fold symmetry and was consistent with published accounts for the antigen (Hsieh et al., 2020). The HexaPro spike was also produced in FreeStyle HEK293F mammalian cells as a control. The protein yielded equivalent structures that were consistent with previously published accounts (Hsieh et al., 2020), and which were indistinguishable from the plant-derived spike (Figure S1).

3.2 Site-specific glycan analysis of spike produced using the NXS/T generation™ system

The site-specific N-glycosylation of the plant-produced antigen was determined using a previously developed analytical pipeline (Figures 2A, S2 and Table S1) (Margolin et al., 2021a). The protein was decorated almost exclusively with oligomannose-type N-glycans, which exhibited low levels of glycan processing. The N-glycosylation of the control mammalian protein was similarly determined (Figures 2B, S3 and Table S2). The mammalian cell-produced spike contained large amounts of complex N-glycans, as well as incompletely processed oligomannose glycans at several N-glycosylation sites (N61, N122, N165, N234, N603, N616, N709, N717, N801, N1074). Minor populations of core glycans were also observed at 3/22 sites in the plant-produced protein (N61, N331 and N616) which were absent when the protein was produced in HEK293F cells. These structures comprise of Hex(3)HexNAc(2) or smaller structures which arise from enzymatic cleavage of the glycan. The N-glycan site occupancy between the 2 systems was largely comparable (Figure 3 and Table S3). Partial unoccupied sites were observed at N234 (4%), N1074 (34%), N1098 (1%) and N1194 (61%) in the plant-produced protein (Table S1).

3.3 Immunogenicity of plant-produced spike in hamsters

Hamsters were immunized with 5 µg of purified trimer, formulated in Alhydrogel®, to compare the immunogenicity of the vaccine when produced in plants and mammalian cells (Figure 4A). The vaccines both elicited neutralizing antibodies against the matched wild type virus, and against the heterologous

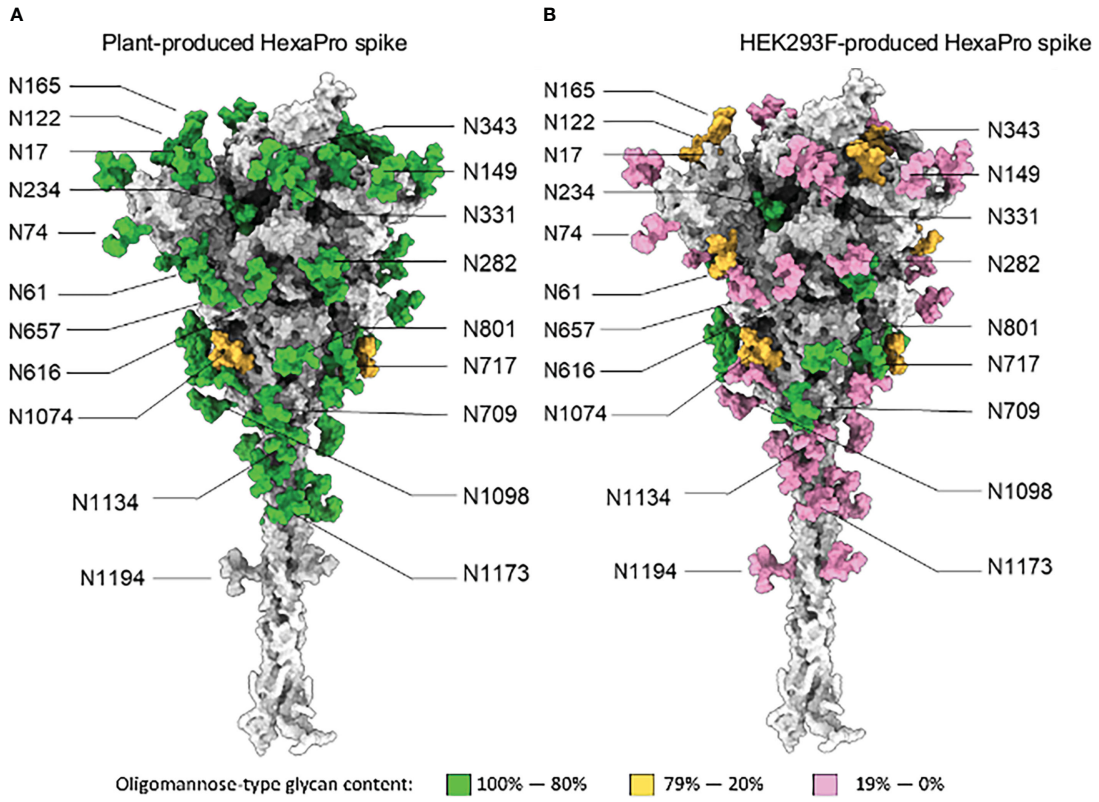

FIGURE 2
Site-specific N-glycosylation of plant and HEK293F-produced spike. **(A)** Fully glycosylated model of the SARS-CoV-2 spike glycoprotein in a native-like prefusion conformation, generated previously by (Zuzic et al., 2022). The individual N-glycan sites were colored according to the site-specific abundance of oligomannose-type glycans determined by LC-MS for spike protein produced using glycan enhanced *N.benthamiana* cells. **(B)** Model of the SARS-CoV-2 S protein produced in an identical manner to panel A except colored according to LC-MS analysis of spike protein produced by transient transfection of HEK293F cells.

Delta virus in all immunized animals after the second injection (Figures 4B, C, respectively). With the exception of a single animal in the plant group, all hamsters developed detectable neutralizing antibodies against the Wuhan virus after a single immunization (Figure 4B). Similarly, 4/5 animals in each group developed neutralizing antibodies against the Delta virus after a single immunization (Figure 4C). The mammalian cell-derived protein induced significantly higher mean titers of neutralizing antibodies against both viral isolates when compared to the plant protein. Irrespective of the producing system, heterologous neutralizing antibody titres were lower than the titres observed against the vaccine-matched virus (Figure 4C).

The hamsters were then challenged with the heterologous Delta virus to emulate the world scenario at the time of the experiment where the approved vaccines were based on the original wild type virus and the predominating variant was Delta. Following challenge, a slight decrease in body weight was witnessed in all groups over the first 2 days with no appreciable differences observed between vaccinated and unvaccinated animals. Both vaccinated groups rapidly recovered the lost weight, whereas the weights of the unvaccinated hamsters continued to decline until the experimental endpoint when a slight increase was observed. Both vaccines afforded significant protection against weight loss compared to the control group which demonstrated protracted weight loss and slower recovery ($p<0.05$) (Figure 5A). Animals immunized with the mammalian cell-produced antigen demonstrated a trend towards faster recovery of the lost weight, although this was not statistically significant ($p>0.05$).

Pathology of lung tissue following challenge was graded based on the observed severity which was reflected as a numerical score of 0-5 where 0 indicates that no significant histological changes were observed and 5 indicates severe changes (Figures 5B, S4). Moderate to marked microscopic lesions were observed in all unvaccinated animals. In contrast, the majority of animals from both vaccinated groups showed only mild or minimal changes on histopathology (Figure 5C). A single animal that was vaccinated with the mammalian cell-produced protein demonstrated complete protection from any observable changes on histopathology. Both vaccines resulted in lower viral loads following challenge when compared to the control group, and this was observed at both time points when viral load was assayed (Figure 5D). Animals vaccinated with the mammalian cell produced spike had a trend towards lower viral loads than animals immunized with the plant-produced spike, although this was only significant at the final time point.

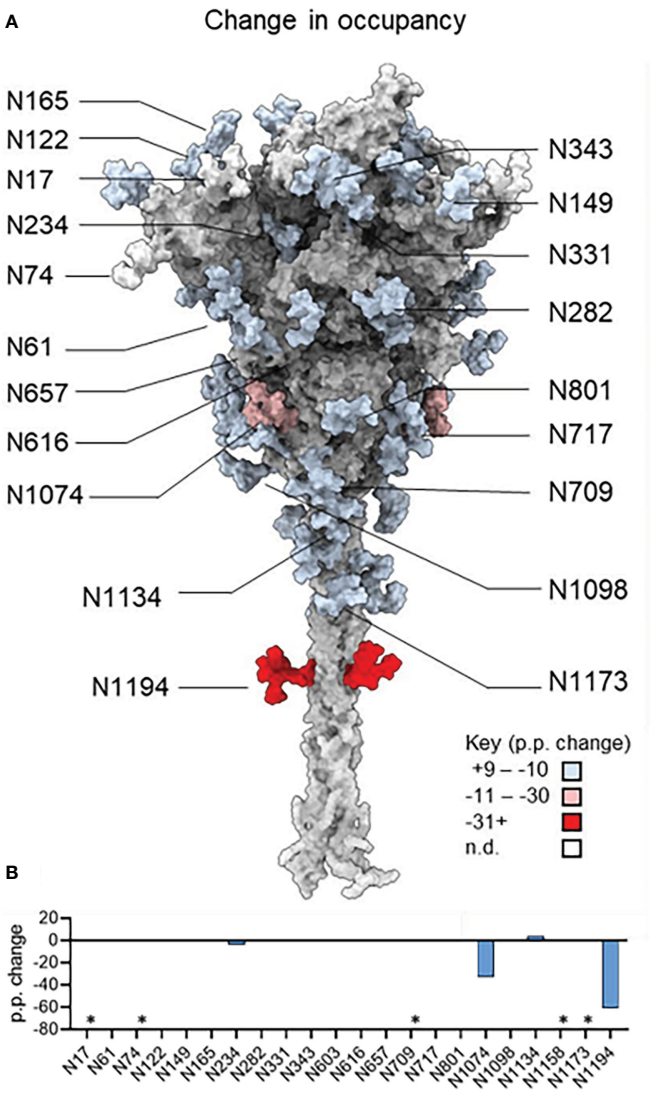

FIGURE 3
The change in site-specific N-glycan occupancy of plant-produced and mammalian cell-derived spike. **(A)** Model of the SARS-CoV-2 S glycoprotein in the native-like prefusion conformation generated by Zuzic et al., (2022). Individual N-glycan sites are colored according to the percentage point change in glycan occupancy of plant-derived protein relative to the comparator HEK293F-produced protein and therefore positive and negative values represent a relative increase or decrease in the glycan occupancy each sequon. **(B)** Bar graph depicting the percentage point changes depicted in panel A. A negative value indicates lower glycan occupancy in the plant-produced spike protein. Sites that could not be resolved are denoted with an asterisk.

4 Discussion

Remodelling the host cell factory has shown promise as a novel paradigm to produce increasingly complex biopharmaceuticals in plants (Frigerio et al., 2022; Ruocco and Strasser, 2022; Ganesan et al., 2023). These approaches enable intrinsic constraints in the host machinery to be addressed resulting in increased accumulation, enhanced folding, improved glycosylation and even tailor-made post-translational modifications (Margolin et al., 2020d). This has important implications for vaccine development and accordingly plant host engineering has shown promise in the production of novel vaccine antigens (Margolin et al., 2020c; Rosenberg et al., 2022; Song et al., 2022; Margolin et al., 2022a; Margolin et al., 2022b; Ruocco and Strasser, 2022; Margolin et al., 2020d) including those from enveloped viruses which historically have posed a challenge for plant-based production.

Following a series of studies to identify constraints in glycosylation-directed folding pathways in plants (Margolin et al., 2020c; Margolin et al., 2021a; Margolin et al., 2022b), we previously developed an integrated approach, NXS/T Generation™, to support improved viral glycoprotein production in *N. benthamiana*. In a proof-of-concept study, we recently used this technology platform to produce a soluble HIV envelope gp140 trimer, which elicited comparable immune responses to the cognate mammalian protein in a rabbit immunogenicity model (Margolin et al., 2022a). In the present study, we applied this approach to the prototype spike glycoprotein from SARS-CoV-2 and compared the resulting protein to the antigen when it was produced in mammalian cells. This work

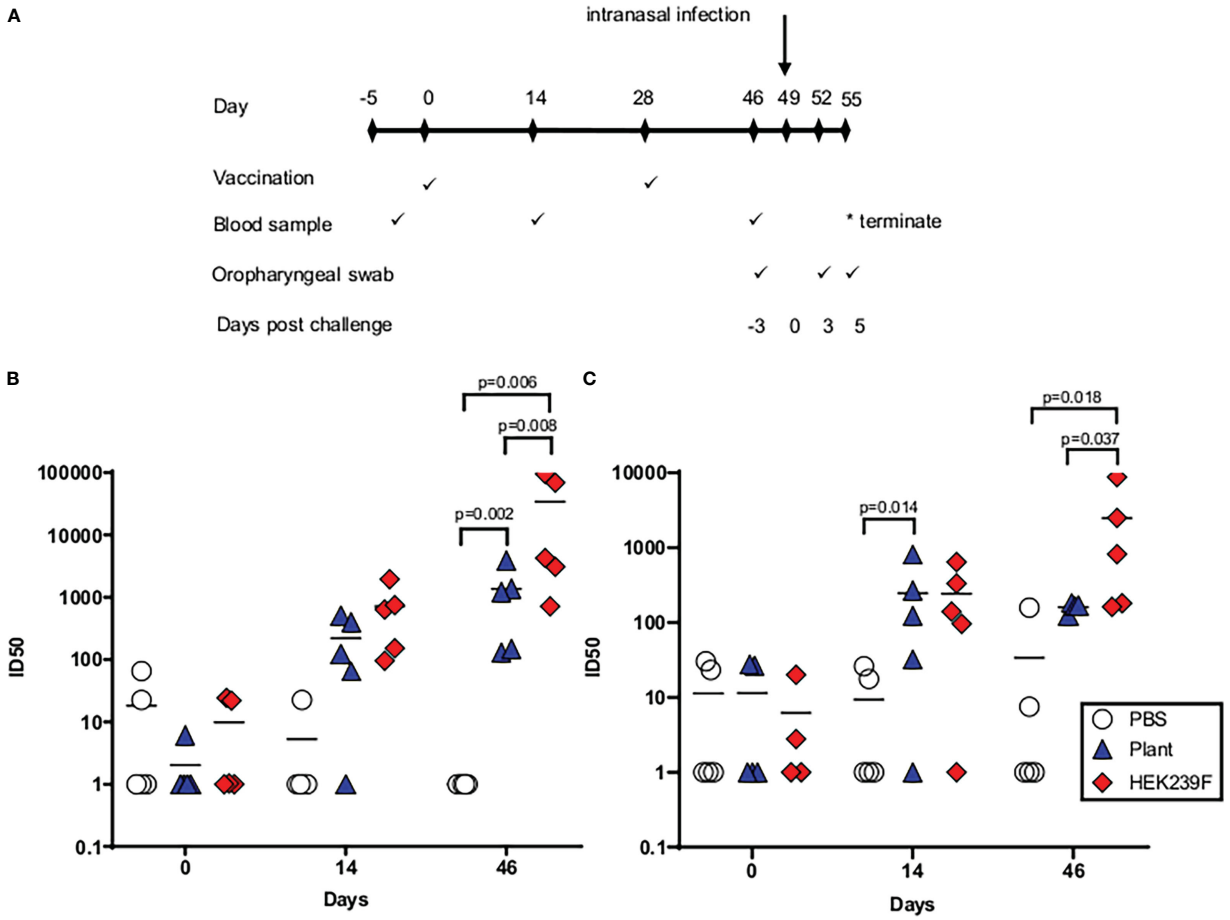

FIGURE 4
Immunogenicity of spike trimers in hamsters when produced in plants and mammalian cells. **(A)** Immunization schematic depicting the timing of immunizations and sampling during the experiment. **(B)** Neutralizing antibody titres (ID_{50}) against the matched wildtype (Wuhan) viral isolate. **(C)** Neutralizing antibody titres (ID_{50}) against heterologous Delta virus. Pre-bleed= day -2, first bleed = day 14, final bleed = day 46.

serves as part of a larger initiative to evaluate the broader applicability of the NXS/T Generation™ technology.

Following production in plants using this platform, the proteins observed by NSTEM were consistent with the prefusion trimer of the SARS-CoV-2 spike (Hsieh et al., 2020), and these were indistinguishable with what was observed for the mammalian control protein. However, despite the apparent similarities, juxtaposition of the site-specific N-glycosylation of the two proteins revealed substantial differences. Whilst the plant-derived protein contained an abundance of poorly processed oligomannose structures, the mammalian cell-derived control displayed a high degree of N-glycan processing with an abundance of mature complex glycans. Other studies have also reported reduced mannose processing in plants for viral glycoproteins (Dobrica et al., 2021; Margolin et al., 2021a), although the extent to which processing was arrested here remains a surprise. Interestingly the N-glycosylation pattern observed for the plant-produced spike in this study contrasts with a recent report describing the production of virus-like particles bearing the full-length protein in wild type *N. benthamiana* (Balieu et al., 2022). In the study conducted by Balieu et al., highly processed mature N-glycans were observed, including typical plant-derived complex glycans with Lewis A epitopes, contrasting against the abundance of immature oligomannose N-glycans that we observed. Although the use of *N. benthamiana* ΔXF as an expression host in the present study would preclude the formation of typical plant complex N-glycans carrying β1,2-xylose and core α1,3-fucose, it should not undermine normal glycan processing along the secretory pathway, and therefore the predominance of unprocessed oligomannose-type N-glycans is puzzling. It is worth noting that the spike protein in this study was soluble and therefore would not have the same association with the endomembrane system as would be expected for a full-length antigen. In the case of the HIV Env glycoprotein, membrane-bound Env has been reported to exhibit enhanced glycan processing and maturation compared to the cognate soluble protein, and this is thought to result from improved association with the membrane-bound host processing machinery (Allen, 2021). Although this could be a contributory factor, it seems unlikely to account for the dramatic retardation of glycan maturation that we observed. Although decreased glycan processing was also observed in our previous work with HIV Env using this production platform, this was less apparent as the extensive glycosylation of the glycoprotein

10.3389/fpls.2023.1146234

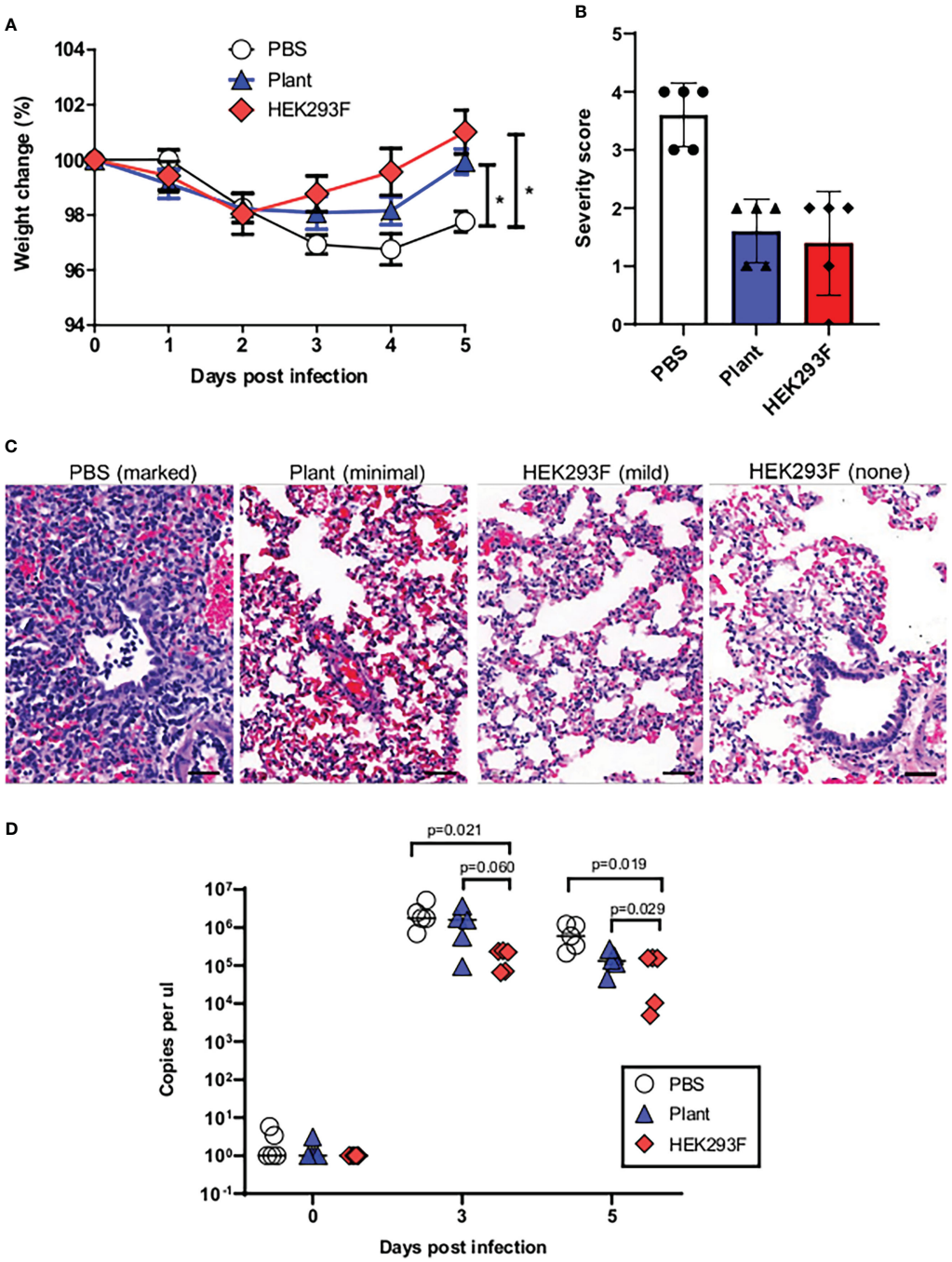

FIGURE 5
Vaccine-mediated protection against heterologous challenge. **(A)** Change in weight following experimental challenge. **(B)** Grading of lung pathology following challenge. **(C)** Representative images of histopathology findings in lung sections. **(D)** Viral load following challenge.

sterically hinders glycan-processing leading to an already elevated oligomannose content (Pritchard et al., 2015; Margolin et al., 2022a).

More encouragingly, the site-specific glycan occupancy of the plant-derived material was similar to that of the mammalian protein and the extensive under glycosylation that we previously observed for viral glycoproteins produced without the NXS/T Generation™ platform (Margolin et al., 2021a) was not seen here. This can be attributed to the co-expression of *Leishmania* LmSTT3D which has been demonstrated to improve glycan occupancy of a broad range of substrates in plants (Castilho et al., 2018; Margolin et al., 2022a).

The impact of impaired glycan maturation on vaccine immunogenicity is largely speculative and probably depends on the antigen in question. In the previous study with HIV, elevated high-mannose glycans did not appear to negatively impact the immunogenicity of the plant-produced vaccine – although it is acknowledged that the sample size was small (Margolin et al.,

2022a) and that the antigen naturally displays increased mannose content (Pritchard et al., 2015). Accordingly, it is less clear how this would impact immunogenicity in the context of an antigen, which would typically have complex glycans as the predominating species, such as the SARS-CoV-2 spike (Chawla et al., 2022). However, robust immune responses have been generated to SARS-CoV-2 spike proteins derived from a wide range of different sources with different glycosylation profiles (Chawla et al., 2022).

Although the plant-produced antigen was immunogenic, hamsters immunized with the vaccine developed significantly lower titres of neutralizing antibodies than animals that were immunized with the mammalian cell-produced protein. This is not unprecedented and these observations mirror studies with influenza virus where haemagglutinin antigens containing high-mannose glycans elicited lower haemagglutinin inhibition antibody titres than equivalent antigens containing typical mammalian-type complex glycans (de Vries et al., 2012). Nonetheless, the plant-produced vaccine still elicited cross-neutralizing antibodies against the Delta variant of SARS-CoV-2.

Following heterologous challenge, both plant-produced and mammalian cell-derived vaccines conferred significant protection from disease. The initial loss of weight indicates that the hamsters were not protected from infection but were able to clear the virus, probably *via* a T cell response. This protected against lung pathology. We had previously reported strong T cell responses to this plant made vaccine in mice (Margolin et al., 2021b). However, the mammalian-cell produced antigen elicited superior protection across multiple parameters including weight change, viral load and lung pathology. This can potentially be attributed to the observed differences in glycosylation. It has been shown that exposure of mannose residues can promote protein turnover, which would potentially result in reduced half-life of the plant-produced protein (Yang et al., 2015). This would in turn result in reduced antigenic stimulation compared to the mammalian cell-derived product, which contains significantly reduced mannose by comparison. In the context of HIV Env, it has also been shown that the abundance of mannose residues impairs immune responses from dendritic cells (Shan et al., 2007) and that enzymatic elimination of these mannose structures can increase the immunogenicity of an Env-derived gp120 antigen (Banerjee et al., 2009). It is unclear if a similar phenomenon is occurring here and further work is required to delineate the mechanism by which the glycosylation impairs the immune response. Lastly, although the differences in immunogenicity have been attributed to the differential glycosylation patterns from the expression hosts, we cannot discount expression-system dependent differences in folding which would also influence vaccine immunogenicity. We also note the limited resolution afforded by negative stain electron microscopy, and cryo-electron microscopy would be required to determine whether meaningful structural differences exist. In conclusion, this study highlights the utility of the NXS/T generation™ platform for remodelling the plant secretory pathway to produce complex viral glycoproteins in plants. Nonetheless, further refinement of the technology could greatly enhance vaccine immunogenicity and this could potentially even be used to generate vaccines with tailor-made glycosylation. Finally, this work highlights the influence of glycosylation in vaccine immunogenicity and reinforces this as an important consideration for production of important vaccine antigens by molecular farming.

Data availability statement

The original contributions presented in the study are included in the article/Supplementary Material. Further inquiries can be directed to the corresponding authors.

Ethics statement

The animal study was reviewed and approved by Animal Ethics Committee of the University of Cape Town, South Africa.

Author contributions

EM conceptualized the study with input from A-LW, RC and ER. Protein production was conducted by EM. JW carried out the negative stain electron microscopy and image processing. JA completed the site-specific N-glycan analysis. AS propagated and titrated the SARS-CoV-2 virus, under the supervision of MS and WP. RC managed the hamster experiment. Immunogenicity assays were conducted by EM and GS. MB cloned the Delta variant of the Spike protein for production of the pseudovirions used for neutralization assays. GS determined the viral loads and performed the neutralization assays. SG carried out the histopathology. EM drafted the manuscript. All authors contributed to data analysis and reviewed the final manuscript before submission. Funding for the project was obtained by RC, EM, MS, WP and A-LW. All authors contributed to the article and approved the submitted version.

Funding

Funding for the recombinant protein production described in this manuscript was supported in part by core funding provided by the Wellcome Trust [203135/Z/16/Z]. For the purpose of open access, the author has applied a CC BY public copyright licence to any Author Accepted Manuscript version arising from this submission. EM was supported by scholarship funding from CIDRI Africa. The immunogenicity and challenge work in this manuscript was funded by the UCT Innovation Builder Fund (Project #IB20-14). Further supplementary funding was provided by the South African Research Chairs Initiative of the Department of Science and Technology and the National Research Foundation (grant number: 64815). GS is supported by EDCTP2 programme

(Training and Mobility Action TMA2018SF-2446) and receives funding from the NRF, the MRC and the PRF. SARS-CoV-2 isolation and propagation was partially supported by the South African Medical Research Council with funds received from the Department of Science and Innovation (MS and WP), and by the Poliomyelitis Research Foundation (WP, grant 21/81). ADS was supported by a bursary from the Poliomyelitis Research Foundation (grant 21/45). RS was supported by the Austrian Science Fund (FWF) Project P31920-B32. MB holds a ACSR Young Investigator Pilot Award and has received funding from the NRF and the Oppenheimer Memorial Trust. This work was also supported by the International AIDS Vaccine Initiative (IAVI) through grant INV- 008352/OPP1153692 funded by the Bill and Melinda Gates Foundation (MC).

Acknowledgments

The authors are grateful to Professor George Lomonossoff (Department of Biological Chemistry, John Innes Centre) for providing the pEAQ-HT expression vector that was used for protein expression in plants. The authors would also like to thank Professor Herta Steinkellner (Department of applied genetics and cell biology, University of Natural Resources and Life Sciences) for providing the *N. benthamiana* ΔXF strain used in this study.

Conflict of interest

EM, AM, RC, A-LW, RS and ER have filed patent applications describing approaches to improve production of glycoproteins in plants. These include WO 2018/069878 A1, WO 2018/220595 A1, PA174002/PCT and PA176498_P.

The remaining authors declare that the research was conducted in the absence of any commercial or financial relationships that could be constructed as a potential conflict of interest.

Publisher's note

Supplementary material

The Supplementary Material for this article can be found online at: https://www.frontiersin.org/articles/10.3389/fpls.2023.1146234/full#supplementary-material

References

Allen, J. (2021). The glycan shields of HIV-1 and SARS-CoV-2 spike proteins and their differential importance in vaccine design. *Doctor philosophy Univ. Southampton*.

Alonzi, D. S., Scott, K. A., Dwek, R. A., and Zitzmann, N. (2017). Iminosugar antivirals: the therapeutic sweet spot. *Biochem. Soc. Trans.* 45 (2), 571–582. doi: 10.1042/BST20160182

Altmann, F. (2007). The role of protein glycosylation in allergy. *Int. Arch. Allergy Immunol.* 142 (2), 99–115. doi: 10.1159/000096114

Arnold, D. F., and Misbah, S. A. (2008). Cetuximab-induced anaphylaxis and IgE specific for galactose-alpha-1,3-galactose. *N Engl. J. Med.* 358 (25), 2735. doi: 10.1056/NEJMc080834

Balieu, J., Jung, J. W., Chan, P., Lomonossoff, G. P., Lerouge, P., and Bardor, M. (2022). Investigation of the n-glycosylation of the SARS-CoV-2 s protein contained in VLPs produced in nicotiana benthamiana. *Molecules* 27 (16), 5119. doi: 10.3390/molecules27165119

Banerjee, K., Andjelic, S., Klasse, P. J., Kang, Y., Sanders, R. W., Michael, E., et al. (2009). Enzymatic removal of mannose moieties can increase the immune response to HIV-1 gp120 *in vivo*. *Virology* 389 (1-2), 108–121. doi: 10.1016/j.virol.2009.04.001

Castilho, A., Beihammer, G., Pfeiffer, C., Goritzer, K., Montero-Morales, L., Vavra, U., et al. (2018). An oligosaccharyltransferase from leishmania major increases the n-glycan occupancy on recombinant glycoproteins produced in nicotiana benthamiana. *Plant Biotechnol. J.* 16 (10), 1700–1709. doi: 10.1111/pbi.12906

Chawla, H., Jossi, S. E., Faustini, S. E., Samsudin, F., Allen, J. D., Watanabe, Y., et al. (2022). Glycosylation and serological reactivity of an expression-enhanced SARS-CoV-2 viral spike mimetic. *J. Mol. Biol.* 434 (2), 167332. doi: 10.1016/j.jmb.2021.167332

Corman, V. M., Landt, O., Kaiser, M., Molenkamp, R., Meijer, A., Chu, D. K., et al. (2020). Detection of 2019 novel coronavirus, (2019-nCoV) by real-time RT-PCR. *Euro Surveill* 25 (3). doi: 10.2807/1560-7917.ES.2020.25.3.2000045

D'Aoust, M. A., Couture, M. M., Charland, N., Trepanier, S., Landry, N., Ors, F., et al. (2010). The production of hemagglutinin-based virus-like particles in plants: a rapid, efficient and safe response to pandemic influenza. *Plant Biotechnol. J.* 8 (5), 607–619. doi: 10.1111/j.1467-7652.2009.00496.x

de Vries, R. P., Smit, C. H., de Bruin, E., Rigter, A., de Vries, E., Cornelissen, L. A., et al. (2012). Glycan-dependent immunogenicity of recombinant soluble trimeric hemagglutinin. *J. Virol.* 86 (21), 11735–11744. doi: 10.1128/JVI.01084-12

Dobrica, M. O., van Eerde, A., Tucureanu, C., Onu, A., Paruch, L., Caras, I., et al. (2021). Hepatitis c virus E2 envelope glycoprotein produced in nicotiana benthamiana triggers humoral response with virus-neutralizing activity in vaccinated mice. *Plant Biotechnol. J.* 19 (10), 2027–2039. doi: 10.1111/pbi.13631

Duan, L., Zheng, Q., Zhang, H., Niu, Y., Lou, Y., and Wang, H. (2020). The SARS-CoV-2 spike glycoprotein biosynthesis, structure, function, and antigenicity: Implications for the design of spike-based vaccine immunogens. *Front. Immunol.* 11. doi: 10.3389/fimmu.2020.576622

Fischer, R., and Buyel, J. F. (2020). Molecular farming – the slope of enlightenment. *Biotechnol. Adv.* 40, 107519. doi: 10.1016/j.biotechadv.2020.107519

Frigerio, R., Marusic, C., Villani, M. E., Lico, C., Capodicasa, C., Andreano, E., et al. (2022). Production of two SARS-CoV-2 neutralizing antibodies with different potencies in nicotiana benthamiana. *Front. Plant Sci.* 13. doi: 10.3389/fpls.2022.956741

Ganesan, P. K., Kulchar, R. J., Kaznica, P., Montoya-Lopez, R., Green, B. J., Streatfield, S. J., et al. (2023). Optimization of biomass and target protein yield for phase III clinical trial to evaluate angiotensin converting enzyme 2 expressed in lettuce chloroplasts to reduce SARS-CoV-2 infection and transmission. *Plant Biotechnol. J.* 21 (2), 244–246. doi: 10.1111/pbi.13954

Group, P. I. W., Multi-National, P.I.I.S.T., Davey, R. T.Jr., Dodd, L., Proschan, M. A., Neaton, J., et al. (2016). A randomized, controlled trial of ZMapp for Ebola virus infection. *N Engl. J. Med.* 375 (15), 1448–1456. doi: 10.1056/NEJMoa1604330

Hager, K. J., Perez Marc, G., Gobeil, P., Diaz, R. S., Heizer, G., Llapur, C., et al. (2022). Efficacy and safety of a recombinant plant-based adjuvanted covid-19 vaccine. *N Engl. J. Med.* 386 (22), 2084–2096. doi: 10.1056/NEJMoa2201300

Hsieh, C. L., Goldsmith, J. A., Schaub, J. M., DiVenere, A. M., Kuo, H. C., Javanmardi, K., et al. (2020). Structure-based design of prefusion-stabilized SARS-CoV-2 spikes. *Science* 369 (6510), 1501–1505. doi: 10.1126/science.abd0826

Jung, J. W., Zahmanova, G., Minkov, I., and Lomonossoff, G. P. (2022). Plant-based expression and characterization of SARS-CoV-2 virus-like particles presenting a native spike protein. *Plant Biotechnol. J.* 20 (7), 1363–1372. doi: 10.1111/pbi.13813

Kang, H., Park, Y., Lee, Y., Yoo, Y.-J., and Hwang, I. (2018). Fusion of a highly n-glycosylated polypeptide increases the expression of ER-localized proteins in plants. *Sci. Rep.* 8 (1), 4612. doi: 10.1038/s41598-018-22860-2

Krammer, F. (2020). Pandemic vaccines: How are we going to be better prepared next time? *Med. (N Y)* 1 (1), 28–32. doi: 10.1016/j.medj.2020.11.004

Maharjan, P. M., Cheon, J., Jung, J., Kim, H., Lee, J., Song, M., et al. (2021). Plant-expressed receptor binding domain of the SARS-CoV-2 spike protein elicits humoral immunity in mice. *Vaccines* 9 (9), 978. doi: 10.3390/vaccines9090978

Mamedov, T., Yuksel, D., Ilgın, M., Gurbuzaslan, I., Gulec, B., Yetiskin, H., et al. (2021). Plant-produced glycosylated and *In vivo* deglycosylated receptor binding domain proteins of SARS-CoV-2 induce potent neutralizing responses in mice. *Viruses* 13 (8), 1595. doi: 10.3390/v13081595

Maponga, T. G., Jeffries, M., Tegally, H., Sutherland, A., Wilkinson, E., Lessells, R. J., et al. (2022). Persistent SARS-CoV-2 infection with accumulation of mutations in a patient with poorly controlled HIV infection. *Clin. Infect. Dis.* 6 (3), e522–e525. doi: 10.1093/cid/ciac548

Mardanova, E. S., Kotlyarov, R. Y., and Ravin, N. V. (2021). High-yield production of receptor binding domain of SARS-CoV-2 linked to bacterial flagellin in plants using self-replicating viral vector pEff. *Plants* 10 (12), 2682. doi: 10.3390/plants10122682

Margolin, E., Allen, J. D., Verbeek, M., Chapman, R., Meyers, A., van Diepen, M., et al. (2022a). Augmenting glycosylation-directed folding pathways enhances the fidelity of HIV env immunogen production in plants. *Biotechnol. Bioeng.* 119 (10), 2919–2937. doi: 10.1002/bit.28169

Margolin, E., Allen, J. D., Verbeek, M., van Diepen, M., Ximba, P., Chapman, R., et al. (2021a). Site-specific glycosylation of recombinant viral glycoproteins produced in nicotiana benthamiana. *Front. Plant Sci.* 12 (1473). doi: 10.3389/fpls.2021.709344

Margolin, E., Burgers, W. A., Sturrock, E. D., Mendelson, M., Chapman, R., Douglass, N., et al. (2020a). Prospects for SARS-CoV-2 diagnostics, therapeutics and vaccines in Africa. *Nat. Rev. Microbiol.* 18 (12), 690–704. doi: 10.1038/s41579-020-00441-3

Margolin, E., Chapman, R., Meyers, A. E., van Diepen, M. T., Ximba, P., Hermanus, T., et al. (2019). Production and immunogenicity of soluble plant-produced HIV-1 subtype c envelope gp140 immunogens. *Front. Plant Sci.* 10. doi: 10.3389/fpls.2019.01378

Margolin, E., Chapman, R., Williamson, A. L., Rybicki, E. P., and Meyers, A. E. (2018). Production of complex viral glycoproteins in plants as vaccine immunogens. *Plant Biotechnol. J.* 19, 1531–1545. doi: 10.1111/pbi.12963

Margolin, E., Crispin, M., Meyers, A., Chapman, R., and Rybicki, E. P. (2020b). A roadmap for the molecular farming of viral glycoprotein vaccines: Engineering glycosylation and glycosylation-directed folding. *Front. Plant Sci.* 11 (1901). doi: 10.3389/fpls.2020.609207

Margolin, E., Oh, Y. J., Verbeek, M., Naude, J., Ponndorf, D., Meshcheriakova, Y. A., et al. (2020c). Co-Expression of human calreticulin significantly improves the production of HIV gp140 and other viral glycoproteins in plants. *Plant Biotechnol. J.* 18 (10), 2109–2117. doi: 10.1111/pbi.13369

Margolin, E. A., Strasser, R., Chapman, R., Williamson, A. L., Rybicki, E. P., and Meyers, A. E. (2020d). Engineering the plant secretory pathway for the production of next-generation pharmaceuticals. *Trends Biotechnol.* 38 (9), 1034–1044. doi: 10.1016/j.tibtech.2020.03.004

Margolin, E., Verbeek, M., de Moor, W., Chapman, R., Meyers, A., Schafer, G., et al. (2021b). Investigating constraints along the plant secretory pathway to improve production of a SARS-CoV-2 spike vaccine candidate. *Front. Plant Sci.* 12. doi: 10.3389/fpls.2021.798822

Margolin, E., Verbeek, M., de Moor, W., Chapman, R., Meyers, A., Schäfer, G., et al. (2022b). Investigating constraints along the plant secretory pathway to improve production of a SARS-CoV-2 spike vaccine candidate. *Front. Plant Sci.* 12 (3056). doi: 10.3389/fpls.2021.798822

Msomi, N., Mlisana, K., de Oliveira, T.Network for Genomic Surveillance in South Africa writing (2020). A genomics network established to respond rapidly to public health threats in south Africa. *Lancet Microbe* 1 (6), e229–e230. doi: 10.1016/S2666-5247(20)30116-6

Murad, S., Fuller, S., Menary, J., Moore, C., Pinneh, E., Szeto, T., et al. (2020). Molecular pharming for low and middle income countries. *Curr. Opin. Biotechnol.* 61, 53–59. doi: 10.1016/j.copbio.2019.10.005

Pambudi, N. A., Sarifudin, A., Gandidi, I. M., and Romadhon, R. (2022). Vaccine cold chain management and cold storage technology to address the challenges of vaccination programs. *Energy Rep.* 8, 955–972. doi: 10.1016/j.egyr.2021.12.039

Pettersen, E. F., Goddard, T. D., Huang, C. C., Couch, G. S., Greenblatt, D. M., Meng, E. C., et al (2004). UCSF Chimera—a visualization system for exploratory research and analysis J. *Comput. Chem.* 25, 1605–12

Pettersen, E. F., Goddard, T. D., Huang, C. C., Meng, E. C., Couch, G. S., Croll, T. I., et al. (2021). UCSF ChimeraX: Structure visualization for researchers, educators, and developers. *Protein Sci.* 30 (1), 70–82. doi: 10.1002/pro.3943

Pritchard, L. K., Vasiljevic, S., Ozorowski, G., Seabright, G. E., Cupo, A., Ringe, R., et al. (2015). Structural constraints determine the glycosylation of HIV-1 envelope trimers. *Cell Rep.* 11 (10), 1604–1613. doi: 10.1016/j.celrep.2015.05.017

Punjani, A., Rubinstein, J. L., Fleet, D. J., and Brubaker, M. A. (2017). cryoSPARC: Algorithms for rapid unsupervised cryo-EM structure determination. *Nat Methods* 14 (3), 290–296. doi: 10.1038/nmeth.4169.

Rogers, T. F., Zhao, F., Huang, D., Beutler, N., Burns, A., He, W. T., et al. (2020). Isolation of potent SARS-CoV-2 neutralizing antibodies and protection from disease in a small animal model. *Science* 369 (6506), 956–963. doi: 10.1126/science.abc7520

Rosenberg, Y. J., Jiang, X., Lees, J. P., Urban, L. A., Mao, L., and Sack, M. (2022). Enhanced HIV SOSIP envelope yields in plants through transient co-expression of peptidyl-prolyl isomerase b and calreticulin chaperones and ER targeting. *Sci. Rep.* 12 (1), 10027. doi: 10.1038/s41598-022-14075-3

Royal, J. M., Simpson, C. A., McCormick, A. A., Phillips, A., Hume, S., Morton, J., et al. (2021). Development of a SARS-CoV-2 vaccine candidate using plant-based manufacturing and a tobacco mosaic virus-like nano-particle. *Vaccines* 9 (11), 1347. doi: 10.3390/vaccines9111347

Ruocco, V., and Strasser, R. (2022). Transient expression of glycosylated SARS-CoV-2 antigens in nicotiana benthamiana. *Plants* 11 (8), 1093. doi: 10.3390/plants11081093

Rybicki, E. P. (2009). Plant-produced vaccines: Promise and reality. *Drug Discov. Today* 14 (1-2), 16–24. doi: 10.1016/j.drudis.2008.10.002

Sainsbury, F., Thuenemann, E. C., and Lomonossoff, G. P. (2009). pEAQ: versatile expression vectors for easy and quick transient expression of heterologous proteins in plants. *Plant Biotechnol. J.* 7 (7), 682–693. doi: 10.1111/j.1467-7652.2009.00434.x

Scheres, S. H. (2012). RELION: Implementation of a Bayesian approach to cryo-EM structure determination J. *Struct. Biol.* 180, 519–30.

Shan, M., Klasse, P. J., Banerjee, K., Dey, A. K., Iyer, S. P., Dionisio, R., et al. (2007). HIV-1 gp120 mannoses induce immunosuppressive responses from dendritic cells. *PloS Pathog.* 3 (11), e169. doi: 10.1371/journal.ppat.0030169

Shin, Y. J., Castilho, A., Dicker, M., Sadio, F., Vavra, U., Grunwald-Gruber, C., et al. (2017). Reduced paucimannosidic n-glycan formation by suppression of a specific beta-hexosaminidase from nicotiana benthamiana. *Plant Biotechnol. J.* 15 (2), 197–206. doi: 10.1111/pbi.12602

Shin, Y.-J., König-Beihammer, J., Vavra, U., Schwestka, J., Kienzl, N. F., Klausberger, M., et al. (2021). N-glycosylation of the SARS-CoV-2 receptor binding domain is important for functional expression in plants. *Front. Plant Sci.* 12. doi: 10.3389/fpls.2021.689104

Siriwattananon, K., Manopwisedjaroen, S., Shanmugaraj, B., Prompetchara, E., Ketloy, C., Buranapraditkun, S., et al. (2021a). Immunogenicity studies of plant-produced SARS-CoV-2 receptor binding domain-based subunit vaccine candidate with different adjuvant formulations. *Vaccines* 9 (7), 744. doi: 10.3390/vaccines9070744

Siriwattananon, K., Manopwisedjaroen, S., Shanmugaraj, B., Rattanapisit, K., Phumiamorn, S., Sapsutthipas, S., et al. (2021b). Plant-produced receptor-binding domain of SARS-CoV-2 elicits potent neutralizing responses in mice and non-human primates. *Front. Plant Sci.* 12. doi: 10.3389/fpls.2021.682953

Song, S. J., Kim, H., Jang, E. Y., Jeon, H., Diao, H. P., Khan, M. R. I., et al. (2022). SARS-CoV-2 spike trimer vaccine expressed in nicotiana benthamiana adjuvanted with alum elicits protective immune responses in mice. *Plant Biotechnol. J.* 20 (12), 2298–2312. doi: 10.1111/pbi.13908

Strasser, R. (2016). Plant protein glycosylation. *Glycobiology* 26 (9), 926–939. doi: 10.1093/glycob/cww023

Strasser, R., Altmann, F., and Steinkellner, H. (2014). Controlled glycosylation of plant-produced recombinant proteins. *Curr. Opin. Biotechnol.* 30, 95–100. doi: 10.1016/j.copbio.2014.06.008

Strasser, R., Stadlmann, J., Schahs, M., Stiegler, G., Quendler, H., Mach, L., et al. (2008). Generation of glyco-engineered nicotiana benthamiana for the production of monoclonal antibodies with a homogeneous human-like n-glycan structure. *Plant Biotechnol. J.* 6 (4), 392–402. doi: 10.1111/j.1467-7652.2008.00330.x

van Diepen, M. T., Chapman, R., Douglass, N., Galant, S., Moore, P. L., Margolin, E., et al. (2019). Prime-boost immunizations with DNA, modified vaccinia virus Ankara, and protein-based vaccines elicit robust HIV-1 tier 2 neutralizing antibodies against the CAP256 superinfecting virus. *J. Virol.* 93 (8), e02155–18. doi: 10.1128/JVI.02155-18

van Diepen, M. T., Chapman, R., Moore, P. L., Margolin, E., Hermanus, T., Morris, L., et al. (2018). The adjuvant AlhydroGel elicits higher antibody titres than AddaVax when combined with HIV-1 subtype c gp140 from CAP256. *PloS One* 13 (12), e0208310. doi: 10.1371/journal.pone.0208310

Ward, B. J., Gobeil, P., Seguin, A., Atkins, J., Boulay, I., Charbonneau, P. Y., et al. (2021). Phase 1 randomized trial of a plant-derived virus-like particle vaccine for COVID-19. *Nat. Med.* 27 (6), 1071–1078. doi: 10.1038/s41591-021-01370-1

Ward, B. J., Landry, N., Trepanier, S., Mercier, G., Dargis, M., Couture, M., et al. (2014). Human antibody response to n-glycans present on plant-made influenza virus-like particle (VLP) vaccines. *Vaccine* 32 (46), 6098–6106. doi: 10.1016/j.vaccine.2014.08.079

Ward, B. J., Makarkov, A., Seguin, A., Pillet, S., Trepanier, S., Dhaliwall, J., et al. (2020). Efficacy, immunogenicity, and safety of a plant-derived, quadrivalent, virus-like particle influenza vaccine in adults (18-64 years) and older adults (>/=65 years): two multicentre, randomised phase 3 trials. *Lancet* 396 (10261), 1491–1503. doi: 10.1016/S0140-6736(20)32014-6

WHO (2021) *Laboratory biosafety guidance related to coronavirus disease (COVID-19): Interim guidance, 28 January 2021 [Online]. world health organisation*. Available at: https://www.who.int/publications/i/item/WHO-WPE-GIH-2021.1 (Accessed 24 October 2022).

Wilbers, R. H., Westerhof, L. B., van Raaij, D. R., van Adrichem, M., Prakasa, A. D., Lozano-Torres, J. L., et al. (2016). Co-Expression of the protease furin in nicotiana benthamiana leads to efficient processing of latent transforming growth factor-beta1 into a biologically active protein. *Plant Biotechnol. J.* 14 (8), 1695–1704. doi: 10.1111/pbi.12530

Yan, W., Zheng, Y., Zeng, X., He, B., and Cheng, W. (2022). Structural biology of SARS-CoV-2: open the door for novel therapies. *Signal Transduct Target Ther.* 7 (1), 26. doi: 10.1038/s41392-022-00884-5

Yang, W. H., Aziz, P. V., Heithoff, D. M., Mahan, M. J., Smith, J. W., and Marth, J. D. (2015). An intrinsic mechanism of secreted protein aging and turnover. *Proc. Natl. Acad. Sci. U.S.A.* 112 (44), 13657–13662. doi: 10.1073/pnas.1515464112

Zhang, J., Xiao, T., Cai, Y., and Chen, B. (2021). Structure of SARS-CoV-2 spike protein. *Curr. Opin. Virol.* 50, 173–182. doi: 10.1016/j.coviro.2021.08.010

Zuzic, L., Samsudin, F., Shivgan, A. T., Raghuvamsi, P. V., Marzinek, J. K., Boags, A., et al. (2022). Uncovering cryptic pockets in the SARS-CoV-2 spike glycoprotein. *Structure* 30 (8), 1062–1074 e1064. doi: 10.1016/j.str.2022.05.006

frontiers | Frontiers in Plant Science

TYPE Brief Research Report
PUBLISHED 02 August 2023
DOI 10.3389/fpls.2023.1202570

OPEN ACCESS

EDITED BY
Balamurugan Shanmugaraj,
Chulalongkorn University, Thailand

REVIEWED BY
Ashwini Malla,
Baiya Phytopharm Co., Ltd, Thailand
Rahul Singh,
University of Pennsylvania, United States

*CORRESPONDENCE
Tarlan Mamedov
tmammedov@gmail.com

RECEIVED 08 April 2023
ACCEPTED 12 July 2023
PUBLISHED 02 August 2023

CITATION
Mamedov T, Yuksel D, Gurbuzaslan I, Ilgin M, Gulec B, Mammadova G, Ozdarendeli A, Pavel STI, Yetiskin H, Kaplan B, Uygut MA and Hasanova G (2023) Plant-produced RBD and cocktail-based vaccine candidates are highly effective against SARS-CoV-2, independently of its emerging variants. *Front. Plant Sci.* 14:1202570. doi: 10.3389/fpls.2023.1202570

Plant-produced RBD and cocktail-based vaccine candidates are highly effective against SARS-CoV-2, independently of its emerging variants

Tarlan Mamedov[1,2]*, Damla Yuksel[1], Irem Gurbuzaslan[1], Merve Ilgin[1], Burcu Gulec[1], Gulshan Mammadova[1], Aykut Ozdarendeli[3,4], Shaikh Terkis Islam Pavel[3,4], Hazel Yetiskin[3,4], Busra Kaplan[3,4], Muhammet Ali Uygut[3] and Gulnara Hasanova[1]

[1]Department of Agricultural Biotechnology, Akdeniz University, Antalya, Türkiye, [2]Institute of Molecular Biology and Biotechnologies, Ministry of Science and Education, Republic of Azerbaijan, Baku, Azerbaijan, [3]Department of Microbiology, Medical Faculty, Erciyes University, Kayseri, Türkiye, [4]Vaccine Research, Development and Application Center, Erciyes University, Kayseri, Türkiye

Severe acute respiratory syndrome coronavirus 2 (SARS-CoV-2) is a novel and highly pathogenic coronavirus that caused an outbreak in Wuhan City, China, in 2019 and then spread rapidly throughout the world. Although several coronavirus disease 2019 (COVID-19) vaccines are currently available for mass immunization, they are less effective against emerging SARS-CoV-2 variants, especially the Omicron (B.1.1.529). Recently, we successfully produced receptor-binding domain (RBD) variants of the spike (S) protein of SARS-CoV-2 and an antigen cocktail in *Nicotiana benthamiana*, which are highly produced in plants and elicited high-titer antibodies with potent neutralizing activity against SARS-CoV-2. In this study, based on neutralization ability, we demonstrate that plant-produced RBD and cocktail-based vaccine candidates are highly effective against SARS-CoV-2, independently of its emerging variants. These data demonstrate that plant-produced RBD and cocktail-based proteins are the most promising vaccine candidates and may protect against Delta and Omicron-mediated COVID-19. This is the first report describing vaccines against SARS-CoV-2, which demonstrate significant activities against Delta and Omicron variants.

KEYWORDS

SARS-CoV-2, plant produced RBD, antigen cocktail, virus neutralization, Delta, Omicron

1 Introduction

The severe acute respiratory syndrome coronavirus 2 (SARS-CoV-2) that causes the coronavirus disease 2019 (COVID-19) infection, a highly infectious RNA virus, has undergone numerous mutations with the formation of genetically diverse linkages since first appearing in the city of Wuhan in 2019. Mutations could potentially have an impact on viral transmission as they affect the interaction between the S protein and its receptor, ACE-2. Among variants of concern (VOCs), the Alpha (B.1.1.7) and Delta (B.1.617.2) variants are associated with a high viral transmission rate and virulence compared to the parental Wuhan strain. Nine mutations were found in the S protein of the Delta variant, including in the amino-terminal domain (NTD) (five mutations) and receptor-binding domain (RBD) (two mutations, L452R, T478K). One mutation (P681R) was found near the furin cleavage site, and the other (D950N) in the S2 domain (Planas et al., 2021). Notably, mutations of G476, F486, T500, and N50, observed within the RBD are close to the receptor (ACE-2) binding site.

On 26 November 2021, a new variant named Omicron (B.1.1.529) was designated the fifth VOC (He et al., 2021), which carries more than 60 mutations compared to the original Wuhan strain. In the new Omicron variant, 36 mutations were found in the S protein sequence, including 30 amino acid substitutions, three deletions, and one insertion. It should be noted that 15 of the 30 amino acid substitutions are in the RBD (Tiecco et al., 2022).

Vaccination is currently the most effective way to prevent pathogenic diseases, including COVID-19. However, currently, available vaccines are less effective or not effective against emerging SARS-CoV-2 variants, such as the Delta strain (B.1.617) and the Omicron (B.1.1.529). Therefore, developing COVID-19 vaccines that are effective against emerging new variants of SARS-CoV-2, such as the Omicron, will be a very challenging task. Recently, we reported the successful production of RBD variants of the S protein of SARS-CoV-2 (Mamedov et al., 2021a) and of an antigen cocktail (Mamedov et al., 2021b) in *Nicotiana benthamiana*, which are highly produced in plants and elicited high-titer antibodies with potent neutralizing activity against SARS-CoV-2. Since the SARS-CoV-2 virus has mutated over time, in this study we tested how RBD or cocktail antigens could elicit specific immune responses against existing SARS-CoV-2 variants, Delta and Omicron. We demonstrate that plant-produced RBD or cocktail antigen-elicited antibodies are capable of neutralizing the Delta or Omicron variants.

2 Materials and method

2.1 Cloning, expression, and purification of gRBD, dRBD, and N+RBD proteins

Cloning, expression, and purification of glycosylated RBD (gRBD), deglycosylated RBD (dRBD), and N+RBD (nucleocapsid protein + receptor binding domain) proteins from *N. benthamiana* plant were performed as described recently (Mamedov et al., 2021a; Mamedov et al., 2021b). The genes encoding RBD of SARS-CoV-2 spike protein (RBD, 319-591 aa, GenBank: QHO60594.1) and nucleocapsid (N, 1–419 aa, GenBank: YP_009724397) were codon optimized using *N. benthamiana* codons and *de novo* synthesized (Biomatik Corp., Kitchener, ON, Canada). The signal peptide (MGFVLFSQLPSFLLVSTLLLFLVISHSCRA) of the tobacco *PR-1a* gene was added to the N-terminus of the RBD and N proteins. The KDEL sequence (ER retention signal) and the FLAG tag sequence (affinity purification tag) were added to the C-terminus. Genes were inserted into the plant expression pEAQ vector and introduced into the AGL1-1 strain of *Agrobacterium tumefaciens* to express genes in *N. benthamiana*. To produce the gRBD protein, pEAQ-RBD was infiltrated into *N. benthamiana* plant. To produce an N+RBD antigen cocktail, RBD and N genes were co-infiltrated into *N. benthamiana* leaves *via* co-agroinfiltration with both pEAQ-RBD and pEAQ-N constructs. To produce dRBD, the RBD and Endo H genes were co-infiltrated into *N. benthamiana* leaves *via* co-agroinfiltration with both pEAQ-RBD or pGreenII–Endo H constructs. Leaves were collected at 5 days after post-infiltration (dpi).

Expression levels of gRBD, dRBD, and N+RBD were determined by ELISA and Western blot analysis. To quantify the expression levels of gRBD, dRBD, and N+RBD, *N. benthamiana* plant leaf extract was filtered through Miracloth and then centrifuged at 20,000×*g* for 25 min at 4°C. The clear extract was analyzed by ELISA and Western blot.

For ELISA, plates were coated with 50 µl of diluted supernatants containing gRBD, dRBD, or N+RBD. The plates were also coated with commercially available RBD protein (Agr319-Phe541 aa, active protein, MBS2563882, MyBiosource, San Diego, CA, USA) as standard protein. Proteins were detected (i) using purified anti-FLAG antibody to detect plant-produced gRBD, dRBD, or N+RBD antigens; (ii) anti-SARS-CoV-2 S protein S1 mAb (cat. no. 945102, BioLegend, USA) to detect plant produced gRBD, dRBD antigens, and commercial RBD protein; (iii) or human novel coronavirus nucleoprotein (N) (1–419 aa) monoclonal antibody (MBS7135930, MyBioSource, San Diego, CA, USA) to detect plant-produced N protein.

For WB analysis, wells were loaded with 20 µl of diluted supernatants containing gRBD, dRBD, or N+RBD. The wells were also loaded with different amounts (100, 50, and 25 ng) of plant-produced, purified FLAG-tagged (Endo H or PNGase F) or commercially available RBD (Arg319–Phe541 aa, active protein, MBS2563882, MyBiosource) proteins as a standard protein. The expression levels of proteins were quantified using highly sensitive Gene Tools software (Syngene Bioimaging, UK). The expression levels were determined based on at least three replicates for each target protein.

Purification of plant-produced gRBD, dRBD, and N+RBD proteins was performed from 20 g of frozen leaves infiltrated with the pEAQ-RBD (with or without pGreenII-Endo H) or pEAQ-RBD+ pEAQ-N constructs, using anti-FLAG affinity chromatography as described recently (Mamedov et al., 2021a; Mamedov et al., 2021b). Plant-produced antigens were purified using anti-DYKDDDDK affinity gel (cat. no. 651503, BioLegend). gRBD-, dRBD-, and N+RBD-expressing leaves weighing 20 g were extracted in 1× PBS buffer and centrifuged at 13,000×*g* for 20 min at 4°C. The column was prepared and equilibrated with 10 column volumes of 1× PBS buffer. After washing the column

with 10 CV of 1× PBS buffer, proteins from the column were eluted with 200 mM glycine buffer, pH 2.2, containing 150 mM NaCl. Eluted fractions were mixed with 2.0 M Tris for neutralization of glycine in elution buffer and concentrated. Purified antigens were analyzed on the SDS-PAGE and Western blotting.

2.2 SDS-PAGE and Western blot

Purified proteins were separated on 10% polyacrylamide gels. For SDS-PAGE analysis, gels were stained with Coomassie (Gel Code Blue, Pierce Rockford, IL, USA). For Western blot, separated samples were transferred to a polyvinylidene fluoride membrane and blocked with 1% I-block. The plant-produced antigens were detected with an anti-DYKDDDDK antibody (cat. no. 637301, BioLegend), followed by horseradish peroxidase (HRP)-conjugated anti-rat polyclonal antibody (cat. no. 405405, BioLegend). Proteins were visualized using the GeneGnome XRQ Chemiluminescence imaging system.

2.3 Immunogenicity studies

Immunogenicity studies of gRBD, dRBD, and N+RBD in mice were performed in groups of 6–7-week-old Balb/c male animals (six mice/group) as described recently (Mamedov et al., 2021a). Mice were immunized intramuscularly (IM) on days 0 and 21 with 5 µg of gRBD, dRBD, and N+RBD adsorbed to 0.3% Alhydrogel. Blood samples were taken from immunized mice on day 42 and used for microneutralization assay (MNT). Mice studies were conducted at Akdeniz University Experimental Animal Care in compliance with the ARRIVE guidelines and with the permission of the Animal Experiments Local Ethics Committee for Animal Experiments at Akdeniz (under protocol number 1155/2020.07.0) with the supervision of a veterinarian.

2.4 MNT assay

We used to live in the SARS-CoV-2 Wuhan (GB-MT327745; GISAID-EPI_ISL_424366), Delta (GB-OM945721; GISAID-EPI_ISL_10844545), and Omicron variants (GB-OM945722; GISAID-EPI_ISL_10844681). SARS-CoV-2 microneutralization (MN) tests were performed as previously described with minor modifications (Mamedov et al., 2021a). Before the day of the experiment, Vero E6 cells (ATCC, CRL-1586) (2×10^4 cells/100 µl/well) were passaged to 96-well plates. The sera collected from vaccinated mice were heat-inactivated for 30 min at 56°C and subjected to twofold serial dilutions (from 1:4 to 1:1,024) with serum-free Dulbecco's modified Eagle's medium (DMEM). Twofold serial dilutions of the mice sera were mixed with an equal volume of DMEM containing 100 tissue culture infectious dose 50 (100 TCID50) of the SARS-CoV-2 variants and incubated for 90 min at 37°C. Following adsorption, inoculums were removed, and cells were incubated for 72 h with DMEM containing 2% FBS and checked for the cytopathic effect (CPE). Microplates were designed as follows: (i) to test two wells for each serum dilution, (ii) six control wells (virus only), and (iii) three wells of growth media for the blank. The CPE evaluation was performed according to the reduction of infection by 50% or more at the serum dilutions. The 50% microneutralization titer (MNT50) was analyzed by the Spearman–Karber method, which was calculated as the reciprocal of the highest serum dilution at which the infectivity was neutralized in 50% of the cell in wells.

2.5 Statistical analysis

We used GraphPad Prism software for statistical analysis. To compare the neutralization activity of gRBD-, dRBD-, and N+RBD-induced serums against live SARS-CoV-2 Wuhan, Delta, and Omicron variants, one way ANOVA test was used. Significant was accepted as $p < 0.05$, and p-values are shown as $^{*}p < 0.05$; $^{**}p < 0.01$; $^{***}p < 0.001$. Each point on the graph was derived from three replicas for each dilution.

3 Results

In this study, glycosylated and nonglycosylated versions of RBD and cocktail antigen obtained by co-expression of RBD with N protein were produced in *N. benthamiana*, as mentioned in our previous studies (Figure 1) (Mamedov et al., 2021a; Mamedov et al., 2021b).

The expression levels of gRBD, dRBD, and N+RBD, determined by ELISA and Western blot analysis, were ~42 mg/kg for dRBD and ~45 mg/kg for gRBD and cocktail antigens (N+RBD), similar to what was previously reported (Mamedov et al., 2021a; Mamedov et al., 2021b). RBD and cocktail antigens were purified from *N. benthamiana* by anti-FLAG affinity chromatography using anti-DYKDDDDK affinity gel, as described in Materials and methods. SDS-PAGE and Western blot analysis of the purified proteins are presented in Figure 1 (and full length gels and blots in the Supplementary Material), which are consistent with the results we recently reported (Mamedov et al., 2021b). Immunogenicity studies of gRBD, dRBD, and N+RBD in mice were performed as described in Materials and methods and as recently reported (Mamedov et al., 2021a; Mamedov et al., 2021b). Antibody levels were determined by ELISA on 42nd-day mouse sera immunized with two doses of plant-produced RBD variants (gRBD or dRBD) or cocktail antigens (N+RBD). As demonstrated in Figure 2, the plant-produced gRBD, dRBD antigens, and cocktail antigens (N+RBD) were able to induce significantly high titers of antibodies with a 5-µg dose. As can be seen from Figure 2, the endpoint titer of N+RBD was 10^7, higher than that of gRBD or dRBD. It should be noted that the endpoint titer of dRBD is higher than that of gRBD, which is consistent with the results we recently reported (Mamedov et al., 2021a).

To evaluate whether RBD or cocktail antigen-elicited antibodies are capable of neutralizing the Delta or Omicron variant, the latter being dominant at the moment, we tested Wuhan (GB-MT327745; GISAID-EPI_ISL_424366), Delta (GB-OM945721; GISAID-EPI_ISL_10844545), and Omicron variants (GB-OM945722;

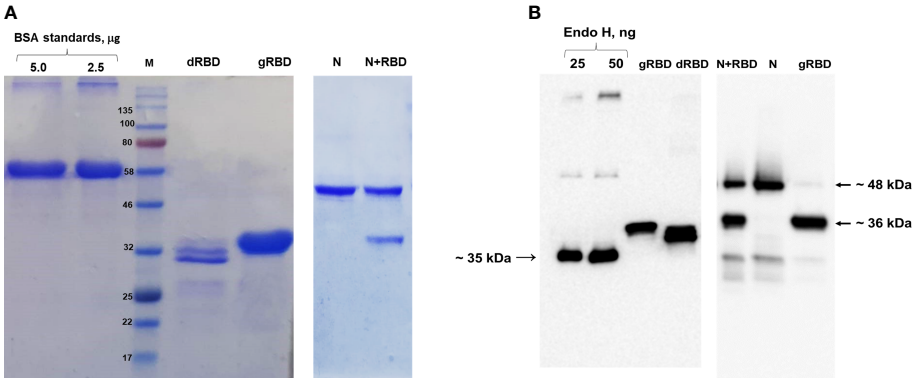

FIGURE 1
SDS-PAGE and Western blot analysis of gRBD, dRBD, and cocktail antigen (N+RBD) proteins, purified from *N. benthamiana* plant. Proteins were purified using anti-DYKDDDDK affinity gel. **(A)** SDS-PAGE for purified antigens. BSA was loaded as a standard, and target proteins were loaded as 5 µg. **(B)** Western blot analysis for plant-produced antigens. Endo H was used as a standard protein, and target proteins were loaded as 50 ng. Proteins were detected using the anti-FLAG antibody.

GISAID-EPI_ISL_10844681) with sera of mice immunized with two doses (5 µg per dose) of the plant-produced RBD variants or cocktail antigen-based COVID-19 vaccines (Figure 2). After two doses, Delta-neutralizing titers were not significantly reduced compared with Wuhan-neutralizing titers. Under the same conditions, Omicron-neutralizing titers were reduced by not more than fourfold compared with neutralizing titers in Wuhan (Figure 3). The plant-produced, deglycosylated RBD vaccine candidate was more effective compared to its glycosylated counterpart, suggesting the negative effect of *N*-glycosylation on protein functionality.

4 Discussion

Recently, we reported the successful production of glycosylated and deglycosylated RBD variants of the S protein of SARS-CoV-2 (Mamedov et al., 2021a) and an antigen cocktail (Mamedov et al., 2021b) in *Nicotiana benthamiana*, which are highly produced in plants and elicited high-titer antibodies with potent neutralizing activity against SARS-CoV-2. In this study, we demonstrate that plant-produced glycosylated and deglycosylated variants of RBD or cocktail antigen-elicited antibodies are capable of neutralizing the Delta or Omicron variant. It should be noted that after two doses (60 µg total synthetic mRNA), the Omicron-neutralizing titers of the messenger RNA (mRNA)-based COVID-19 vaccine (BNT162b2) were reduced by more than 22 times compared to Wuhan-neutralizing titers (Muik et al., 2022). Cele et al. (2022) demonstrated that in two-dose vaccinated individuals with the BNT162b2, the neutralization protection dropped over 40-fold against the Omicron versus the ancestral D614G virus. These results were expected given that the BNT162b2 vaccine is based on the full-length S protein sequence, while the S protein of the Omicron variant is highly mutated compared to other variants (Cele et al., 2022).

As we have described earlier, plant-produced dRBD demonstrated stronger binding to the SARS-CoV-2 receptor, ACE-2, compared with gRBD (Mamedov et al., 2021a). Moreover,

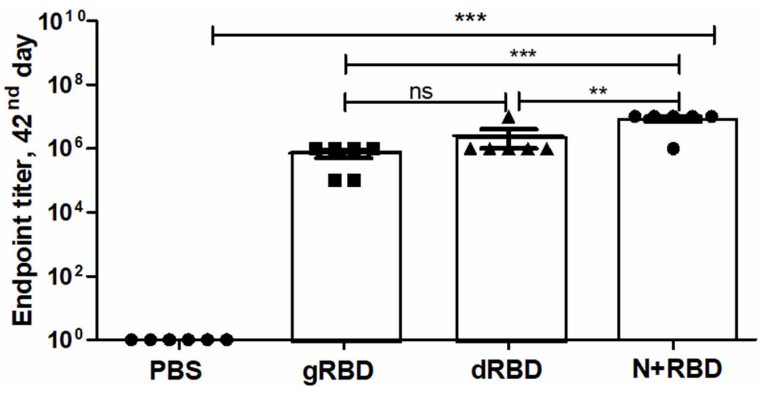

FIGURE 2
Immunogenicity of gRBD, dRBD, and N+RBD antigens in mice on the 42nd day. Mice were immunized with 5 µg of plant-produced proteins in a double injection on days 21 and 42. The endpoint titer was determined as the value corresponding to dilutions of the sera giving an OD value four times greater than the control mouse serum. Data in the graph are shown as the mean standard error of triplicates (SEM) at each sample dilution. The meaning of "**" is that the result is statistically significant. The meaning of "***" is that the result is highly statistically significant. ns, non significant.

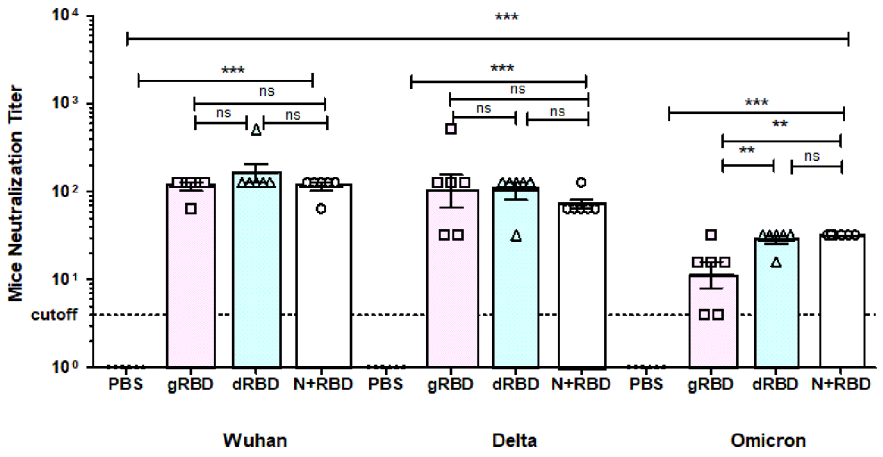

FIGURE 3
Sera from BALB/c mice immunized with gRBD, dRBD, and N+gRBD (cocktail) proteins demonstrated 50% microneutralization titers (MNT50) against live Wuhan, Delta, and Omicron variants of SARS-CoV-2. Microneutralization assay of 42nd-day mouse sera immunized with plant-produced gRBD, dRBD, and N+RBD (~2.7 µg + 2.3 µg, respectively) against live SARS-CoV-2 Wuhan, Delta, and Omicron variants as indicated. The experiment was performed using 4 to 1,024 dilutions of mouse sera collected on day 42. One-way ANOVA and Tukey's multiple comparison tests were used to calculate statistical significance (n = 6 mice/group); ***$p < 0.001$. The meaning of "**" is that the result is statistically significant.

we also demonstrated that both dRBD and dRBD variants induced strong neutralizing antibody responses in mice and sera immunized with the dRBD variant had higher neutralizing activity against live SARS-CoV-2 (Wuhan) compared with gRBD (Mamedov et al, 2021a). The impact of deglycosylation on neutralizing activity can be seen more significantly in the Omicron variant. When comparing Omicron-neutralizing titers, the plant-produced, deglycosylated RBD vaccine candidate was more effective compared to its deglycosylated counterpart, suggesting the negative effect of *N*-glycosylation on protein functionality. The negative effect of *N*-glycosylation on the functionality of proteins has been shown for several proteins. Deglycosylation, achieved by mutation of the *N*-glycosylation sites, increased the expression level and immunogenicity of the RBD protein vaccine (Zhang et al., 2020). The deglycosylation, achieved by the Endo H deglycosylation strategy (Mamedov et al., 2017) in plants significantly enhanced the efficacy of several proteins. For example, deglycosylation improved the SARS-CoV-2 neutralization activity of recombinant ACE2-Fc (Izadi et al., 2023). Deglycosylated Pfs48/45 of *Plasmodium falciparum*, produced in *N. benthamiana* plant using Endo H's *in vivo* deglycosylation strategy had strong inhibition in SMFA, but under the same conditions, glycosylated Pfs48/45 did not display any significant inhibition (Mamedov et al., 2019b). Plant-produced glycosylated PA83 of *Bacillus anthracis* was not functionally active and was not able to combine with LF to form a lethal toxin (LeTx) and induce cell death (Mamedov et al., 2016). In contrast, *in vivo* PNGase F deglycosylated PA83 counterpart was functionally active and showed an EC_{50} value similar to the *Bacillus*-produced recombinant PA (Mamedov et al., 2016). When purified plant-produced PNGase (Mamedov et al., 2016) or Endo H (Mamedov et al., 2017) deglycosylated PA83 proteins were assessed for stability, they appeared to be more stable than the glycosylated counterpart. In addition, the plant-produced deglycosylated PA83 elicited significantly higher levels of TNA titers in immunized mice compared with its glycosylated counterpart (Mamedov et al., 2016). The negative effect of *N*-glycosylation was also demonstrated for plant-produced Pfs25 of *Plasmodium falciparum*. A nonglycosylated form of Pfs25 antigen (N-linked glycosylation sites mutated) generated higher antibody titers and enhanced TB activity compared to its glycosylated counterpart (Farrance et al., 2011). Likewise, the negative effect of *N*-glycosylation was also demonstrated for plant-derived human monoclonal antibodies directed against PA of *Bacillus anthracis*. Deglycosylated (N-linked glycosylation sites mutated), the plant-produced human monoclonal antibody demonstrated superior efficacy compared to a glycosylated form of this mAb in nonhuman primates (Mett et al., 2011).

Plant transient expression systems have proven to be promising alternative expression platforms for the expression of a wide variety of important recombinant proteins, including vaccines (Yusibov & Mamedov, 2010; Mamedov et al., 2016; Mamedov et al., 2019a; Mamedov et al., 2019b; Margolin et al., 2020), therapeutic proteins (Mamedov et al., 2019a), antibodies, and human and industrial enzymes. Importantly, plant expression systems have proven to be capable of high-level production of functionally active SARS-CoV-2 proteins (Mamedov et al., 2020; Mamedov et al., 2021a; Mamedov et al., 2021b) and ACE2 (Mamedov et al., 2021c), receptors of SARS-CoV-2 and SARS-CoV. We recently demonstrated the successful expression of glycosylated and deglycosylated forms of RBD and antigen cocktails, comprising RBD and nucleocapsid (N) proteins, as promising vaccine candidates against COVID-19. We demonstrated that RBD variants of the S protein of SARS-CoV-2 and cocktail antigens are highly produced in the *N. benthamiana* plant and elicited high-titer antibodies with potent neutralizing activity against SARS-CoV-2. Our hypothesis was that if any SARS-CoV-2 variant infects a human, this means that a mutation in the RBD region did not affect its binding to ACE2, the SARS-CoV-2 S protein receptor. Therefore, the correct selection of RBDs is critical

for the successful production of functional RBDs with the ability to induce high neutralizing antibodies against SARS-CoV-2 and its variants. Since SARS-CoV-2 is an mRNA-based virus and mutations were expected, our strategy to eliminate possible emerging mutations was to select not the full sequence of the spike protein (most COVID-19 vaccine developers, including Pfizer-BioNTech and plant-based, Medicago's VLP, which was approved for use by Health Canada, were targeted on the full-length S sequence) but rather a specific region of the S protein covering the RBD. Moreover, to address mutations, the N-protein + RBD multi-antigen, cocktail-antigen-based vaccine was developed and produced for the first time as a potential COVID-19 vaccine candidate (Mamedov et al., 2021b). In this study, we have shown that the N protein probably significantly contributes to the enhancement of neutralizing activity.

Since RBD of SARS-CoV-2 is the primary target for potent virus-neutralizing antibodies (Barnes et al., 2020; Brouwer et al., 2020; Piccoli et al., 2020; Wang et al., 2020; Yang et al., 2020), it is frequently used for COVID-19 vaccine development (Diego-Martin et al., 2020; Rattanapisit et al., 2020; Shin et al., 2021; Siriwattananon et al., 2021; Phoolcharoen et al., 2023) and as an antigen in serological assays and diagnostic reagents (Amanat and Krammer, 2020; Rattanapisit et al., 2020; Makatsa et al., 2021; Jirarojwattana et al., 2023). Several research groups have utilized *N. benthamiana* plants to produce different amino acid regions of RBD variants of SARS-CoV-2 (Diego-Martin et al., 2020; Rattanapisit et al., 2020; Shin et al., 2021; Siriwattananon et al., 2021). The amino acid sequence of R319-F541 is the most widely used sequence domain.

The S protein of SARS-CoV-2 contains a relatively high number of cysteine residues, and eight of the nine cysteine residues found in the RBD are involved in disulfide bridge formation (Lan et al., 2020). Notably, for some viruses, such as HIV, the redox state of the fusion protein was shown to be important for the viral fusion to the target cells (Ryser et al., 1994; Manček-Keber et al., 2021). Thus, the proper formation of disulfide bridges is critical for proper folding of the RBD. We produced the RBD variant (R319-S591 aa), where the number of cysteine residues is even, which forms correct disulfide bridges in the molecule that may stabilize the protein conformation, leading to a functional protein. In fact, as we recently reported, the expression levels of plant-produced gRBD and dRBD variants (Mamedov et al., 2020; Mamedov et al., 2021a) were higher than 45 mg/kg of fresh weight. The purification yields of plant-produced gRBD and dRBD were ~22 and ~20 mg pure protein/kg biomass, respectively, which demonstrate the commercialization feasibility of these vaccine candidates. Moreover, in mice, the plant-produced gRBD and dRBD antigens elicited high titers of antibodies with strong SARS-CoV-2 live virus-neutralizing activity (Mamedov et al., 2021a). We concluded that the correct choice of the amino acid sequence within the RBD of the spike protein is critical for achieving high-level production of soluble and functionally active protein (Mamedov et al., 2021a). On this point, in the study of Rattanapisit et al. (2020), RBD of the spike protein of SARS-CoV-2 was produced in *N. benthamiana* plant, and low yields (2–4 μg/g of fresh weight) were reported (Rattanapisit et al., 2020). In the mentioned study, the amino acid sequence (F318-C617) of RBD was not properly selected, and as a result, cytosine at position 617 remained unpaired (which should form a disulfide bond with cysteine residues at position 649 in the full-length S protein), which may destabilize the protein conformation and lead to a loss of functional activity. In fact, there was no report of neutralization of SARS-CoV-2 in this study. In another study, F318-C617 amino acids of RBD with the Fc region of human immunoglobulin G1 (IgG1) were selected for production in the *N. benthamiana* plant (Siriwattananon et al., 2021). As in the study of Rattanapisit et al., the amino acid sequence of RBD (F318-C617) was not properly selected, and as a result, cytosine at position 617 remained unpaired (Rattanapisit et al., 2020). The expression level of plant-produced SARS-CoV-2 RBD-Fc was low, at 25 μg/g of fresh weight. Low expression levels (2–4 mg/g of fresh weight) of RBD were also reported for RBD variant (His tagged, aa R319-F541, where the number of cysteine residues was not even) (Diego-Martin et al., 2020; Shin et al., 2021), which is too low to be economical for commercialization of these plant-produced RBD variants (Diego-Martin et al., 2020; Shin et al., 2021).

RBD, or full-length S1, of SARC-CoV-2-based VLPs have been also produced in *N. benthamiana* for COVID-19 vaccine development by different research groups (Royal et al., 2021; Moon et al., 2022; O'Kennedy et al., 2023). A number of plant-derived SARS-CoV-2 RBD-based antigens and VLPs are in preclinical and clinical trials (Gobeil et al., 2021; Ward et al., 2021; Hager et al., 2022; Pillet et al., 2022; Ruocco and Strasser, 2022). The studies showed that the plant-produced vaccine is safe without any severe allergic reactions and efficacious against SARS-CoV-2, including the Delta variant of concern (Gobeil et al., 2021; Ward et al., 2021; Hager et al., 2022; Pillet et al., 2022). The plant-produced VLP virus-like particle-based (two doses of 3.75 μg of antigen) vaccine has proven to show efficacy of 75.3% against COVID-19 (original Wuhan strain) and has been approved and authorized for use in Canada; however, there are no reports about the efficacy of this vaccine against Omicron. As this plant-based VLP vaccine is targeted on the full-length S sequence, Medicago is preparing to study an Omicron-adapted version of its vaccine, as reported by D'Aoust (https://www.reuters.com/business/healthcare-pharmaceuticals/canada-approves-medicagos-plant-based-covid-19-vaccine-adults-2022-02-24/) even though Canada has already approved a plant-based VLP Medicago vaccine (designed on S protein of SARS-CoV-2 original Wuhan strain) for COVID-19 for adults.

Collectively, all the above findings demonstrate that plant-produced RBD and cocktail antigens are cost-effective, safe, and promising vaccine candidates against SARS-CoV-2, independently of its variants, and may protect against Delta and Omicron-mediated COVID-19.

5 Conclusion

Since the SARS-CoV-2 virus has mutated over time, developing COVID-19 vaccines that are more effective against emerging variants is a very challenging task. Based on our previous and current studies, all our findings demonstrate that plant viral RBDs

or cocktail antigens can be used as protein subunit vaccines to elicit specific immune responses against all existing SARS-CoV-2 variants, including Delta and Omicron.

Data availability statement

The raw data supporting the conclusions of this article will be made available by the authors, without undue reservation.

Ethics statement

Mice studies were conducted at Akdeniz University Experimental Animal Care in compliance with the ARRIVE guidelines, and with the permission of the Animal Experiments Local Ethics Committee for Animal Experiments at Akdeniz (under protocol number of 1155/2020.07.0) with the supervision of a veterinarian.

Author contributions

TM conceptualized the study. TM designed the experiments. DY, MI, IG, BG, GM, AO, HY, BK, SP, and MU performed the experiments. TM and GH analyzed the data. TM and GH contributed to writing the paper. All authors contributed to the article and approved the submitted version.

Funding

This work was supported by Akdeniz University.

Acknowledgments

The authors are grateful to George P. Lomonossoff (John Innes Center, Biological Chemistry Department) and Plant Bioscience Limited for kindly providing the pEAQ binary expression vector. We thank Philip de Leon at Trade Connections International for his editorial assistance.

Conflict of interest

TM is named as the inventor of the patent applications covering plant-produced COVID-19 vaccine development.

The remaining authors declare that the research was conducted in the absence of any commercial or financial relationships that could be construed as a potential conflict of interest.

Publisher's note

Supplementary material

The Supplementary Material for this article can be found online at: https://www.frontiersin.org/articles/10.3389/fpls.2023.1202570/full#supplementary-material

References

Amanat, F., and Krammer, F. (2020). SARS-coV-2 vaccines: status report. *Immunity* 52, 583–589. doi: 10.1016/j.immuni.2020.03.007

Barnes, C. O., Jette, C. A., Abernathy, M. E., Dam, K. A., Esswein, S. R., Gristick, H. B., et al. (2020). SARS-CoV-2 neutralizing antibody structures inform therapeutic strategies. *Nature* 588 (7839), 682–687. doi: 10.1038/s41586-020-2852-1

Brouwer, P. J. M., Caniels, T. G., van der Straten, K., Snitselaar, J. L., Aldon, Y., Bangaru, S., et al. (2020). Potent neutralizing antibodies from COVID-19 patients define multiple targets of vulnerability. *Science* 369 (6504), 643–650. doi: 10.1126/science.abc5902

Cele, S., Jackson, L., Khoury, D. S., Khan, K., Moyo-Gwete, T., Tegally, H., et al. (2022). Omicron extensively but incompletely escapes Pfizer BNT162b2 neutralization. *Nature* 602, 654–656. doi: 10.1038/s41586-021-04387-1

Diego-Martin, B., González, B., Vazquez-Vilar, M., Selma, S., Mateos-Fernández, R., Gianoglio, S., et al. (2020). Pilot production of SARS-CoV-2 related proteins in plants: a proof of concept for rapid repurposing of indoor farms into biomanufacturing facilities. *Front. Plant Sci.* 11. doi: 10.3389/fpls.2020.612781

Farrance, C. E., Chichester, J. A., Musiychuk, K., Shamloul, M., Rhee, A., Manceva, S. D., et al. (2011). Antibodies to plant-produced *Plasmodium falciparum* sexual stage protein Pfs25 exhibit transmission blocking activity. *Hum. Vaccin.* 7 Suppl, 191–198. doi: 10.4161/hv.7.0.14588

Gobeil, P., Pillet, S., Séguin, A., Boulay, I., Mahmood, A., Vinh, D. C., et al. (2021). Interim report of a phase 2 randomized trial of a plant-produced virus-like particle vaccine for Covid-19 in healthy adults aged 18–64 and older adults Aged 65 and older. *medRxiv*. doi: 10.1101/2021.05.14.21257248

Hager, K. J., Pérez Marc, G., Gobeil, P., Diaz, R. S., Heizer, G., Llapur, C., et al. (2022). Efficacy and safety of a recombinant plant-based adjuvanted Covid-19 vaccine. *N Engl. J. Med.* 386 (22), 2084–2096. doi: 10.1056/NEJMoa2201300

He, X., Hong, W., Pan, X., Lu, G., and Wei, X. (2021). SARS-CoV-2 Omicron variant: Characteristics and prevention. *MedComm* 2 (4), 838–845. doi: 10.1002/mco2.110

Izadi, S., Vavra, U., Melnik, S., Grünwald-Gruber, C., Föderl-Höbenreich, E., Sack, M., et al. (2023). *In planta* deglycosylation improves the SARS-CoV-2 neutralization activity of recombinant ACE2-Fc. *Front. Bioeng Biotechnol.* 11. doi: 10.3389/fbioe.2023.1180044

Jirarojwattana, P., Shanmugaraj, B., Rattanapisit, K., and Phoolcharoen, W. (2023). Development of SARS-CoV-2 neutralizing antibody detection assay by using recombinant plant-produced proteins. *Biotechnol. Rep. (Amst)* 38, e00796. doi: 10.1016/j.btre.2023.e00796

Lan, J., Ge, J., Yu, J., Shan, S., Zhou, H., Fan, S., et al. (2020). Structure of the SARS-CoV-2 spike receptor-binding domain bound to the ACE2 receptor. *Nature* 581, 215–220. doi: 10.1038/s41586-020-2180-5

Makatsa, M. S., Tincho, M. B., Wendoh, J. M., Ismail, S. D., Nesamari, R., Pera, F., et al. (2021). SARS-CoV-2 antigens expressed in plants detect antibody responses in COVID-19 patients. *Front. Plant Sci.* 12. doi: 10.3389/fpls.2021.589940

Mamedov, T., Acsora, R., Gun, N., Gulec, B., Mammadova, G., Cicek, K., et al. (2019a). Engineering, and production of functionally active human Furin in *N. benthamiana* plant: *In vivo* post-translational processing of target proteins by Furin in plants. *PloS One* 14, e0213438. doi: 10.1371/journal.pone.0213438

Mamedov, T., Chichester, J. A., Jones, R. M., Ghosh, A., Coffin, M. V., Herschbach, K., et al. (2016). Production of functionally active and immunogenic non-glycosylated protective antigen from Bacillus anthracis in *Nicotiana benthamiana* by coexpression with Peptide-N-Glycosidase F (PNGase F) of *Flavobacterium meningosepticum*. *PloS One* 11, e0153956. doi: 10.1371/journal.pone.0153956

Mamedov, T., Cicek, K., Gulec, B., Ungor, R., and Hasanova, G. (2017). *In vivo* production of non-glycosylated recombinant proteins in *Nicotiana benthamiana* plants by co-expression with Endo-β-N-acetylglucosaminidase H (Endo H) of *Streptomyces plicatus*. *PloS One* 12 (8), e0183589. doi: 10.1371/journal.pone.0183589

Mamedov, T., Cicek, K., Miura, K., Gulec, B., Akinci, E., Mammadova, G., et al. (2019b). A Plant-Produced in *vivo* deglycosylated full-length Pfs48/45 as a Transmission-Blocking Vaccine candidate against malaria. *Sci. Rep*. 9, 9868. doi: 10.1038/s41598-019-46375-6

Mamedov, T., Gurbuzaslan, I., Yuksel, D., Ilgin, M., Mammadova, G., Ozkul, A., et al. (2021c). Soluble human angiotensin- converting enzyme 2 as a potential therapeutic tool for COVID-19 is produced at high levels in *Nicotiana benthamiana* plant with potent anti-SARS-CoV-2 activity. *Front. Plant Sci.* 12. doi: 10.3389/fpls.2021.742875

Mamedov, T., Yuksel, D., Ilgin, M., Gurbuzaslan, I., Gulec, B., Mammadova, G., et al. (2020). Engineering, production and characterization of Spike and Nucleocapsid structural proteins of SARS–CoV-2 in *Nicotiana benthamiana* as vaccine candidates against COVID-19. *BioRxiv*. doi: 10.1101/2020.12.29.424779

Mamedov, T., Yuksel, D., Ilgin, M., Gurbuzaslan, I., Gulec, B., Yetiskin, H., et al. (2021a). Plant produced glycosylated and in *vivo* deglycosylated receptor binding domain proteins of SARS-CoV-2 induce potent neutralizing responses in mice. *Viruses* 13 (8), 1595. doi: 10.3390/v13081595

Mamedov, T., Yuksel, D., Ilgın, M., Gurbuzaslan, I., Gulec, B., Mammadova, G., et al. (2021b). Production and characterization of nucleocapsid and RBD cocktail antigens of SARS-CoV-2 in *Nicotiana benthamiana* plant as a vaccine candidate against COVID-19. *Vaccines* 9 (11), 1337. doi: 10.3390/vaccines9111337

Manček-Keber, M., Hafner-Bratkovič, I., Lainšček, D., Benčina, M., Govednik, T., Orehek, S., et al. (2021). Disruption of disulfides within RBD of SARS-CoV-2 spike protein prevents fusion and represents a target for viral entry inhibition by registered drugs. *FASEB J.* 35 (6), e21651. doi: 10.1096/fj.202100560R

Margolin, E., Crispin, M., Meyers, A., Chapman, R., and Rybicki, E. P. (2020). A roadmap for the molecular farming of viral glycoprotein vaccines: engineering glycosylation and glycosylation-directed folding. *Front. Plant Sci.* 11. doi: 10.3389/fpls.2020.609207

Mett, V., Chichester, J. A., Stewart, M. L., Musiychuk, K., Bi, H., Reifsnyder, C. J., et al. (2011). A non-glycosylated, plant-produced human monoclonal antibody against anthrax protective antigen protects mice and non-human primates from *B. anthracis* spore challenge. *Hum. Vaccin* 7 (Suppl), 183–190. doi: 10.4161/hv.7.0.14586

Moon, K. B., Jeon, J. H., Choi, H., Park, J. S., Park, S. J., Lee, H. J., et al. (2022). Construction of SARS-CoV-2 virus-like particles in plant. *Sci. Rep.* 12 (1), 1005. doi: 10.1038/s41598-022-04883-y

Muik, A., Lui, B. G., Wallisch, A. K., Bacher, M., Mühl, J., Reinholz, J., et al. (2022). Neutralization of SARS-CoV-2 Omicron by BNT162b2 mRNA vaccine-elicited human sera. *Science* 375 (6581), 678–680. doi: 10.1126/science.abn7591

O'Kennedy, M. M., Abolnik, C., Smith, T., Motlou, T., Goosen, K., Sepotokele, K. M., et al. (2023). Immunogenicity of adjuvanted plant-produced SARS-CoV-2 Beta spike VLP vaccine in New Zealand white rabbits. *Vaccine* 41 (13), 2261–2269. doi: 10.1016/j.vaccine.2023.02.050

Phoolcharoen, W., Shanmugaraj, B., Khorattanakulchai, N., Sunyakumthorn, P., Pichyangkul, S., Taepavarapruk, P., et al. (2023). Preclinical evaluation of immunogenicity, efficacy and safety of a recombinant plant-based SARS-CoV-2 RBD vaccine formulated with 3M-052-Alum adjuvant. *Vaccine* 41 (17), 2781–2792. doi: 10.1016/j.vaccine.2023.03.027

Piccoli, L., Park, Y. J., Tortorici, M. A., Czudnochowski, N., Walls, A. C., Beltramello, M., et al. (2020). Mapping neutralizing and immunodominant sites on the SARS-CoV-2 spike receptor-binding domain by structure-guided high-resolution serology. *Cell* 183 (4), 1024–1042.e21. doi: 10.1016/j.cell.2020.09.037

Pillet, S., Arunachalam, P. S., Andreani, G., Golden, N., Fontenot, J., Aye, P. P., et al. (2022). Safety, immunogenicity, and protection provided by unadjuvanted and adjuvanted formulations of a recombinant plant-derived virus-like particle vaccine candidate for COVID-19 in nonhuman primates. *Cell Mol. Immunol.* 19, 222–233. doi: 10.1038/s41423-021-00809-2

Planas, D., Veyer, D., Baidaliuk, A., Staropoli, I., Guivel-Benhassine, F., Rajah, M. M., et al. (2021). Reduced sensitivity of SARS-CoV-2 variant Delta to antibody neutralization. *Nature* 596, 276–280. doi: 10.1038/s41586-021-03777-9

Rattanapisit, K., Shanmugaraj, B., Manopwisedjaroen, S., Purwono, P. B., Siriwattananon, K., Khorattanakulchai, N., et al. (2020). Rapid production of SARS-CoV-2 receptor binding domain (RBD) and spike specific monoclonal antibody CR3022 in *Nicotiana benthamiana*. *Sci. Rep.* 10, 17698. doi: 10.1038/s41598-020-74904-1

Royal, J. M., Simpson, C. A., McCormick, A. A., Phillips, A., Hume, S., Morton, J., et al. (2021). Development of a SARS-CoV-2 vaccine candidate using plant-based manufacturing and a tobacco mosaic virus-like nano-particle. *Vaccines* 9, 1347. doi: 10.3390/vaccines9111347

Ruocco, V., and Strasser, R. (2022). Transient expression of glycosylated SARS-coV-2 antigens in *Nicotiana benthamiana*. *Plants* 11, 1093. doi: 10.3390/plants11081093

Ryser, H. J., Levy, E. M., Mandel, R., and DiSciullo, G. J. (1994). Inhibition of human immunodeficiency virus infection by agents that interfere with thiol-disulfide interchange upon virus-receptor interaction. *Proc. Natl. Acad. Sci.* 91, 4559–4563. doi: 10.1073/pnas.91.10.4559

Shin, Y. J., König-Beihammer, J., Vavra, U., Schwestka, J., Kienzl, N. F., Klausberger, M., et al. (2021). N-glycosylation of the SARS-CoV-2 receptor binding domain is important for functional expression in plants. *Front. Plant Sci.* 12. doi: 10.3389/fpls.2021.689104

Siriwattananon, K., Manopwisedjaroen, S., Shanmugaraj, B., Rattanapisit, K., Phumiamorn, S., Sapsutthipas, S., et al. (2021). Plant-produced receptor-binding domain of SARS-CoV-2 elicits potent neutralizing responses in mice and non-human primates. *Front. Plant Sci.* 12. doi: 10.3389/fpls.2021.682953

Tiecco, G., Storti, S., Degli Antoni, M., Focà, E., Castelli, F., and Quiros-Roldan, E. (2022). Omicron genetic and clinical peculiarities that may overturn SARS-CoV-2 pandemic: A literature review. *Int. J. Mol. Sci.* 23 (4), 1987. doi: 10.3390/ijms23041987

Wang, C., Li, W., Drabek, D., Okba, N. M. A., van Haperen, R., Osterhaus, A. D. M. E., et al. (2020). A human monoclonal antibody blocking SARS-CoV-2 infection. *Nat. Commun.* 11 (1), 2251. doi: 10.1038/s41467-020-16256-y

Ward, B. J., Gobeil, P., Séguin, A., Atkins, J., Boulay, I., Charbonneau, P. Y., et al. (2021). Phase 1 randomized trial of a plant-derived virus-like particle vaccine for COVID-19. *Nat. Med.* 27, 1071–1078. doi: 10.1038/s41591-021-01370-1

Yang, J., Wang, W., Chen, Z., Lu, S., Yang, F., Bi, Z., et al. (2020). A vaccine targeting the RBD of the S protein of SARS-CoV-2 induces protective immunity. *Nature* 586 (7830), 572–577. doi: 10.1038/s41586-020-2599-8

Yusibov, V. M., and Mamedov, T. G. (2010). Plants as an alternative system for expression of vaccine antigens. *Proc. ANAS (Biol. Sci.)* 65, 195–200.

Zhang, T., Wang, Z., and Xu, X. (2020). Impact of glycosylation and length of RBD of SARS-CoV-2 S protein on the immunogenicity of RBD protein vaccines. *Basic Clin. Med.* 40 (12), 1645–1650.

frontiers | Frontiers in Plant Science

TYPE Original Research
PUBLISHED 08 August 2023
DOI 10.3389/fpls.2023.1233666

OPEN ACCESS

EDITED BY
Balamurugan Shanmugaraj,
Chulalongkorn University, Thailand

REVIEWED BY
Elodie Rivet,
Université de Rouen, France
Mathew Paul,
St George's, University of London,
United Kingdom

*CORRESPONDENCE
Richard Strasser
richard.strasser@boku.ac.at

RECEIVED 02 June 2023
ACCEPTED 17 July 2023
PUBLISHED 08 August 2023

CITATION
Beihammer G, König-Beihammer J, Kogelmann B, Ruocco V, Grünwald-Gruber C, D'Aoust M-A, Lavoie P-O, Saxena P, Gach JS, Steinkellner H and Strasser R (2023) An oligosaccharyltransferase from *Leishmania donovani* increases the N-glycan occupancy on plant-produced IgG1. *Front. Plant Sci.* 14:1233666. doi: 10.3389/fpls.2023.1233666

An oligosaccharyltransferase from *Leishmania donovani* increases the N-glycan occupancy on plant-produced IgG1

Gernot Beihammer[1,2], Julia König-Beihammer[1], Benjamin Kogelmann[1,2], Valentina Ruocco[1], Clemens Grünwald-Gruber[3], Marc-André D'Aoust[4], Pierre-Olivier Lavoie[4], Pooja Saxena[4], Johannes S. Gach[5], Herta Steinkellner[1] and Richard Strasser[1]*

[1]Department of Applied Genetics and Cell Biology, University of Natural Resources and Life Sciences, Vienna, Austria, [2]acib - Austrian Centre of Industrial Biotechnology, Vienna, Austria, [3]Core Facility Mass Spectrometry, University of Natural Resources and Life Sciences, Vienna, Austria, [4]Medicago Inc., Quebec, QC, Canada, [5]Division of Infectious Diseases, University of California, Irvine, Irvine, CA, United States

N-Glycosylation of immunoglobulin G1 (IgG1) at the heavy chain Fc domain (Asn297) plays an important role for antibody structure and effector functions. While numerous recombinant IgG1 antibodies have been successfully expressed in plants, they frequently display a considerable amount (up to 50%) of unglycosylated Fc domain. To overcome this limitation, we tested a single-subunit oligosaccharyltransferase from the protozoan *Leishmania donovani* (LdOST) for its ability to improve IgG1 Fc glycosylation. LdOST fused to a fluorescent protein was transiently expressed in *Nicotiana benthamiana* and confocal microscopy confirmed the subcellular location at the endoplasmic reticulum. Transient co-expression of LdOST with two different IgG1 antibodies resulted in a significant increase (up to 97%) of Fc glycosylation while leaving the overall N-glycan composition unmodified, as determined by different mass spectrometry approaches. While biochemical and functional features of "glycosylation improved" antibodies remained unchanged, a slight increase in FcγRIIIa binding and thermal stability was observed. Collectively, our results reveal that LdOST expression is suitable to reduce the heterogeneity of plant-produced antibodies and can contribute to improving their stability and effector functions.

KEYWORDS

antibody, glycoprotein, glycosylation, *Nicotiana benthamiana*, recombinant protein

1 Introduction

Monoclonal antibodies comprise the most important and fastest-growing class of recombinant biopharmaceuticals used in multiple settings (Walsh and Walsh, 2022). Human immunoglobulin G1 (IgG1) is glycosylated at the conserved asparagine residue 297 (Asn297) in the Fc domain of the heavy chain (HC) and the nature of the attached N-glycan shapes Fc receptor binding and immune-mediated functions (Wang and Ravetch, 2019). Glycosylation is therefore considered an important quality attribute of recombinant antibodies and should be tightly controlled for effective antibody functions, avoidance of unwanted side effects, and development of biosimilars (Reusch and Tejada, 2015).

Plants are increasingly utilized for the production of recombinant biopharmaceuticals (Ruocco and Strasser, 2022; Eidenberger et al., 2023) and successfully used to express different classes of highly effective recombinant antibodies against viruses and human antigens (Chen, 2022; Shanmugaraj et al., 2022). Besides the classical dimeric IgG structure, plants are also able to correctly assemble higher order molecular forms, like dimeric IgA and pentameric IgM (Loos et al., 2014; Dicker et al., 2016; Sun et al., 2021). As shown for IgG antibodies, expression levels of more than 1 g/kg are frequently achieved, making the system economically interesting (Bendandi et al., 2010; Ridgley et al., 2023). Host glycoengineering enables the production of functional IgG antibodies with human-like complex N-glycan structures lacking core fucose residues with increased functional activities (Strasser et al., 2008; Forthal et al., 2010; Zeitlin et al., 2011). However, it has been demonstrated that transient expression of recombinant human IgG1 antibodies in *Nicotiana benthamiana* leaves resulted in the presence of considerable amounts of underglycosylation in the Fc domain (Castilho et al., 2018). Contrary, mammalian cell produced recombinant IgG1 antibodies are typically more than 99% glycosylated at Asn297 (Stadlmann et al., 2008). The observed underglycosylation at the conserved N-glycosylation site increases the heterogeneity ("macroheterogeneity") of a recombinant IgG1 antibody potentially leading to adverse effect on immune effector functions because non-glycosylated (i.e., both HCs in the assembled antibody lack N-glycans) or hemi-glycosylated (i.e., one HC is unglycosylated, the other HC in the assembled antibody is glycosylated) IgG1 antibodies typically display strongly reduced effector functions (Ha et al., 2011; Ju and Jung, 2014).

In eukaryotes N-glycosylation is typically initiated by the transfer of a preassembled oligosaccharide to specific asparagine residues (Asn-X-Ser/Thr consensus sequence motif) of a translocated polypeptide chain in the lumen of the endoplasmic reticulum (ER). In humans, the reaction is catalyzed by the membrane-embedded multi-protein oligosaccharyltransferase (OST) complex (Shrimal and Gilmore, 2019). While the OST subunit composition and known function of individual protein subunits appear largely conserved in plants (Strasser, 2016), the factors causing the differences in the N-glycosylation efficiency are currently elusive. Here, we performed a detailed characterization of the underglycosylation of different transiently expressed recombinant IgG1 antibodies in glycoengineered *N. benthamiana* and provide a robust approach for efficient N-glycosylation of plant-produced IgG1.

2 Materials and methods

2.1 IgG1 expression vectors

Construction of expression vectors for pEAQ-Cetuximab (pEAQ-Cx, two independent expression vectors, one for the heavy chain and one for the light chain), pTra-Cetuximab (pTra-Cx, one expression vector carrying two expression cassettes) and magnICON-Cetuximab (magnICON-Cx, two independent expression vectors, one for the heavy chain and one for the light chain) was described recently (Eidenberger et al., 2022). The expression vector for rituximab (Rx) was provided by Medicago (Li et al., 2016) and is referred to as pCAM-Rx (one expression vector carrying two expression cassettes) in this study. For expression in leaf epidermal cells of *N. benthamiana*, the pEAQ-Cx and magnICON-Cx plasmids, were introduced into *Agrobacterium tumefaciens* strain GV3101, while for pTra-Cx *A. tumefaciens* strain GV3101 pMP90RK was used. Mammalian cell produced Rx (Rituxan) was kindly provided by Friedrich Altmann and described previously (Stadlmann et al., 2008).

2.2 Cloning of sequences encoding OST subunits

Cloning and expression of LmSTT3D has been described previously (Castilho et al., 2018). For cloning of LdOST, the coding sequence (GenBank: TPP46432.1) was amplified by PCR from synthetic DNA using the forward primer 5'-CTTCCG GCTCGTTTGTCTAGAATG-3' and the reverse primer 5'-AAAAACCCTGGCGGGATCC-3'. The PCR fragment was digested with *Xba*I/*Bam*HI and subcloned into *Xba*I/*Bam*HI-digested binary expression vector pPT2 (CaMV35S promoter, Strasser et al., 2005) to obtain pPT2-LdOST or p48 (ubiquitin-10 promoter, Hüttner et al., 2014) to obtain p48-LdOST-TAG. In the p48-LdOST-TAG construct a stop codon was included at the end of the LdOST coding sequence to prevent expression of an RFP-fusion protein. To generate p48-LdOST for expression of LdOST-RFP, the LdOST coding sequence without a stop codon was amplified by PCR using the forward primer 5'-CTTCCGGCTCGTTT GTCTAGAATG-3' and the reverse primer 5'- TATAGGATC CCACCTCACCAAGAGTCCT-3' and cloned into p48. To generate the human OST4-GFP expression construct, the OST4 coding sequence was amplified by PCR from human cDNA using forward primer 5'-TATATCTAGAATGATCACGGACGTGC-3' and reverse primer 5'-tataGGATCCTTCCTGCTTCTTGGG-3', *Xba*I/*Bam*HI-digested and cloned into p47 (ubiquitin-10 promoter, GFP-tag, Hüttner et al., 2014). For ectopic expression, the plasmids were introduced into *A. tumefaciens* strain UIA143 (Strasser et al., 2005).

2.3 Plant material and agroinfiltration

N. benthamiana plants were grown at 23°C under long-day conditions (i.e., 16 h light/8 h dark). Besides wild-type plants a XT/FT-knockout line (ΔXF KO) was used (manuscript in preparation). Infiltration into leaves of 5-week-old *N. benthamiana* was done as previously described (Göritzer et al., 2017). Briefly, the respective *Agrobacteria* were grown in LB-medium overnight at 29°C. Bacteria were centrifuged, resuspended in infiltration buffer (10 mM $MgSO_4$, 10 mM MES and 0.1 mM acetosyringone) and the suspension was used for infiltration. In case of pEAQ-Cx and magnICON-Cx, where light chain and heavy chain are on separate plasmids, *Agrobacteria* suspensions with OD_{600} of 0.15 were infiltrated for the heavy chain while the OD_{600} of *Agrobacteria* suspensions for infiltration of the light chain was 0.1 unless otherwise stated. For pTra-Cx and pCAM-Rx *Agrobacteria* suspensions with OD_{600} of 0.15 were used for infiltration. Binary constructs containing either LdOST or LmSTT3D, respectively, were infiltrated with *Agrobacteria* suspensions with OD_{600} of 0.1.

2.4 Confocal microscopy

Analysis of subcellular localization via confocal microscopy was done as previously described (Schoberer et al., 2019). In short, the acquisition of live-cell confocal images was done on a Leica SP5 microscope using an oil immersion objective (Leica 63x/1.4 NA). For GFP excitation an argon laser at 488 nm and for RFP a diode laser at 561 nm was used. For detection a photomultiplier tube (PMT) and Hybrid detectors (HyD) at 500-530 nm and 600-630 nm respectively were employed.

2.5 Expression of IgG1 and densitometric analysis

For analysis of underglycosylation via densitometry, IgG1 constructs were infiltrated into leaves of *N. benthamiana* and harvested 3 days post infiltration (dpi). Plant material was mechanically disrupted using a ball mill and 4 µL of ice-cold extraction buffer (0.1 M TRIS, 0.5 M NaCl, 1 mM EDTA, 40 mM ascorbic acid, 2% (w/v), pH 6.8) added to 1 mg of plant material. After removal of cell debris via centrifugation Laemmli buffer was added to the extracts and the samples heated to 95°C for 5 min. Samples were then diluted 1:5 before applying them to SDS-PAGE (12% acrylamide). After electrophoretic separation, proteins were blotted to a nitrocellulose membrane and subsequently detected using an anti-IgG antibody conjugated to horseradish peroxidase (Promega). Proteins were visualized using ECL substrate on a Fusion instrument (Vilber). Densitometric analysis of bands corresponding to glycosylated and unglycosylated IgG1 heavy chain was done using the Evolution-Capt software (Vilber). Background subtraction was done using the rolling ball method of the software.

2.6 Mass spectrometric analysis of glycopeptides

For analysis of N-glycans, IgG1 reporters were expressed as described above and enriched via Protein A sepharose as described previously (Castilho et al., 2018). Elution was done using 0.1 M glycine pH 2.8. Following reduction and carbamido-methylation the enriched proteins were subjected to a tryptic in-solution digest (Kolarich and Altmann, 2000) using Trypsin Platinum, Mass Spectrometry Grade (Promega). 10-20 µg protein are routinely digested with 0.5-1.0 µg trypsin for 16 h at 37°C. The resulting glycopeptides were analyzed using an Orbitrap Exploris 480 (Thermo Scientific) and the obtained data analyzed using Skyline Version 22.2 software (MacLean et al., 2010). ANOVA with Tukey *post-hoc* tests were carried out using GraphPad Prism 9.2 software.

2.7 Quantification of underglycosylation via mass spectrometry

To quantify the degree of underglycosylation of plant produced IgG1 via mass spectrometry purified proteins were either measured intact or the fraction of unglycosylated heavy chain analyzed from trypsin-digested glycopeptides. For the intact measurement, 1 µg of protein was applied directly to a Waters BioResolve Column (2.1 x 5 mm). An acetonitrile gradient was used ranging from 15% to 80% (v/v) acetonitrile in 0.1% (v/v) formic acid. Gradient time was 15 minutes, flow rate was set to 400 µL/min at 80°C. Detection was performed on a Q-TOF instrument (Agilent Series 6560 LC-IMS-QTOFMS) equipped with the JetStream ESI source in positive mode. Data analysis was done using MassHunter BioConfirm B.08.00. Spectrum deconvolution was performed using MaxEnt. For quantification on the peptide level, glycopeptides were deglycosylated using Protein-N-glycosidase A (PNGase A, Europa Bioproducts Ltd) which leads to deamidation of the glycosylated asparagine residue present in the N-glycosylation site. The resulting mass shift of + 0.984 can be monitored via mass spectrometry. For normalization, a synthetic peptide EEQYNSTYREEQYDSTYR (JPT Peptide Technologies) was used as described (Castilho et al., 2018). Analysis of mass spectrometry data was done using Skyline Version 22.2. ANOVA with Tukey *post-hoc* tests were carried out using GraphPad Prism 9.2 software.

2.8 Antigen-binding ELISA

A 20-mer peptide (P20) of the extracellular loop of human CD20 was used as an antigen (Blasco et al., 2007). 1 µg/mL of P20 (diluted in PBS buffer, pH 7.4) was coated (50 µL/well) to 96 well microplates (MicroWell™ MaxiSorp™ Merck) for 16 h at 4°C, then saturated by incubation 100 µL/well with 3% fat free milk powder, dissolved in PBS-T (PBS with 0.05% Tween 20) for 1.5 h at 22°C. Solutions of rituximab diluted in blocking solution and applied to the coated plates in two-fold serial dilutions starting from 1000 µg/mL

were then added (50 µL/well) and incubated for 2 h at 22°C to obtain calibration curves. Peroxidase-conjugated goat anti-human gamma chain antibody (Merck) was added at a dilution of 1:5000 and the plates were incubated for a further hour at 22°C. Every step was followed with three-time PBS-T washing. 50 µL/well of the substrate 3,3',5,5'-tetramethylbenzidine (Merck) was added and plates were incubated for 5 to 10 min. The reaction was stopped with 2 M H_2SO_4 and absorbance (λ = 450 nm) with reference to 620 nm was measured with an ELISA reader (Tecan Spark® spectrophotometer). The binding curve was generated using GraphPad Prism 9.2 software.

2.9 Fcγ receptor binding by flow cytometry

FcγRIIIa (CD16a; F158 allotype) expressing TZM-bl cells were used to assess the binding affinity of Rx variants. Flow cytometry was carried out exactly as described (Forthal et al., 2010). The binding curves were generated by plotting the mean fluorescence intensity of positive cells indicating receptor binding as a function of antibody concentration. Unspecific binding to wild-type cells was subtracted from binding to FcγRIIIa-expressing cells. Each antibody concentration was run in duplicate. Binding experiments were repeated three times.

2.10 SPR

In vitro binding experiments of Rx variants to the extracellular domain (amino acids 17-208) of FcγRIIIa/CD16a was performed using a Biacore T200 (Cytiva). First the sensor chip surface was captured with anti-His antibody with the His Capture Kit (Cytiva) to a CM5 chip as described in the manufacturers' protocol. The capturing of anti-His antibody reached 32000 RU. Secondly, immobilization of the His-tagged human FcγRIIIa (F158 allotype) or FcγRIIIa (V158 allotype) (AcroBiosystems) on the chip surface was performed for 60s with a concentration of 1 µg/mL and a flow rate of 10 µL/min in HEPES-EP running buffer. 40 RU units were achieved. The immobilization step was previously optimized in order to avoid avidity effects using lower concentration of FcγRIIIa and shorter times. Flow cell 2 remained unmodified and served as a reference cell for the subtraction of systematic instrument noise and drift. Rx binding curves were generated in multi-cycle kinetic experiments at seven different concentrations ranging from 7.8 to 500 nM with 60 seconds association and 60 seconds dissociation time at a flow rate of 10 µL/min. After each run, surface regeneration was accomplished using 10 mM glycine, pH 1.7, for 120 seconds at a flow rate of 30 µL/min. Binding affinities (K_D) were calculated with Biacore T2 Evaluation software using a 1:1 binding in kinetics (Rx, Rx + LdOST, Rx + LmSTT3D) or steady state (Rituxan). All experiments were repeated as three independent kinetic runs.

2.11 DSF

Protein stability measurements were carried out by differential scanning fluorimetry (DSF) using the CFX96 Real-Time PCR Detection System (Bio-Rad) with a final dilution of 1:500 of the SYPRO Orange dye (Molecular Probes). Fluorescence of a 25 µL sample (final concentration 0.4 mg/mL) in PBS was recorded from 10 - 95°C (0.5°C increments, 10 seconds hold per step) using the FRET channel. The thermograms, both the normalized relative fluorescence units (RFU) and the normalized derivative of relative fluorescence units (d(RFU)/dT) with respect to temperature (T) were recorded and compared. The peaks of the d(RFU)/dT-T thermogram are regarded as the melting temperatures (Tm) of the corresponding protein. Triplicate measurements were performed for each protein. Consistent with previous literature, the first peak of the mAb was attributed to the unfolded Fc fragment, while the second transition was interpreted as the melting of the Fab fragment.

3 Results

3.1 Expression conditions have a minor effect on N-glycosylation site occupancy

A genome edited β1,2-xylosyltransferase and core α1,3-fucosyltransferase *N. benthamiana* knockout line devoid of xylose and fucose carrying N-glycans (ΔXF KO), was used as expression host (manuscript in preparation). Two therapeutic IgG1 antibodies, namely rituximab (Rx) carrying only the conserved N-glycosylation site Asn297 and cetuximab (Cx) which has an additional N-glycosylation site in the Fab domain of the HC were characterized (Castilho et al., 2015; Li et al., 2016; Eidenberger et al., 2022). First, antibodies were transiently expressed under different conditions, including the use of various vector backbones (i.e. magnICON, pEAQ, pCAM, pTra), either as single genes or in tandem repeats, different bacterial concentrations for agroinfiltration and harvesting at diverse time points. Recombinant antibody expression was monitored by immunoblotting of total soluble protein extracts, with focus on the two HC associated bands, representing the glycosylated (~ 53 kDa band) and the underglycosylated HC (~ 50 kDa, Supplemental Figure S1). Densitometric analyses revealed significant amounts of underglycosylated HC in all settings, varying from 15-30% for Rx and 30-55% for Cx. These results are in line with previous observations (Castilho et al., 2018; Eidenberger et al., 2022) and demonstrate that changing expression conditions only had a minor impact on the N-glycosylation efficiency.

3.2 LdOST from the protist *Leishmania donovani* is retained in the ER of plant cells

Recently we characterized LmSTT3D, a single-subunit OST from *Leishmania major* that increases the N-glycosylation efficiencies of plant-produced recombinant glycoproteins (Castilho et al., 2018). GFP tagged LmSTT3D transiently expressed in *N. benthamiana* was located in the ER and displayed punctate structures that resemble Golgi bodies as reported previously (Castilho et al., 2018). A more detailed analysis by confocal microscopy revealed that LmSTT3D-GFP exhibits unusual aggregate-like subcellular structures

(Supplemental Figure S2A) and can alter the N-glycan profile of co-expressed recombinant antibodies towards mannosidic structures (Supplemental Figure S2B). While this negative impact on N-glycan processing was only occasionally observed, these findings indicate a possible interference of LmSTT3D with the plant endogenous glycosylation pathway that should be avoided for the robust production of homogenous recombinant glycoproteins.

To overcome this potential limitation of LmSTT3D, sequence databases of protists were searched for alternative single-subunit OSTs. From the obtained hits we selected the single-subunit OST from *Leishmania donovani*. While this protein termed LdOST displayed less than 80% amino acid sequence identity to LmSTT3D, crucial amino acid residues in the substrate binding region appear all conserved in LdOST and the predicted membrane protein topology is similar to LmSTT3D. This makes LdOST a potential single-subunit OST candidate to overcome IgG1 underglycosylation in plants (Supplemental Figures S3, S4).

We generated an LdOST-RFP fusion protein (Figure 1A), transiently expressed it in *N. benthamiana* and analyzed the subcellular localisation in leaf epidermal cells using confocal microscopy. In contrast to LmSTT3D-GFP (Supplemental Figure S2A), LdOST-RFP displayed exclusively ER labelling and no aberrant cellular structures that are indicative of aggregate formation or mislocalization. Co-localization with a GFP-tagged ER-marker (OST4-GFP) (Figure 1C) confirmed the subcellular localization (Figure 1B). When an untagged LdOST variant was co-expressed with pCAM-Rx and the ER-marker RFP-PDI5 (Shin et al., 2021), a typical ER labelling was observed for the ER marker suggesting that LdOST has no obvious adverse effect on the ER morphology (Figure 1D). By contrast, Rx plus LmSTT3D-GFP and RFP-PDI5 expression resulted in the formation of an aberrant ER with accumulation of the ER marker in punctuate structures (Figure 1E).

3.3 LdOST is a functional single-subunit OST that improves N-glycosylation of IgG1 antibodies

Next, we transiently co-expressed untagged LdOST with pCAM-Rx and Cx, respectively, in *N. benthamiana* ΔXF KO. In crude leaf extracts and on affinity-purified antibodies, the faster migrating HC band at approximately 50 kDa, representing the underglycosylated HC, disappeared in the presence of LdOST suggesting the expression of an active OST subunit (Figures 1F, G). Three different MS-based methods were applied to exactly quantify glycosylated versus non-glycosylated Fc of purified antibodies. First, Rx and Cx antibodies were subjected to tryptic digestion and the respective Asn297 containing polypeptides analyzed by LC-ESI-MS (Figures 2A, 3A). Second, N-glycans were released from the glycopeptides by digestion with PNGase A and the mixture of deglycosylated (EEQYQSTYR) and unglycosylated (EEQYNSTYR) peptides was examined by LC-ESI-MS. A peptide harbouring both the unglycosylated and deglycosylated (N to Q conversion) amino acid sequence motif was used as an internal standard for quantification and processed in the same way as the samples (Figures 2B, 3B) (Castilho et al., 2018). Finally, intact fully assembled IgG1 was analyzed by MS (Figures 2C, D, 3C, D).

Collectively, in the absence of any OST subunit, both antibodies displayed substantial amounts of unglycosylated HC-Fc with clear differences between Rx and Cx (26% and 46% non-glycosylated, respectively) (Figures 2B, 3B). LmSTT3D and LdOST were both able to significantly reduce the underglycosylation at site Asn297 of both antibodies (down to 3 and 10%, respectively). Intact MS-measurement of the assembled antibodies showed considerable amounts of non- and hemi-glycosylated Rx (together 28%) (Figure 2C) and Cx (together 43%) (Figure 3C). These values were significantly reduced by OST subunit co-expression with up to 97% of the assembled antibodies being fully glycosylated. Interestingly, under all tested conditions, the N-glycan occupancy at the Cx Fab N-glycosylation site was more than 99% (Supplemental Figure S5).

Expression of a single-subunit OST might directly or indirectly affect the N-glycan composition on the antibody. The direct effect could be caused by the transfer of an incompletely assembled oligosaccharide precursor ($Man_5GlcNAc_2$ to $Glc_2Man_9GlcNAc_2$ intermediates) (Kelleher and Gilmore, 2006). The indirect effect could be linked to changes in the secretory pathway which may alter the organisation of glycosyltransferases in the Golgi apparatus and thus N-glycan processing. Therefore, the N-glycan composition was determined by LC-ESI-MS. While, the N-glycan profile did not change by overexpression of LdOST, LmSTT3D co-expression resulted in a small but significant increase in oligomannosidic N-glycans (Figure 4; Supplemental Figures S6, S7). This increase was also observed for the Cx Fab N-glycans (Supplemental Figures S5, S8) and is consistent with the observed tendency of LmSTT3D to interfere with ER-morphology.

3.4 Improved N-glycan occupancy on rituximab increases the binding affinity to FcγRIIIa receptors

Having established that LdOST is functional, we further examined the impact of LdOST expression on Rx function. An antigen binding ELISA showed equal binding for the three tested Rx variants - Rx alone, Rx co-expressed with LdOST and Rx co-expressed with LmSTT3D, respectively (Supplemental Figure S9). In accordance, in a cell-based assay, Rx co-expressed with LdOST or with LmSTT3D displayed comparable binding to cells expressing the low affinity FcγRIIIa (F158 allotype) (Supplemental Figure S10). To analyze the binding kinetics in more detail and determine the binding affinities, we carried out SPR with the ectodomains of FcγRIIIa (F158) and FcγRIIIa (V158) (Figure 5). Rx co-expressed with LdOST and LmSTT3D, respectively, displayed reduced K_D values with both receptors indicating that improved N-glycosylation site occupancy increases the binding affinity to the receptor (Supplemental Table S1). The K_D of the mammalian cell-derived Rx (rituxan) was at least 10-fold higher being consistent with the negative impact of the core fucose on FcγRIIIa binding (Shields et al., 2002; Ferrara et al., 2011). Finally, we compared the thermal stability of the antibodies. While all plant-produced Rx variants displayed melting points that were comparable to rituxan, the Rx co-expressed with LdOST variant exhibited a thermal unfolding transition of the CH2 domain at a

10.3389/fpls.2023.1233666

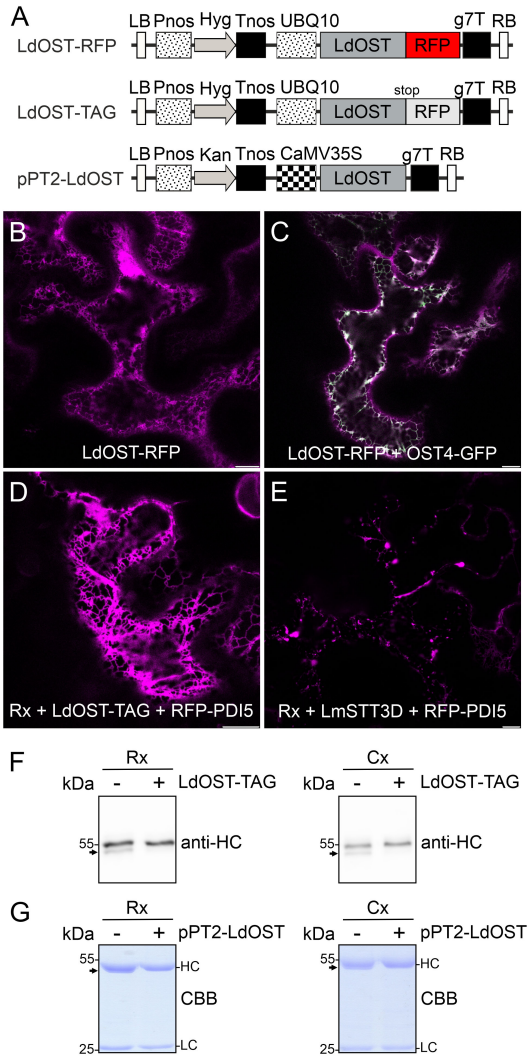

FIGURE 1
LdOST-RFP accumulates in the ER and increases the N-glycan occupancy on the IgG HC. **(A)** Schematic representation of the LdOST expression vectors. LB, left border; Pnos, nopaline synthase gene promoter; Hyg, hygromycin B phosphotransferase gene; Tnos, nopaline synthase gene terminator; UBQ10, *A. thaliana* ubiquitin-10 promoter; LdOST, *L. donovani* OST subunit open reading frame; RFP, red fluorescent protein; g7T, *Agrobacterium* gene 7 terminator; RB, right border. CaMV35S, cauliflower mosaic virus 35S promoter; Kan, neomycin phosphotransferase II gene. LdOST-TAG has a stop-codon that prevents fusion to RFP. **(B)** Confocal microscopy image of LdOST-RFP (magenta) expressed in wild-type *N. benthamiana* leaf epidermal cells. **(C)** Representative wild-type cell co-expressing LdOST-RFP (magenta) and the ER-marker OST4-GFP (green, co-localization in white). **(D)** pCAM-Rx (Rx) was co-expressed with LdOST-TAG and the ER marker RFP-PDI5 (magenta) in wild-type *N. benthamiana* leaf epidermal cells. **(E)** pCAM-Rx (Rx) was co-expressed with LmSTT3D and RFP-PDI5 (magenta) in wild-type *N. benthamiana* leaf epidermal cells. Scale bars = 10 µm. **(F)** pCAM-Rx (Rx) or cetuximab (Cx) antibodies were co-infiltrated with LdOST-TAG. Proteins were extracted from *N. benthamiana* ΔXF KO line 3 dpi and subjected to SDS-PAGE and immunoblotting using anti-IgG (anti-HC) antibodies. **(G)** SDS-PAGE and Coomassie Brilliant Blue (CBB) staining of purified Rx and Cx co-expressed with pPT2-LdOST in *N. benthamiana* ΔXF KO. The arrows indicate the migration position of the unglycosylated HC band.

slightly higher temperature (+ 1°C) than Rx alone (Table 1; Supplemental Figure S11).

4 Discussion

Plant-produced recombinant IgG1 displays considerable amounts of HC that is non-glycosylated at the conserved Asn297 site. This has been shown for transiently produced IgG1 in *N. benthamiana* leaves (Castilho et al., 2018; Jansing et al., 2019; Eidenberger et al., 2022) and for stable expression of antibodies derived from different tissues and species (Rademacher et al., 2008; Vamvaka et al., 2016). In contrast, mammalian cell-derived recombinant IgG1 is fully glycosylated at this site (Stadlmann et al., 2008). As previously reported, the magnICON expression vector-derived antibody displayed reduced glycosylation likely due to high expression levels and a subsequent overload of the endogenous plant OST machinery (Eidenberger et al., 2022). Our attempts to elucidate other factors that cause inefficient Fc glycosylation did not result in noticeable reduced or enhanced N-glycosylation efficiency suggesting that an unknown OST complex intrinsic feature is another major contributor for IgG1 underglycosylation. While most of the OST subunits, including the catalytic STT3 subunit, are present in plants and play a similar role in the N-glycosylation process (Koiwa et al., 2003; Lerouxel et al., 2005;

10.3389/fpls.2023.1233666

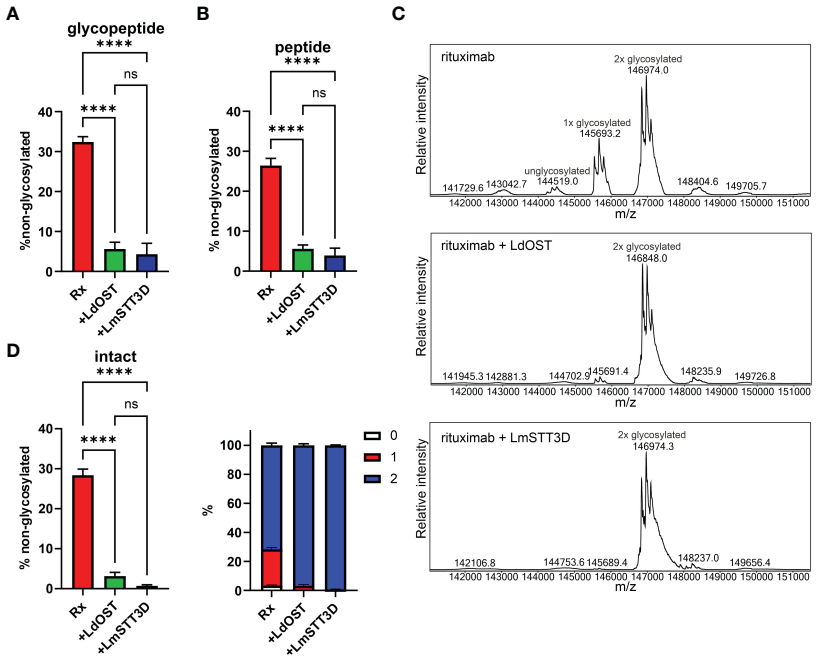

FIGURE 2
Quantification of the underglycosylation of rituximab (Rx). **(A)** % of non-glycosylated Asn297 in the HC of Rx. pCAM-Rx was expressed alone (Rx) (OD_{600} = 0.15) or in combination with LdOST-TAG (OD_{600} = 0.1) and LmSTT3D (OD_{600} = 0.1), respectively, in *N. benthamiana* ΔXF KO, purified and subjected to trypsin digestion. The tryptic peptides were analyzed by LC-ESI-MS. Error bars indicate mean ± SD (n = 3, "****" P < 0.0001 according to ANOVA). **(B)** Purified Rx samples were digested with trypsin, deglycosylated and analyzed by LC-ESI-MS. The amounts of deglycosylated and non-glycosylated peptides were obtained by comparison to an internal standard peptide treated in the same way. Error bars indicate mean ± SD (n = 3, "****" P < 0.0001 according to ANOVA). **(C)** The N-glycan site occupancy of fully assembled intact IgG was determined using LC-ESI-MS. The peaks corresponding to unglycosylated, hemi-glycosylated (1x glycosylated) and fully glycosylated (2x glycosylated) are highlighted. Multiple peaks represent different glycoforms and variations in the clipping of C-terminal lysine. **(D)** Quantification of the peaks from **(C)** Error bars indicate mean ± SD (n = 3, "****" P < 0.0001 according to ANOVA).

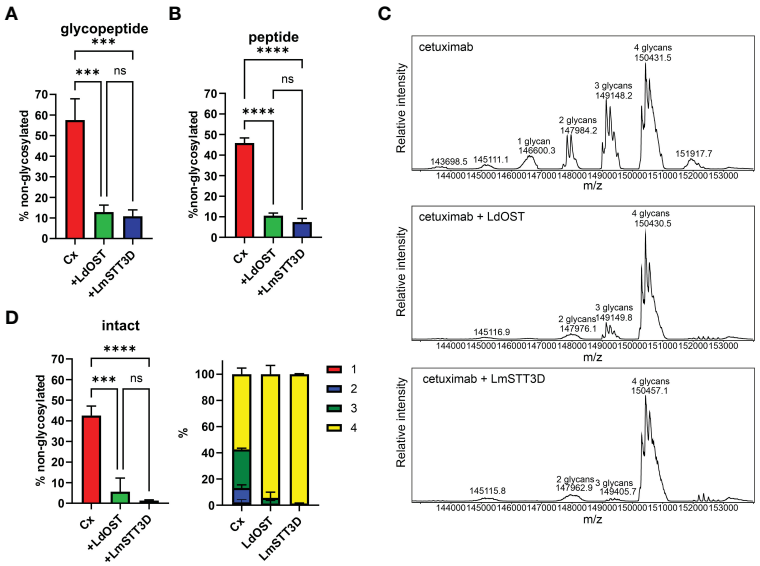

FIGURE 3
Quantification of the underglycosylation of cetuximab (Cx). **(A)** % of non-glycosylated Asn297 in the HC of Cx. Cx was expressed alone (HC OD_{600} = 0.15; LC OD_{600} = 0.1) or in combination with LdOST-TAG (OD_{600} = 0.1) and LmSTT3D (OD_{600} = 0.1), respectively, in *N. benthamiana* ΔXF KO, purified and subjected to trypsin digestion. The tryptic peptides were analyzed by LC-ESI-MS. Error bars indicate mean ± SD (n = 3, "***" P<0.001 according to ANOVA). **(B)** Purified Cx samples were digested with trypsin, deglycosylated and analyzed by LC-ESI-MS. The amounts of deglycosylated and non-glycosylated peptides were obtained by comparison to an internal standard peptide treated in the same way. Error bars indicate mean ± SD (n = 3, "****" P < 0.0001 according to ANOVA). **(C)** The N-glycan site occupancy of fully assembled intact IgG was determined using LC-ESI-MS. The peaks corresponding to assembled antibody carrying 1 to 4 N-glycans highlighted. Multiple peaks represent different glycoforms and variations in the clipping of C-terminal lysine. **(D)** Quantification of the peaks from C. Error bars indicate mean ± SD (n = 3, "***" P < 0.001, "****" P < 0.0001 according to ANOVA).

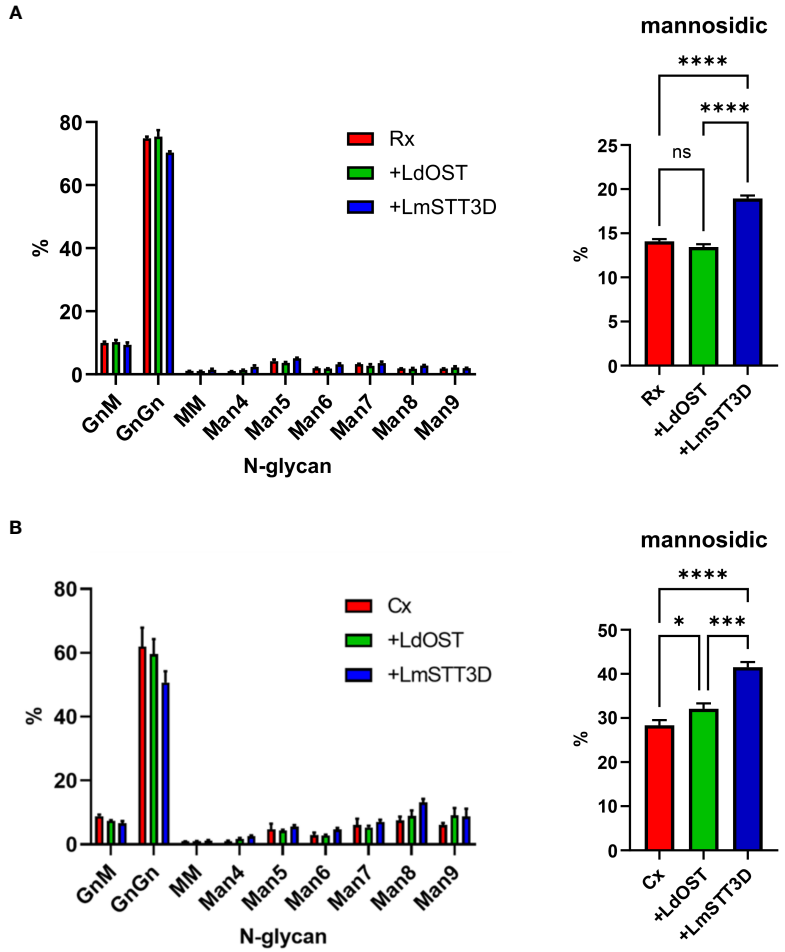

FIGURE 4
Quantification of the N-glycan composition at Asn297 of rituximab and cetuximab expressed in the *N. benthamiana* ΔXF KO line. **(A)** Glycoforms of rituximab (Rx). **(B)** Glycoforms of cetuximab (Cx). Bars represent the relative abundance (%) of glycoforms present at Asn297 in the Fc domain as determined by LC-ESI-MS of the glycopeptide EEQYNSTYR. For abbreviations of N-glycans the ProGlycAn system was used (https://www.proglycan.com/). Mannosidic N-glycans are the sum of Man4 to Man9. Error bars indicate mean ± SD (n = 3, "ns" not significant, "*" $P < 0.05$, "***" $P < 0.001$ "****" $P < 0.0001$ according to ANOVA).

Farid et al., 2013; Jeong et al., 2018), the molecular differences in distinct OST subunits or complex composition that affect substrate recognition or transfer of the oligosaccharide in plants are currently unknown. Since the Fab N-glycosylation site on the Cx HC is almost fully glycosylated, the limitation of the plant OST complex is very specific for distinct sites like Asn297 and is likely caused by the local amino acid environment adjacent to the N-glycosylation site (Murray et al., 2015). While the underglycosylation of highly expressed antibodies could potentially be counterbalanced by overexpression of the whole complex or individual plant OST subunits, expression of non-plant subunits (like LdOST or LmSTT3D) or protein engineering of plant OST subunits can provide solutions to overcome the plant OST complex intrinsic underglycosylation.

In previous studies, we utilized transient expression of LmSTT3D to increase the N-glycan occupancy on different recombinant glycoproteins expressed in plants (Castilho et al., 2018; Göritzer et al., 2020). Nevertheless, we occasionally observed unwanted side effects, like increased amounts of incompletely processed N-glycan structures on recombinant glycoproteins. This suggests an interference with other glycosylation related pathways and cellular processes that is likely related to mislocalization of LmSTT3D to the Golgi apparatus and other vesicular structures and an alteration of ER-derived structures (Castilho et al., 2018). In this regard, LdOST appears superior as it displayed only ER localisation and its co-expression with recombinant antibodies did not lead to unwanted alterations of the overall N-glycan profile (Supplemental Figure S12).

Importantly, biochemical and functional features of LdOST and LmSTT3D co-expression did not negatively impact biochemical and functional activities of the antibodies. In fact, some obvious glycosylation dependent activities, like FcγRIIIa binding affinities, were increased. These results are in line with previous studies that report decreased FcγRIIIa binding of hemi-glycosylated IgG1 (Ha et al., 2011). Also, the melting temperatures of Rx co-expressed with LdOST or with LmSTT3D were slightly higher than the one for Rx which is consistent with a reduced thermal stability of non-glycosylated IgG1 that mainly affects the CH2 domain (Garber and Demarest, 2007; Zheng et al., 2011; Hristodorov et al., 2013).

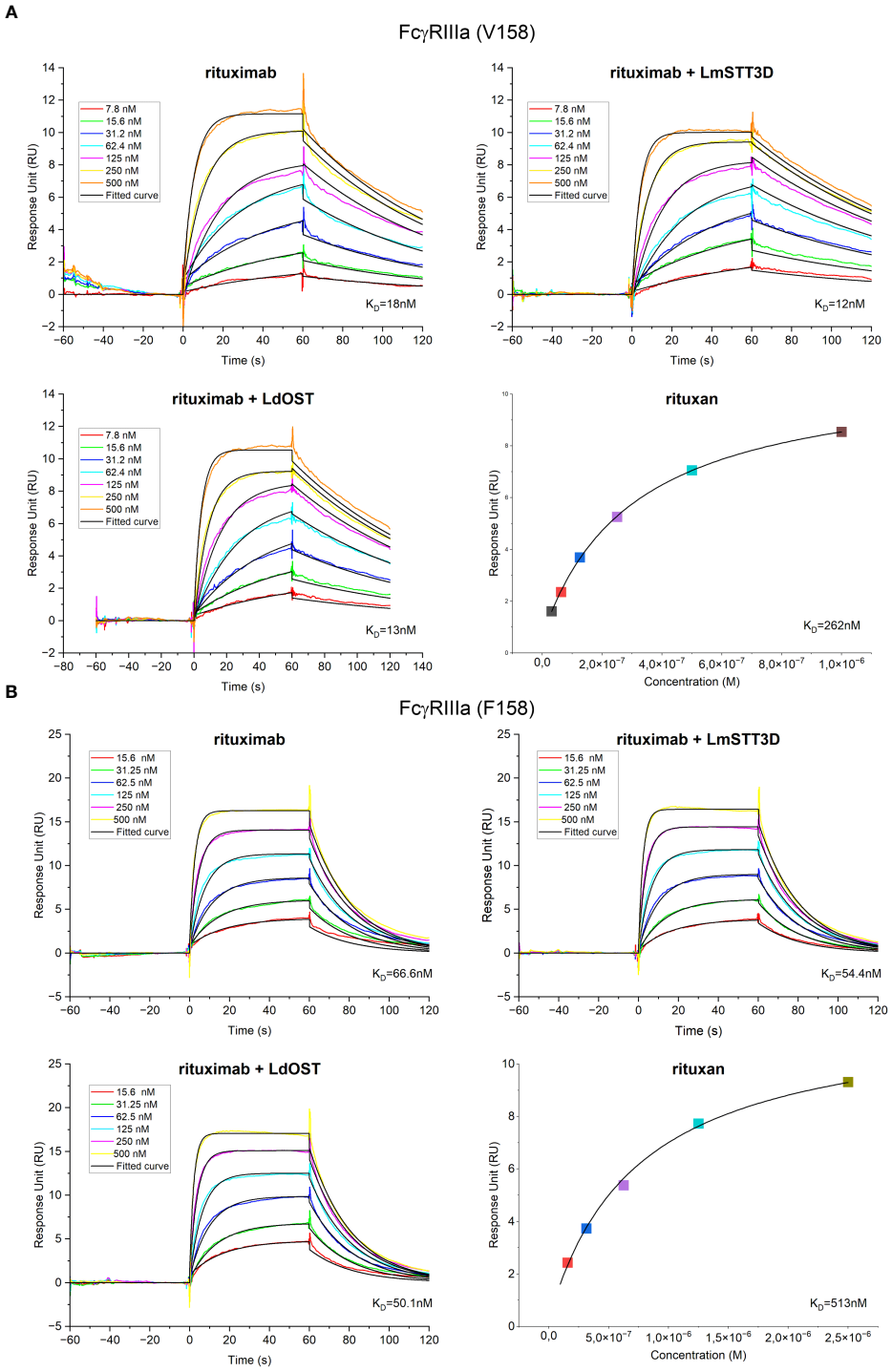

FIGURE 5
Receptor binding characteristics of rituximab (Rx). K_D values were obtained by SPR spectroscopy in multi-cycle kinetic experiments from three independent measurements for **(A)** FcγRIIIa (V158) and **(B)** FcγRIIIa (F158). Sensorgrams exhibit seven different concentrations ranging from 7.8 to 500 nM for FcγRIIIa (V158) and from 15.6 to 500 nM for FcγRIIIa (F158). Binding of the control rituxan was analyzed in steady state.

Augmentation of the N-glycosylation efficiency is not only relevant for IgG1 antibodies but also improves the formation of dimeric IgA antibodies (Göritzer et al., 2020) and is used together with chaperone co-expression as a technology to promote N-glycosylation-directed folding pathways in plants (Margolin et al., 2022; Margolin et al., 2023). We anticipate that LdOST is a useful single-subunit OST that can be broadly applied to overcome constraints in the plant production platform. Taken together, we exploited a novel glycoengineering tool that reduces the heterogeneity of plant made recombinant IgG1 antibodies without any adverse effect on functional properties. Given the high amounts of underglycosylation on plant-produced IgG1 and the noticeable effect

TABLE 1 Thermal stability (DSF).

Antibody	First peak (°C)	Second peak (°C)
Rituxan	68.8 ± 0.4	74.7 ± 0.3
Rituximab	68.8 ± 0.3	75.0 ± 0.0
Rituximab (LmSTT3D)	69.0 ± 0.5	75.2 ± 0.3
Rituximab (LdOST)	69.8 ± 0.4	75.2 ± 0.3

of incompletely glycosylated IgG1 on FcγRIIIa binding, it is advisable to use this glycoengineering approach for recombinant IgG1 production in plants to optimize effector functions.

Data availability statement

The data presented in the study are deposited in the PRIDE repository (Perez-Riverol et al., 2022), accession number PXD043623.

Author contributions

GB, JK-B, BK, VR, CG-G, and JG conducted the experiments. GB, VR, CG-G, M-AD'A, P-OL, PS, HS, and RS analyzed the results. RS conceptualized the study and wrote the paper with support from all authors. All authors contributed to the article and approved the submitted version.

Funding

This work was supported by the Austrian Science Fund (FWF) (P31920-B32 and W1224-B09) and the COMET center acib. The COMET center acib - Next Generation Bioproduction is funded by BMK, BMDW, SFG, Standortagentur Tirol, Government of Lower Austria und Vienna Business Agency in the framework of COMET - Competence Centers for Excellent Technologies (grant 94032). The COMET-Funding Program is managed by the Austrian Research Promotion Agency FFG. This project was supported by EQ-BOKU VIBT GmbH and the BOKU Core Facility Biomolecular & Cellular Analysis. The EQ-BOKU VIBT GmbH was not involved in the study design, collection, analysis, interpretation of data, the writing of this article or the decision to submit it for publication.

Acknowledgments

We thank Dr. David Montefiori and Dr. Gabriel Perez (Duke University School of Medicine, Durham, USA) for providing TZM-bl cells (contributed through the NIH HIV Reagent Program, Division of AIDS, NIAID, NIH). We thank Lin Sun (University of Natural Resources and Life Sciences, Vienna, Austria) for carrying out ELISA experiments, Ulrike Vavra (University of Natural Resources and Life Sciences, Vienna, Austria) for antibody purification, Prof. George Lomonossoff (John Innes Centre, Norwich, United Kingdom) and Plant Bioscience Limited (PBL) (Norwich, United Kingdom) for supplying the pEAQ-*HT* expression vector, Prof. Friedrich Altmann (University of Natural Resources and Life Sciences, Vienna, Austria) for providing Rituxan, Rudolf Figl (University of Natural Resources and Life Sciences, Vienna, Austria) for glycan purification and MALDI analysis and Irene Schaffner (University of Natural Resources and Life Sciences, Vienna, Austria) for assisting with surface plasmon resonance experiments. The SPR equipment was kindly provided by the EQ-BOKU VIBT GmbH and the BOKU Core Facility Biomolecular & Cellular Analysis. The Leica SP5 confocal microscope was kindly provided by the BOKU Core Facilities Multiscale Imaging and the MS equipment was kindly provided by the EQ-BOKU VIBT GmbH and the BOKU Core Facility Mass Spectrometry.

Conflict of interest

Authors M-AD'A, P-OL and PS were employed by the company Medicago.

The remaining authors declare that the research was conducted in the absence of any commercial or financial relationships that could be construed as a potential conflict of interest.

Publisher's note

Supplementary material

The Supplementary Material for this article can be found online at: https://www.frontiersin.org/articles/10.3389/fpls.2023.1233666/full#supplementary-material

References

Bendandi, M., Marillonnet, S., Kandzia, R., Thieme, F., Nickstadt, A., Herz, S., et al. (2010). Rapid, high-yield production in plants of individualized idiotype vaccines for non-Hodgkin's lymphoma. *Ann. Oncol.* 21, 2420–2427. doi: 10.1093/annonc/mdq256

Blasco, H., Lalmanach, G., Godat, E., Maurel, M. C., Canepa, S., Belghazi, M., et al. (2007). Evaluation of a peptide ELISA for the detection of rituximab in serum. *J. Immunol. Methods* 325, 127–139. doi: 10.1016/j.jim.2007.06.011

Castilho, A., Beihammer, G., Pfeiffer, C., Göritzer, K., Montero-Morales, L., Vavra, U., et al. (2018). An oligosaccharyltransferase from *Leishmania major* increases the N-glycan occupancy on recombinant glycoproteins produced in *Nicotiana benthamiana*. *Plant Biotechnol. J.* 16, 1700–1709. doi: 10.1111/pbi.12906

Castilho, A., Gruber, C., Thader, A., Oostenbrink, C., Pechlaner, M., Steinkellner, H., et al. (2015). Processing of complex N-glycans in IgG Fc-region is affected by core fucosylation. *MAbs* 7, 863–870. doi: 10.1080/19420862.2015.1053683

Chen, Q. (2022). Development of plant-made monoclonal antibodies against viral infections. *Curr. Opin. Virol.* 52, 148–160. doi: 10.1016/j.coviro.2021.12.005

Dicker, M., Tschofen, M., Maresch, D., König, J., Juarez, P., Orzaez, D., et al. (2016). Transient glyco-engineering to produce recombinant igA1 with defined N- and O-glycans in plants. *Front. Plant Sci.* 7, 18. doi: 10.3389/fpls.2016.00018

Eidenberger, L., Eminger, F., Castilho, A., and Steinkellner, H. (2022). Comparative analysis of plant transient expression vectors for targeted N-glycosylation. *Front. Bioeng Biotechnol.* 10, 1073455. doi: 10.3389/fbioe.2022.1073455

Eidenberger, L., Kogelmann, B., and Steinkellner, H. (2023). Plant-based biopharmaceutical engineering. *Nat. Rev. Bioeng.* 1, 426–439. doi: 10.1038/s44222-023-00044-6

Farid, A., Malinovsky, F. G., Veit, C., Schoberer, J., Zipfel, C., and Strasser, R. (2013). Specialized roles of the conserved subunit OST3/6 of the oligosaccharyltransferase complex in innate immunity and tolerance to abiotic stresses. *Plant Physiol.* 162, 24–38. doi: 10.1104/pp.113.215509

Ferrara, C., Grau, S., Jäger, C., Sondermann, P., Brünker, P., Waldhauer, I., et al. (2011). Unique carbohydrate-carbohydrate interactions are required for high affinity binding between FcgammaRIII and antibodies lacking core fucose. *Proc. Natl. Acad. Sci. U.S.A.* 108, 12669–12674. doi: 10.1073/pnas.1108455108

Forthal, D. N., Gach, J. S., Landucci, G., Jez, J., Strasser, R., Kunert, R., et al. (2010). Fc-glycosylation influences Fcγ receptor binding and cell-mediated anti-HIV activity of monoclonal antibody 2G12. *J. Immunol.* 185, 6876–6882. doi: 10.4049/jimmunol.1002600

Garber, E., and Demarest, S. J. (2007). A broad range of Fab stabilities within a host of therapeutic IgGs. *Biochem. Biophys. Res. Commun.* 355, 751–757. doi: 10.1016/j.bbrc.2007.02.042

Göritzer, K., Goet, I., Duric, S., Maresch, D., Altmann, F., Obinger, C., et al. (2020). Efficient *N*-glycosylation of the heavy chain tailpiece promotes the formation of plant-produced dimeric igA. *Front. Chem.* 8, 346. doi: 10.3389/fchem.2020.00346

Göritzer, K., Maresch, D., Altmann, F., Obinger, C., and Strasser, R. (2017). Exploring site-specific N-glycosylation of HEK293 and plant-produced human igA isotypes. *J. Proteome Res.* 16, 2560–2570. doi: 10.1021/acs.jproteome.7b00121

Ha, S., Ou, Y., Vlasak, J., Li, Y., Wang, S., Vo, K., et al. (2011). Isolation and characterization of IgG1 with asymmetrical Fc glycosylation. *Glycobiology* 21, 1087–1096. doi: 10.1093/glycob/cwr047

Hristodorov, D., Fischer, R., Joerissen, H., Muller-Tiemann, B., Apeler, H., and Linden, L. (2013). Generation and comparative characterization of glycosylated and aglycosylated human IgG1 antibodies. *Mol. Biotechnol.* 53, 326–335. doi: 10.1007/s12033-012-9531-x

Hüttner, S., Veit, C., Vavra, U., Schoberer, J., Liebminger, E., Maresch, D., et al. (2014). Arabidopsis class I α-mannosidases MNS4 and MNS5 are involved in endoplasmic reticulum-associated degradation of misfolded glycoproteins. *Plant Cell* 26, 1712–1728. doi: 10.1105/tpc.114.123216

Jansing, J., Sack, M., Augustine, S. M., Fischer, R., and Bortesi, L. (2019). CRISPR/Cas9-mediated knockout of six glycosyltransferase genes in *Nicotiana benthamiana* for the production of recombinant proteins lacking β-1,2-xylose and core α-1,3-fucose. *Plant Biotechnol. J.* 17, 350–361. doi: 10.1111/pbi.12981

Jeong, I. S., Lee, S., Bonkhofer, F., Tolley, J., Fukudome, A., Nagashima, Y., et al. (2018). Purification and characterization of *Arabidopsis thaliana* oligosaccharyltransferase complexes from the native host: a protein super-expression system for structural studies. *Plant J.* 94, 131–145. doi: 10.1111/tpj.13847

Ju, M. S., and Jung, S. T. (2014). Aglycosylated full-length IgG antibodies: steps toward next-generation immunotherapeutics. *Curr. Opin. Biotechnol.* 30, 128–139. doi: 10.1016/j.copbio.2014.06.013

Kelleher, D., and Gilmore, R. (2006). An evolving view of the eukaryotic oligosaccharyltransferase. *Glycobiology* 16, 47R–62R. doi: 10.1093/glycob/cwj066

Koiwa, H., Li, F., Mccully, M., Mendoza, I., Koizumi, N., Manabe, Y., et al. (2003). The STT3a subunit isoform of the Arabidopsis oligosaccharyltransferase controls adaptive responses to salt/osmotic stress. *Plant Cell* 15, 2273–2284. doi: 10.1105/tpc.013862

Kolarich, D., and Altmann, F. (2000). N-Glycan analysis by matrix-assisted laser desorption/ionization mass spectrometry of electrophoretically separated nonmammalian proteins: application to peanut allergen Ara h 1 and olive pollen allergen Ole e 1. *Anal. Biochem.* 285, 64–75. doi: 10.1006/abio.2000.4737

Lerouxel, O., Mouille, G., Andème-Onzighi, C., Bruyant, M., Séveno, M., Loutelier-Bourhis, C., et al. (2005). Mutants in DEFECTIVE GLYCOSYLATION, an Arabidopsis homolog of an oligosaccharyltransferase complex subunit, show protein underglycosylation and defects in cell differentiation and growth. *Plant J.* 42, 455–468. doi: 10.1111/j.1365-313X.2005.02392.x

Li, J., Stoddard, T. J., Demorest, Z. L., Lavoie, P. O., Luo, S., Clasen, B. M., et al. (2016). Multiplexed, targeted gene editing in *Nicotiana benthamiana* for glyco-engineering and monoclonal antibody production. *Plant Biotechnol. J.* 14, 533–542. doi: 10.1111/pbi.12403

Loos, A., Gruber, C., Altmann, F., Mehofer, U., Hensel, F., Grandits, M., et al. (2014). Expression and glycoengineering of functionally active heteromultimeric IgM in plants. *Proc. Natl. Acad. Sci. U.S.A.* 111, 6263–6268. doi: 10.1073/pnas.1320544111

MacLean, B., Tomazela, D. M., Shulman, N., Chambers, M., Finney, G. L., Frewen, B., et al. (2010). Skyline: an open source document editor for creating and analyzing targeted proteomics experiments. *Bioinformatics* 26, 966–968. doi: 10.1093/bioinformatics/btq054

Margolin, E., Allen, J. D., Verbeek, M., Chapman, R., Meyers, A., Van Diepen, M., et al. (2022). Augmenting glycosylation-directed folding pathways enhances the fidelity of HIV Env immunogen production in plants. *Biotechnol. Bioeng* 119, 2919–2937. doi: 10.1002/bit.28169

Margolin, E., Schafer, G., Allen, J. D., Gers, S., Woodward, J., Sutherland, A. D., et al. (2023). A plant-produced SARS-CoV-2 spike protein elicits heterologous immunity in hamsters. *Front. Plant Sci.* 14, 1146234. doi: 10.3389/fpls.2023.1146234

Murray, A. N., Chen, W., Antonopoulos, A., Hanson, S. R., Wiseman, R. L., Dell, A., et al. (2015). Enhanced aromatic sequons increase oligosaccharyltransferase glycosylation efficiency and glycan homogeneity. *Chem. Biol.* 22, 1052–1062. doi: 10.1016/j.chembiol.2015.06.017

Perez-Riverol, Y., Bai, J., Bandla, C., Garcia-Seisdedos, D., Hewapathirana, S., Kamatchinathan, S., et al. (2022). The PRIDE database resources in 2022: a hub for mass spectrometry-based proteomics evidences. *Nucleic Acids Res.* 50, D543–D552. doi: 10.1093/nar/gkab1038

Rademacher, T., Sack, M., Arcalis, E., Stadlmann, J., Balzer, S., Altmann, F., et al. (2008). Recombinant antibody 2G12 produced in maize endosperm efficiently neutralizes HIV-1 and contains predominantly single-GlcNAc N-glycans. *Plant Biotechnol. J.* 6, 189–201. doi: 10.1111/j.1467-7652.2007.00306.x

Reusch, D., and Tejada, M. L. (2015). Fc glycans of therapeutic antibodies as critical quality attributes. *Glycobiology* 25, 1325–1334. doi: 10.1093/glycob/cwv065

Ridgley, L. A., Falci Finardi, N., Gengenbach, B. B., Opdensteinen, P., Croxford, Z., Ma, J. K., et al. (2023). Killer to cure: Expression and production costs calculation of tobacco plant-made cancer-immune checkpoint inhibitors. *Plant Biotechnol. J.* 21, 1254–1269. doi: 10.1111/pbi.14034

Ruocco, V., and Strasser, R. (2022). Transient expression of glycosylated SARS-coV-2 antigens in n*icotiana benthamiana*. *Plants (Basel)* 11, 1093. doi: 10.3390/plants11081093

Schoberer, J., König, J., Veit, C., Vavra, U., Liebminger, E., Botchway, S. W., et al. (2019). A signal motif retains Arabidopsis ER-α-mannosidase I in the cis-Golgi and prevents enhanced glycoprotein ERAD. *Nat. Commun.* 10, 3701. doi: 10.1038/s41467-019-11686-9

Shanmugaraj, B., Malla, A., Bulaon, C. J. I., Phoolcharoen, W., and Phoolcharoen, N. (2022). Harnessing the potential of plant expression system towards the production of vaccines for the prevention of human papillomavirus and cervical cancer. *Vaccines (Basel)* 10, 2064. doi: 10.3390/vaccines10122064

Shields, R. L., Lai, J., Keck, R., O'connell, L. Y., Hong, K., Meng, Y. G., et al. (2002). Lack of fucose on human IgG1 N-linked oligosaccharide improves binding to human Fcgamma RIII and antibody-dependent cellular toxicity. *J. Biol. Chem.* 277, 26733–26740. doi: 10.1074/jbc.M202069200

Shin, Y. J., König-Beihammer, J., Vavra, U., Schwestka, J., Kienzl, N. F., Klausberger, M., et al. (2021). N-glycosylation of the SARS-coV-2 receptor binding domain is important for functional expression in plants. *Front. Plant Sci.* 12, 689104. doi: 10.3389/fpls.2021.689104

Shrimal, S., and Gilmore, R. (2019). Oligosaccharyltransferase structures provide novel insight into the mechanism of asparagine-linked glycosylation in prokaryotic and eukaryotic cells. *Glycobiology* 29, 288–297. doi: 10.1093/glycob/cwy093

Stadlmann, J., Pabst, M., Kolarich, D., Kunert, R., and Altmann, F. (2008). Analysis of immunoglobulin glycosylation by LC-ESI-MS of glycopeptides and oligosaccharides. *Proteomics* 8, 2858–2871. doi: 10.1002/pmic.200700968

Strasser, R. (2016). Plant protein glycosylation. *Glycobiology* 26, 926–939. doi: 10.1093/glycob/cww023

Strasser, R., Stadlmann, J., Schähs, M., Stiegler, G., Quendler, H., Mach, L., et al. (2008). Generation of glyco-engineered *Nicotiana benthamiana* for the production of monoclonal antibodies with a homogeneous human-like N-glycan structure. *Plant Biotechnol. J.* 6, 392–402. doi: 10.1111/j.1467-7652.2008.00330.x

Strasser, R., Stadlmann, J., Svoboda, B., Altmann, F., Glössl, J., and Mach, L. (2005). Molecular basis of N-acetylglucosaminyltransferase I deficiency in *Arabidopsis thaliana* plants lacking complex N-glycans. *Biochem. J.* 387, 385–391. doi: 10.1042/BJ20041686

Sun, L., Kallolimath, S., Palt, R., Stiasny, K., Mayrhofer, P., Maresch, D., et al. (2021). Increased *in vitro* neutralizing activity of SARS-CoV-2 IgA1 dimers compared to monomers and IgG. *Proc. Natl. Acad. Sci. U.S.A.* 118, e2107148118. doi: 10.1073/pnas.2107148118

Vamvaka, E., Twyman, R. M., Murad, A. M., Melnik, S., Teh, A. Y., Arcalis, E., et al. (2016). Rice endosperm produces an underglycosylated and potent form of the HIV-neutralizing monoclonal antibody 2G12. *Plant Biotechnol. J.* 14, 97–108. doi: 10.1111/pbi.12360

Walsh, G., and Walsh, E. (2022). Biopharmaceutical benchmarks 2022. *Nat. Biotechnol.* 40, 1722–1760. doi: 10.1038/s41587-022-01582-x

Wang, T. T., and Ravetch, J. V. (2019). Functional diversification of IgGs through Fc glycosylation. *J. Clin. Invest.* 129, 3492–3498. doi: 10.1172/JCI130029

Zeitlin, L., Pettitt, J., Scully, C., Bohorova, N., Kim, D., Pauly, M., et al. (2011). Enhanced potency of a fucose-free monoclonal antibody being developed as an Ebola virus immunoprotectant. *Proc. Natl. Acad. Sci. U.S.A.* 108, 20690–20694. doi: 10.1073/pnas.1108360108

Zheng, K., Bantog, C., and Bayer, R. (2011). The impact of glycosylation on monoclonal antibody conformation and stability. *MAbs* 3, 568–576. doi: 10.4161/mabs.3.6.17922

frontiers | Frontiers in Plant Science

TYPE Original Research
PUBLISHED 08 August 2023
DOI 10.3389/fpls.2023.1215580

OPEN ACCESS

EDITED BY
Kathleen L. Hefferon,
Cornell University, United States

REVIEWED BY
Dhananjay K. Pandey,
Amity University, Jharkhand, India
Kathrin Göritzer,
St. George's, University of London,
United Kingdom

*CORRESPONDENCE
Kazuhito Fujiyama
fujiyama@icb.osaka-u.ac.jp

RECEIVED 02 May 2023
ACCEPTED 03 July 2023
PUBLISHED 08 August 2023

CITATION
Nguyen KD, Kajiura H, Kamiya R, Yoshida T, Misaki R and Fujiyama K (2023) Production and *N*-glycan engineering of Varlilumab in *Nicotiana benthamiana*. *Front. Plant Sci.* 14:1215580. doi: 10.3389/fpls.2023.1215580

Production and *N*-glycan engineering of Varlilumab in *Nicotiana benthamiana*

Kim Dua Nguyen[1], Hiroyuki Kajiura[1,2], Ryo Kamiya[3], Takahiro Yoshida[3], Ryo Misaki[1,2] and Kazuhito Fujiyama[1,2,4]*

[1]International Center for Biotechnology, Osaka University, Osaka, Japan, [2]Industrial Biotechnology Initiative Division, Institute for Open and Transdisciplinary Research Initiatives (OTRI), Osaka University, Osaka, Japan, [3]GreenLand-Kidaya Group Co Ltd., Fukui, Japan, [4]Osaka University Cooperative Research Station in Southeast Asia (OU: CRS), Faculty of Science, Mahidol University, Bangkok, Thailand

N-glycan engineering has dramatically evolved for the development and quality control of recombinant antibodies. Fc region of IgG contains two *N*-glycans whose galactose terminals on Fc-glycan have been shown to increase the stability of CH2 domain and improve effector functions. *Nicotiana benthamiana* has become one of the most attractive production systems for therapeutic antibodies. In this study, Varlilumab, a CD27-targeting monoclonal antibody, was transiently produced in fresh leaves of soil-grown and hydroponic-grown *N. benthamiana*, resulted in the yield of 174 and 618 μg/gram, respectively. However, the IgG produced in wild-type *N. benthamiana* lacked the terminal galactose residues in its *N*-glycan. Therefore, *N*-glycan engineering was applied to fine-tune recombinant antibodies produced in plant platforms. We further co-expressed IgG together with murine β1,4-galactosyltransferase (β1,4-GALT) to modify plant *N*-glycan with β1,4-linked Gal residue(s) and *Arabidopsis thaliana* β1,3-galactosylatransferase (β1,3-GALT) to improve galactosylation. The co-expression of IgG with each of GALTs successfully resulted in modification of *N*-glycan structures on the plant-produced IgG. Notably, IgG co-expressed with murine β1,4-GALT in soil-grown *N. benthamiana* had 42.5% of *N*-glycans variants having galactose (Gal) residues at the non-reducing terminus and 55.3% of that in hydroponic-grown *N. benthamiana* plants. Concomitantly, *N*-glycan profile analysis of IgG co-expressed with β1,3-GALT demonstrated that there was an increased efficiency of galactosylation and an enhancement in the formation of Lewis a structure in plant-derived antibodies. Taken together, our findings show that the first plant-derived Varlilumab was successfully produced with biantennary β1,4-galactosylated *N*-glycan structures.

KEYWORDS

cancer immunotherapy, galactosyltransferase, hydroponics, monoclonal antibody (mAb), *Nicotiana benthamiana*, Varlilumab

Introduction

The use of therapeutic monoclonal antibodies for the treatment of cancers, Alzheimer's disease, and other conditions (Perneczky et al., 2023) has increased substantially over the past years (Kaplon et al., 2023). Accordingly, there has been a demand for high-yield production of recombinant antibodies at low cost. Recently, whole-plant *Nicotiana benthamiana* was selected as a host for such recombinant protein production due to its various advantages, including low production cost, absence of animal contamination, high biomass, and fast and easy scale-up (Sheshukova et al., 2016). These characteristics make *N. benthamiana* an effective alternative production platform for biopharmaceuticals. Moreover, *N. benthamiana* is efficient for agroinfiltration-based transient expression of a variety of antibodies (Sainsbury and Lomonossoff, 2008; Grohs et al., 2010). For instance, ZMapp, a cocktail of three plant-derived antibodies for neutralizing Ebola virus (Qiu et al., 2014), and Covifenz (Medicago), the first plant-based virus-like particles for vaccine against SARS-COV-2 (Pillet et al., 2022), have demonstrated the advantages of *N. benthamiana* over other production platforms during the pandemics. In addition, one of the plant-growing systems is the hydroponic system, which is a method of growing plants in nutrient solutions with or without the use of a mechanical-support medium. The solutions in this system are circulated by a pump, which allows nutrient recovery and minimizes water loss in sustainable agriculture (Kumar and Cho, 2014). Hydroponic system is closed and free from soil-borne diseases, so it was chosen to produce MucoRice-CTB (a rice-based oral vaccine against cholera) to qualify the current good manufacturing practice (cGMP) regulations (Kashima et al., 2016). Several hydroponic systems for *Arabidopsis* and other model plants have been developed (Alatorre-Cobos et al., 2014). Recently, hydroponic system was also employed to transiently produce two SARS-CoV-2 neutralizing antibodies in *N. benthamiana* modified plants (Frigerio et al., 2022). Therefore, the merit of hydroponic-based *N. benthamiana* in producing recombinant proteins such as antibodies should be extensively investigated.

Varlilumab is a human monoclonal antibody IgG1 that targets CD27, a receptor belonging to the tumor necrosis factor (TNF) receptor superfamily. CD27 is well known for its important role in T-cell immunity and as a cell-surface marker of B- and T-cell malignancies. Varlilumab was initially generated using Ig transgenic mice and developed as a potential therapeutic agent for CD27-expressing lymphoma and leukemia (Vitale et al., 2012). In a later study, Varlilumab exhibited potent antitumor activity as both monotherapy and combination therapy in preclinical models (Wasiuk et al., 2017). In combination with Nivolumab (a PD-1 immune checkpoint inhibitor antibody), Varlilumab has shown success in a phase 2 clinical trial as an anti-CD27 agonist antibody against recurrent glioblastoma (Reardon et al., 2018). The safety and activity of Varlilumab have also been evaluated in patients with advanced solid tumors (Burris et al., 2017).

Varlilumab and other IgG molecules contain an *N*-glycosylation site at Asn297 of the Fc region, which plays a critical role in Fc effector functions, such as antibody-dependent cellular cytotoxicity (ADCC) and complement-dependent cytotoxicity (CDC) (Mimura et al., 2018). As a result, *N*-glycan engineering of the Fc regions is a rational strategy for improving the safety and efficacy of recombinant antibodies. *N*-glycosylation occurs first in the endoplasmic reticulum and is subsequently processed during the transport through Golgi apparatus compartments (Seemann et al., 2000; Bard et al., 2006). At each compartment, there are varying compositions of *N*-glycosylation enzymes which catalyze *N*-glycan extension reactions on the secretory *N*-glycoproteins (Elsner et al., 2003). *N*-glycosylation facilitates the correct folding of proteins and provides protease resistance and solubility (Varki, 2017). As mentioned earlier, antibodies are *N*-glycoproteins carrying conserved *N*-glycans at the Fc domain. Different *N*-glycosylation patterns can profoundly affect the biological and therapeutic functions of antibodies (Wang et al., 2019). Highly β1,4-galactosylated antibodies exhibit higher affinity for FcγRIIIa and greater thermal stability because the galactose moiety decreases the conformational entropy of CH2, facilitating the engagement of Fc to FcγRIIIa. Thus, β1,4-galactosylated antibodies possess higher ADCC activity and CDC activity (Kiyoshi et al., 2018). β1,4-galactosyltransferase (β1,4-GALT) catalyzes the transfer of galactose (Gal) from UDP-Gal to the *N*-acetylglucosamine (GlcNAc) residue at the non-reducing terminal of *N*-glycan in mammals, whereas *N. benthamiana* plants lack this enzyme in the Golgi apparatus and instead have β1,3-galactosyltransferase (β1,3-GALT).

Previous studies have focused on expressing human β1,4-GALT in transgenic tobacco cell lines (Palacpac et al., 1999) and transgenic plants of *N. tabacum* (Bakker et al., 2001). In *N. benthaminana*, substantial efforts have been made to achieve plant-derived recombinant proteins with galactose terminated *N*-glycan structures. Notably, different variants of human β1,4-GALT were introduced in *N. benthamiana* to increase the level of biantennary galactosylated *N*-glycans (Hesselink et al., 2014) and multigene vectors containing human sialylation pathway including β1,4-galactosylation were transformed into *N. benthamiana* plants for the generation of complex sialylated structures (Kallolimath et al., 2016). However, these studies employed stable expression in plant cell-lines or transgenic plants, which is a slow and labor-intensive approach (Rivera et al., 2012; Sethi et al., 2021). To circumvent this bottleneck, transient co-expression of β1,4-GALT in *N. benthamiana* was studied (Vézina et al., 2009). This strategy realized a high yield and allowed the fast modification of *N*-glycan profiles of recombinant antibodies. Still, the expression of the original β1,4-GALT or a fusion of β1,4-GALT and N-acetylglucosaminyltransferaseI (GNTI) construct might block the action of other enzymes such as Golgi-α-mannosidase II, which would also result in partially processed glycans (Saint-Jore-Dupas et al., 2006; Vézina et al., 2009). Significant efforts have been contributed to improve β1,4-galactosylation of IgG by targeting β1,4-GALT to the *trans*-Golgi compartments in both stable and transient expression of *N. benthamiana* (Strasser et al., 2009; Forthal et al., 2010; Castilho et al., 2011; Loos et al., 2015; Schneider et al., 2015; Kallolimath et al., 2018). One of the impressive achievements was the transient co-expression of STGalT binary vector with IgG in a glyco-engineered ΔXTFT *N. benthamiana* plants. STGalT is a chimeric protein consisting of

cytoplasmic tail, transmembrane domain and stem (CTS) region of α2,6-sialyltransferas (ST). This co-expression obtained more than 60% of the structures carried galactose terminals after 4 days post-infiltration (Castilho et al., 2011). It is suggested that these approaches were effective to achieve correct localization of β1,4-GALT and hybrid *N*-glycan structures in plants. In previous studies, the CTS of mammalian α2,6-ST was chosen for the fusion with the catalytic domain of β1,4-GALT because this enzyme targeted to the *trans*-Golgi compartments and successfully modified the *N*-glycan profile of plant-derived IgGs. To further investigate and establish simple *in vivo N*-glycan modification steps for the generation of biantennary galactosylated IgG in transient expression of *N. benthamiana*, β1,3-GALT was chosen because the subcellular localization of β1,3-GALT was predicted to be exclusively located in the plant Golgi apparatus. Unlike mammalian β1,4-GALT, plant β1,3-GALT transfers a Gal to a terminal GlcNAc residue in β1,3-linkage (Strasser et al., 2007). This suggests that both mammalian β1,4-GALT and plant β1,3-GALT may have similar localization patterns.

In this study, we expressed recombinant Varlilumab in soil- and hydroponic-based *N. benthamiana* plants. The *N*-glycan profiles of plant-derived Varlilumab were independently modified by introducing β1,4-GALT and over-expressing β1,3-GALT. Our work demonstrated that the first plant-derived Varlilumab was successfully produced with biantennary β1,4-galactosylated *N*-glycan structures using a chimeric β1,3β1,4-GALT.

Materials and methods

Plant expression vector construction

Genes encoding variable regions of Varlilumab H and L chains (clone 1F5, US 2011/0274685 A1) were synthesized by Invitrogen (Carlsbad, CA; USA). The coding regions of H and L chains were introduced to pQCXIP (TaKaRa Bio, Otsu, Japan) and pQCXIH (TaKaRa Bio) while retaining the human H and L, respectively, to form the full-length Varlilumab H and L chains. The modified pPK1-BAR binary plasmid was previously constructed (Sariyatun et al., 2021). Inserts of full-length H and L chains were amplified from pQCXIP-HC and pQCXIH-LC with the addition of *Xba* I sites, respectively. VarHC-*Xba*I-Fw 5'-TAC TCT AGA ATG GAG TTT GGG CTG AGC TGG G-3' and VarHC-*Xba*I-Rv 5'-TAC TCT AGA CTA TTT ACC CGG AGA CAG GGA GA-3' were used for the amplification of Varlilumab H, while Varlilumab L was amplified by the primer pair VarLC-*Xba*I-Fw 5' TAC TCT AGA ATG AGG GTC CTC GCT CAG CT-3' and VarLC-*Xba*I-Rv 5'-TAC TCT AGA CTA ACA CTC TCC CCT GTT GAA GCT-3' (the *Xba* I restriction site is underlined). pFK1-BAR fragments were digested by *Spe*I and the inserts were cleaved by the *Xba* I restriction enzyme (New England Biolabs, Beverly, MA) and subsequently ligated using Ligation High Ver. 2.0 (Toyobo, Osaka, Japan). Both *Spe* I and *Xba* I produced compatible sticky ends (CTAG), so the digested products can be ligated. This resulted in circular binary plasmids containing H and L chain-expression cassettes, which were designated pFK1-BAR-VarHC and pFK1-BAR-VarLC. cDNAs encoding for *A. thaliana* β1,3-GALT (At1g26810) and murine β1,4-GALT were isolated and then introduced in the *Nde* I/*Sac* I restriction site of the binary plasmid pRI201-AN (TaKaRa Bio).

Agroinfiltration

The vectors expressing the Varlilumab H and L chains and GALTs were inserted into *Agrobacterium tumefaciens* strain LBA4404 by electroporation (Bio-Rad, Hercules, CA) with voltage, resistance, and capacitance at 2.4 kV, 200 Ω, and 25 μF, respectively. The RNA silencing suppressor 19 (p19) vector was kindly provided by Prof. Atsushi Takeda (Ritsumeikan University). *A. tumefaciens* transformants were selected using a combination of kanamycin (50 mg/L), rifampicin (50 mg/L), and streptomycin (50 mg/L). A single colony of *Agrobacterium* was first inoculated into 5 ml of 2xYT liquid medium with the above-mentioned antibiotics and cultivated at 28°C overnight, followed by a continuous cultivation of 200 ml of the thus-prepared medium. Cells were collected by centrifugation at 4,000 x *g*. *Agrobacterium* harboring different vectors (H, L, RNA silencing p19 or GALTs) was resuspended and mixed in modified infiltration buffer (10 mM $MgSO_4$, 10 mM MES, 0.56 mM ascorbic acid, 0.03% Tween-20, 100 mM acetosyringone, pH 5.8) at OD_{600} 0.5 following the method of Zhao et al. (2017). The *Agrobacterium* containing H or L was mixed at a 1:1 ratio for expression of Varlilumab. For co-expression with the RNA silencing suppressor p19, the ratio was 1:1:2 for H, L, and p19, respectively. In GALT co-expression experiments, the ratio was 1:1:1:1 for four different constructs (H, L, p19 and GALT). *N. benthamiana* plants were infiltrated by vacuum infiltration (Chen et al., 2013). Infiltrated plants were grown in a controlled plant room with a 16 h light/8 h dark cycle at 28°C for 10 days. The hydroponic-based *N. benthamiana* wild type plants used in this study were prepared by the GreenLand-Kidaya Group (Fukui, Japan). Briefly, *N. benthamiana* seeds were sown into a urethan board in the dark at 21°C. Then, the germinated seedlings were grown at 21°C under a 16 h LED-photoperiod of 420 mmol/m^2s (Yumex Co., Hyogo, Japan) for 10 days, followed by a 16 h yellow LED-photoperiod of 220 mmol/m^2s (RAYS Co.) for 20 days. The nutrient solution used was a mixture of OAT House 1 (71%), OAT House 8 (26%) and OAT House 5 (3%) (all from OAT Agrio Co., Tokyo, Japan). The system was washed with detergent and rinsed twice with tap water between two independent experiments.

Protein expression, SDS-PAGE, and western blotting analysis

Infiltrated leaves were harvested on 2, 4, 6, 8 and 10 days post-infiltration (dpi) to evaluate the transient expression level of antibody. Leaf samples were homogenized in liquid nitrogen using a mortar and pestle, followed by protein extraction in 100 mM sodium phosphate, 100 mM sodium chloride and 40 mM ascorbic acid at pH 6.0 (Husk et al., 2014). The CHO-derived human Varlilumab (Thermo Fisher Scientific, Waltham, MA) and

plant crude extract were separated by sodium dodecyl sulfate polyacrylamide gel electrophoresis (SDS-PAGE) under reducing and non-reducing conditions. For the non-reducing condition, the samples were mixed with non-reducing loading buffer (125 mM Tris-Cl, pH 6.8, 20% glycerol, SDS, 0.1% bromophenol blue) and separated on 10% SDS-PAGE. Under the reducing condition, the buffer contained 5% β-mercaptoethanol. For protein detection, the gels were stained with Coomassie brilliant blue (CBB) (Ready to Use; Nacalai Tesque, Kyoto, Japan) following the manufacturer's instructions. For western blot analysis, the separated proteins in polyacrylamide gel were transferred to a polyvinylidene difluoride (PVDF) membrane (Millipore, Bedford, MA). The membrane was blocked with skim milk (5%) in PBS-T (1.47 mM KH_2PO_4, 10 mM Na_2HPO_4, 2.7 mM KCl, 137 mM NaCl, 0.05% Tween-20, pH 7.4) for 1 h. The membrane was then washed with PBS-T and incubated with primary antibody anti-human IgG (H+L chain) rabbit IgG (lot WI3374611; Invitrogen) at a dilution of 1:5000, followed by secondary antibody anti-rabbit-HRP IgG (Sigma, St. Louis, Missouri, United States) at a dilution of 1:10,000. Finally, the Varlilumab signals were visualized by adding Immobilon Forte Western HRP substrate (Millipore), and the chemiluminescence was imaged by using an iBright Imaging System (Invitrogen).

Protein A Sepharose purification

Leaves were harvested and extracted in a cold extraction buffer (2 ml buffer for 1 g of leaves). The plant debris was removed by centrifugation at 15,000 x *g* for 10 min at 4°C. Then the starches and small plant debris were pelleted by adjusting the pH to 7.0 using sodium hydroxide and centrifuged at 15,000 x *g* for 10 min at 4°C. Finally, the clarified extract was passed through filter paper using a vacuum, and the plant-derived antibody was purified by using rProtein A Sepharose fast flow (Pharmacia Biotech AB, Uppsala, Sweden). The column was equilibrated with a 10 column volume (CV) of equilibration buffer (20 mM sodium phosphate, pH 7.0). The plant extract was loaded at a speed of 2 ml/min. The unbound proteins were washed out of the column using 10 CV of wash buffer (20 mM sodium phosphate, pH 7.0). The purified antibody was eluted from the column by using 10 CV of elution buffer (100 mM glycine, 200 mM L-arginine, pH 3.0) and neutralized immediately with neutralizing buffer (1M Tris buffer, pH 8.0).

Antibody quantification by ELISA

A 96-well plate was coated with 50 µL of goat anti-human IgG (H+L chain) (MBL, Woburn, UK) 1:10000 in 1x PBS buffer and incubated overnight at 4°C. The plate was washed three times with 0.05% Tween-20 in PBS (PBS-T) buffer and blocked with 5% BSA in 1x PBS buffer for 1 h at room temperature (RT). After three additional washings with PBS-T, human plasma IgG (Calbiochem, La Jolla, CA) or plant crude extracts were added into the wells and the plate was incubated at RT for 1 h. The plate was then washed, supplemented with 50 µL of anti-human IgG (H+L chain) conjugated with HRP and incubated for 1 h at RT. The plate was developed using SIGMAFAST™ OPD (Sigma) substrate solution (200 µL/well). The reaction was stopped by addition of 1 M HCl (50 µL/well) and the antibodies were measured at 450 nm with a Bio-Rad imark™ microplate reader.

N-glycan analysis

Purified Varlilumab was separated on SDS-PAGE under reducing conditions and stained with CBB solution. The heavy chain was excised from the gel and destained with 50 mM NH_4HCO_3: acetonitrile (1:1 v/v) with overnight intermittent vortex mixing. Then, the heavy chains of Varlilumab were in-gel digested using Trypsin Gold (Promega, Madison, WI) in ProteaseMAX™ Surfactant (Promega) at 50°C for 1 h. The digested peptides were collected from the gel and the reaction was terminated by adding trifluoacetic acid to a final concentration of 0.5%. Digested glycopeptides were applied to a nanoLC-MS/MS system with an ESI-Qq-TOF mass spectrometer (micrOTOF-Q II; Bruker Daltonics, Bremer, Germany) and a nanoLC system (1,200 series; Agilent Technologies, Palo Alto, CA) incorporating a trap column (5 µm, 0.3 x 5 mm) and an analytical column (3.5 µm, 0.075 x 150 mm), both packed with Zorbax 300SB C-18 (Agilent Technologies).

Antigen-binding assay (CD27 ELISA)

The CD27 ELISA was carried out using recombinant human CD27 (R&D Systems, Minneapolis, MN). Briefly, human CD27 was coated to ELISA plates overnight at 4°C, followed by a blocking with 5% BSA. Each of the following was incubated for 1 h at RT: purified soil-derived Varlilumab, hydroponic-derived Varlilumab, CHO-derived Varlilumab (Thermo Fisher Scientific) as a positive control, and a human plasma IgG (Calbiochem) as a negative control. A goat anti-human IgG (H+L)-HRP (horseradish peroxidase) antibody and substrate SIGMAFAST™ OPD (Sigma) were used for detection. Samples were analyzed at 450 nm using a Bio-Rad imark™ microtiter plate reader.

Statistical analysis

All experiments were performed in three independent replicates. Statistical evaluations were performed using the Minitab software package. Values of $p<0.05$ were considered to indicate statistical significance.

Results

Transient production of Varlilumab in *N. benthamiana*

To produce recombinant Varlilumab in *N. benthamiana* plants, a modified plant expression vector was used (Sariyatun et al., 2021). The genes encoding the heavy and light chain were individually

10.3389/fpls.2023.1215580

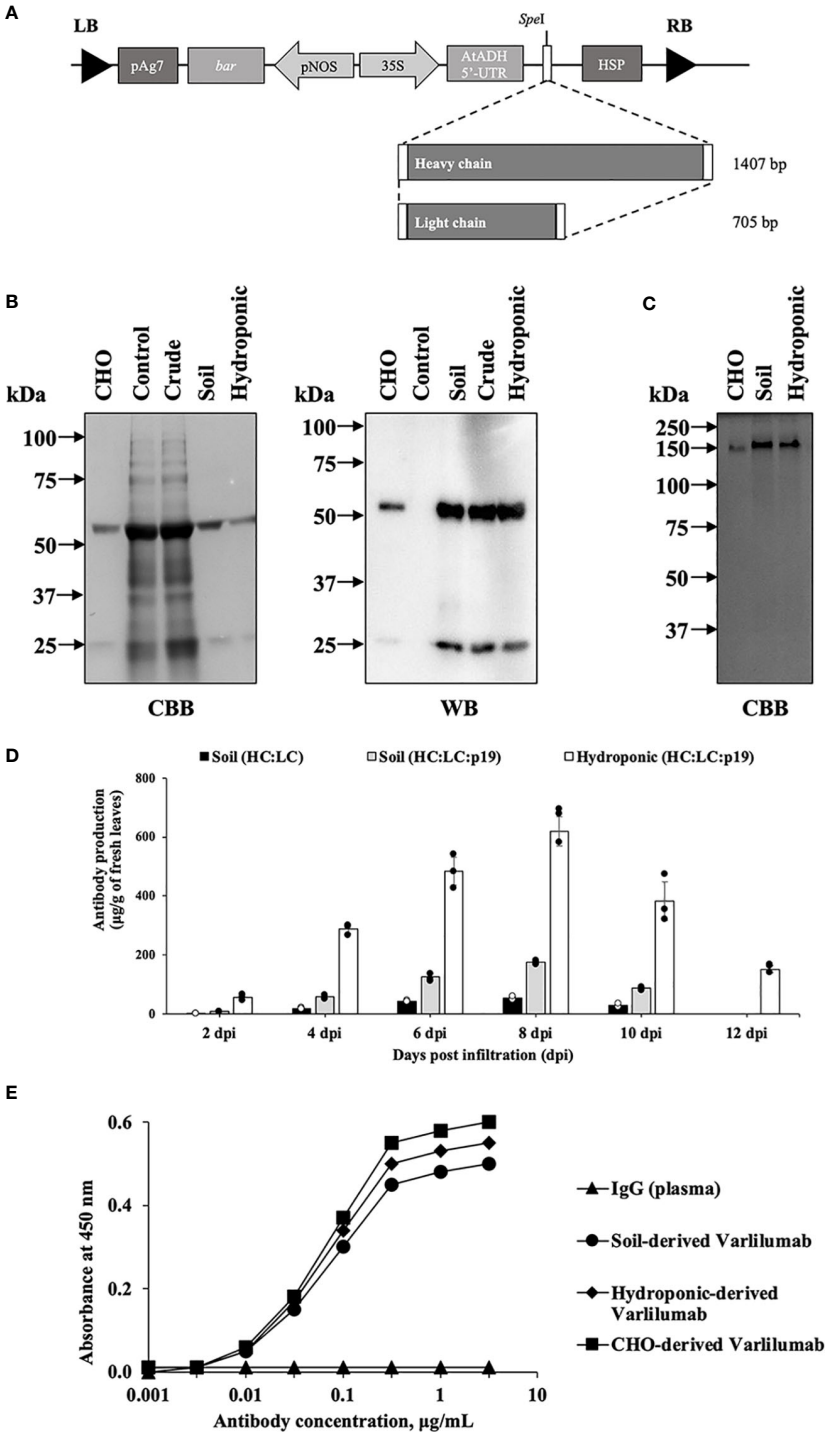

FIGURE 1
Transient production of Varlilumab in *Nicotiana benthamiana*. **(A)** Schematic representation of plant expression vectors of Varlilumab. CaMV 35S, *Cauliflower mosaic virus* 35S promoter; AtADH 5'-UTR, 5'-untranslated region of *Arabidopsis* alcohol dehydrogenase gene as a translational enhancer; HC, heavy chain Varlilumab; LC, light chain Varlilumab; HSP, *Arabidopsis* heat shock protein terminator; pNOS, Nopaline synthase promoter; *bar*, Bialaphos resistant as a selectable marker gene in plant; pAg7, Agropine synthase gene terminator; and LB and RB, left and right borders of T-DNA, respectively. **(B)** CBB staining and western blotting analysis of Varlilumab. The results under reducing conditions are shown as follows. Lane 1: CHO-derived recombinant human Varlilumab as a positive control. Lane 2: Vector control. Lane 3: Crude extract. Lane 4: Purified Varlilumab derived from soil-based *N. benthamiana*. Lane 5: Purified Varlilumab derived from hydroponic-based *N. benthamiana*. **(C)** CBB staining of Varlilumab. The results under non-reducing conditions are shown as follows. Lane 1: CHO-derived Varlilumab. Lane 2: Purified soil-based Varlilumab. Lane 3: Purified hydroponic-based Varlilumab. **(D)** Leaves were collected after 2, 4, 6, 8, 10 and 12 dpi, and quantified by ELISA. The amount of antibody was shown in micrograms of antibody per gram of fresh weight. Data are means ± SD of samples from three independent infiltration experiments. **(E)** Antigen-binding assay of Varlilumab produced in soil- and hydroponic-based *N. benthamiana*.

inserted into the plant expression vector (Figure 1A). The plasmids were transferred into *Agrobacterium tumefaciens* LBA4404 using electroporation. Transient production was performed using vacuum infiltration, followed by protein extraction and protein A affinity chromatography purification. The expression and purity of plant-derived Varlilumab were analyzed by SDS-PAGE to confirm the size and integrity of the antibody (Figures 1B, C). CBB staining and WB using rabbit anti-human IgG (H+L) and anti-rabbit IgG-horseradish peroxidase (HRP) were used to confirm the production of Varlilumab fragments in *N. benthamiana* and successful purification from the Varlilumab-expressing leaves. As shown in Figure 1B, plant-derived Varlilumab was detected at 55 kDa (H) and 26 kDa (L) under reducing conditions. A band corresponding to the assembled antibody was present at approximately 150 kDa under non-reducing conditions, indicating that the antibody was in fully assembled form (H_2L_2). There were no differences in size between the purified soil-based and hydroponic-based Varlilumab in CBB staining or WB (Figure 1C). These results confirmed that H and L were co-expressed, resulting in the expression of fully assembled Varlilumab in *N. benthamiana*.

Infiltrated leaves were harvested at 2, 4, 6, 8, and 10 days post-infiltration (dpi). Varlilumab was quantified in total protein extracts from each sample by an enzyme-linked immunosorbent assay (ELISA). Transient expression of RNA silencing suppressor p19 was tested to determine its efficiency for increasing the expression of Varlilumab. The highest antibody production was observed at 8 dpi (54 ± 4 μg/g of fresh weight), and co-expression with p19 increased the levels of accumulated antibodies by 3.2-fold (174 ± 5 μg/g of fresh weight) in soil-grown plants (Figure 1D). Surprisingly, the expression of Varlilumab in hydroponic-based *N. benthamiana* reached 618 ± 50 μg/gram of fresh weight, 3.5-fold higher than the expression in soil-based *N. benthamiana*. Even at 12 dpi, the hydroponic systems showed high-level Varlilumab production of 151 ± 12 μg/gram of fresh weight, whereas soil-based agroinfiltrated *N. benthamiana* died after 10 dpi. Therefore, co-expression with p19 was necessary and 8 dpi was chosen as the collection day for antibody purification.

We next performed an antigen-binding assay using human CD27 marker (Figure 1E). Both soil- and hydroponic-derived Varlilumab showed human CD27-binding affinity similar to that of commercial Chinese hamster ovary (CHO)-derived Varlilumab. A human plasma antibody that cannot bind to the human CD27 protein was used as a negative control. The results indicated that both soil- and hydroponic-based Varlilumab were successfully produced as functional antibodies in *N. benthamiana*.

N-glycan analysis of Varlilumab produced in CHO cells and *N. benthamiana*

To investigate the *N*-glycan profiles of Varlilumab produced in CHO cells and *N. benthamiana*, we conducted an *N*-glycan analysis of purified Varlilumab produced in CHO cells, soil-based *N. benthamiana*, and hydroponic-based *N. benthamiana* (Figure 2). The trypsin-digested *N*-glycopeptides were analyzed using nanoLC-MS/MS. The percentages of each structure in the total *N*-glycan profile were also determined (Tables 1, 2). In CHO-derived Varlilumab, five *N*-glycoforms were observed. The most abundant *N*-glycopeptide was GN2F, accounting for 51.4% of the total, followed by single-branched β1,4-galactosylated IgG at 21.5% (Table 1). As expected, the *N*-glycan analysis of the soil-based and hydroponic-based Varlilumab revealed high levels of β1,2-xylosylated and α1,3-fucosylated *N*-glycan variants, accounting for 72.3% and 76.8% of the total profile, respectively. GN2XF was also a predominant structure, accounting for 54.5% and 58.5% of the profile in soil- and hydroponic-based Varlilumab, respectively (Table 2). The Lewis a (Le^a) structure was not observed in the un-modified setups of either soil- or hydroponic-grown *N. benthamiana* plants.

Co-expression of Varlilumab with β1,4-galactosyltransferase or β1,3-galactosyltransferase in *N. benthamiana*

To improve the effectiveness of plant-derived Varlilumab, *N*-glycan engineering was performed with the aim of producing Varlilumab with Gal residues on its *N*-glycan. Previous research indicated that Gal residues stabilize the antibody's configuration, improving the binding between the Fc region and Fc receptors (Kiyoshi et al., 2018). In the previous *N*-glycan analysis, single-branched β1,4-galactosylated IgG accounted for 21.5% of CHO-derived Varlilumab, and in un-modified plants, more than half of plant-derived Varlilumab bore a GNGN core structure, which could be extended via β1,4-linked galactose by β1,4-GALT (Bohlender et al., 2022). In this experiment, both soil- and hydroponic-based *N. benthamiana* plants were used for the co-expression of Varlilumab with murine β1,4-GALT. The constituent *N*-glycans of each modification in Varlilumab were determined by *de novo* sequencing of the trypsin-digested *N*-glycopeptides using nanoLC-MS/MS analysis. The *N*-glycopeptides bearing the sequence of N297 were successfully detected. The majority of the *N*-glycans of Varlilumab co-expressed with β1,4-GALT were galactose-terminated, with the galactose-terminated *N*-glycans accounting for 42.5% and 55.3% of total *N*-glycan variants in soil-based and hydroponic-based plants, respectively (Figure 3 and Table 3). However, the modified product formed by β1,4-GALT co-expression was a hybrid structure having a single Galβ1,2-1,4-GlcNAc (42.5% of total *N*-glycan variants in soil-based and 55.3% of that in hydroponic-based plants). Moreover, a non-mature ER-specific glycans (Man9) and high mannose structures were also observed in soil-based plants. Transient expression of β1,4-GALT in *N. benthamiana* results in a partial galactosylation in plant-derived Varlilumab.

To target mammalian β1,4-GALT to the *trans* or late Golgi of plants, the native localization domain of mammalian β1,4-GALT was replaced by the *N*-terminal CTS of *Arabidopsis thaliana* β1,2-XYLT (Saint-Jore-Dupas et al., 2006) or rat α2,6-ST (Strasser et al., 2009). In this study, we chose β1,3-GALT because its subcellular localization was predicted to be exclusively located in the plant Golgi apparatus. *A. thaliana* β1,3-GALT was co-expressed with

10.3389/fpls.2023.1215580

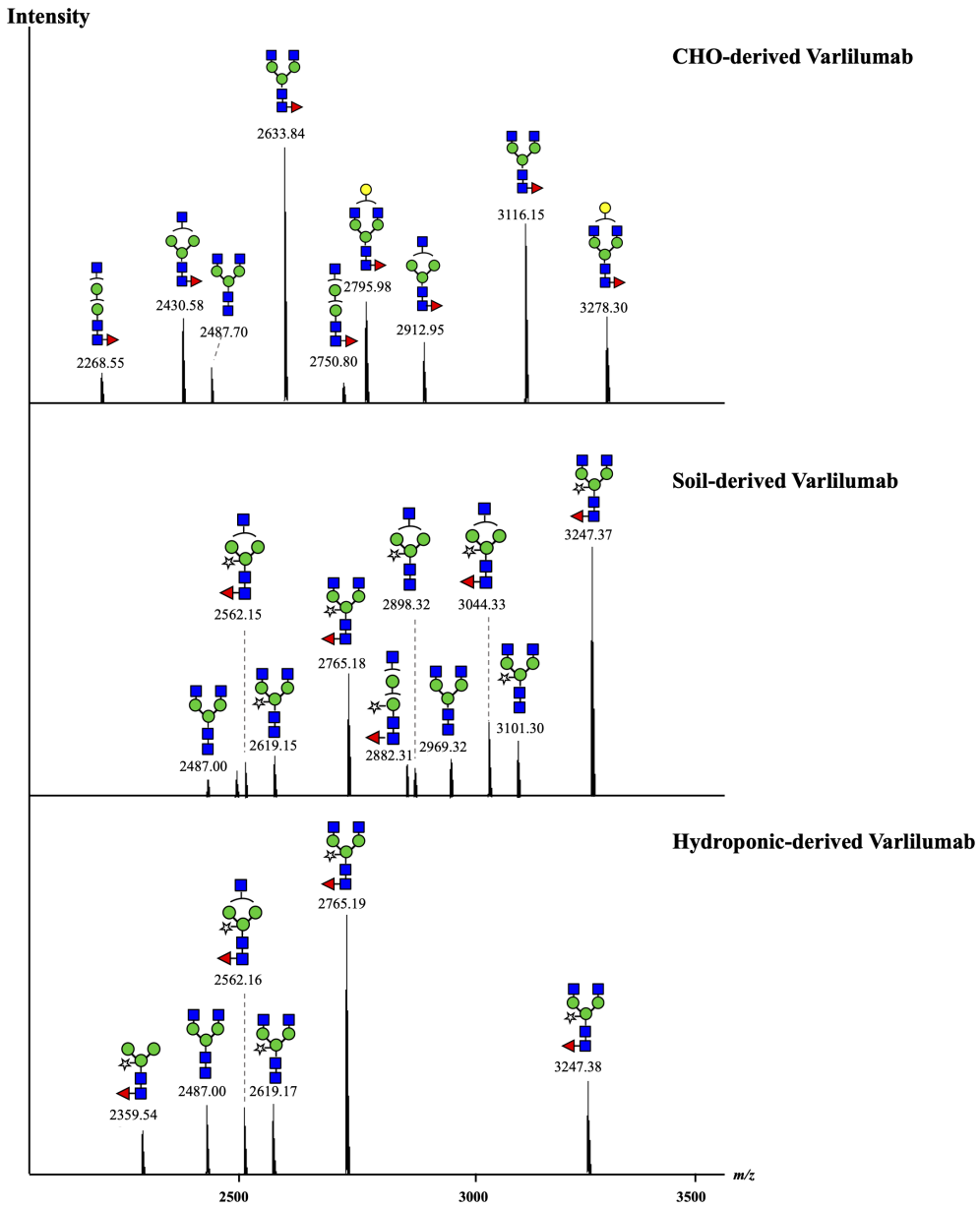

FIGURE 2
N-glycan profile of Varlilumab produced in CHO cells, soil- and hydroponic-based *N. benthamiana*. The deconvoluted MS spectra show the mass $[M + H]^+$ of the tryptic glycopeptides carrying an *N*-glycosylation site. The tryptic glycopeptides contained EEQYNSTYR and TKPREEQYNSTYR with a missed cleavage site in the middle due to the steric hindrance of the glycans or the interference of proline near the cleavage site. Both of the glycopeptides were detected in the three analyzed samples.

TABLE 1 Composition of the *N*-glycan structures in CHO-derived Varlilumab.

Abbreviation	Structure	*N*-glycopeptide ratio (%)
GNM2F	GlcNAcMan2Fuc	5.8
GNF	GlcNAcMan3Fuc	17.1
GN2	GlcNAc2Man3	4.2
GN2F	GlcNAc2Man3Fuc	51.4
Gal(β1,4)GN2F	GalGlcNAc2Man3Fuc	21.5
	Total	**100**

TABLE 2 Composition of the *N*-glycan structures in Varlilumab produced in *N. benthamiana* soil and hydroponic systems.

Abbreviation	Structure	Soil-based (%)	Hydroponic-based (%)
M3XF	Man3XylFuc	–	7.3
GNM2XF	GlcNAcMan2XylFuc	4.5	–
GNX	GlcNAcMan3Xyl	4.0	–
GN2	GlcNAc2Man3	8.9	11.6
GNXF	GlcNAcMan3XylFuc	14.7	11.0
GN2X	GlcNAc2Man3Xyl	13.5	11.6
GN2XF	GlcNAc2Man3XylFuc	54.5	58.5
	Total	**100**	**100**
β1,2-Xylosylated **β1,2-Xylosylated and α1,3-Fucosylated** **Lewis a structure**		17.5 72.3 -	11.6 76.8 -

Varlilumab to observe how it modifies the *N*-glycan profiles of the antibody. The *N*-glycan analysis indicated that the formation of the Le^a structure was enhanced (Figure 3 and Table 4). In previous analysis, there was no Le^a structures observed in the un-modified setups of both soil- and hydroponic-based *N. benthamiana* plants (Table 2). In this modification, there were 46.1% and 22.7% of Le^a structures formed in the soil- and hydroponic-based plants, respectively. In contrast, the percentage of the substrate acceptor of β1,3-GALT, i.e., GN2XF decreased from 54.5% to 25.3% in the soil-based plants and from 58.5% to 27.3% in the hydroponic-based plants. Furthermore, *N*-glycan structures containing both β1,2-Xyl and α1,3-Fuc residues were different between the soil- and hydroponic-based *N. benthamiana* plants. In the soil-based plants, the combined β1,2-XYLT and α1,3-fucosyltransferase (FUCT) worked cooperatively to form 100% of *N*-glycans contained both β1,2-Xyl and α1,3-Fuc residues whereas in hydroponic plants, 13.7% of *N*-glycan structures contained only β1,2-Xyl residues. In short, co-expression with *A. thaliana* β1,3-GALT improved galactosylation efficiency and enhanced the formation of the Le^a structure of plant-derived Varlilumab compared to the un-modified setup.

Co-expression of Varlilumab with a chimeric protein β1,3β1,4-GALT

In our previous experiments, it was suggested that the original CTS region of murine β1,4-GALT acted early in the Golgi network of transiently agroinfiltrated *N. benthamiana* wild type leaves and single β1,4-galactosylated *N*-glycan structures were produced, whereas galactosylation efficiency was improved by co-expression with *A. thaliana* β1,3-GALT. Therefore, we hypothesized that the

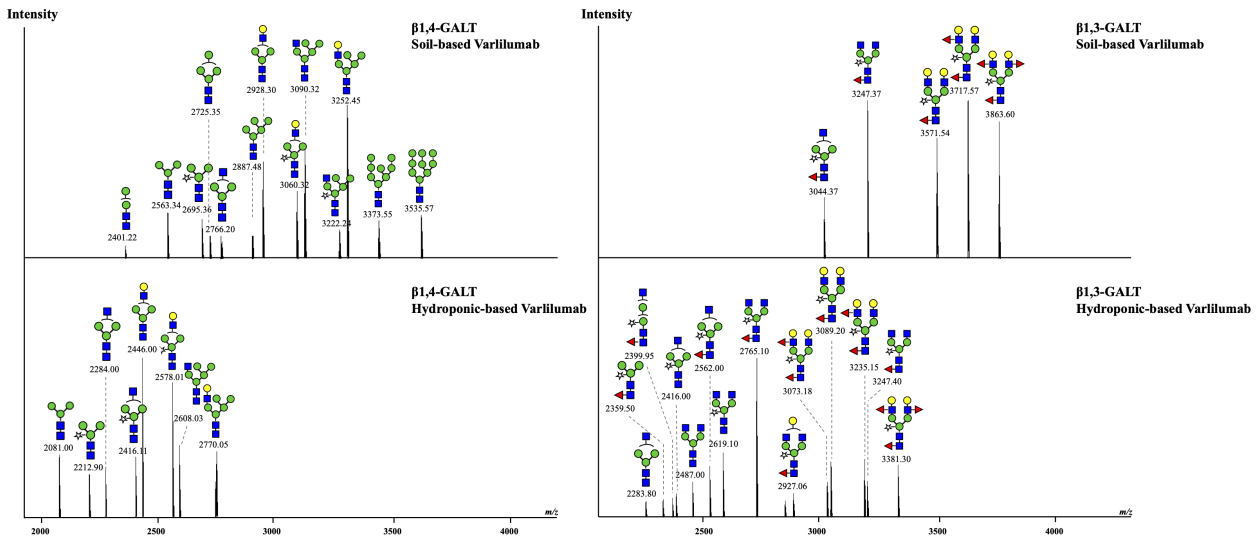

FIGURE 3
Co-expression of Varlilumab with β1,4-galactosyltransferase (β1,4-GALT) or β1,3-galactosyltransferase (β1,3-GALT) in *N. benthamiana* harvested at 8 dpi. Mass spectra of glycopeptides derived from co-expression of Varlilumab with β1,4-GALT or β1,3-GALT produced in soil- and hydroponic-based *N. benthamiana* plants. In this analysis, the trypsin-digested glycopeptides from soil-based Varlilumab, contained TKPREEQYNSTYR while these from hydroponic-based Varlilumab carried EEQYNSTYR.

10.3389/fpls.2023.1215580

TABLE 3 Composition of the *N*-glycan structures in Varlilumab co-expressed with β1,4-GALT *in N. benthamiana*.

Abbreviation	Structure	Soil-based (%)	Hydroponic-based (%)
M2	Man2	1.7	–
M3	Man3	8.2	9.6
M4	Man4	5.4	–
M5	Man5	5.3	–
M8	Man8	5.1	–
M9	Man9	5.7	–
M3X	Man3Xyl	5.2	6.9
GNM3	GlcNAcMan3	2.3	7.7
GNM3X	GlcNAcMan3Xyl	–	9.4
GNM5	GlcNAcMan5	14.8	11.1
GNM5X	GlcNAcMan5Xyl	3.7	–
Gal(β1,4)GNM3	GalGlcNAcMan3	12.5	24.8
Gal(β1,4)GNM3X	GalGlcNAcMan3Xyl	8.8	20.5
Gal(β1,4)GNM5	GalGlcNAcMan5	21.2	10.0
	Total	**100**	**100**
Terminal β1,4-Gal residue **β1,2-Xylosylated** **Oligomannosidic structure**		42.5 17.7 21.5	55.3 36.8 -

TABLE 4 Composition of the *N*-glycan structures in Varlilumab co-expressed with β1,3-GALT *in N. benthamiana*.

Abbreviation	Structure	Soil-based (%)	Hydroponic-based (%)
M3XF	Man3XylFuc	–	2.8
GNM3	GlcNAcMan3	–	2.5
GNX	GlcNAcMan3Xyl	–	3.7
GNXF	GlcNAcMan3XylFuc	9.8	8.0
GN2M2XF	GlcNAc2Man2XylFuc	–	3.0
GN2	GlcNAc2Man3	–	5.4
GN2X	GlcNAc2Man3Xyl	–	10.0
GN2XF	GlcNAc2Man3XylFuc	25.3	27.3
GalGN2XF	GalGlcNAc2Man3XylFuc	–	3.8
Gal(F)GN2XF	GalFucGlcNAc2Man3XylFuc	–	5.6
Gal2GN2XF	Gal2GlcNAc2Man3XylFuc	18.8	10.8
Gal2(F)GN2XF	Gal2FucGlcNAc2Man3XylFuc	24.7	9.0
Gal2F2GN2XF	Gal2Fuc2GlcNAc2Man3XylFuc	21.4	8.1
Total		**100**	**100**
β1,2-Xylosylated **β1,2-Xylosylated and α1,3-Fucosylated** **Lewis a structure**		- 100 64.9	13.7 78.4 22.7

cytoplasmic tail (CT) and transmembrane domain (TMD) of β1,3-GALT would result in hybrid-type *N*-glycans in the antibody. Previous studies have also demonstrated that the *N*-terminal CTS domain of β1,4-GALT is important in determining the *N*-glycosylation profile of recombinant proteins in plants. When the original CTS of β1,4-GALT was replaced with a rat α2,6-sialytransferase CTS domain, more homogeneous biantennary galactosylated *N*-glycan profiles were achieved, as this swapping led to translocation of GALT to the *trans*-Golgi compartments (Schoberer et al., 2009; Castilho et al., 2011). In this study, to investigate whether the expression of CT and TMD of β1,3-GALT results in hybrid-type *N*-glycans in the antibody, the original CT and TMD regions of mouse β1,4-GALT were replaced by the first 23 amino acids encoding for CT and TMD of β1,3-GALT. The chimeric β1,3β1,4-GALT was placed in the pRI201AN vector (Figure 4A). This construct was co-expressed with Varlilumab and the *N*-glycans profile of modified Varlilumab was analyzed using nanoLC-MS/MS. Biantennary galactosylated *N*-glycan (*m/z* 3089.6) was observed (Figure 4B) and accounted for 4.4% of the total *N*-glycan profile. Moreover, non-mature ER-specific glycans (Man9) accounted for 7.3% of the total profile, high mannose structures (Man6, Man7 and Man8) made up 20.8%, and the remaining 67% are complex *N*-glycans carrying both β1,2-Xyl and α1,3-Fuc residues (Table 5). This result suggested that CT and TMD of *A. thaliana* β1,3-GALT are sufficient to form biantennary β1,4-galactosylated *N*-glycans in plant-derived Varlilumab.

Discussion

Cancer immunotherapy has become an attractive treatment option. In particular, the use of monoclonal antibodies—including Varliumab (anti-human CD27)—in cancer treatment has been

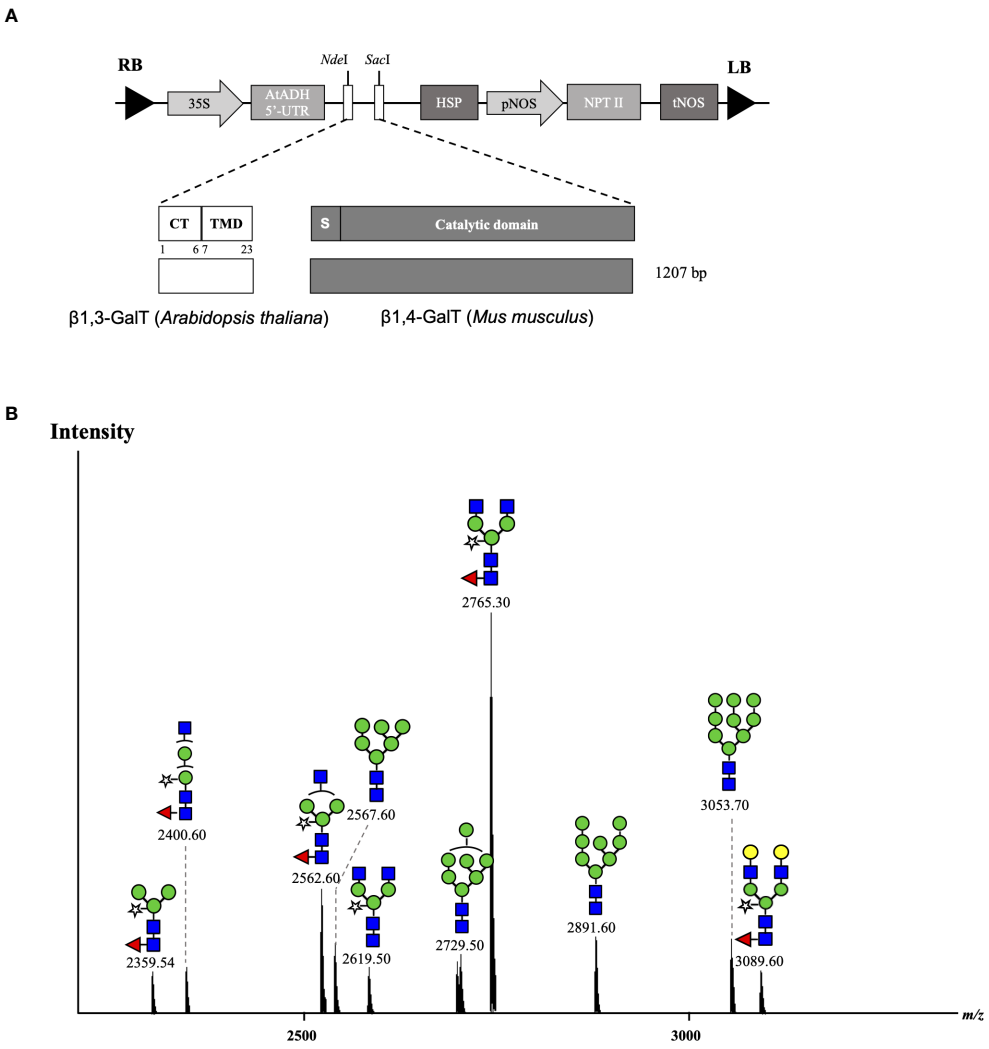

FIGURE 4
Co-expression of Varlilumab with chimeric β1,3β1,4-GALT in *N. benthamiana* harvested at 8 dpi. **(A)** Schematic representation of plant expression vectors of chimeric β1,3β1,4-GALT. CaMV 35S, *Cauliflower mosaic virus* 35S promoter; AtADH 5'-UTR, 5'-untranslated region of the *Arabidopsis* alcohol dehydrogenase gene as a translational enhancer; CT, Cytoplasmic tail; TMD, Transmembrane domain; HSP, *Arabidopsis* heat shock protein terminator; pNOS, Nopaline synthase promoter; NPT II, Neomycin phosphotransferase gene as a selectable marker gene in plant; tNOS, Nopaline synthase terminator; and LB and RB: left and right borders of T-DNA, respectively. **(B)** Mass spectra of glycopeptides (EEQYNSTYR) derived from co-expression with chimeric β1,3β1,4-GALT produced in soil-based *N. benthamiana* plants.

TABLE 5 Composition of the *N*-glycan structures in Varlilumab co-expressed with chimeric β1,3β1,4-GALT *in N. benthamiana.*

Abbreviation	Structure	*N*-glycopeptide ratio (%)
M3XF	Man3XylFuc	4.1
GNM2XF	GlcNAcMan2XylFuc	4.6
GNXF	GlcNAcMan3XylFuc	12.4
GN2X	GlcNAc2Man3Xyl	4.8
GN2XF	GlcNAc2Man3XylFuc	41.5
Gal2(β1,4)GN2XF	Gal2GlcNAc2Man3XylFuc	4.4
M6	Man6	7.2
M7	Man7	5.8
M8	Man8	7.8
M9	Man9	7.3
	Total	100
Terminal β1,4-Gal residue		4.4
β1,2-Xylosylated and α1,3-Fucosylated		67.0
Oligomannosidic structure		20.8
Lewis a structure		-
β1,2-Xylosylated		4.8

studied in multiple clinical trials, but the anti-CD27 mAb has been produced only in CHO cells, and contamination and high cost are concerns when using CHO cells (Nosaki et al., 2021a). Therefore, we developed an alternative platform for producing an effective Varlilumab in plants. Transgenic plants are still prohibited in many countries, and the generation of stable plant transformants is time-consuming (Rivera et al., 2012; Sethi et al., 2021). To tackle these obstacles, transient expression technology was used in this study. The recombinant Varlilumab was expressed in *N. benthamiana* leaves within 8 days of infiltration and successfully assembled. With co-expression of p19, an RNA silencing suppressor, mAb was accumulated at an average of 174 μg/g of fresh leaf weight. This production was higher than that of nivolumab (140 μg/g of fresh leaf weight) in a transient production in *N. benthamiana* using geminiviral vectors (Rattanapisit et al., 2019). The result showed that the purified plant-derived Varlilumab in both soil- and hydroponic-based systems assembled correctly into a tetramer and retained *in vitro* efficacy similar to those of commercial mammalian cell-produced Varlilumab.

Of note, a high expression of Varlilumab was observed in hydroponic systems. Varlilumab expression reached 618 μg/g of fresh leaf weight in hydroponic *N. benthamiana*, which was 3.5 times greater than the expression achieved in soil-based *N. benthamiana*. The antibody production was rapidly increased from 4 dpi (288 μg/g of fresh leaf weight) and stayed high until 12 dpi (151 μg/g of fresh leaf weight). Hydroponic cultivating conditions have been shown to increase the accumulation of ascorbic acid in plants (Buchanan and Omaye, 2013). Ascorbic acid has been shown to suppress necrosis caused by transient expression in *N. benthamiana* (Nosaki et al., 2021b) and to scavenge excess reactive oxygen species (ROS) generated by *A. tumefaciens* (Wojtaszek, 1997). Therefore, an accumulation of ascorbate acid in hydroponic-based *N. benthamiana* plants might contribute to an improvement of transformation, enhancement of agroinfiltration and maintenance of the health of agroinfiltrated plants. To our knowledge, this is the first study to produce recombinant Varlilumab in a plant-based platform. Our results indicate that this system has the potential to be competitive for the recombinant production of antibodies with high yield.

Previous reports described that the antibodies produced in tobacco do not have β1,4-Gal terminals, which show better performance in their effector functions, as plants lack mammalian β1,4-GALT. Previous studies reported the stable expression of human β1,4-GALT in tobacco cell-lines and transgenic tobacco plants (Palacpac et al., 1999; Bakker et al., 2001). Although these approaches achieved galactosylated IgGs, the hurdles are laborious and time-intensive. Therefore, transient expression of Varlilumab and co-expression of GALT were selected to obtain galactosylated Varlilumab produced in *N. benthamiana* in a short period of time. Despite the fact that transient expression of β1,4-GALT in tobacco plants results in galactosylation of Varlilumab, the *N*-glycan modification was partially processed. The GalGNM5 structure was found and β1,2-Xyl residue was also present in β1,4-Gal-containing *N*-glycans, suggesting that β1,4-GALT blocked the function of Golgi-α-mannosidase II and acted early in the Golgi apparatus together with β1,2-xylosyltransferase (XYLT). Moreover, the presence of xylose-bearing *N*-glycan structures (GNM5X or GNM3X) in soil-based Varlilumab (17.7%) and hydroponic-based Varlilumab (36.8%) indicated that β1,2-XYLT worked actively in the *medial*-Golgi (Figure 5). On the contrary, Varlilumab with β1,4-GALT co-expressed contained glycans with no detectable α1,3-fucose. This may suggest that the introduced β1,4-GALT is

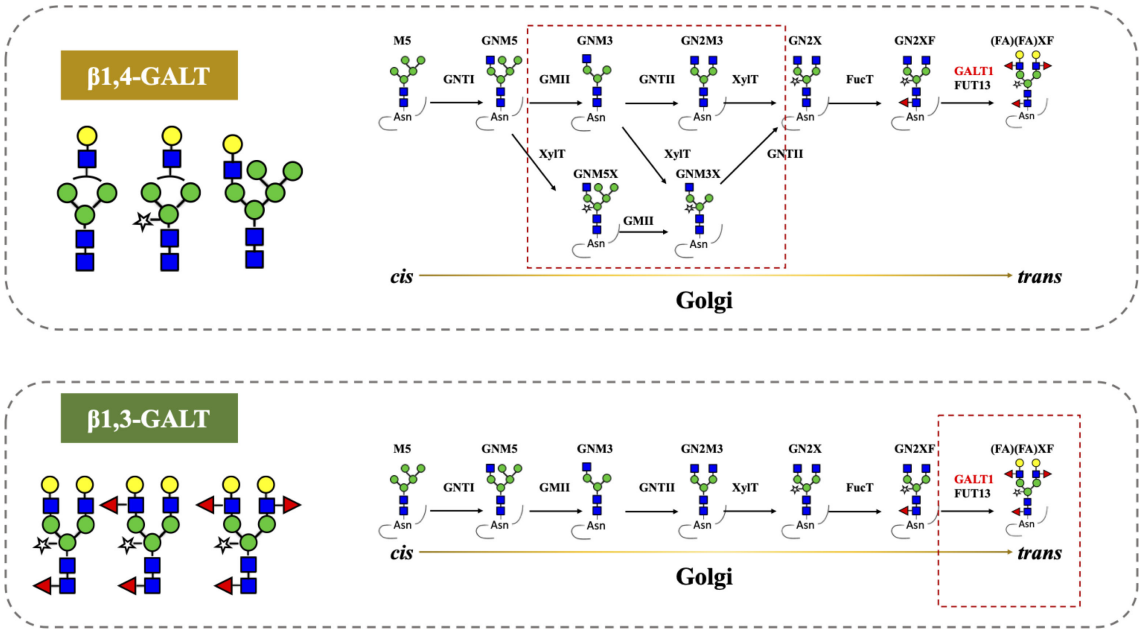

FIGURE 5
Co-expression of β1,4-galactosyltransferase (β1,4-GALT) and β1,3-galactosyltransferase (β1,3-GALT) in *N. benthamiana*. GnTI, *N*-Acetylglucosaminyltransferase I; GMII, Golgi-α-mannosidase II; GnTII, *N*-Acetylglucosaminyltransferase II; XylT, β1,2-Xylosyltransferase; FucT, core α1,3-Fucosyltransferase; GALT1, β1,3-Galactosyltransferase; FUT13, α1,4-Fucosyltransferase. M5, Man5; GNM5, GlcNAcMan5; GNM3, GlcNAcMan3; GN2M3, GlcNAc2Man3; GN2X, GlcNAc2Man3Xyl; GN2XF, GlcNAc2Man3XylFuc; (FA)(FA)XF, Gal2Fuc2GlcNAc2Man3XylFuc.

integrated in the Golgi apparatus at a location which is adjacent to the α1,3-FUCT. Thus, the two glycosyltransferases are competing for the same substrates passing by. This was previously observed with the stable expression of human β1,4-GALT in transgenic tobacco cell lines and transgenic plants of *N. tabacum* (Palacpac et al., 1999; Bakker et al., 2001; Bakker et al., 2006). Moreover, the presence of 5.7% of a non-mature ER-specific glycans (Man9) and 21.5% of high-mannose-type glycans could be associated with a fraction of proteins "en-route", as reported previously for other plant-derived antibodies produced by transient expression in soil-based *N. benthamiana* (Sriraman et al., 2004). However, hydroponic-derived Varlilumab showed a dissimilar *N*-glycan profile to Varlilumab produced in soil-based *N. benthamiana*, indicating that the hydroponic cultivation would alter *N*-glycosylation patterns. Although galactosylated Varlilumab was found in this co-expression with β1,4-GALT, biantennary *N*-glycans with β1,4-Gal were not achieved. To improve galactosylation by β1,4-GALT in plants, β1,4-GALT has been coupled with different membrane anchorage domains of tobacco, such as GNTI (Vézina et al., 2009), XYLT (Saint-Jore-Dupas et al., 2006), and ST (Strasser et al., 2009; Forthal et al., 2010; Castilho et al., 2011; Loos et al., 2015; Schneider et al., 2015; Kallolimath et al., 2018).

In this study, we also investigated *A. thaliana* β1,3-GALT, the subcellular localization of which was predicted to lie exclusively in the Golgi apparatus (Strasser et al., 2007). In parallel, we co-expressed β1,3-GALT with Varlilumab in both soil- and hydroponic-grown *N. benthamiana* plants. The *N*-glycan analysis of Varlilumab revealed successful modification in both soil- and hydroponic-based *N. benthamiana* plants when compared to the un-modified setup (Figure 3 and Table 4). Le^a structures were found in the soil- and hydroponic-based plants at rates of 64.9% and 22.7%, respectively. Le^a [Fucα1-4(Galβ1-3)GlcNAc-R] structures require the continuous extension of β1,3-galactose and α1,4-fucose residues by β1,3-GALT and α1,4-fucosyltransferase (FUT13) in the *trans*-Golgi compartments (Strasser et al., 2007). In soil-based *N. benthamiana*, all of the *N*-glycan structures of Varlilumab carried both β1,2-Xyl and α1,3-Fuc residues and 64.9% of Le^a structures were formed, suggesting that Varlilumab produced in the soil-based plants properly passed through the *trans*-Golgi network. By contrast, Varlilumab produced in a hydroponic system had a smaller amount of Le^a structures (22.7%), and 13.7% of the *N*-glycan variants carried only the β1,2-Xyl residue, indicating these amounts of Varlilumab being en-routed in hydroponic-based *N. benthamiana* plants (Sriraman et al., 2004).

The transient expression of mammalian GALT in *N. benthamiana* results in galactosylation of antibodies and reflects a dynamic state of the *N*-glycosylation process with the presence of non-mature ER-specific glycans and fucose-carrying glycan structures. β1,4-GALT localizes correctly but early in the plant Golgi apparatus, while the endogenous β1,3-GALT acts in the *trans*-Golgi compartments (Figure 5). Thus, a chimeric of the mammalian β1,4-GALT catalytic domain and transmembrane domain of β1,3-GALT was generated to improve the galactosylation of β1,4-GALT in *N. benthamiana*. Specifically, the first 23 aa encoding for CT and TMD of β1,3-GALT fused with the stem, and the catalytic domain of β1,4-GALT (Figure 4A) was co-expressed with Varlilumab. *N*-glycan analysis of the modified Varlilumab indicated that 4.4% of the total Varlilumab had

biantennary β1,4-galactosylated *N*-glycans (*m/z* 3089.6) (Figure 4B and Table 5). This finding revealed that CT and TMD of *A. thaliana* β1,3-GALT are sufficient to form biantennary β1,4-galactosylated *N*-glycans in plant-derived Varlilumab.

Conclusion

In this study, we established a plant-based platform to rapidly produce Varlilumab. Our data demonstrated that Varlilumab can be transiently produced in *N. benthamiana* with a large amount of mAb in a hydroponic system. We also found that co-expression with chimeric β1,4-GALT successfully achieved biantennary β1,4-galactosylated Varlilumab. Gal is important for the effector functions of antibodies, and transient expression significantly reduces the time and material required as compared with the generation of transgenic plants stably expressing antibodies, so this is a major improvement in the *in planta* engineering of antibodies and a critical step toward obtaining recombinant therapeutic *N*-glycoproteins with fully humanized *N*-glycans.

Data availability statement

The original contributions presented in the study are included in the article/Supplementary Material. Further inquiries can be directed to the corresponding author.

Author contributions

KN performed the experiments and wrote a manuscript. HK assisted with nanoLC-MS/MS analysis and RM helped to verify DNA sequences of Varlilumab. RK and TY established the growing conditions for hydroponic-based *N. benthaminana*. KF supervised the findings of this work. All authors contributed to the article and approved the submitted version.

Funding

This study was supported by the Ministry of Education, Culture, Sports, Science and Technology (MEXT).

Acknowledgments

We thank Professor Atsushi Takeda from Ritsumeikan University, Japan for providing the RNA silencing suppressor 19 (p19) vector and Akitoshi Suzuki for the preparation of hydroponic-based plants.

Conflict of interest

Authors RK and TY was employed by the company GreenLand-Kidaya group Co Ltd.

The remaining authors declare that the research was conducted in the absence of any commercial or financial relationships that could be construed as a potential conflict of interest.

Publisher's note

Supplementary material

The Supplementary Material for this article can be found online at: https://www.frontiersin.org/articles/10.3389/fpls.2023.1215580/full#supplementary-material

References

Alatorre-Cobos, F., Calderón-Vázquez, C., Ibarra-Laclette, E., Yong-Villalobos, L., Pérez-Torres, Claudia-Anahí, Oropeza-Aburto, A., et al. (2014). An improved, low-cost, hydroponic system for growing arabidopsis and other plant species under aseptic conditions. *BMC Plant Biol.* 14 (1), 69. doi: 10.1186/1471-2229-14-69

Bakker, H., Bardor, M., Molthoff, J. W., Gomord, V., Elbers, I., Stevens, L. H., et al. (2002). Galactose-extended glycans of antibodies produced by transgenic plants. *Proc. Natl. Acad. Sci.* 98 (5), 2899–2804. doi: 10.1073/pnas.031419998

Bakker, H., Rouwendal, G. J.A., Karnoup, A. S., Florack, D. E.A., Stoopen, G. M., Helsper, J. P.F.G., et al. (2006). An antibody produced in tobacco expressing a hybrid β-1,4-galactosyltransferase is essentially devoid of plant carbohydrate epitopes. *Proc. Natl. Acad. Sci.* 103 (20), 7577–7825. doi: 10.1073/pnas.0600879103

Bard, F., Casano, L., Mallabiabarrena, A., Wallace, E., Saito, K., Kitayama, H., et al. (2006). Functional genomics reveals genes involved in protein secretion and golgi organization. *Nature* 439 (7076), 604–607. doi: 10.1038/nature04377

Bohlender, L. L., Parsons, J., Hoernstein, S. N.W., Bangert, N., Rodríguez-Jahnke, F., Reski, R., et al. (2022). Unexpected arabinosylation after humanization of plant protein N-glycosylation. *Front. Bioeng. Biotechnol.* 10 (February). doi: 10.3389/fbioe.2022.838365

Buchanan, D. N., and Omaye, S. T. (2013). Comparative study of ascorbic acid and tocopherol concentrations in hydroponic- and soil-grown lettuces. *Food Nutr. Sci.* 04 (10), 1047–1535. doi: 10.4236/fns.2013.410136

Burris, H. A., Infante, J. R., Ansell, S. M., Nemunaitis, J. J., Weiss, G. R., Villalobos, V. M., et al. (2017). Safety and activity of varlilumab, a novel and first-in-class agonist anti-CD27 antibody, in patients with advanced solid tumors. *J. Clin. Oncol.* 35 (18), 2028–2036. doi: 10.1200/JCO.2016.70.1508

Castilho, A., Bohorova, N., Grass, J., Bohorov, O., Zeitlin, L., Whaley, K., et al. (2011). Rapid high yield production of different glycoforms of ebola virus monoclonal antibody. *PloS One* 6 (10), e260405. doi: 10.1371/journal.pone.0026040

Chen, Q., Lai, H., Hurtado, J., Stahnke, J., Leuzinger, K., and Dent, M. (2013). Agroinfiltration as an effective and scalable strategy of gene delivery for production of pharmaceutical proteins. *Adv. Tech Biol. Med.* doi: 10.4172/atbm.1000103

Elsner, M., Hashimoto, H., and Tommy, N. (2003). Cisternal maturation and vesicle transport: join the band wagon! (Review). *Mol. Membrane Biol.* 20 (3), 221–295. doi: 10.1080/0968768031000114024

Forthal, D. N., Gach, J. S., Landucci, G., Jez, J., Strasser, R., Kunert, R., et al. (2010). "Fc-glycosylation influences fcγ receptor binding and cell-mediated anti-HIV activity of monoclonal antibody 2G12.". *J. Immunol.* 185 (11), 6876–6882. doi: 10.4049/jimmunol.1002600

Frigerio, R., Marusic, C., Villani, M. E., Lico, C., Capodicasa, C., Andreano, E., et al. (2022). "Production of two SARS-CoV-2 neutralizing antibodies with different potencies in nicotiana benthamiana.". *Front. Plant Sci.* 13. doi: 10.3389/fpls.2022.956741

Grohs, B. M., Niu, Y., Veldhuis, L. J., Trabelsi, S., Garabagi, F., Hassell, J. A., et al. (2010). Plant-produced trastuzumab inhibits the growth of HER2 positive cancer cells. *J. Agric. Food Chem.* 58 (18), 10056–10635. doi: 10.1021/jf102284f

Hesselink, T., Rouwendal, G. J.A., Henquet, M. G.L., Florack, D. E.A., Helsper, J. P.F.G., and Bosch, D. (2014). Expression of natural human B1,4-galT1 variants and of non-mammalian homologues in plants leads to differences in galactosylation of N-glycans. *Transgenic Res.* 23 (5), 717–285. doi: 10.1007/s11248-014-9806-z

Husk, A., Hamorsky, K. T., and Matoba, N. (2014). Monoclonal antibody purification (Nicotiana benthamiana plants). *Bio-Protocol* 4 (2), e1034–e1034. doi: 10.21769/bioprotoc.1034

Kallolimath, S., Castilho, A., Strasser, R., Grünwald-Gruber, C., Altmann, F., Strubl, S., et al. (2016). Engineering of complex protein sialylation in plants. *Proc. Natl. Acad. Sci.* 113 (34), 9498–9503. doi: 10.1073/pnas.1604371113

Kallolimath, S., Gruber, C., Steinkellner, H., and Castilho, A. (2018). "Promoter choice impacts the efficiency of plant glyco-engineering.". *Biotechnol. J.* 13 (1), 1700380. doi: 10.1002/biot.201700380

Kaplon, Hélène, Crescioli, S., Chenoweth, A., Visweswaraiah, J., and Reichert, J. M. (2023). Antibodies to watch in 2023. *MAbs* 15 (1). doi: 10.1080/19420862.2022.2153410

Kashima, K., Yuki, Y., Mejima, M., Kurokawa, S., Suzuki, Y., Minakawa, S., et al. (2016). "Good manufacturing practices production of a purification-free oral cholera vaccine expressed in transgenic rice plants.". *Plant Cell Rep.* 35 (3), 667–679. doi: 10.1007/s00299-015-1911-9

Kiyoshi, M., Caaveiro, J. M.M., Tada, M., Tamura, H., Tanaka, T., Terao, Y., et al. (2018). Assessing the heterogeneity of the fc-glycan of a therapeutic antibody using an engineered fcγReceptor IIIa-immobilized column. *Sci. Rep.* 8 (1), 3955. doi: 10.1038/s41598-018-22199-8

Kumar, R. R., and Cho, J. Y. (2014). Reuse of hydroponic waste solution. *Environ. Sci. pollut. Res.* 21 (16), 9569–9775. doi: 10.1007/s11356-014-3024-3

Loos, A., Gach, J. S., Hackl, T., Maresch, D., Henkel, T., Porodko, A., et al. (2015). "Glycan modulation and sulfoengineering of anti–HIV-1 monoclonal antibody PG9 in plants.". *Proc. Natl. Acad. Sci.* 112 (41), 12675–12680. doi: 10.1073/pnas.1509090112

Mimura, Y., Katoh, T., Saldova, R., O'Flaherty, R., Izumi, T., Mimura-Kimura, Y., et al. (2018). Glycosylation engineering of therapeutic igG antibodies: challenges for the safety, functionality and efficacy. *Protein Cell* 9 (1), 47–62. doi: 10.1007/s13238-017-0433-3

Nosaki, S., Hoshikawa, K., Ezura, H., and Miura, K. (2021a). Transient protein expression systems in plants and their applications. *Plant Biotechnol.* 38 (3), 610a. doi: 10.5511/plantbiotechnology.21.0610a

Nosaki, S., Kaneko, M. K., Tsuruta, F., Yoshida, H., Kato, Y., and Miura, K. (2021b). Prevention of necrosis caused by transient expression in nicotiana benthamiana by application of ascorbic acid. *Plant Physiol.* 186 (2), 832–355. doi: 10.1093/plphys/kiab102

Palacpac, N. Q., Yoshida, S., Sakai, H., Kimura, Y., Fujiyama, K., Yoshida, T., et al. (1999). Stable expression of human B1,4-galactosyltransferase in plant cells modifies N-linked glycosylation patterns. *Proc. Natl. Acad. Sci.* 96 (8), 4692–4975. doi: 10.1073/pnas.96.8.4692

Perneczky, R., Jessen, F., Grimmer, T., Levin, J., Flöel, A., Peters, O., et al. (2023). Anti-amyloid antibody therapies in alzheimer's disease. *Brain* 146 (3), 842–495. doi: 10.1093/brain/awad005

Pillet, Stéphane, Arunachalam, P. S., Andreani, G., Golden, N., Fontenot, J., Pyone Aye, P., et al. (2022). Safety, immunogenicity, and protection provided by unadjuvanted and adjuvanted formulations of a recombinant plant-derived virus-like particle vaccine candidate for COVID-19 in nonhuman primates. *Cell. Mol. Immunol.* 19 (2), 222–233. doi: 10.1038/s41423-021-00809-2

Qiu, X., Wong, G., Audet, J., Bello, A., Fernando, L., Alimonti, J. B., et al. (2014). Reversion of advanced ebola virus disease in nonhuman primates with ZMapp. *Nature* 514 (7520), 47–53. doi: 10.1038/nature13777

Rattanapisit, K., Phakham, T., Buranapraditkun, S., Siriwattananon, K., Boonkrai, C., Pisitkun, T., et al. (2019). Structural and in vitro functional analyses of novel plant-produced anti-human PD1 antibody. *Sci. Rep.* 9 (1), 152055. doi: 10.1038/s41598-019-51656-1

Reardon, D., Kaley, T., Iwamoto, F., Baehring, J., Subramaniam, D., Rawls, T., et al. (2018). ATIM-23. Anti-CD27 agonist antibody varlilumab in combination with nivolumab for recurrent glioblasma (RGBM): phase 2 clinical trial results. *Neuro-Oncology* 20 (suppl_6). doi: 10.1093/neuonc/noy148.018. vi6–vi6.

Rivera, A. L., Gómez-Lim, M., Fernández, F., and Loske, A. M. (2012). Physical methods for genetic plant transformation. *Phys. Life Rev.* 9 (3), 308–455. doi: 10.1016/j.plrev.2012.06.002

Sainsbury, F., and Lomonossoff, G. P. (2008). Extremely high-level and rapid transient protein production in plants without the use of viral replication. *Plant Physiol.* 148 (3), 1212–1185. doi: 10.1104/pp.108.126284

Saint-Jore-Dupas, C., Nebenführ, A., Boulaflous, Aurélia, Follet-Gueye, M.-L., Plasson, C., Hawes, C., et al. (2006). Plant *N* -glycan processing enzymes employ different targeting mechanisms for their spatial arrangement along the secretory pathway. *Plant Cell* 18 (11), 3182–3200. doi: 10.1105/tpc.105.036400

Sariyatun, R., Florence, H. K., Ohashi, T., Misaki, R., and Fujiyama, K. (2021). Production of human acid-alpha glucosidase with a paucimannose structure by glycoengineered arabidopsis cell culture. *Front. Plant Sci.* 12 (July). doi: 10.3389/fpls.2021.703020

Schoberer, J., Vavra, U., Stadlmann, J., Hawes, C., Mach, L., Steinkellner, H., et al. (2009). Arginine/lysine residues in the cytoplasmic tail promote ER export of plant glycosylation enzymes. *Traffic* 10 (1), 101–155. doi: 10.1111/j.1600-0854.2008.00841.x

Schneider, J., Castilho, A., Pabst, M., Altmann, F., Gruber, C., Strasser, R., et al. (2015). "Characterization of plants expressing the human β1,4-galactosyltrasferase gene.". *Plant Physiol. Biochem.* 92 (July), 39–47. doi: 10.1016/j.plaphy.2015.04.010

Seemann, J., Jokitalo, E., Pypaert, M., and Warren, G. (2000). Matrix proteins can generate the higher order architecture of the golgi apparatus. *Nature* 407 (6807), 1022–1026. doi: 10.1038/35039538

Sethi, L., Kumari, K., and Nrisingha, D. (2021). Engineering of plants for efficient production of therapeutics. *Mol. Biotechnol.* 63 (12), 1125–1375. doi: 10.1007/s12033-021-00381-0

Sheshukova, E. V., Komarova, T. V., and Dorokhov, Y. L. (2016). Plant factories for the production of monoclonal antibodies. *Biochem. (Moscow)* 81, 1118–1135. doi: 10.1134/s0006297916100102

Sriraman, R., Bardor, M., Markus, S., Carmen, V., Loïc, F., Rainer, F., et al. (2004). Recombinant anti-HCG antibodies retained in the endoplasmic reticulum of transformed plants lack core-xylose and core-α(1,3)-fucose residues. *Plant Biotechnol. J.* 2 (4), 279–875. doi: 10.1111/j.1467-7652.2004.00078.x

Strasser, R., Bondili, J. S., Vavra, U., Schoberer, J., Svoboda, B., Glössl, J., et al. (2007). A unique B1,3-galactosyltransferase is indispensable for the biosynthesis of *N* -glycans containing lewis a structures in *arabidopsis thaliana*. *Plant Cell* 19 (7), 2278–2292. doi: 10.1105/tpc.107.052985

Strasser, R., Castilho, A., Stadlmann, J., Kunert, R., Quendler, H., Gattinger, P., et al. (2009). "Improved virus neutralization by plant-produced anti-HIV antibodies with a homogeneous β1,4-galactosylated n-glycan profile.". *J. Biol. Chem.* 284 (31), 20479–20485. doi: 10.1074/jbc.M109.014126

Varki, A. (2017). Biological roles of glycans. *Glycobiology* 27 (1), 3–49. doi: 10.1093/glycob/cww086

Vézina, L.-P., Faye, Loïc, Lerouge, P., D'Aoust, Marc-André, Marquet-Blouin, E., Burel, C., et al. (2009). Transient co-expression for fast and high-yield production of antibodies with human-like N -glycans in plants. *Plant Biotechnol. J.* 7 (5), 442–555. doi: 10.1111/j.1467-7652.2009.00414.x

Vitale, L. A., He, Li Z., Thomas, L. J., Widger, J., Weidlick, J., Crocker, A., et al. (2012). Development of a human monoclonal antibody for potential therapy of CD27-expressing lymphoma and leukemia. *Clin. Cancer Res.* 18 (14), 3812–3821. doi: 10.1158/1078-0432.CCR-11-3308

Wang, L.-X., Tong, X., Li, C., Giddens, J. P., and Li, T. (2019). Glycoengineering of antibodies for modulating functions. *Annu. Rev. Biochem.* 88 (1), 433–595. doi: 10.1146/annurev-biochem-062917-012911

Wasiuk, A., Testa, J., Weidlick, J., Sisson, C., Vitale, L., Widger, J., et al. (2017). CD27-mediated regulatory T cell depletion and effector T cell costimulation both contribute to antitumor efficacy. *J. Immunol.* 199 (12), 4110–4123. doi: 10.4049/jimmunol.1700606

Wojtaszek, Przemysław. (1997). Oxidative burst: an early plant response to pathogen infection. *Biochem. J.* 322 (3), 681–692. doi: 10.1042/bj3220681

Zhao, H., Tan, Z., Wen, X., and Wang, Y. (2017). An improved syringe agroinfiltration protocol to enhance transformation efficiency by combinative use of 5-azacytidine, ascorbate acid and tween-20. *Plants (Basel).* 6 (1), 9. doi: 10.3390/plants6010009

frontiers | Frontiers in Plant Science

TYPE Original Research
PUBLISHED 29 August 2023
DOI 10.3389/fpls.2023.1149455

OPEN ACCESS

EDITED BY
Kathleen L. Hefferon,
Cornell University, United States

REVIEWED BY
Ekaterina Sheshukova,
Russian Academy of Sciences, Russia
Jinping Zhao,
Texas A and M University, United States

*CORRESPONDENCE
Waranyoo Phoolcharoen
Waranyoo.P@chula.ac.th

RECEIVED 22 January 2023
ACCEPTED 16 August 2023
PUBLISHED 29 August 2023

CITATION
Bulaon CJI, Khorattanakulchai N, Rattanapisit K, Sun H, Pisuttinusart N, Strasser R, Tanaka S, Soon-Shiong P and Phoolcharoen W (2023) Antitumor effect of plant-produced anti-CTLA-4 monoclonal antibody in a murine model of colon cancer.
Front. Plant Sci. 14:1149455.
doi: 10.3389/fpls.2023.1149455

Antitumor effect of plant-produced anti-CTLA-4 monoclonal antibody in a murine model of colon cancer

Christine Joy I. Bulaon[1,2,3], Narach Khorattanakulchai[4], Kaewta Rattanapisit[4], Hongyan Sun[5], Nuttapat Pisuttinusart[1,2,3], Richard Strasser[6], Shiho Tanaka[7], Patrick Soon-Shiong[7] and Waranyoo Phoolcharoen[1,2*]

[1]Center of Excellence in Plant-Produced Pharmaceuticals, Chulalongkorn University, Bangkok, Thailand, [2]Department of Pharmacognosy and Pharmaceutical Botany, Faculty of Pharmaceutical Sciences, Chulalongkorn University, Bangkok, Thailand, [3]Graduate Program of Pharmaceutical Sciences and Technology, Faculty of Pharmaceutical Sciences, Chulalongkorn University, Bangkok, Thailand, [4]Baiya Phytopharm Co., Ltd, Bangkok, Thailand, [5]GemPharmatech Co., Ltd, Nanjing, China, [6]Department of Applied Genetics and Cell Biology, University of Natural Resources and Life Sciences, Vienna, Austria, [7]ImmunityBio, Inc., Culver City, CA, United States

Cytotoxic T lymphocyte-associated protein 4 (CTLA-4) is an immune checkpoint regulator exclusively expressed on T cells that obstructs the cell's effector functions. Ipilimumab (Yervoy®), a CTLA-4 blocking antibody, emerged as a notable breakthrough in modern cancer treatment, showing upfront clinical benefits in multiple carcinomas. However, the exhilarating cost of checkpoint blockade therapy is discouraging and even utmost prominent in developing countries. Thereby, affordability of cancer care has become a point of emphasis in drug development pipelines. Plant expression system blossomed as a cutting-edge platform for rapid, facile to scale-up, and economical production of recombinant therapeutics. Here, we describe the production of an anti-CTLA-4 2C8 antibody in *Nicotiana benthamiana*. ELISA and bio-layer interferometry were used to analyze antigen binding and binding kinetics. Anticancer responses in vivo were evaluated using knocked-in mice implanted with syngeneic colon tumor. At 4 days post-infiltration, the antibody was transiently expressed in plants with yields of up to 39.65 $\pm$ 8.42 µg/g fresh weight. Plant-produced 2C8 binds to both human and murine CTLA-4, and the plant-produced IgG1 also binds to human FcγRIIIa (V158). In addition, the plant-produced 2C8 monoclonal antibody is as effective as Yervoy® in inhibiting tumor growth in vivo. In conclusion, our study underlines the applicability of plant platform to produce functional therapeutic antibodies with promising potential in cancer immunotherapy.

KEYWORDS

cytotoxic T lymphocyte-associated protein 4, 2C8, anti-CTLA-4 antibody, *Nicotiana benthamiana*, cancer immunotherapy

Introduction

Cancer is a multifaceted disease that exerts a heavy toll on society. It is still the leading cause of fatality worldwide with the developing nations shouldering most of the burden. Since then, cancer management with surgery, radiotherapy and chemotherapy has provided a chance of cure and achieved satisfactory results (Arruebo et al., 2011). However, shortcomings of these current cancer modalities including post-operative recurrence, resistance, and side effects limit their clinical success. In attempt to augment the traditional methods for cancer therapy, developments in the treatment landscape represent major areas of focus. The worthwhile advancement in cancer therapeutics have shifted the paradigm for cancer treatment. Among these, cancer immunotherapy has drawn significant attention in the oncology field. The concept of immunotherapy involves variety of approaches aimed at harnessing the immune system to target cancerous cells. The efficacy of these immune-based therapies is being actively evaluated in several clinical trials (Behrouzieh et al., 2021; Juat et al., 2022; Liu et al., 2022) and has shown considerable promise in a number of human malignancies, for which immunotherapy is regarded as a standard of care.

Immune checkpoint blockade (ICB) therapy has become one of the most common options for cancer immunotherapy within the therapeutic armamentarium. Several immune checkpoint proteins, such as programmed cell death protein 1 (PD-1), programmed cell death ligand 1 (PD-L1), and cytotoxic T lymphocyte-associated protein 4 (CTLA-4), enable peripheral immune tolerance under physiological conditions although often become coopted in the cancer context. Immune checkpoint inhibitors (ICIs) could reverse T cell enervation and restore antitumor effector functions, ultimately leading to cancer eradication. ICB therapy has gained prominence and is being approved in multiple cancer indications largely due to durable response (Tang et al., 2018) and improved safety (Khan et al., 2018) observed in clinical practice. The CTLA-4 checkpoint receptor provided the first target for antibody-based immunotherapy and is a homolog of CD28 receptor, which both belong to the immunoglobulin superfamily on T cells. It is postulated that CTLA-4 can negatively regulate T cell signaling by directly antagonizing CD28. Due to the higher affinity binding of CTLA-4 to CD80 and CD86, CTLA-4 can outcompete CD28 for co-stimulatory ligands, thus inhibiting T cell activation. Additionally, CTLA-4 is constitutively expressed on regulatory T cells (Tregs), indicating that CTLA-4 receptor plays a vital role for direct and indirect immunosuppressive activity of Tregs. To that end, the relevance of CTLA-4 function led to the development of inhibitory antibodies obturating its actions to enhance T cell antitumor responses. The two approved monoclonal antibodies (mAbs) that target CTLA-4 are Ipilimumab (Yervoy®, MDX-010, BMS-734016) and Tremelimumab (tremelimumab-actl; IMJUDO®). They are currently used as monotherapy or in combination to treat a variety of malignant tumors, including hepatocellular carcinoma, non-small cell lung cancer, melanoma and other solid tumors (Cameron et al., 2011; Cabel et al., 2017; Morse et al., 2019; Keam, 2023). With the substantial number of preclinical and clinical studies, anti-CTLA-4 mAb has proven the unprecedented potentials of ICB immunotherapy. Interestingly, while cancer remains a universal concern, the staggering high production cost of recombinant blocking antibodies is expected to impact in low- and middle-income countries.

The use of plant expression systems to produce pharmaceutical and non-pharmaceuticals is constantly expanding and gaining recognition in the research (Bulaon et al., 2020; Shanmugaraj et al., 2020a; Rattanapisit et al., 2021; Shanmugaraj et al., 2021) and manufacturing industries (Nosaki et al., 2021). Some of its key advantages include rapid and ease of cultivation, scalability, lack or low risk of pathogen contamination, ability to carry out posttranslational modifications and cost-effectiveness (Nandi et al., 2016; Shanmugaraj et al., 2020a; Nosaki et al., 2021). For several years, mammalian cell cultures (i.e., CHO cells) have been the dominant expression system for mAbs. Nonetheless, the plant-based facility is projected to lower operating expenses and cost of goods sold compared to the CHO facility (Kelley, 2009; Petrides et al., 2014; Nandi et al., 2016). The downstream processing costs for a mAb produced using a conventional CHO cell platform at a high production capacity (1,000 kg/year) were estimated to be $232/g. Even at a much lower production capacity (600 kg/year), the plant-derived platform has a cost of goods sold of ~$99/g, which includes both upstream and downstream process operations, corresponding to decrease of over 50% in manufacturing costs. According to the presented techno-economic model (Nandi et al., 2016), plant-based expression technology is a promising platform for the production of mAbs. Our team (Rattanapisit et al., 2019; Phakham et al., 2021; Yiemchavee et al., 2021; Phetphoung et al., 2022) have previously expressed recombinant immunotherapeutic antigens and antibodies in plants, providing proof of principle for its viability. To attenuate striking disparities and improve access to treatment in impoverished countries, plant-based approach offers a competitive platform for the development of immunomodulatory agents for cancer immunotherapy. Herein, we describe the rapid transient expression of an anti-CTLA-4 antibody, 2C8, in *Nicotiana benthamiana*. This plant-produced antibody was purified and characterized for its physicochemical and functional properties. We found that the plant-produced anti-CTLA-4 2C8 mAb binds to human and murine CTLA-4 proteins as well as to one of the Fcγ receptors (FcγRs). Further, this plant-produced anti-CTLA-4 2C8 mAb demonstrated similar antitumor efficacy with the commercial anti-CTLA-4 mAb (Yervoy®) in a humanized mouse tumor model. These results imply that the plant-produced anti-CTLA-4 mAb may have comparable therapeutic potentials to clinically effective Ipilimumab.

Materials and methods

Expression vector constructs

The nucleotide sequences encoding the variable regions of anti-CTLA-4 2C8 heavy chain (HC) and light chain (LC) (Wang et al., 2017) were codon optimized *in silico* for expression in *N.*

benthamiana and synthesized commercially (Bioneer, South Korea). To construct the full-length HC and LC of 2C8 mAb, the plant-optimized variable HC and LC genes were fused with the constant regions of human immunoglobulin 1 (IgG1) gamma chain and kappa chain, respectively. In addition, both the HC and LC of 2C8 mAb harbor a signal peptide at the N-terminus and a SEKDEL retention peptide at the C-terminus of HC. The HC and LC of anti-CTLA-4 2C8 mAb were subcloned using *Xba*I and *Sac*I restriction enzymes in a plant expression vector (pBYR2e) (Chen et al., 2011; Diamos and Mason, 2019). The constructed anti-CTLA-4 pBYR2e-2C8 HC and pBYR2e-2C8 LC expression vectors were introduced into *Agrobacterium tumefaciens* strain GV3101 by electroporation and the recombinant colonies were selected on appropriate antibiotic (50 mg l^{-1} kanamycin; 50 mg l^{-1} gentamycin; 50 mg l^{-1} rifampicin) supplemented Luria Bertani (LB) agar plate. All expression vectors (pBYR2e-2C8 HC and pBYR2e-2C8 LC) in *A. tumefaciens* cells were sequenced verified (U2Bio, Thailand) prior to infiltration in *Nicotiana benthamiana* plants.

Transient expression in *Nicotiana benthamiana*

The *Agrobacterium* harboring either the pBYR2e-2C8 HC or pBYR2e-2C8 LC plasmids were cultivated on liquid LB media containing 50 mg l^{-1} kanamycin, 50 mg l^{-1} gentamycin, and 50 mg l^{-1} rifampicin overnight with shaking (200 rpm) at 28°C in the dark. The *Agrobacterium* cells were pelleted and resuspended with 1X infiltration buffer (10 mM 2-N-morpholino-ethanesulfonic acid (MES); 10 mM $MgSO_4$) at pH 5.5. A 1:1 ratio of HC and LC cultures were mixed to get a final OD_{600} of 0.2.

Approximately 6–8-week-old *N. benthamiana* plants were grown in a plant room under controlled conditions (16 h light and 8 h dark cycle at 28°C) and used for expression. The method for small-scale infiltration in plants was adopted from (Phakham et al., 2021). Briefly, the HC and LC genes were co-agroinfiltrated into *N. benthamiana* leaves using needle-less syringes. The infiltrated plant leaves were maintained and harvested within 2-, 3-, 4-, 5-, and 6-days post-infiltration (dpi) to initially evaluate the expression level of plant-produced anti-CTLA-4 antibody.

Isolation and quantification of plant-produced anti-CTLA-4

Infiltrated leaf samples collected at different dpi were chopped into small leaf discs and pooled to obtain ~20-50 mg leaf fresh weight. The leaves were extracted by a tissue lyser (Retsch, Model: MM 400) with stainless steel grinding balls (diameter 3 mm) (Retsch, Germany) in 200 µl 1X phosphate-buffered saline (PBS: 137 mM NaCl; 2.7 mM KCl; 4.3 mM Na_2HPO_4; 1.47 mM KH_2PO_4) at pH 7.4. The resultant crude extract was subjected to centrifugation (20,000 × *g* for 5 min) at 4°C and the supernatant was analyzed to determine the yield of plant-produced 2C8 mAb by enzyme-linked immunosorbent assay (ELISA).

Briefly, a 96-well microtiter plate (3690, Corning, United States) was coated with 25 µl of goat anti-human IgG, Fc specific antibody (dilution 1:1000) (ab97221, Abcam, United Kingdom) and incubated overnight at 4°C. The ELISA plate was washed with 1X PBST (PBS with 0.05% (v/v) Tween 20) for three times and blocked with 5% (w/v) skim milk in 1X PBS for 2 h at 37°C. After washing, two-fold serial dilutions of standard human IgG1 isotype control (ab206198, Abcam, United Kingdom) and plant crude extracts were added and incubated for 2 h at 37°C. Then, the plate was washed and treated with peroxidase-conjugated goat anti-human kappa antibody (dilution 1:2500) (2060-05, SouthernBiotech, United States) for 1 h at 37°C. After three-time washes with 1X PBST, the plate was developed using TMB one solution substrate (Promega, United States) and the reaction was stopped with 1M H_2SO_4. The absorbance was measured at 450 nm by a microplate reader (Hercuvan, Model: NS-100).

Purification of plant-produced anti-CTLA-4

The production of plant-produced anti-CTLA-4 2C8 mAb was scaled up by vacuum infiltration. In brief, *Agrobacterium* cultures harboring recombinant HC and LC vectors were mixed together at a ratio of 1:1 in 1X infiltration buffer to achieve an OD_{600} of 0.2. Plant leaves were then submerged in an infiltration medium containing an *Agrobacterium* suspension and infiltrated under vacuum at 600–760 mmHg for 1-2 min. Infiltrated tobacco plants were incubated in an indoor plant room and harvested at optimal dpi. About 70 g of infiltrated *N. benthamiana* leaves were harvested at 4 dpi and homogenized by blender with 140 mL 1X PBS. The plant crude extract was centrifuged (13,000 rpm for 30 min) at 4°C and filtered by a cheesecloth and a 0.22-µm S-Pak filter (Merck Millipore, United States). The clarified supernatant was loaded onto a polypropylene column (diameter 15 mm) (Qiagen, Germany) packed with MabSelect SuRe™ LX protein A resin (Cytiva, Sweden). The column was washed with 1X PBS, and the plant-produced antibody was eluted using a 0.15 M citrate buffer at pH 2.7 and immediately neutralized with 1.5 M Tris-HCl pH 8.8 until a final pH of approximately 7.4. The purified antibody was buffer-exchanged with 1X PBS using a Snakeskin™ dialysis tubing (3.5K MWCO) (Thermo Scientific, United States) and concentrated in Amicon® Ultra (50K) centrifugal filter (Merck, Germany). The purified plant-produced anti-CTLA-4 antibody was quantified by ELISA and characterized in succeeding experiments.

Sodium dodecyl sulfate polyacrylamide gel electrophoresis and immunoblot analysis

Plant crude extracts and purified antibody samples were separated by SDS-PAGE and analyzed by western blot to confirm the antibody expression. For non-reducing condition, protein samples were mixed with 10X loading buffer (125 mM Tris-HCl at pH 6.8; 12% (w/v) SDS; 10% (v/v) glycerol; 0.001% (w/v) bromophenol blue). Whereas, for reducing condition, protein samples were mixed with 10X loading buffer containing 22% (v/v) β-mercaptoethanol. The proteins were heated for 5 min at 95°C and separated on a 4-15% gel. For visualization of purified plant-produced antibody (~2 µg) on SDS gel, the bands were stained with InstantBlue® dye (Abcam, United Kingdom).

For western blotting, about 20-40 µg total soluble protein of plant crude extracts and 0.1-1.0 µg of purified antibody were transferred to a nitrocellulose membrane (Bio-Rad, United States). Then, the membrane was blocked with 5% (w/v) skim milk in 1X PBS. The blot membranes were incubated either with peroxidase conjugated goat anti-human IgG gamma chain antibody (dilution 1:5000) (2040-05, SouthernBiotech, United States) or peroxidase-conjugated goat anti-human kappa antibody (dilution 1:5000) (2060-05, SouthernBiotech, United States) for the detection of HC and LC of plant-produced anti-CTLA-4 2C8 mAb. A non-infiltrated plant crude extract was used as a negative control. The membranes were washed with 1X PBST and exposed to a medical X-ray green film (Carestream, United States) using enhanced chemiluminescence substrate solution (Promega, United States).

Size exclusion chromatography

To determine the antibody purity and aggregation status of the antibody, the plant-produced anti-CTLA-4 mAb was injected into a SEC BEH 200 column (4.6 x 300 mm, 2.5 µM particle size) (Waters, United States) attached on an UHPLC system (Waters, United States). The 1X PBS buffer at pH 7.4 was used as an elution buffer and operated at 0.3 mL/min flow rate. The column was maintained at 25°C and the sample was run for 20 min. The UV absorbance signal was monitored at 280 nm and the peak was integrated by using Empower 3 software (Waters, United States).

N-Glycan analysis

Liquid chromatography-electrospray ionization-mass spectrometry (LC-ESI-MS) was performed to assess the *N*-glycan profile of our purified plant-produced anti-CTLA-4. In brief, the antibody was initially subjected to reducing SDS-PAGE and then the protein band of heavy chain was cut into slices, S-alkylated and proteolytically digested. The tryptic glycopeptides were analyzed by LC-ESI-MS following the protocol of (Strasser et al., 2008).

CTLA-4 binding ELISA

Recombinant human CTLA-4 protein (huCTLA-4) (11159-H08H, SinoBiological, China) and mouse CTLA-4 protein (muCTLA-4) (50503-M08H, SinoBiological, China) were used to verify the binding activity of plant-produced anti-CTLA-4 2C8 mAb to its target. Briefly, microtiter plates (3690, Corning, United States) were coated at a concentration of 2 µg/mL overnight at 4°C. Then, the plates were washed with 1X PBST and blocked with 5% (w/v) skim milk in 1X PBS for 1 h at 37°C. Two-fold serial dilutions starting from 8 µg/mL of plant-produced anti-CTLA-4 2C8 antibody or plant-produced irrelevant antibody (anti-PD-1) (Rattanapisit et al., 2019) or human IgG1 isotype control (ab206198, Abcam, United Kingdom) were added into the plates and incubated for 2 h at 37°C. After three-time washes with 1X PBST, the plates were incubated with peroxidase-conjugated goat anti-human kappa antibody (dilution 1:2500) (2060-05, SouthernBiotech, United States) for 1 h at 37°C. The plates were washed and then developed using TMB one solution substrate (Promega, United States) for 15 min at room temperature, before quenching with 1 M H_2SO_4. The absorbance was measured at 450 nm by a microplate reader (Hercuvan, Model: NS-100).

Equilibrium dissociation constant (K_D) determination by bio-layer interferometry

BLI buffer used in all experiments was 10 mM HEPES, 150 mM NaCl, pH 7.4, with 0.02% Tween 20, and 0.1% BSA. Commercially purchased recombinant human and mouse CTLA-4 proteins (SinoBiological, China) and human FcγRIIIa (V158) protein (R&D systems, United States) were used in the experiments. For determining the binding affinity for huCTLA-4 and muCTLA-4, plant-produced anti-CTLA-4 2C8 mAb was immobilized on anti-hIgG Fc Capture (AHC) biosensors (Sartorius Corporation, Germany). A concentration series of 100, 50, 25, 12.5 nM of huCTLA-4 and a concentration series of 100, 25, 6.25, 3.13 of muCTLA-4 were used to determine the kinetic constants (k_{on}, k_{off}, K_D) for huCTLA-4 and muCTLA-4, respectively, using 1:1 binding curve fit. For determining binding affinity for huFcγRIIIa (V 158), the receptor protein was loaded on the HIS1K sensor, and a concentration series of 4000, 2000, 1000, 500, 250, 125, 62.5 nM of anti-CTLA-4 2C8 was used to determine K_D using steady state analysis.

In vivo analysis in mouse tumor model

The study protocol (Animal Protocol No. GPTAP20220128-4) was reviewed and approved by the Institutional Animal Care and Use Committee (IACUC) of GemPharmatech Co., Ltd., China prior execution. The procedures involving care and utilization of animals were conducted in accordance with the laws and regulations stated in the Animal Welfare Act and the Association for Assessment and Accreditation of Laboratory Animal Care (AAALAC).

Six to eight weeks old female knocked-in mice were used in this study. Accordingly, humanized mice model (BALB/c-hPD-1/hPD-L1/hCTLA-4) was developed by GemPharmatech, Co., Ltd with experimental animal using license (SYXK (SU) 2018-0027) and experimental animal production license (SCXK (SU) 2018-0008). CRISPR/Cas9 technology was used to replace the extracellular regions of murine PD-1, PD-L1, and CTLA-4 with human PD-1, PD-L1, and CTLA-4 on a BALB/c background. Following, the expression of human proteins was detected in this strain, with no apparent difference in T/B/NK cell proportion observed between wild type and humanized mice. Thereby, this strain can be used to test immune-oncology drugs. BALB/c-hPD-1/hPD-L1/hCTLA-4 were implanted with CT26 murine colon cancer cells expressing humanized PD-L1 (CT26-hPDL1) subcutaneously on the right flank (1×10^6/100 µL cells). When the average tumor size reached 100.07 mm^3, all mice (n = 18) were randomly allocated into 3 treatment groups (n = 6 per group). 1X PBS as vehicle or anti-CTLA-4 antibodies (3 mg/kg), such as plant-produced 2C8 and

commercially available Ipilimumab (Yervoy®), were administered via., intraperitoneal injection on days 0, 3, 6, 9, 12, 15. To evaluate the treatment efficacy, tumor growth inhibition (TGI) models based on tumor volume (TV) and tumor weight (TW) measurements were utilized. Furthermore, body weight changes were measured by an electronic weighing scale three times in a week.

Statistical analysis

All data were expressed as mean ± standard deviation (mean ± SD). One way ANOVA followed by multiple comparison procedures was performed. Data were analyzed with SPSS and all tests were two-sided. A p value < 0.001 was considered to be statistically significant and noted with ***.

Results

Transient expression of 2C8, an anti-CTLA-4 mAb

The genetic cassettes of anti-CTLA-4 pBYR2e-2C8 HC and pBYR2e-2C8 LC (Figure 1A) were co-delivered into *N. benthamiana* by *Agrobacterium*-mediated transformation to produce complete recombinant antibody with 2 HC and 2 LC (Figure 1B). Expression of anti-CTLA-4 2C8 mAb was determined over a 5-day timepoints and infiltrated leaves were collected daily from 2 dpi. The morphological changes in *N. benthamiana* leaves at the infiltrated site were examined (Figure 2A, indicated in circles). At 3 dpi, visible necrotic lesion was observed, while the surrounding non-infiltrated leaf area showed no necrosis. Necrosis with associated wilting was later developed from 4 to 6 dpi. The effect of dpi on antibody expression level was quantified by ELISA. Infiltrated leaves with evidence of infection or necrosis were collected and used to extract recombinant antibody. Based on the result, the highest expression of plant-produced antibody was achieved at 4 dpi, amounting up to 39.65 ± 8.42 μg/g fresh weight (Figure 2B; Supplementary Table 1). The presence of plant-produced antibody in crude leaf extracts was confirmed by immunoblotting. Under a non-reduced condition, the infiltrated crude extract (+ Crude) showed a single band at ~150 kDa while non-infiltrated crude extract (- Crude) did not show any detectable band (Figure 2C). The HC and LC bands at ~150 kDa could correspond to the expression of a fully assembled antibody when detected by anti-human IgG gamma and anti-human kappa antibodies. Overall, our findings indicated that plant-produced anti-CTLA-4 2C8 mAb was successfully and rapidly produced in plants via., transient expression approach.

Characterization of anti-CTLA-4 2C8 mAb produced in *N. benthamiana*

The plant-produced mAb was purified from crude leaf extracts using protein A affinity chromatography and the purity was determined by InstantBlue® staining. The purified plant-produced antibody was further confirmed by immunblot assay using peroxidase-conjugated HC-specific and LC-specific antibodies. Under non-reducing condition, the plant-produced antibody was shown as a single distinct band at ~150 kDa (Figure 3A), with trace levels of antibody fragments also observed. The results indicated the

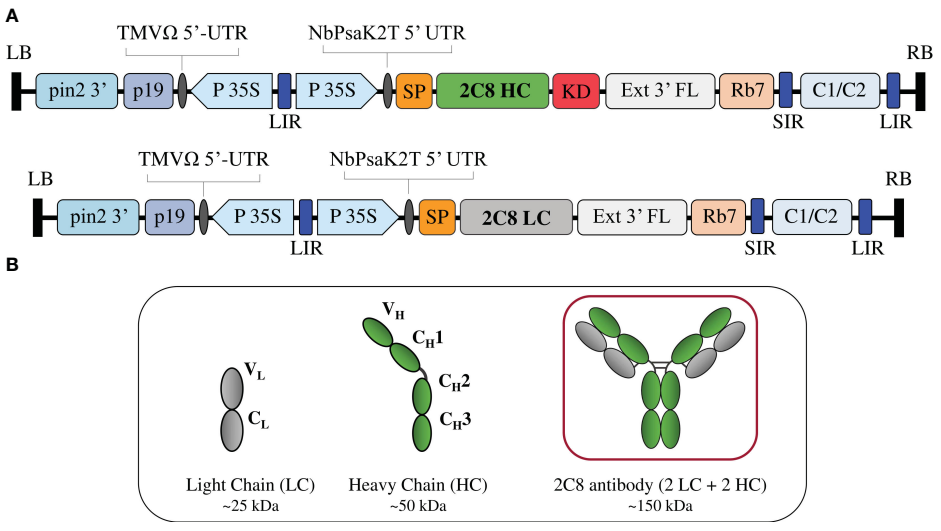

FIGURE 1
Construction of anti-CTLA-4 2C8 mAb. **(A)** Schematic representation of the gene expression vectors used in the study. The T-DNA elements flanked between the LB (left border) and RB (right border) of pBYR2e comprises of P19: silencing suppressor gene derived from TBSV; TMV 5′ UTR: tobacco mosaic virus Ω 5′ UTR; P35S: CaMV 35S promoter; NbPsaK2T 5′UTR: *Nicotiana* photosystem I reaction center subunit *psaK* 5′UTR; Ext3′FL: 3′ region of the tobacco extension gene; Rb 7: tobacco RB7 promoter; and C1/C2: BeYDV ORFs C1 and C2 encoding for Rep and RepA. The 2C8 HC and 2C8 LC contained DNA sequences encoding for the HC (heavy chain) and LC (light chain) of anti-CTLA-4 2C8 antibody. These expression cassettes are fused either with SP (signal peptide) and/or KD (SEKDEL tag) and inserted between the LIR and SIR (long and short intergenic regions of the BeYDV genome). **(B)** Schematic and structure diagram of HC, LC, and assembled plant-produced anti-CTLA-4 2C8 mAb.

assembly of a full length IgG containing two identical HCs and two identical LCs as identified by anti-human gamma and anti-human kappa antibodies. Meanwhile, under reducing condition, protein bands at ~50 kDa and ~25 kDa were detected corresponding to the expected HC and LC of plant-produced antibody (Figure 3B). SDS-PAGE and immunoblot results verified the presence of unassembled free HC and LC in the blots containing reducing agent β-mercaptoethanol. To identify intact antibody and aggregates, plant-produced anti-CTLA-4 2C8 mAb was analyzed by SEC separation. Figure 3C shows a chromatogram of SEC fractions containing a plant-produced anti-CTLA-4 IgG monomer (major peak) and some observed amounts of aggregated forms (minor peaks). According to our results, plant-produced monoclonal antibody largely assembled and remained as a monomeric species. Moreover, to determine the *N*-glycosylation pattern, plant-produced anti-CTLA-4 2C8 mAb was first digested with trypsin followed by LC-ESI-MS analysis. The attachment of SEKDEL or KD tag to the C-terminus of heavy chain revealed the presence of oligomannosidic *N*-glycans $Man_{5-9}GlcNAc_2$ on the plant-derived antibody (Figure 3D), which is expected for ER-retained proteins.

Plant-produced anti-CTLA-4 2C8 mAb binds to CTLA-4 and FcγRIIIa (V158)

The affinity of plant-produced anti-CTLA-4 2C8 mAb to purified CTLA-4 recombinant proteins was investigated by ELISA. Plates were coated either with human CTLA-4 or mouse CTLA-4 and then treated with increasing concentrations of plant-produced anti-CTLA-4 antibody, alongside with plant-produced anti-PD-1 (Rattanapisit et al., 2019) and human IgG1 isotype antibody as negative controls. Specific and dose-dependent binding to CTLA-4 proteins was observed for our plant-produced anti-CTLA-4 2C8 antibody (Figures 4A, B), whereas plant-produced anti-PD-1 antibody and human IgG1 did not elicit any binding as expected. Moreover, plant-produced 2C8 mAb was able to recognize both human and mouse CTLA-4 his-tagged proteins. Altogether, the anti-CTLA-4 2C8 mAb produced in *N. benthamiana* is deemed to be functional as it exhibits effective binding and human-mouse cross-reactivity to its target.

We further evaluated the binding kinetics using BLI with huCTLA-4 and muCTLA-4. The plant-produced 2C8 mAb demonstrated high binding affinity with human CTLA-4 and mouse CTLA-4 targets, having a subnanomolar to low nanomolar equilibrium dissociation constant (K_D) of 8.8×10^{-10} M and 2.2×10^{-9} M (Figure 5A). In addition, we also characterized the plant-produced 2C8 IgG1 binding to one of the Fcγ receptors using BLI and obtained K_D values from steady-state analysis. Data showed that the plant-produced IgG1 exhibited binding affinity for FcγRIIIa (V158) with a K_D of 3.2×10^{-7} M (Figures 5B). Collectively, these results confirmed the high binding affinity of plant-produced 2C8 for CTLA-4 protein and its ability to bind FcγR.

Plant-produced anti-CTLA-4 2C8 mAb exhibits antitumor activity *in vivo*

The antitumor efficacy of plant-produced anti-CTLA-4 2C8 mAb was evaluated in BALB/c-hPD-1/hPD-L1/hCTLA-4 mice. The humanized mice were subcutaneously implanted with mouse colon CT26-hPDL-1 tumor cells. The plant-produced anti-CTLA-4 or commercial anti-CTLA-4 (Yervoy®) or 1X PBS (vehicle) was

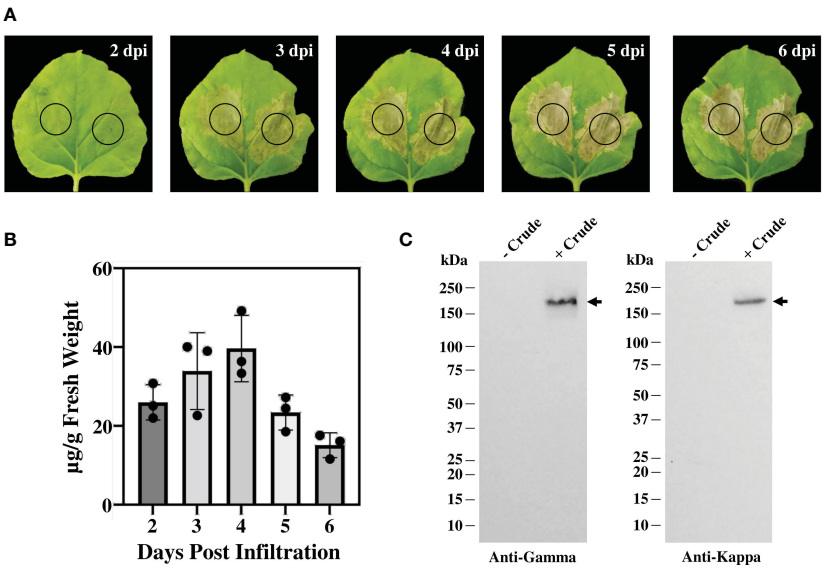

FIGURE 2
Transient expression of anti-CTLA-4 2C8 mAb in tobacco plants. **(A)** Physical morphology of *N. benthamiana* leaves for 2-6 days after infiltration with *Agrobacterium* carrying pBYR2e-2C8 HC + LC expression vectors. Black circle indicates infiltration site. **(B)** The expression levels of mAb (µg/g fresh weight) in *N. bethamiana* on days 2, 3, 4, 5, and 6 post-infiltration were quantified by ELISA. The data are presented as mean ± SD of three independent experiments. **(C)** The expression of mAb from crude leaf extracts was verified by western blot and detected by either peroxidase-conjugated anti-human IgG gamma chain or anti-human kappa antibody. Numbers on the left indicate molecular weight (kDa). – Crude: non-infiltrated crude extract as the control and + Crude: infiltrated crude extract. Black arrows indicate antibody bands.

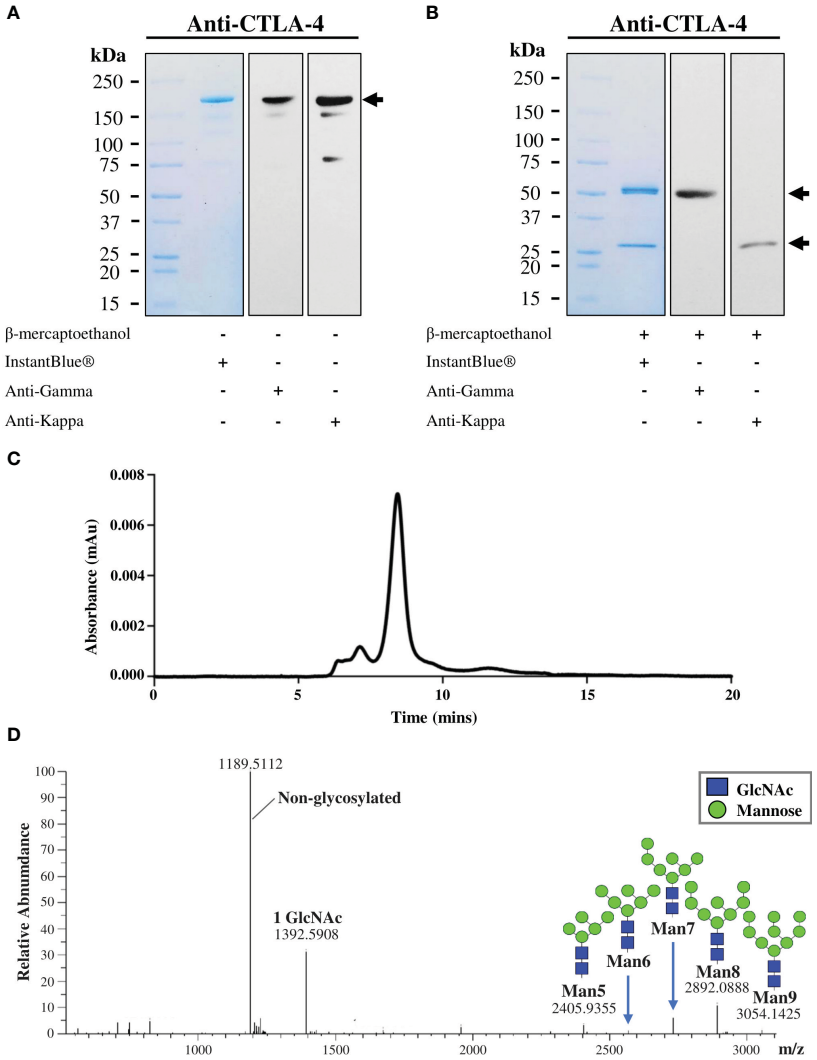

FIGURE 3
Characterization of purified plant-produced anti-CTLA-4 2C8 mAb. The purified plant-produced antibody was characterized by SDS-PAGE under **(A)** non-reducing and **(B)** reducing conditions. Separated proteins were either visualized by InstantBlue® staining (left) or transferred onto nitrocellulose membrane probed either with peroxidase-conjugated anti-human IgG gamma chain (middle) or anti-human kappa antibody (right). Numbers on the left indicate molecular weight (kDa). −: without β-mercaptoethanol and +: with β-mercaptoethanol. **(C)** Elution profile of purified plant-produced anti-CTLA-4 by size exclusion chromatography. **(D)** The *N*-glycosylation profile of plant-produced glycopeptide EEQYNSTYR (glycosylation site is underlined) from the Fc domain is shown, and the major glycosylated peaks are described. Black arrows indicate antibody bands.

administered following the dosage regimen shown on Figure 6A. Tumor growth inhibition based on tumor volume (TGI_{TV}) and tumor weight (TGI_{TW}) were monitored to evaluate the anti-tumor effect. As shown in Figure 6B; Supplementary Table 2, treatment with plant-produced anti-CTLA-4 at 3 mg/kg significantly regressed the tumor volume (TGI_{TV} = 96.58%) relative to the vehicle group ($p < 0.001$). Furthermore, our plant-produced anti-CTLA-4 antibody demonstrated comparable tumor volume reduction to those observed in the Yervoy® group at same dose (TGI_{TV} = 98.83%). At the conclusion of the study, tumors were collected and weighed. Data was used as a reference for the evaluation of antitumor effect. As shown in Figure 6C and summarized in Supplementary Table 3, results revealed that treatment with plant-produced anti-CTLA-4 significantly repressed tumor weight (TGI_{TW} = 96.93%) similarly to that of Yervoy®-treated group (TGI_{TW} = 99.20%). Hence, our findings demonstrated that the plant-produced anti-CTLA-4 2C8 mAb elicited strong antitumor responses and established similar degree of tumor growth inhibition with the commercially available anti-CTLA-4 drug. Meanwhile, tumor-bearing mice also showed good safety and tolerability to continuous administration of plant-produced anti-CTLA-4 antibody since no apparent body weight loss (>10%) were observed throughout the experiment (Figure 6D).

Discussion

The evasive mechanisms and immunosuppressive microenvironment of most malignant cells provided monumental strides for cancer immunotherapy. Several immunotherapeutic

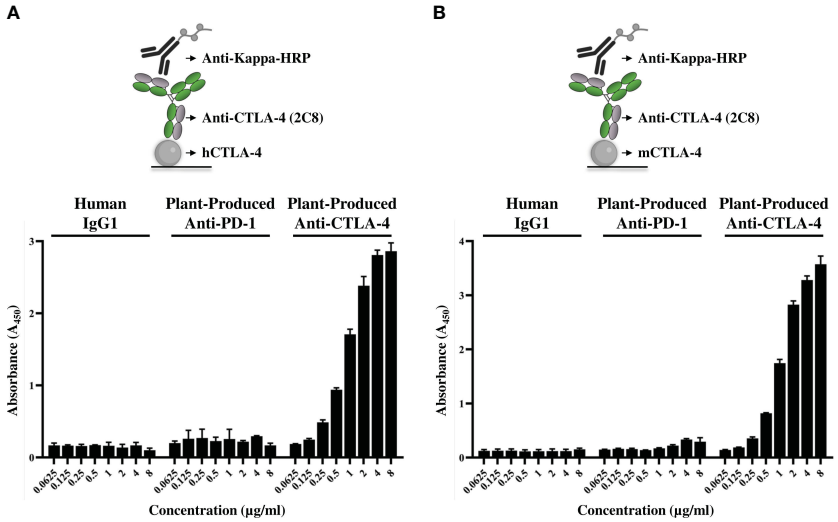

FIGURE 4
Binding properties of plant-produced anti-CTLA-4 2C8 mAb. The purified plant-produced anti-CTLA-4 antibody 2C8 mAb was tested to confirm their binding activities and cross-reactivity to huCTLA-4/His **(A)** or mCTLA-4/His **(B)**. The plant-produced anti-PD-1 and human IgG1 were used in parallel assays as negative controls. The data are presented as mean ± SD of three independent experiments.

maneuvers have been developed, with effective ICIs receiving most attention. This treatment aims to redirect the host immune system to eliminate cancer via., blockade of immunological checkpoints. Seven first-generation ICIs have been marketed and entered clinical use as of this writing, while over 5,000 trials currently being conducted (Upadhaya et al., 2022). These ICIs have demonstrated remarkable clinical efficacy in an array of recalcitrant carcinomas, including aggressive melanoma, difficult-to-treat lymphomas, and some cancers of the lung, liver, and kidney. Although minority of cancer patients benefitted from such treatments (Taefehshokr et al., 2022), ICIs have pushed the frontiers in cancer care, joining the ranks of conventional therapies. According to a pooled-analysis of anti-CTLA-4 Ipilimumab, more than 20% of treated patients with unresectable or metastatic melanoma experienced long-term survival for up to 10 years and suggested no cancer recurrence thereafter (Schadendorf et al., 2015). Nevertheless, despite favorable outcomes, the expensive cost of ICIs constraints access to and affordability of treatment.

The absolute cost of cancer medications is undoubtedly a crucial and growing global problem. While cancer occurs in all populations, the low- and middle-income countries suffer a double burden due to limited access to treatment. As a result, numerous initiatives to overcome these barriers must be prioritized. The advent of recombinant technology has transformed the standard of care regimens for cancer and a wide range of diseases. Currently, majority of the approved recombinant biopharmaceuticals, including the commercially available ICIs, are routinely produced in mammalian cell cultures. Mammalian cells remain to be the preferred platform; however, this system is rather expensive and requires complex culture conditions (Schillberg and Finnern, 2021). Plants seem to be a desirable alternative and inexpensive method for producing highly valuable proteins. It is well known that economic benefits, speed, and simplicity of scale-up drove concerted attention towards plant systems. The emergence of COVID-19 pandemic intensified the applications of plant platforms with the development of effective vaccine candidates and mAbs against the rapidly spreading SARS-CoV-2 and its variants (Shanmugaraj et al., 2020b; Khorattanakulchai et al., 2022). To this day, many plant-made mAbs are in various stages of development and hold promises for treating a plethora of infections as well as cancer. For example, Ma et al. (Ma et al., 2015) successfully produced P2G12 mAb from transgenic tobacco plants and tested it in a phase I clinical trial as an anti-HIV microbicidal agent. Safety evaluation of plant-based P2G12 in 11 volunteers revealed that no side effects or adverse immune effects were observed following vaginal administration. Furthermore, a tobacco-derived mAb against the *Bacillus anthracis* protective antigen demonstrated toxin-neutralizing activity *in vitro* and *in vivo* (Hull et al., 2005). More importantly, a non-glycosylated version of this mAb was found to be more effective in protecting mice and primates contracted with *B. anthracis* (Mett et al., 2011). In the case of cancer, manufacturing of Rituximab and Trastuzumab in *N. bethamiana* resulted in the development of biosimilar plant products that were as effective as the original drug in terms of inducing ADCC, inhibiting cancer cell proliferation and reducing tumor growth (Komarova et al., 2011; Holtz et al., 2015).

CTLA-4 is regarded as one of the best characterized inhibitory immune checkpoints. Engagement of CTLA-4 receptor to CD80 and CD86 ligands mediate negative co-stimulatory signal, impeding T cell effector functions and abrogating antitumor immune responses. It is widely known that anti-CTLA-4 antibodies block this checkpoint pathway by specifically binding to CTLA-4, disrupting ligand-receptor interactions and then T cell activation. Ipilimumab is the only approved antibody-based therapy produced in CHO cells with some limitations, such as production costs, sterility requirements, and contamination risks (Siddiqui and Rajkumar, 2012; Dhara et al., 2018). To facilitate the economical production of ICI, we produced an anti-CTLA-4 antibody in *N. benthamiana* plants for effective cancer immunotherapy. Here, 2C8

A

Ligand	Analyte	k_{on} (1/Ms)	k_{off} (1/M)	K_D (M)
2C8	huCTLA-4	2.13E+05	1.88E-04	8.83E-10
2C8	muCTLA-4	2.53E+05	5.42E-04	2.15E-09

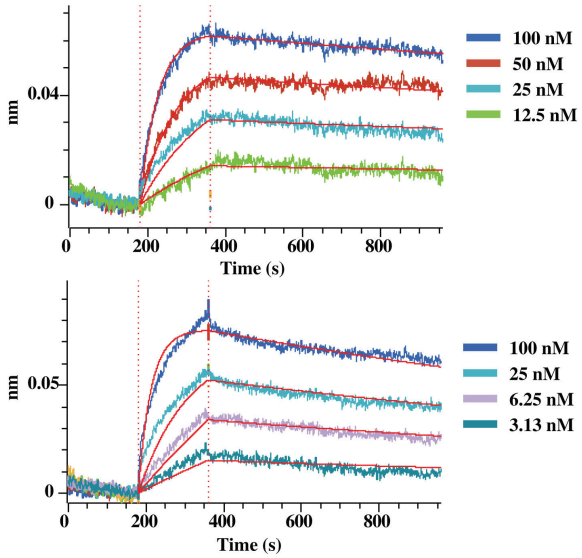

B

Ligand	Analyte	K_D (M)
huFcγRIIIa (V158)	2C8	3.20E-7

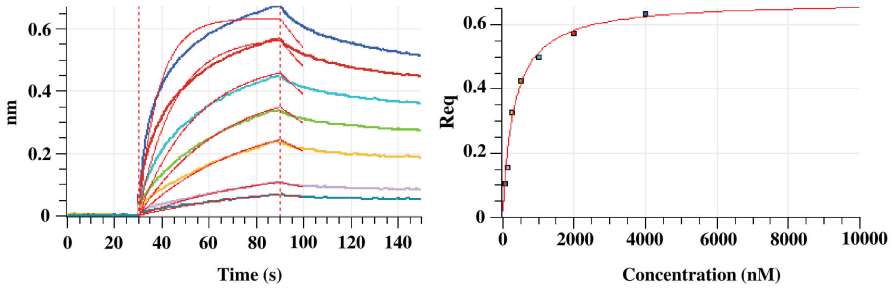

FIGURE 5
BLI binding analysis of plant-produced anti-CTLA-4 2C8 mAb. **(A)** BLI kinetic analysis of anti-CTLA-4 2C8 against huCTLA-4 (top) and muCTLA-4 (bottom). **(B)** BLI steady state analysis of anti-CTLA-4 2C8 against huFcγRIIIa (V158).

heavy chain and light chain genes were inserted into a plant expression vector and coordinately co-expressed in tobacco leaves. The reliability of *N. benthamiana* to produce functional ICIs has been proven in our earlier reports (Rattanapisit et al., 2019; Phakham et al., 2021; Phetphoung et al., 2022). Similarly, we have adopted an *Agrobacterium*-mediated expression for the production of anti-CTLA-4 checkpoint inhibitor. Based on the results, the infiltrated leaves at 2 dpi showed the least damage while apparent necrosis and wilting were observed at 3-6 dpi. In line with previous studies (Boonyayothin et al., 2022), leaf damage and/or necrosis was observed when a recombinant antibody was transiently expressed, whereas an *Agrobacterium* culture containing no antibody showed no response after infiltration. Relevant literatures also showed similar responses for the expression of recombinant proteins, for example hemagglutinin (Matsuda et al., 2012), hepatitis B (Huang et al., 2008), human growth hormone (Gils et al., 2005), and tumor associated MUC1 peptide (Pinkhasov et al., 2011). The expression level of anti-CTLA-4 antibody increased until 4 dpi, accumulating up to 39.65 ± 8.42 μg/g fresh weight, and then decreased on later dpi. This demonstrates influence of transfection time and necrosis with protein yield (Hamorsky et al., 2015) and suggests that protein expression may be less optimal from 5 dpi and later. Western blotting was also carried out to verify antibody expression in *N. benthamiana* crude extracts. The anti-CTLA-4 2C8 mAb was successfully expressed as expected and was only detected in infiltrated plant crude extracts. According to the obtained results, the anti-CTLA-4 antibody was optimally produced in *N. benthamiana* at 4 dpi, which is an undoubted advantage over transgenic expression (Ma et al., 2015) and mammalian expression (Ahmadi et al., 2017). For antibody purification, protein A-based affinity chromatography was used. SDS-PAGE and western blot analyses revealed that the purified plant-produced anti-CTLA-4 2C8 mAb assembled into its tetrameric isoform under a non-reduced condition whereas heavy chain and light chain monomers were observed in the presence of a reducing agent. Plant systems have distinctive *N*-glycosylation machinery

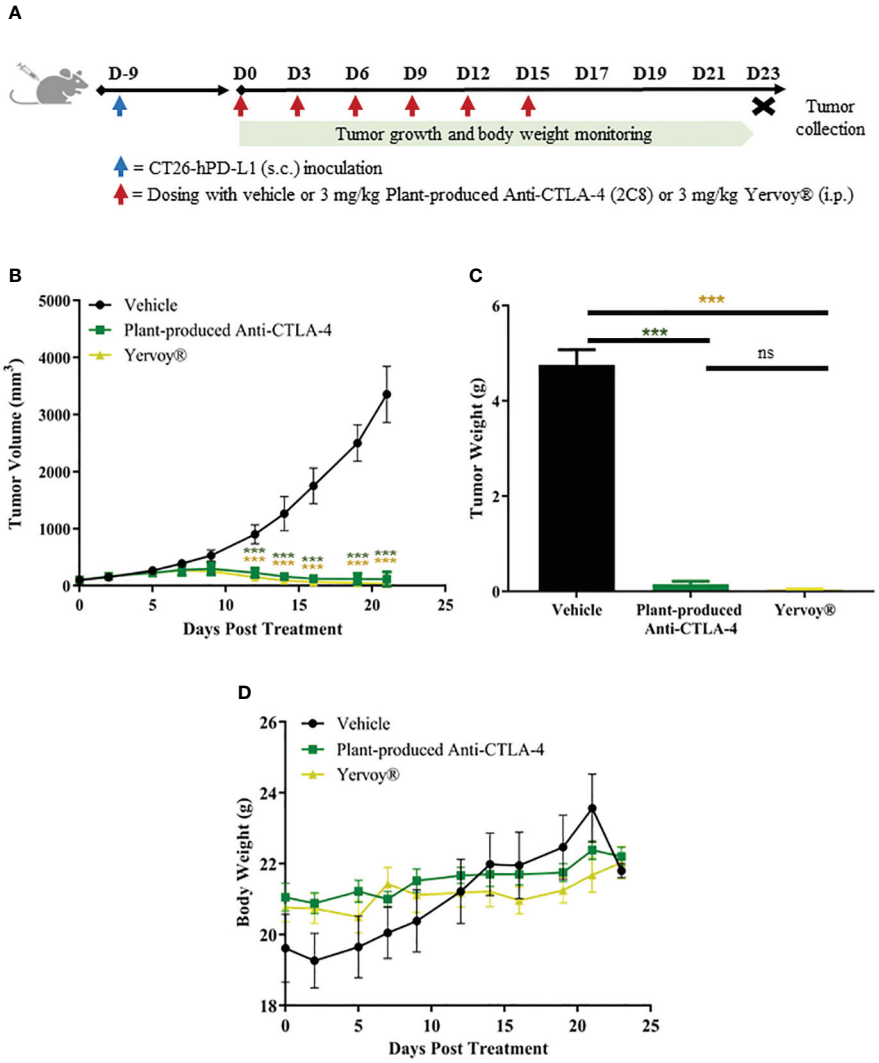

FIGURE 6
In vivo antitumor activity of plant-produced anti-CTLA-4 2C8 mAb. **(A)** Schematic representation of the experimental design used to evaluate antitumor effects in mice model. In this experiment, syngeneic humanized mice bearing CT26-hPD-L1 colon cancer were treated with plant-produced anti-CTLA-4 (3 mg/kg) or commercial anti-CTLA-4 (Yervoy®) (3 mg/kg) or vehicle. The generated graphs show **(B)** tumor volume changes over time, **(C)** tumor weight data of mice in different treatment groups, and **(D)** body weight changes during evaluation period. The data are presented as mean ± SD. ns: not significant and ***$p < 0.001$ by one way ANOVA test, the *post-hoc* test was LSD.

from humans (Strasser et al., 2008) that differ substantially during the late stages of *N*-linked glycan processing. Plants often have high-mannose-type *N*-glycans with $Man_{5-9}GlcNAc_2$ structure (Rayon et al., 1998). Here, the *N*-glycan profile of plant-produced anti-CTLA-4 depicted high-mannose oligosaccharides, as a result of targeted accumulation in the ER via., SEKDEL peptide sequence. The presence or absence of localization signals causes differences in the *N*-glycosylation of proteins when synthesized in plants (Triguero et al., 2011), with complex-type glycans of β(1,2)-xylose and α(1,3)-fucose residues abundant in plantibodies lacking KDEL and oligomannose-type glycans predominant in plantibodies with KDEL, as seen in our study and others (Ko et al., 2003; Triguero et al., 2005). These oligomannosidic glycans found in SEKDEL-containing plant glycoproteins are non-immunogenic as reported elsewhere (Sriraman et al., 2004). Additionally, in previously published *N*-glycan analyses of anti-PD-1/PD-L1 mAbs by our team (Phakham et al., 2021; Phetphoung et al., 2022), *N*-glycosylation patterns differed among antibodies produced in plants to that of mammalian cells, at which authentic plant glycan structures were derived in plant-produced antibodies but absent in aglycosylated Atezolizumab (Tecentriq®) while only mammalian-type glycans were observed in commercial Pembrolizumab (Keytruda®). Meanwhile, glycoengineered plants offers another approach to diminish or abolish plant-specific *N*-glycan repertoire (Fischer et al., 2021).

The ability of purified plant-produced 2C8 mAb to bind to its target antigen has been demonstrated *in vitro*. Using human and mouse CTLA-4 proteins, the plant-produced anti-CTLA-4 antibody exhibited concentration-dependent binding. In contrary, both controls such as non-related anti-PD-1 antibody and human IgG1 isotype only showed background binding. Likewise, BLI analysis confirmed subnanomolar or low nanomolar affinity for

human and mouse CTLA-4 proteins, demonstrating the successful production of a functional mAb in plants with binding activity and mouse-human cross-reactivity. The binding properties of our plant-produced 2C8 differ from that of Ipilimumab, owing to its low cross-reactivity for mouse CTLA-4 (He et al., 2017; Li et al., 2020; Passariello et al., 2020), which we have not confirmed. Moreover, the Fcγ receptor engagement of plant-produced 2C8 was also investigated by BLI. The anti-CTLA-4 antibody exhibited sub-micromolar binding for FcγRIIIa (V158) typical for IgG1 and is consistent with previous studies (Gombos et al., 2018), suggesting potential effector function. Moreover, the presence of plant mannosidic *N*-glycans did not significantly alter the binding affinity of plant-produced mAb to its CTLA-4 target, which is in line with other earlier findings (Phakham et al., 2021; Phetphoung et al., 2022), and also to one of the FcγRs. Previous reports have indicated the relevance of FcγR-dependent functions via., ADCC and ADCP in anti-CTLA-4 therapies (Arce Vargas et al., 2018; Ingram et al., 2018), which contributes to antitumor responses in mouse tumor models. However, preclinical design of an anti-CTLA-4 IgG2 isotype to minimize Fc effector function (Hanson et al., 2004) implicates the unclear roles of FcγRs in the activity of mAbs.

In order to elucidate a preclinical rationale for plant-based checkpoint inhibitors, we preliminarily tested the antitumor activity of our plant-produced anti-CTLA-4 antibody *in vivo*. Here, we utilized a PD-1/PD-L1/CTLA-4 humanized BALB/c mice with established CT26-hPD-L1 colon carcinoma. The CT26 colon cancer cell line is categorized to be highly immunogenic (Lechner et al., 2013) and has been used in a variety of *in vivo* studies, including our current study. Based on the results, we found that plant-produced anti-CTLA-4 2C8 elicited significant antitumor efficacy in syngeneic CT26-hPD-L1 tumor model. More importantly, treatment with plant-produced anti-CTLA-4 reduced the tumor size and repressed the tumor weight comparably with the mammalian cell produced anti-CTLA-4 (Yervoy®). In contrast, treatment with vehicle failed to control tumor growth. These data reveal the direct effects of anti-CTLA-4 antibodies in the reversal of CTLA-4-induced T cell tolerance and anergy (Peggs et al., 2009; Pardoll, 2012). In particular, our plant-produced anti-CTLA-4, together with Yervoy®, blocked the CTLA-4 function on tumor cells, leading to a marked inhibition of tumor growth as a result of T cell activation. Interestingly, the syngeneic murine tumor model shown substantial sensitivity to anti-CTLA-4 immunotherapy, wherein our plant-produced anti-CTLA-4 was as sensitive as the commercial anti-CTLA-4 in suppressing growth of tumors positive for PD-L1 expression. In line with our study, the efficacy of anti-CTLA-4 antibody was reported in other murine tumor models of colon cancer (*ie.*, CT26, Colon 26, and MC38) which showed high sensitivity and durable responses to CTLA-4 blockade (Grosso and Jure-Kunkel, 2013; Wei et al., 2017; Sato et al., 2021). On the other hand, treatment-related toxicity was assessed based on body weight. An obvious decrease in the body weight has been associated with the prospective occurrence of toxicity and side effects in treated mice, which eventually undermines their chance of survival (Chapman et al., 2013). In the present study, no significant body weight changes were recorded in any of the treatment groups such that serious body weight loss of over 10% was not evident following the treatment of either anti-CTLA-4 antibodies or vehicle. These results, in turn, translate into the favorable safety and tolerability of the plant-produced anti-CTLA-4 treatment. Although notable differences in body weight may not completely establish overall treatment-associated toxicities, preliminary results reported here provide sufficient basis for future exploration in non-clinical toxicology studies.

Altogether, a recombinant anti-CTLA-4 2C8 antibody has been successfully produced in *N. benthamiana*. This plant-derived antibody cross-reacts to both human and mouse CTLA-4, binds to FcγRIIIa (V158) and elicits excellent antitumor effects in syngeneic mouse model. To our knowledge, this study addresses the first preclinical assessment of a plant-produced anti-CTLA-4 immunotherapy. More so, the cost-effective production of plant-based immune checkpoint inhibitor further affirms the suitability of the current platform to relieve financial strain and improve treatment accessibility in the developing countries.

Data availability statement

The original contributions presented in the study are included in the article/Supplementary Material. Further inquiries can be directed to the corresponding author.

Ethics statement

The animal study was approved by the Institutional Animal Care and Use Committee (IACUC) of GemPharmatech Co., Ltd., China. The study was conducted in accordance with the local legislation and institutional requirements.

Author contributions

WP and CJIB conceived the study. NK and KR performed gene synthesis and cloning. CJIB performed antibody expression, purification, quantification and binding assays. CJIB and NP performed size exclusion chromatography. RS performed N-glycan analysis. ST and PS-S performed BLI analysis. HS performed *in vivo* antitumor assays. All authors contributed to the article and approved the submitted version.

Funding

This study was supported by the National Research Council of Thailand, Scholarship Program for ASEAN and Non-ASEAN countries, and BOKU Core Facility Mass Spectrometry.

Conflict of interest

WP from Chulalongkorn University is a founder/shareholder of Baiya Phytopharm Co., Ltd. Thailand. Authors NK and KR are employed by Baiya Phytopharm Co., Ltd. Author HS is an employee

in GemPharmatech Co., Ltd. Authors ST and PS-S are employees in ImmunityBio, Inc.

The remaining authors declare that the research was conducted in the absence of any commercial or financial relationship that could be construed as a potential conflict of interest.

Publisher's note

All claims expressed in this article are solely those of the authors and do not necessarily represent those of their affiliated organizations, or those of the publisher, the editors and the reviewers. Any product that may be evaluated in this article, or claim that may be made by its manufacturer, is not guaranteed or endorsed by the publisher.

Supplementary material

The Supplementary Material for this article can be found online at: https://www.frontiersin.org/articles/10.3389/fpls.2023.1149455/full#supplementary-material

References

Ahmadi, S., Davami, F., Davoudi, N., Nematpour, F., Ahmadi, M., Ebadat, S., et al. (2017). Monoclonal antibodies expression improvement in CHO cells by PiggyBac transposition regarding vectors ratios and design. *PloS One* 12 (6), e0179902. doi: 10.1371/journal.pone.0179902

Arce Vargas, F., Furness, A. J. S., Litchfield, K., Joshi, K., Rosenthal, R., Ghorani, E., et al. (2018). Fc effector function contributes to the activity of human anti-CTLA-4 antibodies. *Cancer Cell* 33 (4), 649–663.e644. doi: 10.1016/j.ccell.2018.02.010

Arruebo, M., Vilaboa, N., Sáez-Gutierrez, B., Lambea, J., Tres, A., Valladares, M., et al. (2011). Assessment of the evolution of cancer treatment therapies. *Cancers (Basel)* 3 (3), 3279–3330. doi: 10.3390/cancers3033279

Behrouzieh, S., Sheida, F., and Rezaei, N. (2021). Review of the recent clinical trials for PD-1/PD-L1 based lung cancer immunotherapy. *Expert Rev. Anticancer Ther.* 21 (12), 1355–1370. doi: 10.1080/14737140.2021.1996230

Boonyayothin, W., Kobtrakul, K., Khositanon, P., Vimolmangkang, S., and Phoolcharoen, W. (2022). Development of a plant-produced recombinant monoclonal antibody against Δ-9-tetrahydrocannabinol (Δ9-THC) for immunoassay application. *Biotechnol. Rep.* 34, e00725. doi: 10.1016/j.btre.2022.e00725

Bulaon, C. J. I., Shanmugaraj, B., Oo, Y., Rattanapisit, K., Chuanasa, T., Chaotham, C., et al. (2020). Rapid transient expression of functional human vascular endothelial growth factor in Nicotiana benthamiana and characterization of its biological activity. *Biotechnol. Rep.* 27, e00514. doi: 10.1016/j.btre.2020.e00514

Cabel, L., Loir, E., Gravis, G., Lavaud, P., Massard, C., Albiges, L., et al. (2017). Long-term complete remission with Ipilimumab in metastatic castrate-resistant prostate cancer: case report of two patients. *J. Immunother. Cancer* 5, 31. doi: 10.1186/s40425-017-0232-7

Cameron, F., Whiteside, G., and Perry, C. (2011). Ipilimumab: first global approval. *Drugs* 71 (8), 1093–1104. doi: 10.2165/11594010-000000000-00000

Chapman, K., Sewell, F., Allais, L., Delongeas, J.-L., Donald, E., Festag, M., et al. (2013). A global pharmaceutical company initiative: An evidence-based approach to define the upper limit of body weight loss in short term toxicity studies. *Regul. Toxicol. Pharmacol.* 67 (1), 27–38. doi: 10.1016/j.yrtph.2013.04.003

Chen, Q., He, J., Phoolcharoen, W., and Mason, H. S. (2011). Geminiviral vectors based on bean yellow dwarf virus for production of vaccine antigens and monoclonal antibodies in plants. *Hum. Vaccines* 7 (3), 331–338. doi: 10.4161/hv.7.3.14262

Dhara, G., Naik, H. M., Majewska, N., and Betenbaugh, M. (2018). Recombinant antibody production in CHO and NS0 cells: differences and similarities. *BioDrugs* 32, 1–14. doi: 10.1007/s40259-018-0319-9

Diamos, A. G., and Mason, H. S. (2019). Modifying the replication of geminiviral vectors reduces cell death and enhances expression of biopharmaceutical proteins in nicotiana benthamiana leaves. *Front. Plant Sci.* 9 (1974). doi: 10.3389/fpls.2018.01974

Fischer, R., Holland, T., Sack, M., Schillberg, S., Stoger, E., Twyman, R. M., et al. (2021). Glyco-engineering of plant-based expression systems. *Adv. Biochem. Eng. Biotechnol.* 175, 137–166. doi: 10.1007/10_2018_76

Gils, M., Kandzia, R., Marillonnet, S., Klimyuk, V., and Gleba, Y. (2005). High-yield production of authentic human growth hormone using a plant virus-based expression system. *Plant Biotechnol. J.* 3 (6), 613–620. doi: 10.1111/j.1467-7652.2005.00154.x

Gombos, R. B., Gonzalez, A., Manrique, M., Chand, D., Savitsky, D., Morin, B., et al. (2018). Toxicological and pharmacological assessment of AGEN1884, a novel human IgG1 anti-CTLA-4 antibody. *PloS One* 13 (4), e0191926. doi: 10.1371/journal.pone.0191926

Grosso, J. F., and Jure-Kunkel, M. N. (2013). CTLA-4 blockade in tumor models: an overview of preclinical and translational research. *Cancer Immun.* 13, 5. doi: 10.1158/1424-9634.DCL-5.13.1

Hamorsky, K. T., Kouokam, J. C., Jurkiewicz, J. M., Nelson, B., Moore, L. J. , Husk, A. S., et al. (2015). N-Glycosylation of cholera toxin B subunit in Nicotiana benthamiana: impacts on host stress response, production yield and vaccine potential. *Sci. Rep.* 5 (1), 8003. doi: 10.1038/srep08003

Hanson, D., Canniff, P., Primiano, M., Donovan, C., Gardner, J., Natoli, E., et al. (2004). Preclinical in *vitro* characterization of anti-CTLA4 therapeutic antibody CP-675,206. *Cancer Res.* 64.

He, M., Chai, Y., Qi, J., Zhang, C. W. H., Tong, Z., Shi, Y., et al. (2017). Remarkably similar CTLA-4 binding properties of therapeutic ipilimumab and tremelimumab antibodies. *Oncotarget* 8 (40), 67129–67139. doi: 10.18632/oncotarget.18004

Holtz, B. R., Berquist, B. R., Bennett, L. D., Kommineni, V. J. M., Munigunti, R. K., White, E. L., et al. (2015). Commercial-scale biotherapeutics manufacturing facility for plant-made pharmaceuticals. *Plant Biotechnol. J.* 13 (8), 1180–1190. doi: 10.1111/pbi.12469

Huang, Z., LePore, K., Elkin, G., Thanavala, Y., and Mason, H. S. (2008). High-yield rapid production of hepatitis B surface antigen in plant leaf by a viral expression system. *Plant Biotechnol. J.* 6 (2), 202–209. doi: 10.1111/j.1467-7652.2007.00316.x

Hull, A. K., Criscuolo, C. J., Mett, V., Groen, H., Steeman, W., Westra, H., et al. (2005). Human-derived, plant-produced monoclonal antibody for the treatment of anthrax. *Vaccine* 23 (17-18), 2082–2086. doi: 10.1016/j.vaccine.2005.01.013

Ingram, J. R., Blomberg, O. S., Rashidian, M., Ali, L., Garforth, S., Fedorov, E., et al. (2018). Anti–CTLA-4 therapy requires an Fc domain for efficacy. *Proc. Natl. Acad. Sci. U. S. A.* 115 (15), 3912–3917. doi: 10.1073/pnas.1801524115

Juat, D. J., Hachey, S. J., Billimek, J., Del Rosario, M. P., Nelson, E. L., Hughes, C. C. W., et al. (2022). Adoptive T-cell therapy in advanced colorectal cancer: A systematic review. *Oncologist* 27 (3), 210–219. doi: 10.1093/oncolo/oyab038

Keam, S. J. (2023). Tremelimumab: first approval. *Drugs* 83 (1), 93–102. doi: 10.1007/s40265-022-01827-8

Kelley, B. (2009). Industrialization of mAb production technology: the bioprocessing industry at a crossroads. *MAbs* 1 (5), 443–452. doi: 10.4161/mabs.1.5.9448

Khan, M., Lin, J., Liao, G., Tian, Y., Liang, Y., Li, R., et al. (2018). Comparative analysis of immune checkpoint inhibitors and chemotherapy in the treatment of advanced non-small cell lung cancer: A meta-analysis of randomized controlled trials. *Medicine* 97 (33), e11936. doi: 10.1097/MD.0000000000011936

Khorattanakulchai, N., Manopwisedjaroen, S., Rattanapisit, K., Panapitakkul, C., Kemthong, T., Suttisan, N., et al. (2022). Receptor binding domain proteins of SARS-CoV-2 variants produced in Nicotiana benthamiana elicit neutralizing antibodies against variants of concern. *J. Med. Virol.* 94, 4265–4276. doi: 10.1002/jmv.27881

Ko, K., Tekoah, Y., Rudd, P. M., Harvey, D. J., Dwek, R. A., Spitsin, S., et al. (2003). Function and glycosylation of plant-derived antiviral monoclonal antibody. *Proc. Natl. Acad. Sci. U.S.A.* 100 (13), 8013–8018. doi: 10.1073/pnas.0832472100

Komarova, T. V., Kosorukov, V. S., Frolova, O. Y., Petrunia, I. V., Skrypnik, K. A., Gleba, Y. Y., et al. (2011). Plant-made trastuzumab (Herceptin) inhibits HER2/neu+ Cell proliferation and retards tumor growth. *PloS One* 6 (3), e17541. doi: 10.1371/journal.pone.0017541

Lechner, M. G., Karimi, S. S., Barry-Holson, K., Angell, T. E., Murphy, K. A., Church, C. H., et al. (2013). Immunogenicity of murine solid tumor models as a defining feature of in *vivo* behavior and response to immunotherapy. *J. Immunother.* 36 (9), 477–489. doi: 10.1097/01.cji.0000436722.46675.4a

Li, D., Li, J., Chu, H., and Wang, Z. (2020). A functional antibody cross-reactive to both human and murine cytotoxic T-lymphocyte-associated protein 4 via binding to an N-glycosylation epitope. *MAbs* 12 (1), 1725365. doi: 10.1080/19420862.2020.1725365

Liu, J., Fu, M., Wang, M., Wan, D., Wei, Y., and Wei, X. (2022). Cancer vaccines as promising immuno-therapeutics: platforms and current progress. *J. Hematol. Oncol.* 15 (1), 28. doi: 10.1186/s13045-022-01247-x

Ma, J. K., Drossard, J., Lewis, D., Altmann, F., Boyle, J., Christou, P., et al. (2015). Regulatory approval and a first-in-human phase I clinical trial of a monoclonal antibody produced in transgenic tobacco plants. *Plant Biotechnol. J.* 13 (8), 1106–1120. doi: 10.1111/pbi.12416

Matsuda, R., Tahara, A., Matoba, N., and Fujiwara, K. (2012). Virus vector-mediated rapid protein production in Nicotiana benthamiana: effects of temperature and photosynthetic photon flux density on hemagglutinin accumulation. *Environ. Control. Biol.* 50(4), 375–381. doi: 10.2525/ecb.50.375

Mett, V., Chichester, J. A., Stewart, M. L., Musiychuk, K., Bi, H., Reifsnyder, C. J., et al. (2011). A non-glycosylated, plant-produced human monoclonal antibody against anthrax protective antigen protects mice and non-human primates from B. anthracis spore challenge. *Hum. Vaccin* 7 Suppl, 183–190. doi: 10.4161/hv.7.0.14586

Morse, M. A., Overman, M. J., Hartman, L., Khoukaz, T., Brutcher, E., Lenz, H. J., et al. (2019). Safety of nivolumab plus low-dose ipilimumab in previously treated microsatellite instability-high/mismatch repair-deficient metastatic colorectal cancer. *Oncologist* 24 (11), 1453–1461. doi: 10.1634/theoncologist.2019-0129

Nandi, S., Kwong, A. T., Holtz, B. R., Erwin, R. L., Marcel, S., and McDonald, K. A. (2016). Techno-economic analysis of a transient plant-based platform for monoclonal antibody production. *MAbs* 8 (8), 1456–1466. doi: 10.1080/19420862.2016.1227901

Nosaki, S., Hoshikawa, K., Ezura, H., and Miura, K. (2021). Transient protein expression systems in plants and their applications. *Plant Biotechnol. (Tokyo)* 38 (3), 297–304. doi: 10.5511/plantbiotechnology.21.0610a

Pardoll, D. M. (2012). The blockade of immune checkpoints in cancer immunotherapy. *Nat. Rev. Cancer* 12 (4), 252–264. doi: 10.1038/nrc3239

Passariello, M., Vetrei, C., Sasso, E., Froechlich, G., Gentile, C., D'Alise, A., et al. (2020). Isolation of two novel human anti-CTLA-4 mAbs with intriguing biological properties on tumor and NK cells. *Cancers* 12, 2204. doi: 10.3390/cancers12082204

Peggs, K. S., Quezada, S. A., Chambers, C. A., Korman, A. J., and Allison, J. P. (2009). Blockade of CTLA-4 on both effector and regulatory T cell compartments contributes to the antitumor activity of anti–CTLA-4 antibodies. *J. Exp. Med.* 206 (8), 1717–1725. doi: 10.1084/jem.20082492

Petrides, D., Carmichael, D., Siletti, C., and Koulouris, A. (2014). Biopharmaceutical process optimization with simulation and scheduling tools. *Bioengineering (Basel)* 1 (4), 154–187. doi: 10.3390/bioengineering1040154

Phakham, T., Bulaon, C. J. I., Khorattanakulchai, N., Shanmugaraj, B., Buranapraditkun, S., Boonkrai, C., et al. (2021). Functional characterization of pembrolizumab produced in nicotiana benthamiana using a rapid transient expression system. *Front. Plant Sci.* 12. doi: 10.3389/fpls.2021.736299

Phetphoung, T., Malla, A., Rattanapisit, K., Pisuttinusart, N., Damrongyot, N., Joyjamras, K., et al. (2022). Expression of plant-produced anti-PD-L1 antibody with anoikis sensitizing activity in human lung cancer cells via., suppression on epithelial-mesenchymal transition. *PloS One* 17 (11), e0274737. doi: 10.1371/journal.pone.0274737

Pinkhasov, J., Alvarez, M. L., Rigano, M. M., Piensook, K., Larios, D., Pabst, M., et al. (2011). Recombinant plant-expressed tumour-associated MUC1 peptide is immunogenic and capable of breaking tolerance in MUC1.Tg mice. *Plant Biotechnol. J.* 9 (9), 991–1001. doi: 10.1111/j.1467-7652.2011.00614.x

Rattanapisit, K., Bulaon, C. J. I., Khorattanakulchai, N., Shanmugaraj, B., Wangkanont, K., and Phoolcharoen, W. (2021). Plant-produced SARS-CoV-2 receptor binding domain (RBD) variants showed differential binding efficiency with anti-spike specific monoclonal antibodies. *PloS One* 16 (8), e0253574. doi: 10.1371/journal.pone.0253574

Rattanapisit, K., Phakham, T., Buranapraditkun, S., Siriwattananon, K., Boonkrai, C., Pisitkun, T., et al. (2019). Structural and *in vitro* functional analyses of novel plant-produced anti-human PD1 antibody. *Sci. Rep.* 9 (1), 15205. doi: 10.1038/s41598-019-51656-1

Rayon, C., Lerouge, P., and Faye, L. (1998). The protein N-glycosylation in plants. *J. Exp. Bot.* 49 (326), 1463–1472. doi: 10.1093/jxb/49.326.1463

Sato, Y., Fu, Y., Liu, H., Lee, M. Y., and Shaw, M. H. (2021). Tumor-immune profiling of CT-26 and Colon 26 syngeneic mouse models reveals mechanism of anti-PD-1 response. *BMC Cancer* 21 (1), 1222. doi: 10.1186/s12885-021-08974-3

Schadendorf, D., Hodi, F. S., Robert, C., Weber, J. S., Margolin, K., Hamid, O., et al. (2015). Pooled analysis of long-term survival data from phase II and phase III trials of ipilimumab in unresectable or metastatic melanoma. *J. Clin. Oncol.* 33 (17), 1889–1894. doi: 10.1200/jco.2014.56.2736

Schillberg, S., and Finnern, R. (2021). Plant molecular farming for the production of valuable proteins - Critical evaluation of achievements and future challenges. *J. Plant Physiol.* 258-259, 153359. doi: 10.1016/j.jplph.2020.153359

Shanmugaraj, B., Bulaon, C. J. I., Malla, A., and Phoolcharoen, W. (2021). Biotechnological insights on the expression and production of antimicrobial peptides in plants. *Molecules* 26(13), 4032. doi: 10.3390/molecules26134032

Shanmugaraj, B., Bulaon, C. J. I., and Phoolcharoen, W. (2020a). Plant molecular farming: a viable platform for recombinant biopharmaceutical production. *Plants (Basel)* 9 (7), 842 doi: 10.3390/plants9070842

Shanmugaraj, B., Rattanapisit, K., Manopwisedjaroen, S., Thitithanyanont, A., and Phoolcharoen, W. (2020b). Monoclonal Antibodies B38 and H4 Produced in Nicotiana benthamiana Neutralize SARS-CoV-2 in *vitro*. *Front. Plant Sci.* 11. doi: 10.3389/fpls.2020.589995

Siddiqui, M., and Rajkumar, S. V. (2012). The high cost of cancer drugs and what we can do about it. *Mayo Clinic Proc.* 87 (10), 935–943. doi: 10.1016/j.mayocp.2012.07.007

Sriraman, R., Bardor, M., Sack, M., Vaquero, C., Faye, L., Fischer, R., et al. (2004). Recombinant anti-hCG antibodies retained in the endoplasmic reticulum of transformed plants lack core-xylose and core-alpha(1,3)-fucose residues. *Plant Biotechnol. J.* 2 (4), 279–287. doi: 10.1111/j.1467-7652.2004.00078.x

Strasser, R., Stadlmann, J., Schähs, M., Stiegler, G., Quendler, H., Mach, L., et al. (2008). Generation of glyco-engineered Nicotiana benthamiana for the production of monoclonal antibodies with a homogeneous human-like N-glycan structure. *Plant Biotechnol. J.* 6 (4), 392–402. doi: 10.1111/j.1467-7652.2008.00330.x

Taefehshokr, S., Parhizkar, A., Hayati, S., Mousapour, M., Mahmoudpour, A., Eleid, L., et al. (2022). Cancer immunotherapy: Challenges and limitations. *Pathol. - Res. Pract.* 229, 153723. doi: 10.1016/j.prp.2021.153723

Tang, J., Yu, J. X., Hubbard-Lucey, V. M., Neftelinov, S. T., Hodge, J. P., and Lin, Y. (2018). Trial watch: The clinical trial landscape for PD1/PDL1 immune checkpoint inhibitors. *Nat. Rev. Drug Discov.* 17 (12), 854–855. doi: 10.1038/nrd.2018.210

Triguero, A., Cabrera, G., Cremata, J. A., Yuen, C. T., Wheeler, J., and Ramírez, N. I. (2005). Plant-derived mouse IgG monoclonal antibody fused to KDEL endoplasmic reticulum-retention signal is N-glycosylated homogeneously throughout the plant with mostly high-mannose-type N-glycans. *Plant Biotechnol. J.* 3 (4), 449–457. doi: 10.1111/j.1467-7652.2005.00137.x

Triguero, A., Cabrera, G., Rodríguez, M., Soto, J., Zamora, Y., Pérez, M., et al. (2011). Differential N-glycosylation of a monoclonal antibody expressed in tobacco leaves with and without endoplasmic reticulum retention signal apparently induces similar in *vivo* stability in mice. *Plant Biotechnol. J.* 9 (9), 1120–1130. doi: 10.1111/j.1467-7652.2011.00638.x

Upadhaya, S., Neftelinov, S. T., Hodge, J., and Campbell, J. (2022). Challenges and opportunities in the PD1/PDL1 inhibitor clinical trial landscape. *Nat. Rev. Drug Discov.* 21 (7), 482–483. doi: 10.1038/d41573-022-00030-4

Wang, C.-I., Ngoh, E., and Yeo, S. P. (2017). *Anti-CTLA-4 antibodies* (Singapore: United States patent application).

Wei, S. C., Levine, J. H., Cogdill, A. P., Zhao, Y., Anang, N. A. S., Andrews, M. C., et al. (2017). Distinct cellular mechanisms underlie anti-CTLA-4 and anti-PD-1 checkpoint blockade. *Cell* 170 (6), 1120–1133.e1117. doi: 10.1016/j.cell.2017.07.024

Yiemchavee, S., Wong-Arce, A., Romero-Maldonado, A., Shanmugaraj, B., Monsivais-Urenda, A. E., Phoolcharoen, W., et al. (2021). Expression and immunogenicity assessment of a plant-made immunogen targeting the cytotoxic T-lymphocyte associated antigen-4: a possible approach for cancer immunotherapy. *J. Biotechnol.* 329, 29–37. doi: 10.1016/j.jbiotec.2021.01.016

frontiers | Frontiers in Plant Science

TYPE Original Research
PUBLISHED 06 October 2023
DOI 10.3389/fpls.2023.1275228

OPEN ACCESS

EDITED BY
Balamurugan Shanmugaraj,
Chulalongkorn University, Thailand

REVIEWED BY
Ario De Marco,
University of Nova Gorica, Slovenia
Linda Avesani,
University of Verona, Italy

*CORRESPONDENCE
Richard Strasser
richard.strasser@boku.ac.at

RECEIVED 09 August 2023
ACCEPTED 22 September 2023
PUBLISHED 06 October 2023

CITATION
Ruocco V, Vavra U, König-Beihammer J, Bolaños–Martínez OC, Kallolimath S, Maresch D, Grünwald-Gruber C and Strasser R (2023) Impact of mutations on the plant-based production of recombinant SARS-CoV-2 RBDs. *Front. Plant Sci.* 14:1275228. doi: 10.3389/fpls.2023.1275228

Impact of mutations on the plant-based production of recombinant SARS-CoV-2 RBDs

Valentina Ruocco[1], Ulrike Vavra[1], Julia König-Beihammer[1], Omayra C. Bolaños–Martínez[1], Somanath Kallolimath[1], Daniel Maresch[2], Clemens Grünwald-Gruber[2] and Richard Strasser[1]*

[1]Department of Applied Genetics and Cell Biology, University of Natural Resources and Life Sciences, Vienna, Austria, [2]Core Facility Mass Spectrometry, University of Natural Resources and Life Sciences, Vienna, Austria

Subunit vaccines based on recombinant viral antigens are valuable interventions to fight existing and evolving viruses and can be produced at large-scale in plant-based expression systems. The recombinant viral antigens are often derived from glycosylated envelope proteins of the virus and glycosylation plays an important role for the immunogenicity by shielding protein epitopes. The receptor-binding domain (RBD) of the SARS-CoV-2 spike is a principal target for vaccine development and has been produced in plants, but the yields of recombinant RBD variants were low and the role of the N-glycosylation in RBD from different SARS-CoV-2 variants of concern is less studied. Here, we investigated the expression and glycosylation of six different RBD variants transiently expressed in leaves of *Nicotiana benthamiana*. All of the purified RBD variants were functional in terms of receptor binding and displayed almost full N-glycan occupancy at both glycosylation sites with predominately complex N-glycans. Despite the high structural sequence conservation of the RBD variants, we detected a variation in yield which can be attributed to lower expression and differences in unintentional proteolytic processing of the C-terminal polyhistidine tag used for purification. Glycoengineering towards a human-type complex N-glycan profile with core α1,6-fucose, showed that the reactivity of the neutralizing antibody S309 differs depending on the N-glycan profile and the RBD variant.

KEYWORDS

antigen, glycoprotein, glycosylation, *Nicotiana benthamiana*, spike protein, vaccine, virus

Introduction

The SARS-CoV-2 pandemic has dramatically shown that efforts need to be increased for the fast and efficient development of counter measurements to combat newly emerging viruses. The rapid production of potent vaccines is one way to fight emerging and reemerging viral pathogens. The heavily glycosylated SARS-CoV-2 spike protein that is exposed at the viral surface is one of the key targets for vaccine development. Glycosylation is a major posttranslational modification that is found on a vast number of mammalian proteins and on surface proteins of viruses that use mammalian cells as a host. Since glycosylation is important for virus transmission and cell entry, understanding of biological processes governed by glycosylation is crucial to prevent virus infection and disease progression. N-glycosylation is the major type of glycosylation found on SARS-CoV-2 and other enveloped viruses (Watanabe et al., 2020b). N-glycosylation is initiated in the endoplasmic reticulum (ER) by transfer of a preassembled oligosaccharide to specific asparagine residues present on nascent polypeptide chains (Strasser, 2016). While the attached N-glycans promote protein folding and serve important functions during quality control in the ER, the complex type N-glycans that are generated in the Golgi apparatus have more diverse functions. For example, a single fucose residue is transferred in the Golgi apparatus to the conserved complex N-glycan present in the IgG1 heavy chain. The presence of this core fucose alters the affinity of antibodies to cellular receptors and thus controls effector functions (Wang and Ravetch, 2019). Other complex N-glycan modifications on viral or recombinant glycoproteins enable the interaction with specific lectin-type receptors (Hoffmann et al., 2021).

The SARS-CoV-2 spike protein monomer on the surface of the virus contains 22 highly conserved N-glycosylation sites. N-glycosylation of these sites is important for expression, conformational dynamics and virus infectivity as shown for the original SARS-CoV-2 strain (Yang et al., 2020b; Zhao et al., 2020; Newby et al., 2023). Many viral envelope proteins and subunits are explored as vaccine candidates and glycosylation is critical for vaccine development (Bagdonaite and Wandall, 2018; Ozdilek and Avci, 2022). Glycosylation is frequently required for proper folding of viral antigens expressed in heterologous systems (Casalino et al., 2020). The attached N-glycans are bound by lectin-like molecular chaperones calnexin/calreticulin which promote folding (Shin et al., 2021; Margolin et al., 2023). Moreover, the presence or absence of glycans on vaccines can have completely detrimental effects on the potency. For example, masking of epitopes by attachment of additional glycans can divert the immune response to distinct regions of the polypeptide and enhance the induction of neutralizing antibodies (Shi et al., 2022). Deletion of glycans can also be beneficial and enhance the immune response with a broader protection as shown for SARS-CoV-2 vaccination approaches (Huang et al., 2022; Wu et al., 2022). In addition to glycan occupancy of viral proteins, also the glycan structure has an impact on the immunogenicity as indicated by differences in reactivity with specific SARS-CoV-2 neutralizing antibodies (Pinto et al., 2020; Samuelsson et al., 2022). Since its emergence, SARS-CoV-2 has undergone continuous mutations and recent evidence shows that some variants of concern like Delta or Omicron display differences in N-glycan processing (Zheng et al., 2022; Baboo et al., 2023) which may affect the infectivity like shown for the Omicron BA.1 variant (Lusvarghi et al., 2023). These findings underscore the importance of N-glycosylation for SARS-CoV-2 virus infection (Gong et al., 2021; Maity and Acharya, 2023) and the requirement for platforms and expression systems that allow the production of defined homogenous glycan structures on recombinant viral proteins (Yang et al., 2015; Schwestka et al., 2021; Hsu et al., 2023). Since even small differences in glycosylation may alter the immune response (Samuelsson et al., 2022), a controlled glycosylation profile on protein subunit vaccines is highly desirable.

The receptor-binding domain (RBD) of the spike protein binds to the human angiotensin-converting enzyme 2 (ACE2) receptor when RBD is exposed in the up state. RBD has two N-glycans at sites N331 and N343 that are preserved in all SARS-CoV-2 variants of concern. The N343 glycan plays an important role in shielding RBD in the down state and through glycan-protein interaction it contributes to opening of the spike protein for receptor binding (Sztain et al., 2021; Pang et al., 2022). The N331 glycan is involved in the interaction of the spike protein with the glycocalyx of the host cell and thus also contributes to the host cell infectivity (Mycroft-West et al., 2020; Kim et al., 2022). RBD carries dominant neutralizing epitopes and is therefore a prime candidate for protein subunit vaccines (Yang et al., 2020a).

In recent years, plants have emerged as commercially relevant production systems for recombinant biopharmaceuticals like antibodies or vaccines (Chung et al., 2022; Eidenberger et al., 2023). Transient expression in plants provides a very flexible platform for safe and fast production of recombinant proteins. Using transient production in *Nicotiana benthamiana* a virus-like particle vaccine (Covifenz®) was produced by the company Medicago and approved by Health Canada as COVID-19 vaccine (Hager et al., 2022). Despite the fact that production of Covifenz® was not continued and Medicago ceased operations due to a management decision from its parent company (Benvenuto et al., 2023), the approval showed that this plant-made vaccine is safe and effective in preventing COVID-19. An RBD-based subunit vaccine that was effective, safe and non-toxic in animal studies is currently tested in phase 1 clinical trials (Phoolcharoen et al., 2023). In several other studies the huge potential of transient expression in plants for RBD subunit vaccine production has been demonstrated (Ruocco and Strasser, 2022). Most of these studies focused on the original RBD sequence. By contrast, comparable little information is available how mutations in different variants affect the plant-based production and glycosylation of recombinant RBD. Here, we produced glycoengineered RBD from different SARS-CoV-2 variants and functionally characterized the plant-produced viral proteins to reveal challenges associated with their production in *N. benthamiana*.

10.3389/fpls.2023.1275228

Results

The yield of transiently expressed RBD-215 variants differs

In previous studies, we have transiently expressed recombinant SARS-CoV-2 RBD (Wuhan-Hu-1 strain, region R319-L533 from the spike protein, length 215 amino acids and here referred to as RBD-215) by agroinfiltration in *N. benthamiana* leaves (Schwestka et al., 2021; Shin et al., 2021; König-Beihammer et al., 2022). The expressed protein has the barley α-amylase signal peptide for targeting the protein to the secretory pathway, two N-glycosylation sites (N331 and N343, numbering according to the full-length SARS-CoV-2 spike sequence) (Watanabe et al., 2020a) and a polyhistidine-tag attached to the C-terminus (Figure 1A). We used the same expression vector (pEAQ-*HT*) (Sainsbury et al., 2009) to examine the effect of different mutations occurring in the RBD of SARS-CoV-2 variants on their expression and functionality (Figure 1B). We aimed to express seven RBD-215 variants (Delta, Omicron sublineages BA.1, BA.2, BA.2.75, BA.4/BA.5, BQ.1.1 and XBB.1.5) (Figures 1C, D; Table S1). DNA sequences coding for the RBD-215 variants were codon-optimized for *N. benthamiana* and *in vitro* synthesized. Despite several attempts, no positive transformation clones were obtained for the BA.4/BA.5 sequence cloned into the expression vector pEAQ-*HT* and this variant was therefore not further investigated. The remaining six RBD-215 variants were all successfully cloned into pEAQ-*HT*.

To compare the yield of the transiently expressed RBD-215 variants, *Agrobacteria* carrying the respective pEAQ-*HT* expression constructs were infiltrated into leaves of *N. benthamiana* ΔXT/FT plants which are glycoengineered to produce mainly complex N-glycans lacking β1,2-xylose and core α1,3-fucose (Strasser et al., 2008). 4 days after infiltration, leaves were harvested and polyhistidine-tagged RBD-215 variants were purified from the apoplastic fluid via immobilized metal affinity chromatography (IMAC). All variants except BA.2.75 could be purified and displayed mainly the monomeric RBD-215 form upon SDS-PAGE under non-reducing conditions which is consistent with previous data (Figure 2) (Shin et al., 2021). For some variants an

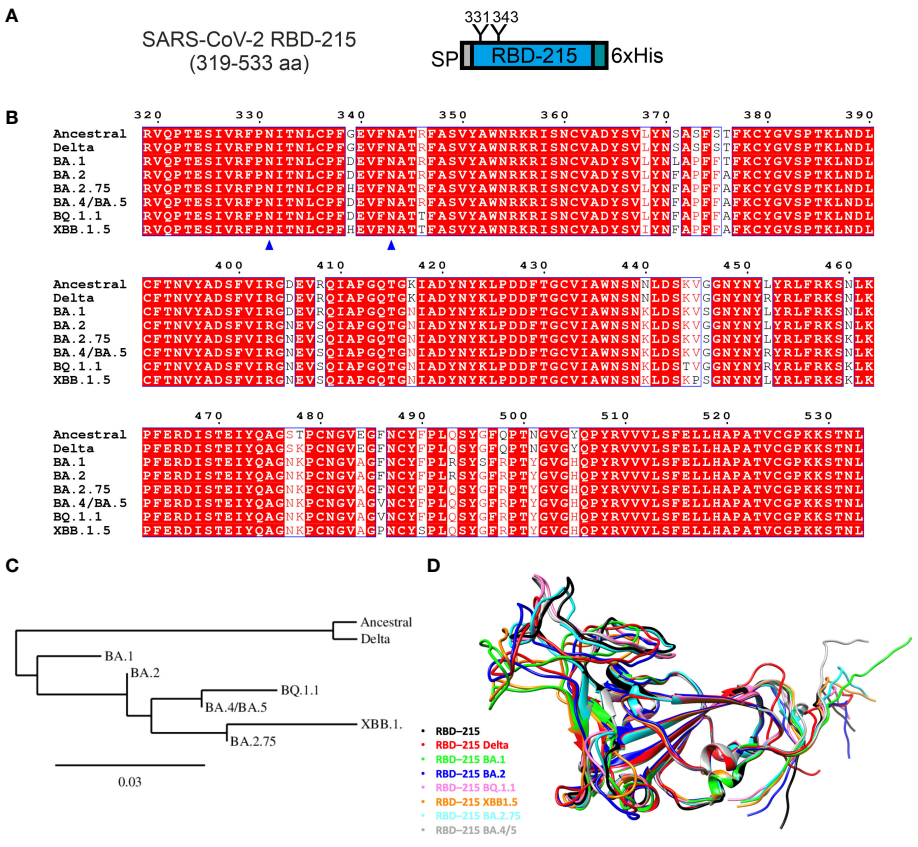

FIGURE 1
Comparison of expressed RBD-215 variants. **(A)** Schematic illustration of the expressed SARS-CoV-2 RBD-215 protein. SP, signal peptide; "Y", N-glycosylation sites, numbering according to the full-length SARS-CoV-2 spike sequence (UniProt: P0DTC2); 6xHis, polyhistidine tag composed of six histidine residues. **(B)** Sequence alignment of the amino acid region 319-533 from different SARS-CoV-2 variants was done using T-Coffee (https://www.ebi.ac.uk/Tools/msa/tcoffee/) and displayed using ESPript3.0 (https://espript.ibcp.fr/ESPript/cgi-bin/ESPript.cgi). N-glycosylation sites are marked by blue triangles. **(C)** Phylogenetic tree of RBD-215 sequences constructed using Phylogeny.fr (https://www.phylogeny.fr/). **(D)** Comparison of RBD-215 models produced by AlphaFold CoLab, showcasing their distinct and common structures and secondary features. The models were superimposed using the MatchMaker tool from UCSF Chimera (https://www.cgl.ucsf.edu/chimera/), which allows a direct comparison, highlighting conserved regions and structural variations (see also Table S1).

10.3389/fpls.2023.1275228

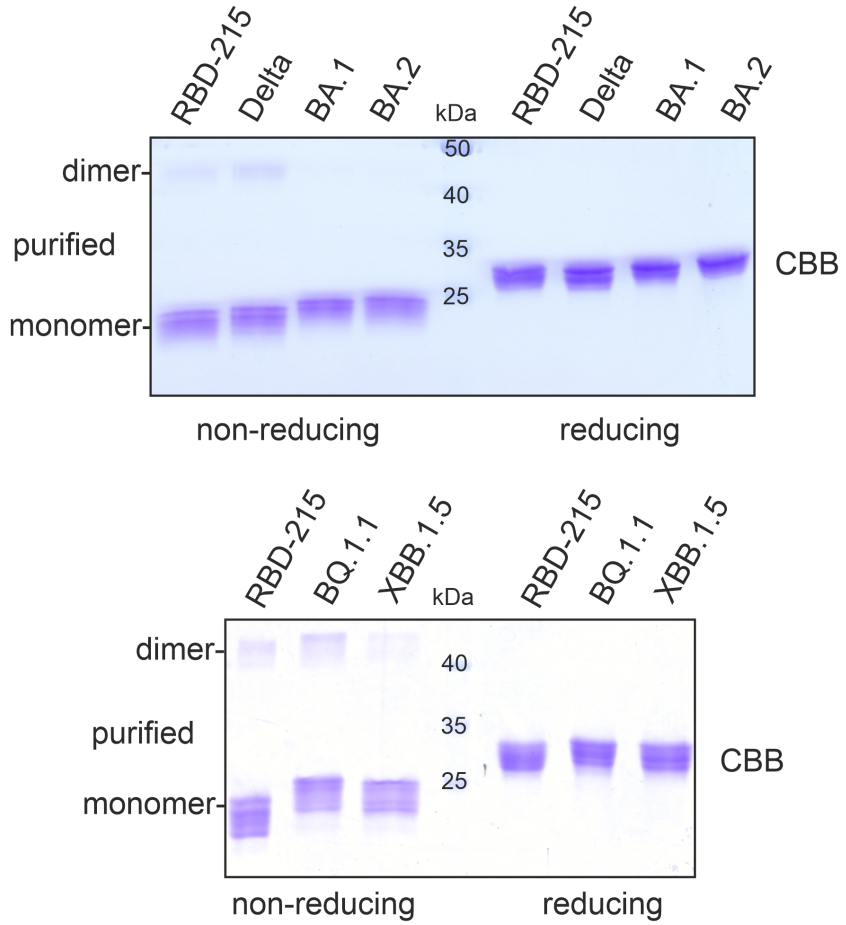

FIGURE 2
SDS-PAGE of purified RBD-215 variants. IMAC-purified RBD-215 variants were subjected to SDS-PAGE under non-reducing and reducing conditions and stained with Coomassie Brilliant Blue (CBB).

additional faint band between 40 and 50 kDa was visible under non-reducing conditions which disappeared under reducing conditions. This band likely comes from a dimer formed by intermolecular disulfide bonds.

The purification yield of the Delta variant ranged from 10 – 20 µg/g fresh leaves and was comparable to yields for RBD-215 (10-20 µg/g fresh leaves; Shin et al., 2021). For Omicron variants BA.1 and BA.2, 5-10 µg/g fresh leaves were obtained by purification. By contrast, only small amounts could be purified from BQ.1.1 (1-2 µg/g fresh leaves) and XBB.1.5 (~ 0.5 µg/g fresh leaves).

The RBD-215 variants display differences in stability in the apoplastic fluid

The yield of BQ.1.1 and XBB.1.5 was 10-20 times lower and even further reduced for BA.2.75. Therefore, we investigated the expression and fate of these three low-yield variants more in detail and included RBD-215 for comparison. When we analysed the apoplastic fluid, the signal intensity was comparable for RBD-215, BQ.1.1 and XBB.1.5, but the amount of polyhistidine-tagged BA.2.75 was much lower (Figure 3A). Consistent with the immunoblot analysis, the apoplastic fluid isolated from BA.2.75 expressing plants displayed less RBD-215-specific bands and the amount of BA.2.75 was also reduced in total soluble protein showing that the expression of this variant is lower (Figure 3B). Previously we found that poorly expressing RBD variants are misfolded and retained in the ER (Shin et al., 2021). ER-retained proteins typically carry Endo H-sensitive oligomannosidic N-glycans. BA.2.75 in total soluble protein was resistant to Endo H, but the N-glycans could be cleaved by PNGase F which can remove oligomannosidic and Golgi-processed complex N-glycans lacking core α1,3-fucose (Figure 3C). Likewise, BQ.1.1 and XBB.1.5 present in total soluble protein extracts exhibited mainly Endo H-resistant glycans (Figure 3D). Taken together, these findings indicate that the expressed RBD-215 variants are not misfolded and secreted through the Golgi to the apoplast.

Immunoblots and SDS-PAGE of proteins isolated from the apoplastic fluid confirmed that the expression levels of RBD-215, BQ.1.1 and XBB.1.5 are comparable (Figures 3A, E). Therefore, in

10.3389/fpls.2023.1275228

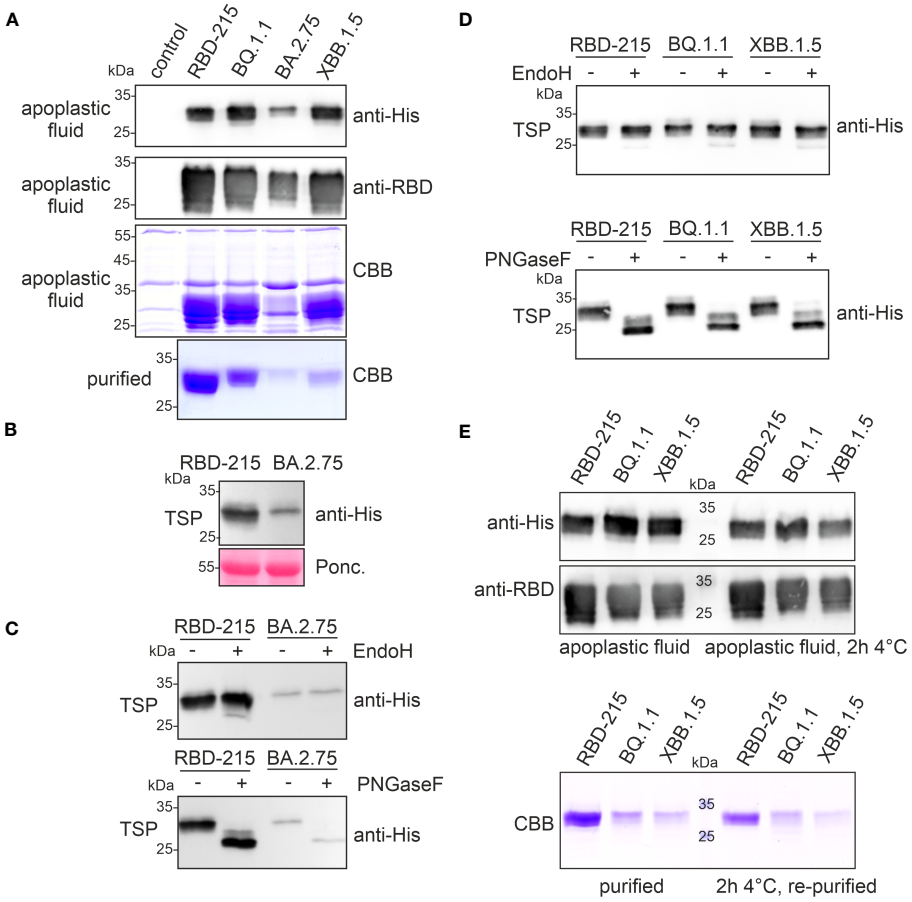

FIGURE 3
RBD-215 variants display differences in expression and yield after purification. **(A)** Immunoblot analysis (anti-histidine and anti-RBD antibodies) and SDS-PAGE with CBB-staining of isolated apoplastic fluid and purified RBD-215 variants. **(B)** Immunoblot of total soluble protein (TSP). Leaves from infiltrated *N. benthamiana* ΔXT/FT plants were harvested 4 days after infiltration and TSP was analysed with anti-histidine antibody. **(C, D)** Immunoblot of Endo H or PNGase F digested TSP. TSP was obtained by infiltration of *N. benthamiana* ΔXT/FT with *Agrobacteria* carrying the expression vectors for the indicated RBD-215 proteins. **(E)** Immunoblot and SDS-PAGE with CBB staining of the apoplastic fluid. The apoplastic fluid or the purified proteins were incubated for 2 h at 4°C followed by SDS-PAGE and immunoblotting or IMAC-purification (re-purified) and SDS-PAGE with CBB staining.

contrast to BA.2.75, the low yield of XBB.1.5 cannot be explained by lower expression levels or an inaccessible tag. On Coomassie Brilliant Blue-stained gels, RBD-215, BQ.1.1 and XBB.1.5 exhibited different faster migrating bands that likely represent RBD-215 protein with a cleaved polyhistidine-tag because these proteins are not detectable on immunoblots. It is therefore conceivable that the RBD-215 variants differ in their susceptibility to cleavage of the polyhistidine-tag which impacts their purification and overall yield. Indeed, the RBD-215 variants lost their polyhistidine tag in the apoplastic fluid rather rapidly, and this instability correlates with the observed low yields during IMAC purification (Figure 3E). A faster IMAC purification protocol with magnetic beads and continuous cooling resulted in a more than threefold (~1.8 µg/g fresh weight) increase of the yield for XBB.1.5. However, even under these conditions, the polyhistidine tag on XBB.1.5 was more unstable compared to RBD-215 or BQ.1.1, as less protein was purified after incubation for 2h at 4°C (Figure 3E).

The RBD-215 variants are glycosylated and functional

Next, we analysed the N-glycans to see if the mutations affect the N-glycan occupancy and/or N-glycan processing. Purified RBD-215 proteins were proteolytically digested and glycopeptides were analysed by mass spectrometry (MS). All purified RBD-215 variants carried primarily complex N-glycans with $GlcNAc_2Man_3GlcNAc_2$ (GnGn) as major N-glycan on both N-glycosylation sites (Figure 4; Supplemental Figure S1). In addition, all RBD-215 variants displayed small amounts of truncated N-glycans with removed terminal GlcNAc residues (MM and GnM N-glycans). These N-glycans are likely generated in the apoplast by β-hexosaminidase 3 (HEXO3) (Shin et al., 2017). On Omicron BA.2 the amounts of truncated N-glycans were modestly increased on both N-glycosylation sites suggesting that the N-glycans are more accessible for removal of terminal GlcNAc residues (Table 1). The

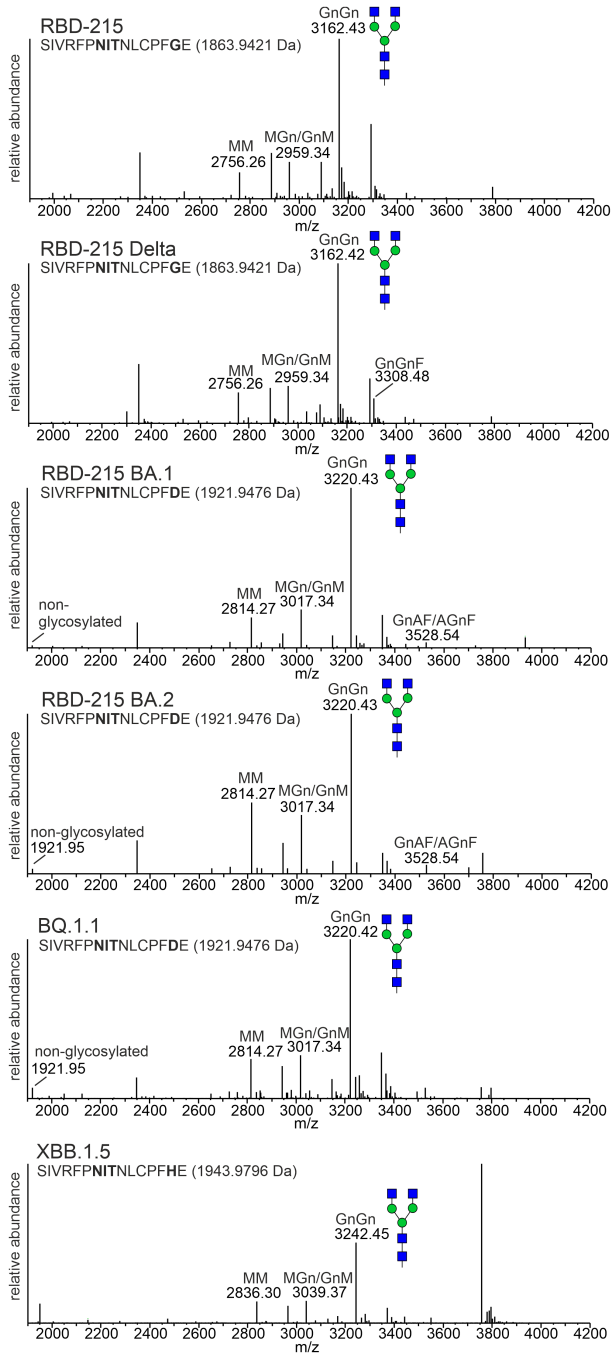

FIGURE 4
MS spectra of the RBD-215 glycopeptide containing N-glycosylation site N331 of the SARS-CoV-2 spike protein. The assigned N-glycan structures were labelled according to the ProGlycAn nomenclature (http://www.proglycan.com/). A cartoon illustration (filled green circle, mannose; filled blue square, GlcNAc; for details see http://www.functionalglycomics.org/) highlights the main N-glycan structures detected for each peptide.

overall very low amounts of oligomannosidic N-glycans (0.0-3.4%) are consistent with the secretion trough the Golgi and high accessibility of the N-glycans for processing. In all variants more than 96% of both N-glycosylation sites are fully glycosylated showing that both sites are very well recognized by the plant oligosaccharyltransferase complex (Castilho et al., 2018).

To examine whether the RBD-215 variants are functional in terms of binding to the human cellular receptor ACE2, we carried out binding assays using SPR. All six RBD-215 variants displayed binding to ACE2-Fc (Figure 5; Table S2). The binding curves for some variants appeared slightly out of phase which can be attributed to protein-intrinsic properties. By contrast, a comparison of SEC and non-SEC purified RBD-215 and BA.1 showed that the small amounts of dimers or oligomers do not affect the binding (Supplemental Figure S2). The binding affinity of the more recently evolved variants BQ.1.1. and XBB.1.5 was higher than RBD-215, Delta, BA.1 and BA.2 being consistent with the evolution of the virus towards better binding to ACE2 and higher infection capability (Ito et al., 2023; Yue et al., 2023).

To further investigate characteristics of the plant-produced RBD-215 variants, we analysed the thermostability of the purified proteins using differential scanning fluorimetry (DSF). The RBD-215 and Delta variants displayed a higher melting temperature (48.3°C and 50.1°C, respectively) than the Omicron variants BA.1 (41.2°C, lowest melting temperature of the analysed variants) and BA.2 (44.5°C). The reduced stability of BA.1 compared to BA.2 and the other variants is in close agreement with thermostability assays using mammalian-cell produced RBDs (Lin et al., 2022; Stalls et al., 2022) suggesting that the plant-produced variants display a similar folding. The thermostability of RBD-215 BQ.1.1 was 48.6°C and XBB.1.5. showed an increased (52.3°C) melting temperature (Figure 6; Supplemental Figure S3) which is consistent with the presence of amino acid changes (e.g. F486P) that are predicted to increase the stability (Verkhivker et al., 2023).

Glycoengineering shows improved binding of S309 to fucosylated RBD-215 Omicron BA.1

Distinct glycans attached to viral glycoproteins used as vaccine candidates may alter the immune response (Lusvarghi et al., 2023; Margolin et al., 2023). It is therefore of interest to produce glycosylation variants by glycoengineering to make vaccine candidates more potent. MS analysis of the N-glycans attached to N331 and N343 did not reveal huge differences in N-glycan composition (Figure 4). To see if RBD-215 variants can be subjected to glycoengineering in plants, we expressed RBD-215 and Omicron BA.1 in the presence of kifunensine to block α-mannosidases and produce oligomannosidic N-glycans. In another approach, we co-expressed the human core α1,6-fucosyltransferase (FUT8) to generate complex N-glycans carrying core α1,6-fucose as the vast majority of the complex N-glycans from mammalian cell-produced spike and RBD carry core fucose (Allen et al., 2021; Hsu et al., 2023). MS analysis showed that oligomannosidic N-glycans were present when kifunensine was co-infiltrated (Figure 7A; Supplemental Figure S4; Table 2). Upon FUT8 expression, complex N-glycans of RBD-215 and Omicron BA.1 were efficiently modified with fucose residues (~76-87% of all N-glycans fucosylated, Table 2). To examine the impact of the glycoengineered variants on receptor binding and thermostability we carried out SPR analysis and DSF. The K_D values were almost

10.3389/fpls.2023.1275228

TABLE 1 Relative N-glycan composition at the two N-glycosylation sites of the RBD-215 variants.

Site N331	RBD-215[5]	Delta[5]	BA.1[6]	BA.2[6]	BQ.1.1[6]	XBB.1.5[7]
Peptide[1]	1,6	2,5	1,0	1,4	3,4	1,5
Truncated[2]	16,3	14,0	13,0	23,2	17,1	16,8
Complex[3]	82,1	83,4	85,2	73,5	78,9	80,7
Mannosidic[4]	0,0	0,1	0,8	1,9	0,6	1,0
Total	100	100	100	100	100	100
Site N343	**RBD-215[8]**	**Delta[8]**	**BA.1[8]**	**BA.2[8]**	**BQ.1.1[9]**	**XBB.1.5[9]**
Peptide[1]	0,1	0,1	0,1	0,1	0,0	0,0
Truncated[2]	15,9	13,9	12,5	21,7	20,6	26,8
Complex[3]	83,4	85,5	85,4	74,8	78,4	71,3
Mannosidic[4]	0,6	0,5	2,1	3,4	1,0	1,9
Total	100	100	100	100	100	100

[1]non-glycosylated peptide. [2]processed N-glycans lacking GlcNAc residues at the non-reducing end (MM, MU, MMF, MUF) or carrying only Asn-GlcNAc. [3]complex N-glycans with at least one GlcNAc residues at the non-reducing end (e.g. GnGn, MGn/GnM, GnA/AGn, GnGnF, MGnF/GnMF, GnAF/AGnF). [4]mannosidic N-glycans ranging from Glc1Man9 to Man4. [5]peptide: SIVRFP**NIT**NLCPFGE; [6]peptide: SIVRFP**NIT**NLCPFDE; [7]peptide: SIVRFP**NIT**NLCPFHE; [8]peptide: VF**NAT**RFASVYAWNRK; [9]peptide: VF**NAT**TFASVYAWNRK.

identical to the GnGn containing glycoforms (Figures 5, 7B) and the melting points were in the same range (see Figure 6) suggesting that folding and the thermostability of the RBD-215 variants are not affected by changes in N-glycan composition (Figure 7C).

Next, we examined whether two well-characterized SARS-CoV-2 neutralizing antibodies (S309 and P5C3) (Pinto et al., 2020; Fenwick et al., 2021) can bind to RBD-215 and Omicron BA.1 as well as glycovariants thereof. P5C3 is a class 1 antibody that binds to the receptor binding motif of RBD in the "up" conformation (Fenwick et al., 2022; Chen et al., 2023). The monoclonal class 3 antibody S309 whose binding site does not overlap with the receptor binding motif, binds to an epitope that includes the fucose attached to the N-glycan on site N343 (Pinto et al., 2020; Qu et al., 2023). S309 and P5C3 bound quite similar to RBD-215 and neither the presence of fucose (RBD-215 + FUT8) nor oligomannosidic N-glycans (RBD-215 + kif) affected their binding (Figures 8A, B). In contrast to P5C3, S309 binding to Omicron BA.1 was strongly affected, but the reduced binding was improved 5-fold in the presence of the core fucose (BA.1 + FUT8) (Figure 8B). RBD-215 BA.1 with oligomannosidic N-glycans (BA.1 + kif) exhibited a modest (~1.6-fold) increase in binding to S309. These findings indicate that the fucosylated N-glycan at N343 plays a more important role for binding of the class 3 neutralizing antibody S309 to the Omicron BA.1 variant. In summary our data demonstrate that plant-produced RBD-215 variants are functional and behave like mammalian cell-derived RBD antigens.

Discussion

Viral glycoprotein antigens produced in different expression systems are used for vaccination and can elicit protecting neutralising antibodies (Yang et al., 2020a; Allen et al., 2021). However, glycosylation is species- and cell-type specific and the production of more authentic glycosylation profiles or modification with distinct sugar residues can prevent a skewed immune response and lead to more efficient immunogens. Challenges in RBD protein production have been observed in different expression systems (Chen et al., 2021; Guo et al., 2021; Dalvie et al., 2022) including plants which displayed generally low yields (Diego-Martin et al., 2020; Shin et al., 2021; Siriwattananon et al., 2021). Here, we found differences in the yield after purification between the variants. For some RBD-215 variants the low yield is not a primary consequence of low expression levels, but rather related to proteolytic processing of the polyhistidine-tag. Degradation or cleavage of tags is a common limitation of plant-produced secreted recombinant proteins (Gattinger et al., 2021). Optimization of production requires either a protein design that reduces the susceptibility to tag cleavage or identification and inactivation of the involved proteases in the apoplastic fluid (Jutras et al., 2020). An alternative strategy is the attachment of a KDEL ER-retrieval motif that results in the accumulation of recombinant proteins in the ER and therefore prevents the contact with proteases present in the apoplast. The drawbacks of this strategy are, however, the modification of recombinant proteins with an additional peptide motif (KDEL or SEKDEL) that could result in an unwanted immune response (Petruccelli et al., 2006), inefficient purification of polyhistidine-tagged proteins from total soluble protein extracted from plant tissues, and ER inherent oligomannosidic N-glycans that interfere with glycoengineering approaches and could affect the viral antigen function.

In the analysed plant-produced RBD variants, the two N-glycosylation sites, N331 and N343, are almost fully occupied with N-glycans which has also been shown for mammalian cell-produced RBD (Allen et al., 2021; Hsu et al., 2023). In addition, we detected only minor differences in the N-glycan profile of the variants and found mainly complex N-glycans that are the dominant glycan structures on mammalian cell-produced RBD,

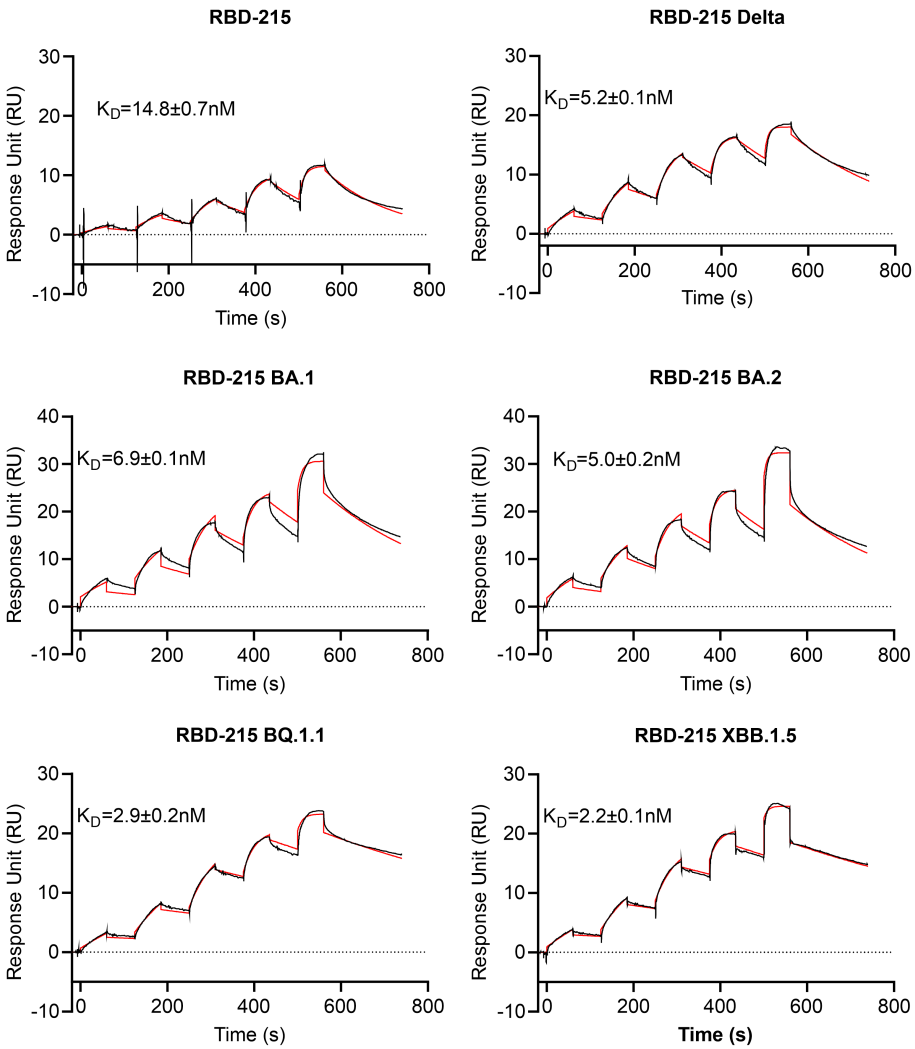

FIGURE 5
ACE2-Fc receptor binding of RBD-215 variants. SPR sensorgrams are shown and the K_D values (mean ± SD, n = 3) are given (red line fitted curves).

on recombinant spike trimers, virus derived spike trimer and a plant-produced virus-like particle (Allen et al., 2021; Brun et al., 2021; Gstöttner et al., 2021; Balieu et al., 2022; Hsu et al., 2023). In contrast to that, the N-glycan profile of plant-produced trimeric HexaPro spike differs markedly from the HEK293-produced one (Margolin et al., 2023). The plant HexaPro spike displayed predominately unprocessed oligomannosidic N-glycans. While the plant HexaPro spike elicited neutralizing antibodies in hamsters, the titers were lower compared to hamsters immunized with HEK293 HexaPro spike and animals were less well protected against the virus. This highlights that the differences in N-glycan composition have an impact on the potency of the produced SARS-CoV-2 vaccines and binding of neutralizing antibodies (Lusvarghi et al., 2023).

In a previous study, no differences were found in the binding affinity between RBD carrying different types of N-glycans and S309 antibody (Hsu et al., 2023). The experiments were carried out with the original RBD sequence and are consistent with our ELISA data. By contrast, we observed a clear fucose-dependent binding of S309 to the Omicron BA.1 variant. Due to mutations in the S309 epitope which includes G339D close to N343, BA.1 binds less well to S309 (Dejnirattisai et al., 2022; Qu et al., 2023). Our data show that the presence of the core fucose in the S309 epitope can to some extent compensate for the reduced binding to BA.1. For newly emerging variants, recombinant subunit vaccines with discrete glycoforms should therefore be explored to improve the immune response.

In summary, the characteristics of the produced RBD-215 variants were very similar to mammalian cell-produced RBD which emphasizes that the transient plant-based expression system is highly suitable for RBD subunit vaccine production. Our findings are relevant for attempts aiming at the production of mosaic or cocktail vaccines in plants to induce an immune response that

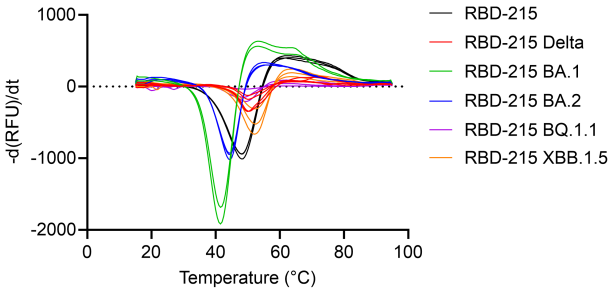

RBD variant	Tm (°C)
RBD-215	48.3 ± 0.0
RBD-215 Delta	50.1 ± 0.3
RBD-215 BA.1	41.2 ± 0.0
RBD-215 BA.2	44.5 ± 0.0
RBD-215 BQ.1.1	48.6 ± 0.8
RBD-215 XBB.1.5	52.3 ± 0.3

FIGURE 6
Thermal stability of RBD-215 variants. DSF profiles of the RBD-215 variants show changes in protein intrinsic fluorescence. For each RBD-215 protein, three overlaid curves (technical replicates) are shown and the Tm is given for every protein (mean ± SD, n = 3).

protects against a wide range of SARS-CoV-2 variants (Cohen et al., 2022; Zhang et al., 2022). In a previous study, a Delta RBD-Fc fusion was produced in *N. benthamiana* and shown to elicit broadly neutralizing antibodies against different strains in cynomolgus monkeys (Khorattanakulchai et al., 2022). A combination of plant-produced RBD variants in one vaccine could result in an even broader protection against circulating and emerging variants. The control of the N-glycan structures on plant-produced viral antigens could further improve such vaccines. The production of potent vaccines in plants will allow a more cost-effective manufacturing which is very important for low- and middle-income countries and thus contributes to overcome current inequities in access to such biologicals.

Materials and methods

Cloning of RBD-215 expression constructs

The cloning of pEAQ-RBD-215 carrying the original SARS-CoV-2 WT was described previously (Shin et al., 2021). The RBD-215 variants were cloned in the same way. Briefly, *N. benthamiana* codon-optimized DNA fragments harbouring the coding sequence for the barley α-amylase signal peptide, the RBD of SARS-CoV-2 (amino acids 319-533) and a 6x-histidine tag were PCR amplified using flanking primers, *Age*I/*Xho*I digested and ligated into *Age*I/*Xho*I digested plant expression vector pEAQ-*HT* (Sainsbury et al., 2009). The pEAQ-*HT* plant expression vectors containing RBD-215 sequence variants were transformed into *Agrobacterium tumefaciens* strain UIA143 (Strasser et al., 2005).

Purification of his-tagged RBD-215 variants

5-week-old *N. benthamiana* ΔXT/FT plants (Strasser et al., 2008) grown at 24°C were used for transient expression of RBD-215 variants. Leaves were manually infiltrated with *Agrobacteria* (OD_{600} = 0.2) carrying the respective pEAQ-RBD-215 expression vector. For the purification, infiltrated leaves were harvested 4 days after infiltration and intracellular fluid was collected by low-speed centrifugation as described in detail previously (Castilho et al., 2011b). His-tagged RBD-215 variants were purified from collected intracellular fluid by loading onto a 5 ml HisTrap HP column (Cytiva), elution with imidazole and subsequent dialysis and concentration by ultracentrifugation as described in detail previously (Göritzer et al., 2019). For production of RBD-215 variants with oligomannosidic N-glycans, 50 µM kifunensine (Santa Cruz Biotechnology) was co-infiltrated with the *Agrobacteria* suspension. For production of RBD-215 variants with core α1,6-fucose on complex N-glycans, a previously described FUT8 expression vector was used (Castilho et al., 2011a) and *Agrobacteria* harboring the FUT8 expression vector were co-infiltrated with an OD_{600} = 0.1.

For faster purification, the intracellular fluid in 20 mM Na_2HPO_4, 500 mM NaCl, 10 mM imidazole, pH 7.4 was incubated with pre-washed His Mag Sepharose® Ni magnetic beads (Cytiva) and incubated at 4°C for 30 min. After removal of the magnetic particles and washing with 20 mM Na_2HPO_4, 500 mM NaCl, 30 mM imidazole, pH 7.4, bound proteins were eluted with 20 mM Na_2HPO_4, 500 mM NaCl, 500 mM imidazole, pH 7.4 and the samples were dialyzed against PBS for 16 h at 4°C using SnakeSkin™ Dialysis Tubing 10K MWCO (Thermo Fisher Scientific).

SDS-PAGE and immunoblot analysis

Total soluble protein (TSP) extracts were prepared by dissolving homogenized leaf material in 20 mM Na_2HPO_4, 500 mM NaCl, pH 7.4. Proteins separated by SDS-PAGE were either visualized by Coomassie Brilliant Blue staining or immunoblotting with anti-His (Thermo Fisher Scientific) or anti-RBD (Sino Biological) antibodies. For *in vitro* deglycosylation, purified RBD-215 or total soluble protein extracts were incubated with endoglycosidase H (EndoH) (New England Biolabs) or peptide-N-glycosidase F (PNGaseF) (New England Biolabs) according to the manufacturer's instructions and subjected to SDS-PAGE and immunoblotting.

MS analysis

Purified RBD-215 was S-alkylated with iodoacetamide and digested in-solution with endoproteinases LysC (Roche) and

10.3389/fpls.2023.1275228

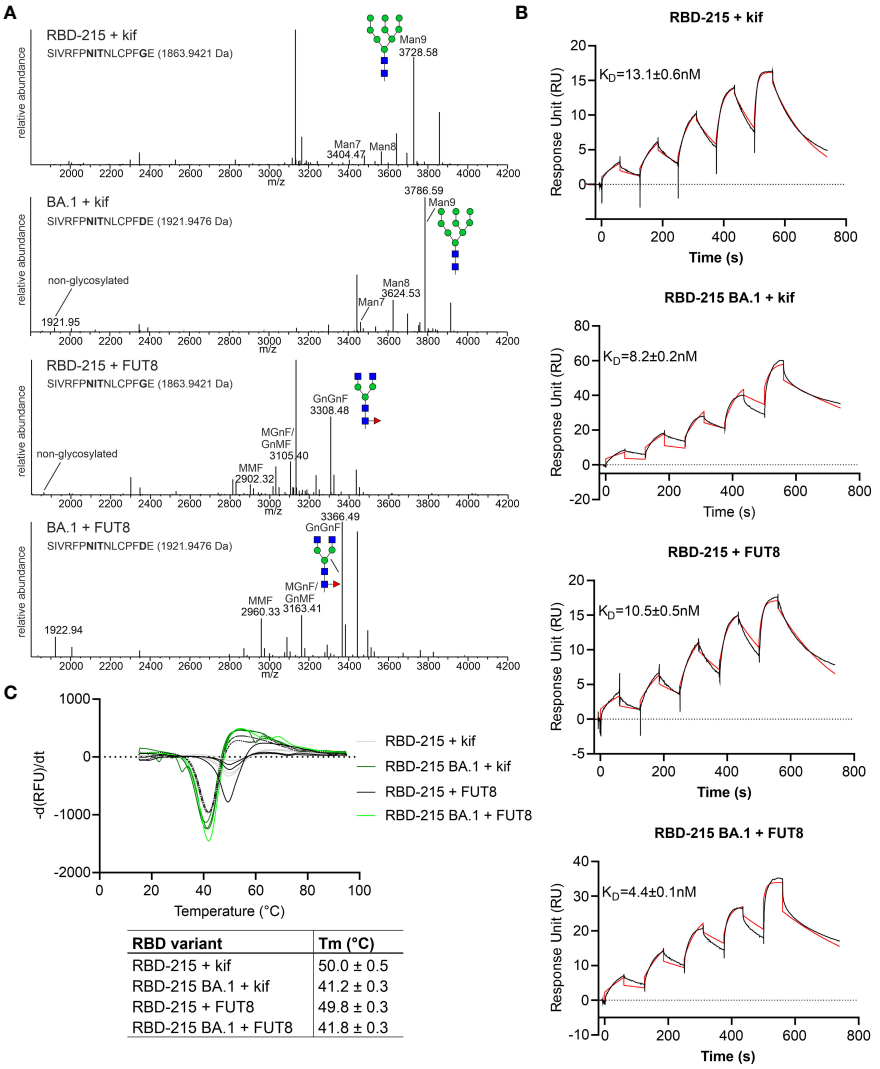

RBD variant	Tm (°C)
RBD-215 + kif	50.0 ± 0.5
RBD-215 BA.1 + kif	41.2 ± 0.3
RBD-215 + FUT8	49.8 ± 0.3
RBD-215 BA.1 + FUT8	41.8 ± 0.3

FIGURE 7
Glycoengineering results in RBD-215 variants with oligomannosidic or fucosylated complex N-glycans whose Tm and K_D values are not affected by changes in N-glycan structures. **(A)** MS spectra of RBD-215 + kif, Omicron BA.1 + kif, RBD-215 + FUT8, Omicron BA.1 + FUT8. A cartoon illustration (filled green circle, mannose; filled blue square, GlcNAc; red triangle, fucose) highlights the main N-glycan structures detected for each peptide **(B)** SPR analysis of ACE2-Fc binding to RBD-215 variants and **(C)** DSF curves and values (mean ± SD, n = 3) of RBD-215 + kif, Omicron BA.1 + kif, RBD-215 + FUT8, Omicron BA.1 + FUT8.

TABLE 2 Relative N-glycan composition of glycoengineered RBD-215 and Omicron BA.1.

Site N331	RBD-215 + FUT8	BA.1 + FUT8	RBD-215 + kif	BA.1 + kif
Peptide	1,7	0,2	3,0	2,4
Truncated	6,9	14,2	1,8	1,6
Complex	87,6	81,4	0,0	0,0
Mannosidic	3,8	4,2	95,2	96,0
Total	100	100	100	100
Fucosylated	76,7	82,3	0,0	0,0

(Continued)

TABLE 2 Continued

Site N343	RBD-215 + FUT8	BA.1 + FUT8	RBD-215 + kif	BA.1 + kif
Peptide	0,0	0,0	0,1	0,1
Truncated	10,4	11,7	1,6	0,8
Complex	87,7	84,4	0,0	0,0
Mannosidic	1,9	3,9	98,3	99,1
Total	100	100	100	100
Fucosylated	86,5	86,0	0,0	0,0

GluC (Promega). Glycopeptides were analysed using a Vanquish™ Neo UHPLC (Thermo Fisher Scientific) system coupled to an Orbitrap Exploris 480 mass spectrometer (Thermo Fisher Scientific). The possible N-glycopeptides were identified as sets of peaks consisting of the peptide moiety and the attached N-glycan varying in the number of HexNAc units, hexose, pentose and deoxyhexose residues. The theoretical masses of these glycopeptides were determined with an EXCEL spread sheet using the monoisotopic masses for amino acids and monosaccharides. The expected glycopeptides were manually detected and analysed with FreeStyle 1.8 program (Thermo Fisher Scientific). The deconvoluted, positively charged glycopeptides are shown in a mass range of 1900-4200 Da.

ELISA

Plant-produced RBD-215 variants (6 nM) in PBS were coated onto NUNC Maxisorp 96 well plates (Thermo Fisher Scientific) overnight at 4°C. Plates were washed 3 times with PBS supplemented with 0.1% (v/v) Tween 20 (PBST) and subsequently blocked for 1 hour with 1% (w/v) BSA in PBST. Recombinant S309 (VIR7831) IgG1 antibody (a kind gift from Hugo Mouquet) (Planas et al., 2022) or plant-produced P5C3 IgG1 (Kallolimath et al., 2023) was diluted in PBST supplemented with 1% BSA (4-fold dilution series starting with 4 nM) and incubated for 2 hours. The plates were washed 3 times with PBST and incubated for 1.5 hours with anti-IgG (H+L) horseradish peroxidase conjugated antibody (Promega) diluted 1:5000 in PBST + 1% (w/v) BSA. After 3 washes, substrate solution (10 mM sodium acetate, pH 5 + 1:60 diluted TMB-stock solution (0.4% (w/v) tetramethylbenzidine (Fluka) in DMSO) + 1:300 diluted H_2O_2 (0.6% in H_2O)) was applied (150 µL/well) and plates were incubated for 5-10 min with shaking. Reactions were stopped by the addition of 1 M sulfuric acid (25 µL/well) and absorbance was measured at 450 nm on a Tecan Sunrise Microplate (Tecan) reader using a reference wavelength of 620 nm. All samples were analysed at least twice with three technical replicates. EC50 values were calculated by non-linear regression of the blank-corrected data points based on a four-parametric log model with GraphPad Prism version 9.0 (Kallolimath et al., 2023).

SPR

The surface plasmon resonance (SPR) experiments were performed using a Biacore T200 (Cytiva). All assays were performed with HBS-EP running buffer (Cytiva) at 25°C. To determine the binding kinetics between the RBD-215 variants (MW = ~24 kDa without glycans) and ACE2-Fc (MW = 189,8 kDa, produced in HEK293 cells) (Castilho et al., 2021), a CM5 chip was coated with 150 pg of Protein A via amine coupling in the active cell (5500 RU). The reference flow cell was left blank without Protein A. The ligand ACE2-Fc was immobilized non covalently at 2.63 nM. The analytes, RBD-215 variants, were injected over the two flow cells at a range of five concentrations (200, 80, 32, 12.8 and 5.12 nM) prepared by serial 2.5-fold dilutions, at a flow rate of 30 µL/min using a single-cycle kinetics program. Prior to SPR measurements protein concentration for each sample was verified by averaging 5 independent measurements taken with a NanoDrop spectrophotometer in the UV-mode (at 280 nm using sample-specific extinction coefficients). Running buffer was also injected using the same program for background subtraction. The chip was regenerated at each measurement with 10 mM glycine-HCl pH 1.7. The ligand ACE2-Fc was captured at every run. All data were fitted to a 1:1 binding model using Biacore T200 Evaluation Software 3.1. Measurements were repeated three times for RBD-215 variants and are reported with standard deviation. The sensorgrams were plotted using GraphPad Prism version 9.0.

DSF

Protein stability measurements were carried out by differential scanning fluorimetry (DSF) using the CFX96 Real-Time PCR Detection System (Bio-Rad) with a final dilution of 1:500 of the SYPRO Orange dye (Molecular Probes). Fluorescence of a 25 µL sample (final concentration 0.4 mg/mL) in PBS was recorded from 10 - 95°C (0.5°C increments, 10 seconds hold per step) using the FRET channel. The thermograms, both the normalized relative fluorescence units (RFU) and the normalized derivative of relative fluorescence units (d(RFU)/dT) with respect to temperature (T) were recorded and compared. The peaks of the d(RFU)/dT-T thermogram are regarded as the melting temperatures (Tm)

A

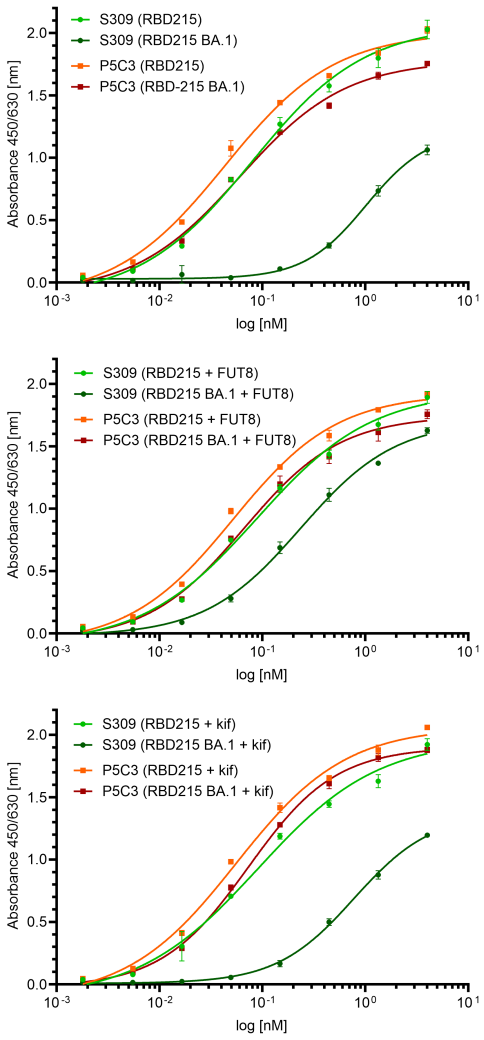

B

antibody	RBD215 EC50 (nM)	RBD215+FUT8 EC50 (nM)	RBD215+kif EC50 (nM)
S309	0,092	0,092	0,094
P5C3	0,050	0,062	0,055

antibody	BA.1 EC50 (nM)	BA.1+FUT8 EC50 (nM)	BA.1+kif EC50 (nM)
S309	1,133	0,225	0,711
P5C3	0,062	0,061	0,064

FIGURE 8
ELISA showing differences in binding of S309 antibody to glycoengineered Omicron BA.1. Binding to antibody P5C3 was used for comparison. **(A)** ELISA binding curves. **(B)** EC50 values (mean values, n = 3).

of the corresponding protein. Triplicate measurements were performed for each protein.

Data availability statement

The datasets presented in this study can be found in online repositories. The names of the repository/repositories and accession number(s) can be found below: https://www.ebi.ac.uk/pride/archive/, PXD044462.

Author contributions

VR: Conceptualization, Investigation, Visualization, Writing – review & editing. UV: Formal Analysis, Investigation, Writing – review & editing. JK-B: Formal Analysis, Investigation, Methodology, Writing – review & editing. OB: Formal Analysis, Investigation, Writing – review & editing. SK: Resources, Writing – review & editing. DM: Formal Analysis, Writing – review & editing. CG-G: Data curation, Investigation, Writing – review & editing. RS: Conceptualization, Data curation, Funding acquisition, Supervision, Writing – original draft.

Funding

The author(s) declare financial support was received for the research, authorship, and/or publication of this article. This work was supported by the Austrian Science Fund (FWF) (P31920-B32 and W1224-B09) and the BOKU COVID-19 Initiative.

Acknowledgments

The authors thank Professor George Lomonossoff (John Innes Centre, Norwich, UK) and Plant Bioscience Limited (Norwich, UK) for supplying the pEAQ-*HT* expression vector and Hugo Mouquet (Humoral Immunology Laboratory, Institut Pasteur, Université Paris Cité, Paris, France) for the kind gift of S309 (VIR7831) antibody. We thank Irene Schaffner and Jakob Wallner (University of Natural Resources and Life Sciences, Vienna, Austria) for help with the interpretation of SPR data. The SPR equipment was kindly provided by the EQ-BOKU VIBT GmbH and the BOKU Core Facility Biomolecular & Cellular Analysis. The MS equipment was kindly provided by the EQ-BOKU VIBT GmbH and the BOKU Core Facility Mass Spectrometry.

Conflict of interest

The authors declare that the research was conducted in the absence of any commercial or financial relationships that could be construed as a potential conflict of interest.

The author(s) declared that they were an editorial board member of Frontiers, at the time of submission. This had no impact on the peer review process and the final decision.

Publisher's note

Supplementary material

The Supplementary Material for this article can be found online at: https://www.frontiersin.org/articles/10.3389/fpls.2023.1275228/full#supplementary-material

References

Allen, J. D., Chawla, H., Samsudin, F., Zuzic, L., Shivgan, A. T., Watanabe, Y., et al. (2021). Site-specific steric control of SARS-CoV-2 spike glycosylation. *Biochemistry* 60, 2153–2169. doi: 10.1021/acs.biochem.1c00279

Baboo, S., Diedrich, J. K., Torres, J. L., Copps, J., Singh, B., Garrett, P. T., et al. (2023). Evolving spike-protein N-glycosylation in SARS-CoV-2 variants. *bioRxiv*, 539897. doi: 10.1101/2023.05.08.539897

Bagdonaite, I., and Wandall, H. H. (2018). Global aspects of viral glycosylation. *Glycobiology* 28, 443–467. doi: 10.1093/glycob/cwy021

Balieu, J., Jung, J. W., Chan, P., Lomonossoff, G. P., Lerouge, P., and Bardor, M. (2022). Investigation of the N-glycosylation of the SARS-CoV-2 S protein contained in VLPs produced in *nicotiana benthamiana*. *Molecules* 27, 5119. doi: 10.3390/molecules27165119

Benvenuto, E., Broer, I., D'Aoust, M. A., Hitzeroth, I., Hundleby, P., Menassa, R., et al. (2023). Plant molecular farming in the wake of the closure of Medicago Inc. *Nat. Biotechnol.* 41, 893–894. doi: 10.1038/s41587-023-01812-w

Brun, J., Vasiljevic, S., Gangadharan, B., Hensen, M., V. Chandran, A., Hill, M. L., et al. (2021). Assessing antigen structural integrity through glycosylation analysis of the SARS-CoV-2 viral spike. *ACS Cent. Sci.* 7, 586–593. doi: 10.1021/acscentsci.1c00058

Casalino, L., Gaieb, Z., Goldsmith, J. A., Hjorth, C. K., Dommer, A. C., Harbison, A. M., et al. (2020). Beyond shielding: the roles of glycans in the SARS-CoV-2 spike protein. *ACS Cent. Sci.* 6, 1722–1734. doi: 10.1021/acscentsci.0c01056

Castilho, A., Beihammer, G., Pfeiffer, C., Göritzer, K., Montero-Morales, L., Vavra, U., et al. (2018). An oligosaccharyltransferase from *Leishmania major* increases the N-glycan occupancy on recombinant glycoproteins produced in *Nicotiana benthamiana*. *Plant Biotechnol. J.* 16, 1700–1709. doi: 10.1111/pbi.12906

Castilho, A., Bohorova, N., Grass, J., Bohorov, O., Zeitlin, L., Whaley, K., et al. (2011a). Rapid high yield production of different glycoforms of Ebola virus monoclonal antibody. *PloS One* 6, e26040. doi: 10.1371/journal.pone.0026040

Castilho, A., Gattinger, P., Grass, J., Jez, J., Pabst, M., Altmann, F., et al. (2011b). N-glycosylation engineering of plants for the biosynthesis of glycoproteins with bisected and branched complex N-glycans. *Glycobiology* 21, 813–823. doi: 10.1093/glycob/cwr009

Castilho, A., Schwestka, J., Kienzl, N. F., Vavra, U., Grünwald-Gruber, C., Izadi, S., et al. (2021). Generation of enzymatically competent SARS-CoV-2 decoy receptor ACE2-Fc in glycoengineered *Nicotiana benthamiana*. *Biotechnol. J.* 16, e2000566. doi: 10.1002/biot.202000566

Chen, W. H., Wei, J., Kundu, R. T., Adhikari, R., Liu, Z., Lee, J., et al. (2021). Genetic modification to design a stable yeast-expressed recombinant SARS-CoV-2 receptor binding domain as a COVID-19 vaccine candidate. *Biochim. Biophys. Acta Gen. Subj* 1865, 129893. doi: 10.1016/j.bbagen.2021.129893

Chen, Y., Zhao, X., Zhou, H., Zhu, H., Jiang, S., and Wang, P. (2023). Broadly neutralizing antibodies to SARS-CoV-2 and other human coronaviruses. *Nat. Rev. Immunol.* 23, 189–199. doi: 10.1038/s41577-022-00784-3

Chung, Y. H., Church, D., Koellhoffer, E. C., Osota, E., Shukla, S., Rybicki, E. P., et al. (2022). Integrating plant molecular farming and materials research for next-generation vaccines. *Nat. Rev. Mater.* 7, 372–388. doi: 10.1038/s41578-021-00399-5

Cohen, A. A., Van Doremalen, N., Greaney, A. J., Andersen, H., Sharma, A., Starr, T. N., et al. (2022). Mosaic RBD nanoparticles protect against challenge by diverse sarbecoviruses in animal models. *Science* 377, eabq0839. doi: 10.1126/science.abq0839

Dalvie, N. C., Rodriguez-Aponte, S. A., Hartwell, B. L., Tostanoski, L. H., Biedermann, A. M., Crowell, L. E., et al. (2022). Engineered SARS-CoV-2 receptor binding domain improves manufacturability in yeast and immunogenicity in mice. *Proc. Natl. Acad. Sci. U S A.* 118, e2106845118. doi: 10.1073/pnas.2106845118

Dejnirattisai, W., Huo, J., Zhou, D., Zahradnik, J., Supasa, P., Liu, C., et al. (2022). SARS-CoV-2 Omicron-B.1.1.529 leads to widespread escape from neutralizing antibody responses. *Cell* 185, 467–484.e415. doi: 10.1016/j.cell.2021.12.046

Diego-Martin, B., González, B., Vazquez-Vilar, M., Selma, S., Mateos-Fernández, R., Gianoglio, S., et al. (2020). Pilot production of SARS-CoV-2 related proteins in plants: A proof of concept for rapid repurposing of indoor farms into biomanufacturing facilities. *Front. Plant Sci.* 11, 612781. doi: 10.3389/fpls.2020.612781

Eidenberger, L., Kogelmann, B., and Steinkellner, H. (2023). Plant-based biopharmaceutical engineering. *Nat. Rev. Bioeng.* 1, 426–439. doi: 10.1038/s44222-023-00044-6

Fenwick, C., Turelli, P., Ni, D., Perez, L., Lau, K., Herate, C., et al. (2022). Patient-derived monoclonal antibody neutralizes SARS-CoV-2 Omicron variants and confers full protection in monkeys. *Nat. Microbiol.* 7, 1376–1389. doi: 10.1038/s41564-022-01198-6

Fenwick, C., Turelli, P., Perez, L., Pellaton, C., Esteves-Leuenberger, L., Farina, A., et al. (2021). A highly potent antibody effective against SARS-CoV-2 variants of concern. *Cell Rep.* 37, 109814. doi: 10.1016/j.celrep.2021.109814

Gattinger, P., Izadi, S., Grunwald-Gruber, C., Kallolimath, S., and Castilho, A. (2021). The instability of dimeric fc-fusions expressed in plants can be solved by monomeric fc technology. *Front. Plant Sci.* 12, 671728. doi: 10.3389/fpls.2021.671728

Gong, Y., Qin, S., Dai, L., and Tian, Z. (2021). The glycosylation in SARS-CoV-2 and its receptor ACE2. *Signal Transduct. Target Ther.* 6, 396. doi: 10.1038/s41392-021-00809-8

Göritzer, K., Turupcu, A., Maresch, D., Novak, J., Altmann, F., Oostenbrink, C., et al. (2019). Distinct Fcα receptor *N*-glycans modulate the binding affinity to immunoglobulin A (IgA) antibodies. *J. Biol. Chem.* 294, 13995–14008. doi: 10.1074/jbc.RA119.009954

Gstöttner, C., Zhang, T., Resemann, A., Ruben, S., Pengelley, S., Suckau, D., et al. (2021). Structural and functional characterization of SARS-CoV-2 RBD domains produced in mammalian cells. *Anal. Chem.* 93, 6839–6847. doi: 10.1021/acs.analchem.1c00893

Guo, Y., He, W., Mou, H., Zhang, L., Chang, J., Peng, S., et al. (2021). An engineered receptor-binding domain improves the immunogenicity of multivalent SARS-CoV-2 vaccines. *mBio* 12, e00930-21. doi: 10.1128/mBio.00930-21

Hager, K. J., Pérez Marc, G., Gobeil, P., Diaz, R. S., Heizer, G., Llapur, C., et al. (2022). Efficacy and safety of a recombinant plant-based adjuvanted Covid-19 vaccine. *N Engl. J. Med.* 386, 2084–2096. doi: 10.1056/NEJMoa2201300

Hoffmann, D., Mereiter, S., Jin Oh, Y., Monteil, V., Elder, E., Zhu, R., et al. (2021). Identification of lectin receptors for conserved SARS-CoV-2 glycosylation sites. *EMBO J.* 40, e108375. doi: 10.15252/embj.2021108375

Hsu, Y. P., Frank, M., Mukherjee, D., Shchurik, V., Makarov, A., and Mann, B. F. (2023). Structural remodeling of SARS-CoV-2 spike protein glycans reveals the regulatory roles in receptor-binding affinity. *Glycobiology* 33, 126–137. doi: 10.1093/glycob/cwac077

Huang, H. Y., Liao, H. Y., Chen, X., Wang, S. W., Cheng, C. W., Shahed-Al-Mahmud, M., et al. (2022). Vaccination with SARS-CoV-2 spike protein lacking glycan shields elicits enhanced protective responses in animal models. *Sci. Transl. Med.* 14, eabm0899. doi: 10.1126/scitranslmed.abm0899

Ito, J., Suzuki, R., Uriu, K., Itakura, Y., Zahradnik, J., Kimura, K. T., et al. (2023). Convergent evolution of SARS-CoV-2 Omicron subvariants leading to the emergence of BQ.1.1 variant. *Nat. Commun.* 14, 2671. doi: 10.1038/s41467-023-38188-z

Jutras, P. V., Dodds, I., and van der Hoorn, R. A. (2020). Proteases of *Nicotiana benthamiana*: an emerging battle for molecular farming. *Curr. Opin. Biotechnol.* 61, 60–65. doi: 10.1016/j.copbio.2019.10.006

Kallolimath, S., Palt, R., Foderl-Hobenreich, E., Sun, L., Chen, Q., Pruckner, F., et al. (2023). Glyco engineered pentameric SARS-CoV-2 IgMs show superior activities compared to IgG1 orthologues. *Front. Immunol.* 14, 1147960. doi: 10.3389/fimmu.2023.1147960

Khorattanakulchai, N., Srisutthisamphan, K., Shanmugaraj, B., Manopwisedjaroen, S., Rattanapisit, K., Panapitakkul, C., et al. (2022). A recombinant subunit vaccine candidate produced in plants elicits neutralizing antibodies against SARS-CoV-2 variants in macaques. *Front. Plant Sci.* 13, 901978. doi: 10.3389/fpls.2022.901978

Kim, S. H., Kearns, F. L., Rosenfeld, M. A., Casalino, L., Papanikolas, M. J., Simmerling, C., et al. (2022). GlycoGrip: cell surface-inspired universal sensor for betacoronaviruses. *ACS Cent. Sci.* 8, 22–42. doi: 10.1021/acscentsci.1c01080

König-Beihammer, J., Vavra, U., Shin, Y. J., Veit, C., Grunwald-Gruber, C., Gillitschka, Y., et al. (2022). In planta production of the receptor-binding domain from SARS-CoV-2 with human blood group A glycan structures. *Front. Chem.* 9, 816544. doi: 10.3389/fchem.2021.816544

Lin, S., Chen, Z., Zhang, X., Wen, A., Yuan, X., Yu, C., et al. (2022). Characterization of SARS-CoV-2 Omicron spike RBD reveals significantly decreased stability, severe evasion of neutralizing-antibody recognition but unaffected engagement by decoy ACE2 modified for enhanced RBD binding. *Signal Transduct. Target Ther.* 7, 56. doi: 10.1038/s41392-022-00914-2

Lusvarghi, S., Stauft, C. B., Vassell, R., Williams, B., Baha, H., Wang, W., et al. (2023). D614G and Omicron SARS-CoV-2 variant spike proteins differ in the effects of N-glycan modifications on spike expression, virus infectivity, and neutralization by some therapeutic antibodies. *bioRxiv*, 540228. doi: 10.1101/2023.05.10.540228

Maity, S., and Acharya, A. (2023). Many roles of carbohydrates: A computational spotlight on the coronavirus S protein binding. *ACS Appl. Bio Mater.*, acsabm.2c01064. doi: 10.1021/acsabm.2c01064

Margolin, E., Schafer, G., Allen, J. D., Gers, S., Woodward, J., Sutherland, A. D., et al. (2023). A plant-produced SARS-CoV-2 spike protein elicits heterologous immunity in hamsters. *Front. Plant Sci.* 14, 1146234. doi: 10.3389/fpls.2023.1146234

Mycroft-West, C. J., Su, D., Pagani, I., Rudd, T. R., Elli, S., Gandhi, N. S., et al. (2020). Heparin inhibits cellular invasion by SARS-CoV-2: structural dependence of the interaction of the spike S1 receptor-binding domain with heparin. *Thromb. Haemost.* 120, 1700–1715. doi: 10.1055/s-0040-1721319

Newby, M. L., Fogarty, C. A., Allen, J. D., Butler, J., Fadda, E., and Crispin, M. (2023). Variations within the glycan shield of SARS-CoV-2 impact viral spike dynamics. *J. Mol. Biol.* 435, 167928. doi: 10.1016/j.jmb.2022.167928

Ozdilek, A., and Avci, F. Y. (2022). Glycosylation as a key parameter in the design of nucleic acid vaccines. *Curr. Opin. Struct. Biol.* 73, 102348. doi: 10.1016/j.sbi.2022.102348

Pang, Y. T., Acharya, A., Lynch, D. L., Pavlova, A., and Gumbart, J. C. (2022). SARS-CoV-2 spike opening dynamics and energetics reveal the individual roles of glycans and their collective impact. *Commun. Biol.* 5, 1170. doi: 10.1038/s42003-022-04138-6

Petruccelli, S., Otegui, M. S., Lareu, F., Tran Dinh, O., Fitchette, A. C., Circosta, A., et al. (2006). A KDEL-tagged monoclonal antibody is efficiently retained in the endoplasmic reticulum in leaves, but is both partially secreted and sorted to protein storage vacuoles in seeds. *Plant Biotechnol. J.* 4, 511–527. doi: 10.1111/j.1467-7652.2006.00200.x

Phoolcharoen, W., Shanmugaraj, B., Khorattanakulchai, N., Sunyakumthorn, P., Pichyangkul, S., Taepavarapruk, P., et al. (2023). Preclinical evaluation of immunogenicity, efficacy and safety of a recombinant plant-based SARS-CoV-2 RBD vaccine formulated with 3M-052-Alum adjuvant. *Vaccine* 41, 2781–2792. doi: 10.1016/j.vaccine.2023.03.027

Pinto, D., Park, Y. J., Beltramello, M., Walls, A. C., Tortorici, M. A., Bianchi, S., et al. (2020). Cross-neutralization of SARS-CoV-2 by a human monoclonal SARS-CoV antibody. *Nature* 583, 290–295. doi: 10.1038/s41586-020-2349-y

Planas, D., Saunders, N., Maes, P., Guivel-Benhassine, F., Planchais, C., Buchrieser, J., et al. (2022). Considerable escape of SARS-CoV-2 Omicron to antibody neutralization. *Nature* 602, 671–675. doi: 10.1038/s41586-021-04389-z

Qu, P., Faraone, J. N., Evans, J. P., Zheng, Y. M., Carlin, C., Anghelina, M., et al. (2023). Enhanced evasion of neutralizing antibody response by Omicron XBB.1.5, CH.1.1, and CA.3.1 variants. *Cell Rep.* 42, 112443. doi: 10.1016/j.celrep.2023.112443

Ruocco, V., and Strasser, R. (2022). Transient expression of glycosylated SARS-CoV-2 antigens in *nicotiana benthamiana*. *Plants (Basel)* 11, 1093. doi: 10.3390/plants11081093

Sainsbury, F., Thuenemann, E. C., and Lomonossoff, G. P. (2009). pEAQ: versatile expression vectors for easy and quick transient expression of heterologous proteins in plants. *Plant Biotechnol. J.* 7, 682–693. doi: 10.1111/j.1467-7652.2009.00434.x

Samuelsson, E., Mirgorodskaya, E., Nystrom, K., Backstrom, M., Liljeqvist, J. A., and Norden, R. (2022). Sialic acid and fucose residues on the SARS-CoV-2 receptor-binding domain modulate igG antibody reactivity. *ACS Infect. Dis.* 8, 1883–1893. doi: 10.1021/acsinfecdis.2c00155

Schwestka, J., König-Beihammer, J., Shin, Y. J., Vavra, U., Kienzl, N. F., Grünwald-Gruber, C., et al. (2021). Impact of specific N-glycan modifications on the use of plant-produced SARS-CoV-2 antigens in serological assays. *Front. Plant Sci.* 12, 747500. doi: 10.3389/fpls.2021.747500

Shi, J., Zheng, J., Tai, W., Verma, A. K., Zhang, X., Geng, Q., et al. (2022). A Glycosylated RBD Protein Induces Enhanced Neutralizing Antibodies against Omicron and Other Variants with Improved Protection against SARS-CoV-2 Infection. *J. Virol.* 96, e0011822. doi: 10.1128/jvi.00118-22

Shin, Y. J., Castilho, A., Dicker, M., Sádio, F., Vavra, U., Grünwald-Gruber, C., et al. (2017). Reduced paucimannosidic N-glycan formation by suppression of a specific β-hexosaminidase from *Nicotiana benthamiana*. *Plant Biotechnol. J.* 15, 197–206. doi: 10.1111/pbi.12602

Shin, Y. J., König-Beihammer, J., Vavra, U., Schwestka, J., Kienzl, N. F., Klausberger, M., et al. (2021). N-glycosylation of the SARS-CoV-2 receptor binding domain is important for functional expression in plants. *Front. Plant Sci.* 12, 689104. doi: 10.3389/fpls.2021.689104

Siriwattananon, K., Manopwisedjaroen, S., Shanmugaraj, B., Rattanapisit, K., Phumiamorn, S., Sapsutthipas, S., et al. (2021). Plant-produced receptor-binding domain of SARS-CoV-2 elicits potent neutralizing responses in mice and non-human primates. *Front. Plant Sci.* 12, 682953. doi: 10.3389/fpls.2021.682953

Stalls, V., Lindenberger, J., Gobeil, S. M., Henderson, R., Parks, R., Barr, M., et al. (2022). Cryo-EM structures of SARS-CoV-2 Omicron BA.2 spike. *Cell Rep.* 39, 111009. doi: 10.1016/j.celrep.2022.111009

Strasser, R. (2016). Plant protein glycosylation. *Glycobiology* 26, 926–939. doi: 10.1093/glycob/cww023

Strasser, R., Stadlmann, J., Schähs, M., Stiegler, G., Quendler, H., Mach, L., et al. (2008). Generation of glyco-engineered *Nicotiana benthamiana* for the production of monoclonal antibodies with a homogeneous human-like N-glycan structure. *Plant Biotechnol. J.* 6, 392–402. doi: 10.1111/j.1467-7652.2008.00330.x

Strasser, R., Stadlmann, J., Svoboda, B., Altmann, F., Glössl, J., and Mach, L. (2005). Molecular basis of N-acetylglucosaminyltransferase I deficiency in *Arabidopsis thaliana* plants lacking complex N-glycans. *Biochem. J.* 387, 385–391. doi: 10.1042/BJ20041686

Sztain, T., Ahn, S. H., Bogetti, A. T., Casalino, L., Goldsmith, J. A., Seitz, E., et al. (2021). A glycan gate controls opening of the SARS-CoV-2 spike protein. *Nat. Chem.* 13, 963–968. doi: 10.1038/s41557-021-00758-3

Verkhivker, G., Alshahrani, M., and Gupta, G. (2023). Balancing functional tradeoffs between protein stability and ACE2 binding in the SARS-CoV-2 omicron BA.2, BA.2.75 and XBB lineages: dynamics-based network models reveal epistatic effects modulating compensatory dynamic and energetic changes. *Viruses* 15, 1143. doi: 10.3390/v15051143

Wang, T. T., and Ravetch, J. V. (2019). Functional diversification of IgGs through Fc glycosylation. *J. Clin. Invest.* 129, 3492–3498. doi: 10.1172/JCI130029

Watanabe, Y., Allen, J. D., Wrapp, D., Mclellan, J. S., and Crispin, M. (2020a). Site-specific glycan analysis of the SARS-CoV-2 spike. *Science* 369, 330–333. doi: 10.1126/science.abb9983

Watanabe, Y., Berndsen, Z. T., Raghwani, J., Seabright, G. E., Allen, J. D., Pybus, O. G., et al. (2020b). Vulnerabilities in coronavirus glycan shields despite extensive glycosylation. *Nat. Commun.* 11, 2688. doi: 10.1038/s41467-020-16567-0

Wu, C. Y., Cheng, C. W., Kung, C. C., Liao, K. S., Jan, J. T., Ma, C., et al. (2022). Glycosite-deleted mRNA of SARS-CoV-2 spike protein as a broad-spectrum vaccine. *Proc. Natl. Acad. Sci. U.S.A.* 119, e2119995119. doi: 10.1073/pnas.2119995119

Yang, Q., Hughes, T. A., Kelkar, A., Yu, X., Cheng, K., Park, S., et al. (2020b). Inhibition of SARS-CoV-2 viral entry upon blocking N- and O-glycan elaboration. *Elife* 9, e61552. doi: 10.7554/eLife.61552

Yang, J., Wang, W., Chen, Z., Lu, S., Yang, F., Bi, Z., et al. (2020a). A vaccine targeting the RBD of the S protein of SARS-CoV-2 induces protective immunity. *Nature* 586, 572–577. doi: 10.1038/s41586-020-2599-8

Yang, Z., Wang, S., Halim, A., Schulz, M. A., Frodin, M., Rahman, S. H., et al. (2015). Engineered CHO cells for production of diverse, homogeneous glycoproteins. *Nat. Biotechnol.* 33, 842–844. doi: 10.1038/nbt.3280

Yue, C., Song, W., Wang, L., Jian, F., Chen, X., Gao, F., et al. (2023). ACE2 binding and antibody evasion in enhanced transmissibility of XBB.1.5. *Lancet Infect. Dis.* 23, 278–280. doi: 10.1016/S1473-3099(23)00010-5

Zhang, J., Han, Z. B., Liang, Y., Zhang, X. F., Jin, Y. Q., Du, L. F., et al. (2022). A mosaic-type trimeric RBD-based COVID-19 vaccine candidate induces potent neutralization against Omicron and other SARS-CoV-2 variants. *Elife* 11, e78633. doi: 10.7554/eLife.78633.sa2

Zhao, P., Praissman, J. L., Grant, O. C., Cai, Y., Xiao, T., Rosenbalm, K. E., et al. (2020). Virus-receptor interactions of glycosylated SARS-CoV-2 spike and human ACE2 receptor. *Cell Host Microbe* 28, 586–601. doi: 10.1016/j.chom.2020.08.004

Zheng, L., Wang, K., Chen, M., Qin, F., Yan, C., and Zhang, X. E. (2022). Characterization and function of glycans on the spike proteins of SARS-CoV-2 variants of concern. *Microbiol. Spectr.* 10, e0312022. doi: 10.1128/spectrum.03120-22

frontiers | Frontiers in Plant Science

TYPE Original Research
PUBLISHED 23 October 2023
DOI 10.3389/fpls.2023.1271757

OPEN ACCESS

EDITED BY
Balamurugan Shanmugaraj,
Chulalongkorn University, Thailand

REVIEWED BY
Rahul Singh,
University of Pennsylvania, United States
Tarlan Mammedov,
Akdeniz University, Türkiye

*CORRESPONDENCE
Nataliia Shcherbak
natalia@icbge.org.ua

†These authors have contributed equally to this work

RECEIVED 02 August 2023
ACCEPTED 02 October 2023
PUBLISHED 23 October 2023

CITATION
Shcherbak N, Prochaska H, Lystvan K, Prokhorova Y, Giritch A and Kuchuk M (2023) Accumulation of colicin M protein and its biological activity in transgenic lettuce and mizuna plants.
Front. Plant Sci. 14:1271757.
doi: 10.3389/fpls.2023.1271757

Accumulation of colicin M protein and its biological activity in transgenic lettuce and mizuna plants

Nataliia Shcherbak[1*†], Heike Prochaska[2†], Kateryna Lystvan[1], Yelizaveta Prokhorova[1], Anatoli Giritch[2] and Mykola Kuchuk[1]

[1]Department of Genetic Engineering, Institute of Cell Biology and Genetic Engineering of National Academy of Sciences (NAS) of Ukraine, Kyiv, Ukraine, [2]Nomad Bioscience GmbH, Halle (Saale), Germany

Food-borne illnesses caused by pathogenic *Escherichia coli* strains, especially enterohaemorrhagic *E. coli* (EHEC), are a serious public health problem, as debilitating disease and even death from such food poisonings have been repeatedly reported. Colicin M (ColM), a non-antibiotic antimicrobial protein produced by some strains of *E. coli*, has shown promising activity in controlling multiple enteropathogenic strains of *E. coli* and related pathogens. As contaminated green leafy vegetables are a frequent source of pathogenic *E. coli* infections, we genetically modified (GM) two edible crops, lettuce (*Lactuca sativa* L.) and mizuna (*Brassica rapa* subsp. nipposinica var. laciniata), to stably express the ColM gene and assessed the antibacterial activity of tissue extracts from these plants against selected *E. coli* strains *in vitro*. Transgenic plants of these species were developed using *Agrobacterium*-mediated transformation with a vector containing the ColM-coding gene (*cma*) under the control of the 35S promoter. Western blot analysis of recombinant ColM protein was performed in selected transgenic plants to confirm *cma* gene expression and quantify ColM accumulation. Extracts of transgenic plants expressing ColM showed significant activity against two major strains of EHEC (O157:H7 and O104:H4) as well as *E. coli* strains resistant to beta-lactam- and carbapenem-class antibiotics. Importantly, the antibacterial activity persisted in several subsequent generations of transgenic lettuce and mizuna plants that stably expressed the ColM gene. In addition, our results also show that the antibacterial activity of dried (up to 40°C) biomass of transgenic plants remained stable without a decrease for at least three months.

KEYWORDS

bacteriocins, colicin M, transgenic lettuce, transgenic mizuna, pathogenic *Escherichia coli*, STEC, EHEC, multi-drug resistance

1 Introduction

Food contamination by Shiga-toxin producing *Escherichia coli* (STEC) strains, especially their subset which can cause hemorrhagic colitis (enterohemorrhagic *E. coli*, EHEC), has repeatedly resulted in outbreaks of debilitating intestinal infections affecting the health of millions of people worldwide. *E. coli* of serotype O104:H4, which combines enteroaggregative and Shiga-toxin producing properties (EAEC/EHEC), was responsible for a large outbreak of gastrointestinal disease in multiple countries in Europe in 2011. The high virulence and multidrug resistance (MDR) of this uncommon *E. coli* strain led to the infection of almost 4,000 people and resulted in 54 deaths (Navarro-Garcia, 2014; Tietze et al., 2015). *E. coli* O157:H7 is currently the predominant STEC serotype causing severe illnesses with a low infectious dose (50–100 colony-forming units (CFU/g or mL) (Puligundla and Lim, 2022). Frequently the spread of these pathogenic bacteria is associated with the consumption of animal products because they are commonly found in the intestinal tract of cattle (Low et al., 2005; Munns et al., 2015). However, green leafy vegetables, which are usually eaten raw without heat treatment from cooking, can be contaminated in the field through improperly composted manure, or contaminated irrigation water or soil (Alegbeleye et al., 2018; Waltenburg et al., 2021; Xu et al., 2021). A multistate outbreak of STEC O157:H7 associated with the consumption of Romaine lettuce was reported in the USA in 2011 (Slayton et al., 2013). Subsequently, the U.S. Centers for Disease Control and Prevention (USCDC) reported that in 2018 and 2019, several large outbreaks of *E. coli* O157:H7 linked to Romaine lettuce resulted in 439 illnesses and 5 deaths (USCDC, 2020). In spite of these experiences and the implementation of mitigation measures that followed, contaminated fresh leafy vegetables have continued to cause foodborne disease outbreaks (Irvin et al., 2021; Waltenburg et al., 2021).

The food industry employs various sanitizing methods both for disinfection of food processing equipment and for reduction of common foodborne pathogens associated with fresh-cut vegetables and fruit products. Currently, thermal inactivation is one of the most effective methods for the destruction of pathogenic bacteria in food, but the method is not generally amenable to decontaminating green leafy vegetables or some types of animal feed. For such products, sodium hypochlorite (NaClO) solutions can be used, but their residues are potentially harmful, can impart an undesirable taste, and the process is not environmentally benign (Tomás-Callejas et al., 2011). Antibiotics are often used prophylactically to prevent the spread of pathogenic bacteria on farms and in livestock. In response to the significant increase of MDR bacteria, legislative measures have widely been taken to limit or eliminate the use of antibiotics, including in the form of feed additives for livestock (Urban-Chmiel et al., 2022). According to the U.S. Food and Drug Administration (FDA), medically important antimicrobial drugs approved for use in food-producing animals decreased by 38% since 2015, which was the peak year of sales (FDA, 2021). However, this is only the beginning of the implementation of measures to prevent the increase of MDR bacteria and the problem of the constantly growing number of bacteria resistant to widely used antibiotics, including drugs of last resort, remains relevant. Antibiotics used in food-producing animals are closely related to those used in human medicine and antibiotic-resistant pathogenic bacteria foreshadow a growing global health crisis. Numerous studies have confirmed that bacteria use both phenotypic and genetic strategies that ensure the emergence of antibiotic resistance (Urban-Chmiel et al., 2022). There is already evidence of bacterial resistance to highly effective antibiotics, including transmission among *E. coli* strains of the resistance gene for the antibiotic colistin, considered the antibacterial of last resort in the management of severe and life-threatening Gram-negative infections (Liu et al., 2016; Paveenkittiporn et al., 2017). Also of concern is the rapidly increasing prevalence of *Enterobacteriaceae* harbouring carbapenemases and becoming resistant to carbapenem-class antibiotics. The spread of carbapenem resistance has led the World Health Organization (WHO) to designate carbapenem-resistant enterobacteria (CRE) as «priority pathogens» that pose the greatest global threat to human health (Willyard, 2017; Sheu et al., 2019). Alternative management strategies are therefore urgently needed, especially to control Gram-negative bacterial pathogens.

The spread of bacterial infections caused by food contamination with pathogenic microorganisms could be effectively prevented by bacteriocins, which are non-antibiotic antimicrobial proteins produced by bacteria to kill closely related strains, presumably by affording producing strains a competitive advantage for resources in their ecological niche (Gabrielsen et al., 2014; Kumariya et al., 2019; Benitez-Chao et al., 2021). Due to their high species and strain specificity (i.e., narrow spectrum of activity), the use of bacteriocins as antimicrobial agents offers important advantages over current chemistries, including sparing beneficial bacteria and thus avoiding microbial imbalances in the gastrointestinal (GI) tract (Cleveland et al., 2001; Cavera et al., 2015). Further, bacteriocins are natively produced by bacteria resident in the GI tract of humans and other animals, underscoring their evolutionary importance as well as their safety.

Therefore, bacteriocins offer unique advantages as potential alternatives to antibiotics, especially for prophylactic use in both food and feed. Within the bacteriocin family, colicins are antibacterial proteins produced by certain strains of *E. coli* that are effective against pathogenic strains of the same or closely related species (Callaway et al., 2004; Chérier et al., 2021). Colicins can be recombinantly produced using several platforms, including various plant hosts. Several plant-produced colicins have been approved as GRAS (Generally Recognized as Safe) antimicrobial food processing aids by FDA (GRAS Notice (GRN) No. 593, 2015). Colicin M (ColM) is the only one colicin interfering with peptidoglycan biosynthesis. Targeting such an essential bacterial component potentially makes the ColM-like proteins “universal” antibacterial agents (Chérier et al., 2021). ColM was first produced using transient gene expression methods in *Nicotiana benthamiana* plants, a well-accepted standard species for recombinant protein manufacturing, as well as in edible species of plants such as spinach and leafy beet (Schulz et al., 2015; Stephan et al., 2017; Hahn-Löbmann et al., 2019). Among the various colicins evaluated, ColM had the broadest antimicrobial activity against the seven major

foodborne enterohemorrhagic *E. coli* (EHEC) strains, including the O157:H7 serotype (Schulz et al., 2015; Hahn-Löbmann et al., 2019) and *Klebsiella pneumoniae* (Łojewska et al., 2020).

The goal of our work was to create genetically modified edible plants that could stably express recombinant ColM. Previously, ColM had been recombinantly expressed only in non-food species of plants, including transiently and transgenically in *N. benthamiana* (Hahn-Löbmann et al., 2019) and transgenically in *N. tabacum* (Łojewska et al., 2020). The ColM isolated from these plants retained its conformation and was fully active. In the present study, we report for the first time the successful development of stable transgenic green leafy vegetables, lettuce and mizuna, expressing ColM and confirm the *antibacterial activity of* plant extracts for several generations of transgenic plants. We also demonstrate that heat dried (up to 40°C) transgenic plant biomass retained antimicrobial activity without significant reduction for at least 3 months. Our results suggest that bacteriocin-expressing leafy vegetables that are often the vectors for environmentally acquired Gram-negative bacterial infections could be used instead as a functional food to help control foodborne illnesses.

2 Materials and methods

2.1 Vector construction and bacterial strains

The vector pNMD46772 containing the ColM-coding *cma* gene under the control of a 35S promoter and selective *bar* gene under the control of a nos promoter was transformed to *Agrobacterium tumefaciens* strain GV3101. The transformed bacteria were grown on selective LB (Bertani, 1951) agar medium containing rifampicin 50 mg/L, gentamicin 25 mg/L and kanamycin 100 mg/L. Colonies were confirmed to be transformed with vector pNMD46772 using PCR analysis with primers specific for the *cma* gene.

2.2 Plant transformation and regeneration

Agrobacterium-mediated transformation of lettuce 'Odeskyj curling'; with the vector pNMD46772 containing the *cma* gene was carried out as described in Shcherbak et al. (2013). After 48 h of co-cultivation with diluted *Agrobacterium* suspension supplemented with 100 mM acetosyringone, explants were placed on modified B5 (Gamborg et al., 1968) regeneration medium (B5 medium salts with 2.5% sucrose, 3 mg/L kinetin, 0.5 mg/L NAA) supplemented with 5 mg/L phosfinothricin (PPT) for selection. As shoot appeared, each one was removed and placed on the MS (Murashige and Skoog, 1962) medium supplemented with 0.5 mg/L of indole-3-butyric acid for rooting. Well established plants were transferred into the soil and grown in a greenhouse.

For genetic transformation of mizuna, hypocotyls of 5-7-day-old seedlings were used as explants. After co-cultivation with *Agrobacterium*, the explants were cultivated on callus induction MS medium containing 2,4-D (2 mg/L) and BAP (0.5 mg/L) for one week. Further regeneration of shoots took place on a nutrient medium containing zeatin (2 mg/L), BAP (1 mg/L) and NAA (0.5 mg/L). PPT at concentrations of 5 mg/L was used for the first step of mizuna transformants selection and after two weeks of cultivation on the regeneration medium the PPT concentration was increased to 10 mg/L. Regenerated plants were also rooted, transferred to the soil and grown in a greenhouse.

2.3 PCR and RT-PCR

Genomic DNA was isolated from plant leaves using the CTAB protocol for isolating DNA from plant tissues. PCR was carried out in 20 µl reaction volume containing 50 ng DNA, 200 µM each of forward and reverse primers, 200 µM dNTPs and 1 U Taq DNA polymerase (Thermo Scientific, USA). Amplification was performed on a Mastercycler® personal (Eppendorf, USA). Sequences of the primers used were as follows:

for *bar* gene amplification.

bar_fwd 5'-ACATCGAGACAAGCACGGTC-3'.
bar_rev 5'-GCCAGAAACCCACGTCATGC-3'.

for *cma* gene amplification.

colM_fwd 5'-ATGGAAACCCTTACTGTGCACGCTC-3'.
colM_rev 5'-CCTCTTACCAGACTCTTTGATGTG-3'.

The products of the amplification (411 bp when using primers for *bar* gene and 1003 bp for *cma* gene) were separated on 1% (w/v) agarose gels.

RT-PCR was performed for previously selected transgenic plants to detect *cma* gene transcripts. Total RNA was prepared from 100 mg of transgenic plant leaf tissue using an GeneJET RNA Purification Kit (Thermo Fischer Scientific, Waltham, USA) and reverse-transcribed using a RevertAid First Strand cDNA Synthesis Kit (Thermo Scientific, USA) with oligo dT primers. Genomic DNA from RNA preparation was removed by DNase I (RNase-free) treatment for 30 min at 37°C. A negative control for each sample consisted of the same reaction mixture without reverse transcriptase. The obtained cDNA was used as a template for PCR with gene-specific primers.

2.4 Extraction of plant material for protein analysis

Leaf material of transgenic and non-transgenic plants was ground in liquid nitrogen and total soluble protein (TSP) extracts were prepared with 5 volumes of extraction buffer (50 mM HEPES pH7.0, 10 mM K acetate, 5 mM Mg acetate, 10% glycerol, 0.05% Tween-20, 300 mM NaCl). After incubation for 20 min on ice and centrifugation for 10 min at 13000 rpm at 4°C, supernatant was used for immunoblot analysis and determination of antimicrobial activity. Protein concentration in the extracts was determined by the Bradford method using Bio-Rad Protein Assay (Bio-Rad

Laboratories, Hercules, USA) and bovine serum albumin (BSA) (Sigma-Aldrich, Saint Louis, USA) as a standard.

2.5 Drying of plant material and extraction of dried material

Plant leaf material was harvested, frozen in liquid nitrogen and stored at -80°C. After 262 days, part of the material was thawed and incubated for 1 day at 40°C in an oven for drying. For final drying, material was incubated at room temperature for an additional 10 days. Dried material was further stored at room temperature. Fresh and frozen plant material was extracted with 5 volumes of extraction buffer, while dried material was extracted with 20 volumes of extraction buffer.

To allow direct comparison of activities for fresh and dried plant material, the weight factor for normalization of different extraction volumes and the weight loss during drying process were calculated as follows: Weight factor = fresh weight/dry weight * 5 (vol fresh extraction)/20 (vol dry extraction).

2.6 Purification of colicin M

ColM was transiently expressed in *N. benthamiana* and purified according to Stephan et al. (2017) with minor modifications. For purification plant material was extracted with the buffer containing 20 mM citric acid (pH4.0), 20mM NaH_2PO_4 and 30 mM NaCl in a 5:1 (v/w) buffer:biomass ratio. Ground leaf material admixed with pre-chilled extraction buffer was incubated on ice for 10 min followed by centrifugation at 10,000 x g for 15 min at 22°C. The supernatant was filtered using Miracloth (Merck KGaA, Darmstadt, Germany) and mixed with 10 mg/ml diatomaceous earth (Sigma-Aldrich, Saint Louis, USA) followed by incubation of the filtrate for 20 min at room temperature and centrifugation for 15 min at 10,000 x g at 22°C. The resulting supernatant was filtrated using filter discs with a pore size of 8–12 µm and the final filtrate was used for further purification by column chromatography. The filtrate was loaded on a HiTrap™Capto™MMC (GE Healthcare, Munich, Germany) column equilibrated with extraction buffer. The column was washed in two steps. The first wash step was performed with extraction buffer. The second wash step was done using diluted (30%) elution buffer consisting of 50 mM Na_2HPO_4 (pH 7.84), 10 mM citric acid and 1 M NaCl. The elution of ColM was carried out in a linear gradient from 30 to 100% of elution buffer concentration. The eluted fractions were analyzed by SDS-PAGE and Coomassie staining using Instant Blue™ staining solution (Expedeon, San Diego, CA, USA). The colicin containing fractions were pooled and dialyzed overnight at 4°C against 20 mM Na_2HPO_4 (pH 7.5), 10 mM citric acid and 50 mM NaCl. After dialysis, purified protein was frozen in liquid nitrogen and finally freeze-dried by lyophilization using freeze dryer Alpha 1–2 LDplus (Martin Christ Gefriertrocknungsanlagen, Osterode am Harz, Germany). Purified ColM batch 12 was used as a reference standard for antimicrobial activity and in immunoblot analysis.

2.7 Immunoblot analysis

Protein-containing plant extracts were mixed 1:1 with 2xLaemmli buffer and denatured at 95°C for 10 min. The total proteins were separated by sodium dodecyl sulfate polyacrylamide gel electrophoresis (SDS-PAGE) using a 15% polyacrylamide gel under reducing conditions and then transferred to a PVDF membrane. The membrane was incubated with a rabbit polyclonal ColM antibody 30365 (diluted 1:5,000) or monoclonal ColM antibody 3F9 (diluted 1:2,000) overnight. Polyclonal ColM antibody was generated against purified full length ColM by BioGenes GmbH (Berlin, Germany). Monoclonal ColM antibody 3F9 was generated against purified full-length ColM by Fraunhofer Institute for Cell Therapy and Immunology (IZI, Halle (Saale), Germany). Secondary antibodies were IgG (whole molecule) peroxidase affinity isolated antibody (Sigma-Aldrich, Saint Louis, USA), anti-mouse (diluted 1:5,000) or anti-rabbit (diluted 1:10,000). Determination of ColM concentration in extracts was done semi-quantitatively by comparison of different amounts of extracts with known amounts of purified ColM batch 12 reference protein.

2.8 Antimicrobial activity determinations

Microbiological studies were carried out on two laboratory strains of *E. coli* (DH10B and XL1-Blue) and a set of reference strains (Table 1). The bacteria were incubated at 37°C in LB medium (Bertani, 1951).

Semi-quantitative determinations of antimicrobial bacteriocin activity by a spot-on-lawn soft-agar overlay assay were performed as described in Schulz et al. (2015). Specific activity was calculated by normalization of arbitrary colicin activity units to TSP concentrations determined via Bradford assay to exclude effects of different extraction efficiencies.

TABLE 1 Reference *E. coli* strains used in activity determinations.

collection number/strain designation (origin)	serotype	origin
ATCC BAA-2326	O104:H4	Doenitz Prolab e. Kfr., Augsburg (distributed Microbiologics product; obtained from ATCC collection)
ATCC 35150	O157:H7	Doenitz Prolab e. Kfr., Augsburg (distributed Microbiologics product; obtained from ATCC collection)
NCTC13352		The National Collection of Type Cultures (NCTC), UK (Public Health England)
NCTC13919		The National Collection of Type Cultures (NCTC), UK (Public Health England)
ATCC BAA-2452		Microbiologics (#01242P)

2.9 Determination of minimal inhibitory concentration

Each respective bacterial test culture was grown in LB medium until OD600 of 0.2 and diluted to approximately $2x10^3$ CFU/µl. 5 µl of diluted culture were spotted on LB medium supplemented with 0.75% (w/v) agar, 0.1 mg/ml BSA (AppliChem, Darmstadt, Germany) and a dilution series of purified ColM (10 µg/ml to 1 ng/ml). Plates were incubated for 16-20 h at 37°C before MIC readout. The MIC was defined as the lowest concentration of ColM that inhibited visible growth of the test culture.

3 Results

3.1 Generation and analysis of transgenic plants expressing colicin M gene

We generated transgenic plants of lettuce (*Lactuca sativa* L.) 'Odeskyj curling' and mizuna (*Brassica rapa subsp. nipposinica* var. *laciniata*) using *Agrobacterium*-mediated transformation with a vector carrying the ColM-coding gene (*cma*). The vector pNMD46772 contains two expression cassettes: a *cma* gene under the control of a 35S promoter and the selective *bar* gene under the control of a nos promoter. Expression of the *bar* gene in transgenic plants provides for their resistance to the herbicide phosphinothricin (PPT). After five- or six-weeks incubation of lettuce cotyledons on the regeneration medium supplemented with the selective agent PPT (5 mg/L), green shoots were formed on the explants (Figure 1A). Regenerated plants developed roots after transfer to the medium supplemented with 0.5 mg/L of indole-3-butyric acid (Figure 1B). The resulting rooted lettuce plants were transferred to soil and grown in a greenhouse (Figure 1C). Mizuna plants were regenerated on the zeatin-containing media after 3-5 weeks of cultivation (Figure 1D). The selected plant lines resistant to 5 mg/L of PPT were cultivated under aseptic conditions (Figure 1E). Two lines were transferred to soil and grown in a greenhouse (Figures 1F, G). Greenhouse-maintained lettuce and mizuna plants bloomed and formed seeds in 3-4 months.

All putative transgenic plants were initially screened for the integration of *bar* and *cma* genes using primers which should produce fragments of 411 bp and 1003 bp respectively. Amplification of the DNA of all plants revealed the expected fragments whose position is indicated by the arrows (Figures 2A, B). This result confirms the presence of *cma* and *bar* genes in the genome of the plants generated on the selective medium. A total of 5 independent transgenic lettuce plants and 2 mizuna plants were confirmed as PCR-positive for the transgenes integration. The purified RNA of transgenic plants along with wild type plants were used for cDNAs synthesis by reverse transcription. PCR

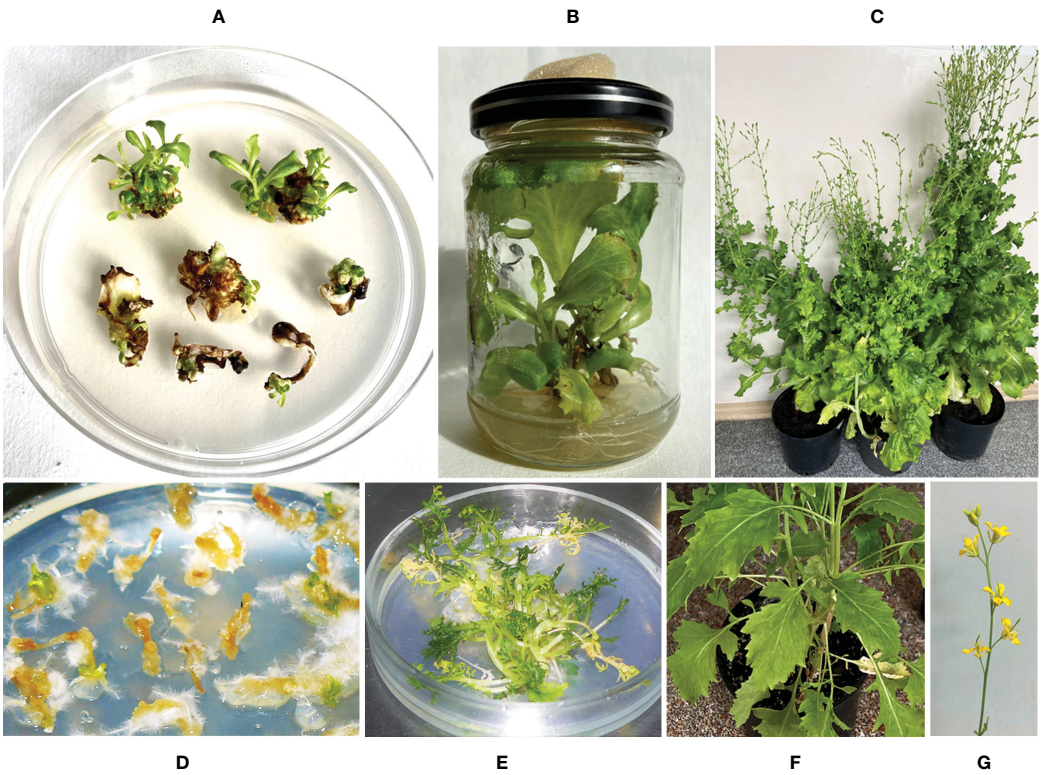

FIGURE 1
Generation of lettuce and mizuna transgenic plants expressing the gene of ColM. **(A)** *In vitro* lettuce plant regeneration from cotyledon explants after six weeks cultivation on selective medium; **(B)** rooting of regenerated lettuce shoots; **(C)** transgenic lettuce plants in a greenhouse; **(D, E)** *in vitro* regeneration of mizuna plants after four weeks **(D)** and 3 months **(E)** of cultivation on selective medium; **(F, G)** transgenic mizuna plants in a greenhouse.

product (1003 bp) obtained from the cDNAs by PCR with primers complementary to the *cma* gene confirmed ColM expression at the transcription level for transgenic plants of lettuce and mizuna (Figure 2C). A negative control for each sample consisted of the same reaction mixture without reverse transcriptase and no PCR products have been detected (lanes (1- to 6-), Figure 2C).

3.2 Transgenic lettuce and mizuna plants exhibit antibacterial activity against *E. coli*

In an initial screen for antibacterial activity, the transgenic plants were tested by placing explants on agar medium covered with diluted bacterial suspension. Clear bacterial growth inhibition zones were observed around the explants of transgenic lettuce plants grown in a greenhouse (Figure 3A) and two transgenic mizuna plant lines maintained *in vitro* (Figure 3B).

Antimicrobial activity was also evaluated semi-quantitatively using a soft-agar overlay assay with plant extracts based on the highest dilution of each that caused a clearing effect. The results of these experiments are presented in Table 2. The data showed very comparable levels of antibacterial activity in different transgenic lines and even between the two analyzed species. However, a decrease or complete absence of antibacterial activity in some plants of T1 generation was also noted. The antibacterial activity of two T1 generation plants of the transgenic lettuce line Ls#21 (Ls#21/T1#3 and Ls#21/T1#5) differed by almost 10 times (Table 2). This result was also confirmed by analysis of recombinant ColM expression detected using immunoblot: the lower antibacterial activity values correlated with less pronounced immunoblot signals (Figure 4A, these lines are marked in blue).

3.3 Antibacterial activity was retained in T2 and T3 generations of transgenic plants

The same correlation between the antibacterial activity of the extracts, determined by soft-agar overlay assay, and the intensity of the immunoblot signals was observed when analyzing plants of the T2 generation of transgenic lettuce. Table 3 summarizes results of analysis of the transgenic trait associated with ColM gene expression in the T2 generation of lettuce plants.

These results show that lettuce transgenic line Ls#6.2 retained significant antibacterial activity in almost all plants of the next generations T1 and T2. Only three plants of T2 generation of Ls#6.2/T1#2 line showed very low or no antibacterial activity (Table 3). One of the plants of T1 generation of lettuce line Ls#21 (namely Ls#21/T1#3) had high antibacterial activity as did all of its T2 descendants (Table 3; Figure 4B). Another T1 plant of line Ls#21 (Ls#21/T1#5) had low antibacterial activity and so did most of its offspring, except line Ls#21/T1#5/T2#4 (Table 3; Figure 4B). This line showed high antibacterial activity despite its parental line showing low activity. This observation could be the result of silencing of the ColM gene in transgenic line Ls#21/T1#5 (T1 generation) and the reversion of silencing in one of the descendants. In addition, the offspring of Ls#21/T1#3/T2#3 was analyzed for ColM expression by immunoblot. All 20 analyzed plants of the T3 generation, which were selected on PPT-containing medium, showed ColM expression (Figure 4C).

For lettuce and mizuna transgenic plants, we selected lines that had high antibacterial activity and calculated the concentration of recombinant ColM in total soluble protein (TSP) extracts generated by addition of 5 volumes of extraction buffer. The content of ColM in transgenic plant extracts (mg/ml) and fresh weight (FW) of plant biomass (mg/g) was calculated via antibacterial activity (Table 4) and by semiquantitative immunoblot analysis (Figure 5).

3.4 Extracts of edible transgenic plants showed antimicrobial activity against pathogenic serotypes and multidrug-resistant strains

After finding high antibacterial activity in ColM-containing transgenic plant extracts against *E. coli* DH10B, we subsequently

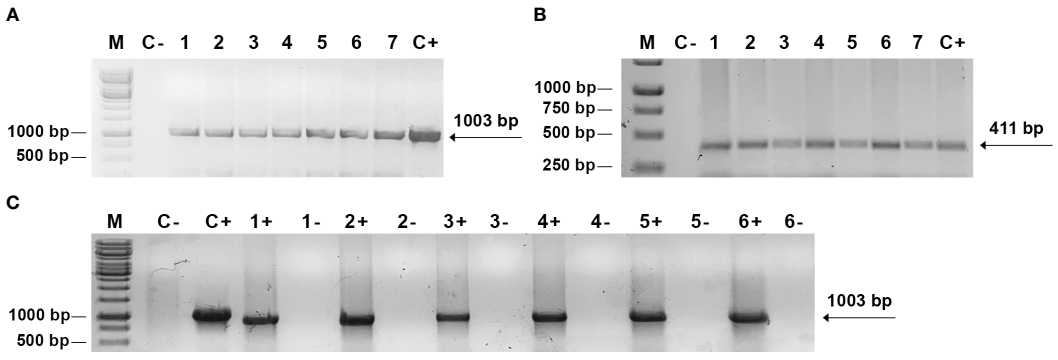

FIGURE 2
PCR and RT-PCR analysis of transgenic plants. **(A, B)** PCR analysis of genomic DNA. M - DNA mass ladder *O`GeneRuler*^{TM} *1 kb DNA Ladder (Thermo Fischer Scientific);* C- negative control with DNA from non-transformed plant; C+ - positive control, pNMD46772 plasmid DNA; 1-7 - independent transgenic lettuce (1-5) and mizuna (6-7) lines with primers to *cma* **(A)** and *bar* **(B)** genes; **(C)** RT-PCR analysis: C- negative control with RNA from non-transformed plant; C+ - positive control, pNMD46772 plasmid DNA; 1+ - transgenic mizuna RNA, 2+, 3+, 4+, 5+, 6+ - transgenic lettuce RNA; lanes 1-, 2-, 3-, 4-, 5-,6- - negative control for each corresponding sample, consisting of the same reaction mixture without reverse transcriptase.

10.3389/fpls.2023.1271757

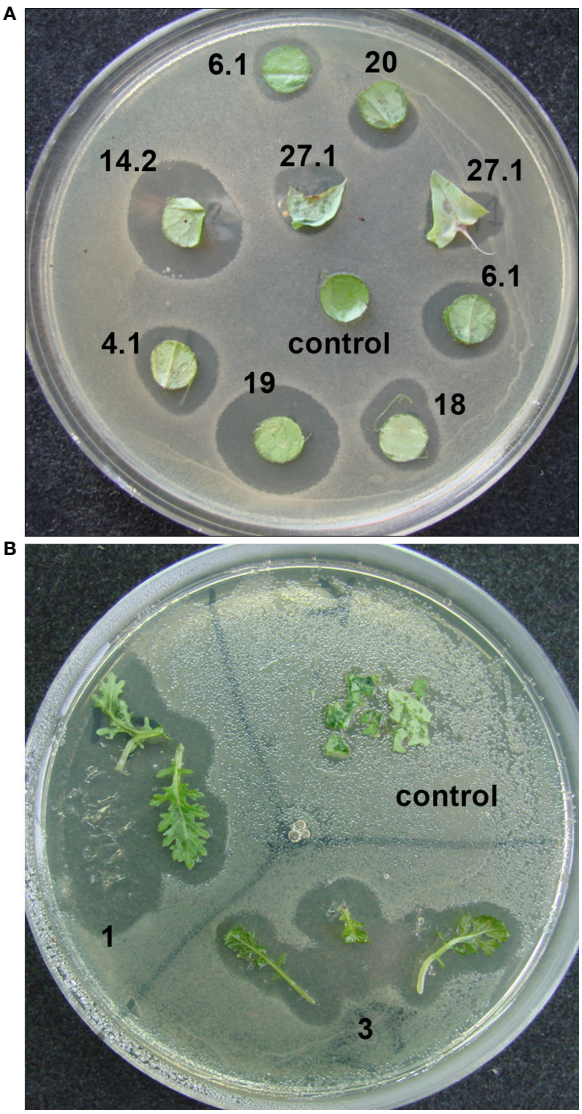

FIGURE 3
Determination of the antibacterial activity of ColM in transgenic lettuce and mizuna explants using a laboratory strain of *E. coli* XL1-Blue. **(A)** explants of different transgenic lines of lettuce; **(B)** leaves of two different transgenic lines of mizuna (BrT0#1, BrT0#3).

evaluated the activity of the extracts against a set of reference strains of *E. coli*, including two EHEC pathogenic serotypes (Figure 6). Antibacterial activity against the emerging pathogenic serotype O104:H4 was higher than against the other EHEC serotype, O157:H7. In addition, ColM-containing extracts of edible plants, as well as purified ColM, also inhibited the growth of MDR *E. coli* strains. All three strains, including NCTC13352 that produces beta-lactamase and is therefore resistant to beta-lactam antibiotics, NCTC13919 that produces carbapenemases conferring resistance to carbapenems, and ATCC BAA-2452 that is resistant to both classes of these antibiotics, were sensitive to ColM-containing plant extracts.

Plant-derived purified recombinant ColM was used for determined Minimal Inhibitory Concentrations (MIC) for

TABLE 2 Antibacterial activity of transgenic lettuce and mizuna plant extracts against *E. coli* strain DH10B.

Transgenic line	Protein concentration, mg/ml	Antibacterial activity, AU	Specific activity, AU/mg/ml
Ls#16	2.42	5800	2396
Ls#19	1.77	2600	1465
Ls#6.2/T1#1	n.d.	2600	n.d.
Ls#6.2/T1#2	n.d.	3800	n.d.
Ls#6.2/T1#3	n.d.	3800	n.d.
Ls#6.2/T1#4	1.41	3800	2699
Ls#21/T1#3	n.d.	1100	n.d.
Ls#21/T1#5	n.d.	150	n.d.
Br#1	n.d.	2600	n.d.
Br#3	n.d.	3800	n.d.
Br#1/T1#1	1.64	1100	670
Br#1/T1#2	2.04	0	0
Br#1/T1#3	1.77	2600	1467
Br#1/T1#4	1.00	510	512
Br#1/T1#5	1.27	2600	2044
Br#3/T1#1	2.24	512	229
Br#3/T1#3	2.03	2048	1011

n.d. – no data/not determined.

analyzed *E. coli* strains. The results showed that ColM was active against most of the *E. coli* strains used in the study with MIC values ranging from 4.0 to 78.0 ng/ml (Table 5). Only for *E. coli* strain ATCC 35150 O157:H7 the MIC of recombinant ColM was significantly higher (5 μg/ml). The MIC value serves as the basis for assessing the sensitivity or resistance of the pathogen to an antimicrobial agent. The data presented in Table 4 show that the amount of ColM in transgenic lettuce plants extracts and mizuna line Br#1/T1#12 ranged from 1.06 to 3.36 μg/ml and these values are significantly higher than the MIC of purified recombinant ColM for the studied pathogenic bacterial strains (except for ATCC 35150 O157:H7). These results suggest the feasibility of using the obtained edible transgenic plants expressing ColM to help control foodborne disease.

3.5 Antimicrobial activity in dried plant material does not decrease for at least 3 months

For edible plants producing pharmaceuticals, the issue of long-term storage conditions without loss of recombinant protein activity is highly important. Therefore, in our studies we also evaluated the antibacterial activity of dried samples of transgenic lettuce and mizuna plants expressing ColM. In these studies, leaf material stored at -80°C for 9 months was subsequently dried at 40° C and

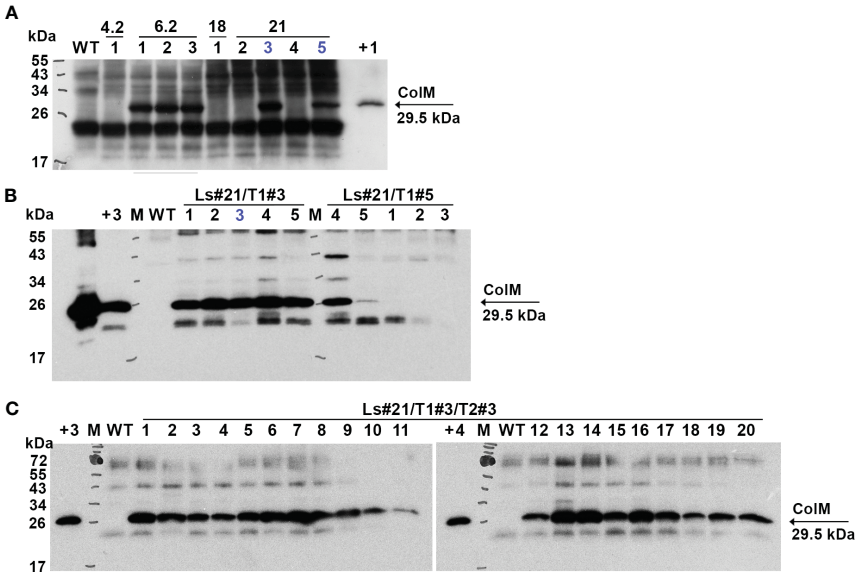

FIGURE 4
Expression of recombinant ColM detected by immunoblot in T1 **(A)**, T2 **(B)** and T3 **(C)** generations of transgenic lettuce (Ls46722). Transgenic or wild-type (WT) leaf material was extracted with 5 volumes of buffer. 7.5 µl of TSP were resolved using SDS-PAGE (15% gel) and expression was analyzed by immunoblot with polyclonal ColM antibody. **(A)** M - molecular weight marker; WT - wild-type non-transgenic lettuce plant; track numbers (1-5) correspond to different lettuce plants of the T1 generation of transgenic lines 4.2; 6.2; 18; 21 (indicated in the top row); +1 - positive control: 80 ng *N. benthamiana* TSP extract after *Agrobacterium*-mediated transient expression of ColM; blue color indicates plants which progeny analysis shown in **(B)**. **(B)** Track numbers correspond to different lettuce plants of the T2 generation of transgenic line 21; +2 - positive control: 1 µg purified ColM; +3 - positive control: TSP extract of Ls#6.2/2; blue color indicates plant which progeny analysis is shown in **(C)**. **(C)** Track numbers (1-20) correspond to different lettuce plants of the T3 generation of transgenic line 21 (Ls#21/3/3); +4 - positive control: 38 ng purified ColM.

TABLE 3 The antibacterial activity and expression of the ColM detected by immunoblot in the T1 and T2 generations of transgenic lettuce.

Lettuce transgenic plants T1 generation	Antibacterial activity, AU	Lettuce transgenic plants T2 generation	Protein concentration, mg/ml	Antibacterial activity, AU	Specific activity, AU/mg/ml	WB signal
Ls#6.2/T1#1	2600	T2#1	1.50	3800	2541	+++
		T2#2	1.07	2600	2420	+++
		T2#3	1.28	2600	2034	++
		T2#4	1.33	5800	4346	+++
		T2#5	1.08	2600	2413	+++
Ls#6.2/T1#2	3800	T2#1	1.35	10	7	–
		T2#2	1.30	1700	1304	+++
		T2#3	1.23	225	183	+
		T2#4	0.89	2600	2909	+++
		T2#5	1.26	340	271	+
Ls#6.2/T1#3	3800	T2#1	1.35	3800	2818	+++
		T2#2	1.16	3800	3286	+++
		T2#3	1.23	3800	3097	+++
		T2#4	1.02	3800	3712	+++
		T2#5	1.07	3800	3555	+++
Ls#21/T1#3	1100	T2#1	1.30	2600	1999	+++

(Continued)

TABLE 3 Continued

Lettuce transgenic plants T1 generation	Antibacterial activity, AU	Lettuce transgenic plants T2 generation	Protein concentration, mg/ml	Antibacterial activity, AU	Specific activity, AU/mg/ml	WB signal
		T2#2	1.04	3800	3661	+++
		T2#3	0.87	2600	2994	+++
		T2#4	1.32	5800	4383	+++
		T2#5	1.04	2600	2512	+++
Ls#21/T1#5	150	T2#1	1.29	10	8	–
		T2#2	1.14	1	1	–
		T2#3	1.07	150	141	–
		T2#4	1.29	1100	855	+++
		T2#5	1.15	340	297	+

TABLE 4 Determination of ColM content in transgenic plant extracts by antibacterial activity and semiquantitative immunoblot analysis.

	ColM concentration, µg/ml extract		ColM concentration, µg/g FW	
	by activity	by WB	by activity	by WB
Ls#6.2/T1#1/T2#12	2.37 ± 1.75	1.06 ± 0.74	11.87 ± 8.76	5.28 ± 3.70
Ls#21/T1#3/T2#16	3.36 ± 2.50	2.08 ± 1.27	16.81 ± 12.50	10.40 ± 6.35
Ls#16/T1#11	2.72 ± 2.98	1.59 ± 0.87	13.61 ± 14.89	7.93 ± 4.33
Br#1/T1#12	2.46 ± 0.76	1.29 ± 0.80	12.28 ± 3.78	6.44 ± 3.99
Br#3/T1#13	0.54 ± 0.37	0.24 ± 0.26	2.70 ± 1.83	1.18 ± 1.28

The concentration was calculated in µg/ml extract and µg/g fresh weight (FW) of plant biomass and as a percentage of TSP and represented as an average value and standard deviation (AV ± SD) of three experiments.

antibacterial activity was evaluated after 1 week, 4 weeks and 3 months of storage at room temperature. The results are shown in Figure 7.

Except for an initial drop in ColM antibacterial activity after 9 months of storage at -80°C, no additional activity decrease was observed that could be correlated to either the drying procedure or the length of time of additional storage. These results underscore the advantages of edible transgenic plants over other methods of recombinant ColM production. The levels of specific antimicrobial activity observed in plant extracts (Figure 6), and the stability of ColM under various storage regimes (Figure 7), suggest a new and inexpensive method for producing recombinant pharmaceutical products that does not require costly protein purification steps and is suitable for transportation and long-term storage without loss of activity.

4 Discussion

Plants have emerged as a reliable platform for production of recombinant proteins providing a safe and low-cost alternative to bacterial and mammalian cells systems. Transient expression in *Nicotiana benthamiana* has shown great potential for the manufacturing of recombinant biopharmaceuticals. Consequently, a wide range of medicinal proteins including recombinant vaccine antigens, monoclonal antibodies and other biotherapeutics have been synthesized in plants, some of which have advanced to clinical development (Daniell et al., 2009; Bendandi et al., 2010; Chichester et al., 2012; Gleba et al., 2014; Tusé et al., 2015; Ward et al., 2020; Leroux-Roels et al., 2022). The practice of using plants to produce valuable recombinant proteins has advanced significantly in recent decades (Ghequire and De Mot, 2017; Stander et al., 2022). With regard to antimicrobial proteins specifically, the cost of goods sold (COGS) for such proteins made by transient expression in plants at commercial scale was estimated to be comparable to those of products made by traditional food processing methods (McNulty et al., 2020). Despite the undoubted effectiveness of transient expression systems, the stable expression of antimicrobial proteins in transgenic edible plants makes it possible to reduce the costs of the most expensive part of production, namely, the extraction and purification of the recombinant protein (Łojewska et al., 2016). Such vegetables can be used as an antibacterial food or feed supplement without, or with minimal, downstream purification of the product.

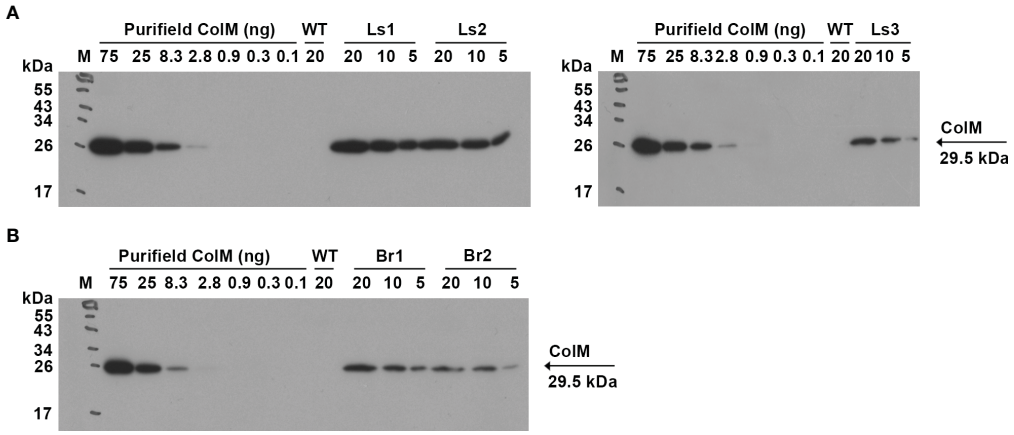

FIGURE 5
(A) Determination of ColM content in transgenic plant extracts by semiquantitative immunoblot analysis. Leaf material of ColM-expressing transgenic lettuce **(A)** and mizuna **(B)** plants was extracted with 5 volumes of buffer. The numbers above the tracks indicate the amount of purified ColM in ng or TSP extracts of transgenic plants in µl. Samples were resolved using SDS-PAGE (15% gel) and expression was analyzed by immunoblot with monoclonal ColM antibody. **(A)** M - molecular weight marker; WT - wild-type non-transgenic lettuce plant; Ls1 – transgenic lettuce plant of T2 generation Ls#6.2/T1#1/T2#12; Ls2 - transgenic lettuce plant of T2 generation Ls#21/T1#3/T2#16; Ls3 – transgenic lettuce plant of T1 generation Ls#16/T1#11. **(B)** M - molecular weight marker; WT - wild-type non-transgenic mizuna plant; Br1 – transgenic mizuna plant of T1 generation Br#1/T1#12; Br2 - transgenic mizuna plant of T1 generation Br#3/T1#13.

The original idea of obtaining biopharmaceuticals in transgenic plants was implemented primarily for production of edible vaccines, and lettuce (*Lactuca sativa* L.) has often been used as a host plant for such studies (Matsui et al., 2009; Hamabata et al., 2019; Matsui et al., 2021). The main advantage of lettuce is that it is a fast-growing plant whose leaves are eaten raw and therefore can be used as an oral preparation. Lyophilized lettuce tissue has been used as a vehicle of oral vaccines against tuberculosis (Lakshmi et al., 2013), fasciolosis of cattle and sheep (Wesołowska et al., 2018) as well as to induce tolerance in hemophilia therapy (Su et al., 2015). The acceptance of lettuce plants for such studies is also explained by the fact that *in vitro* cultivation and genetic transformation techniques have been developed for lettuce, and it is also easy to grow indoors in the greenhouse, in hydroponic systems, and in the

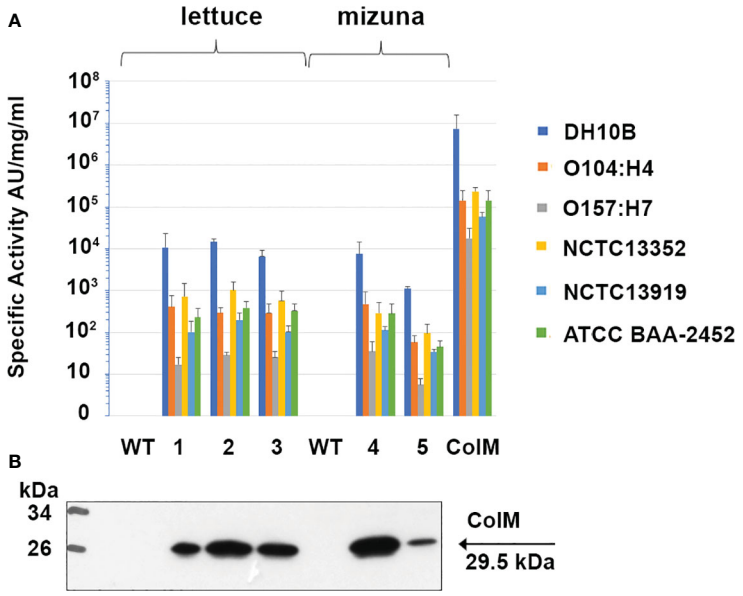

FIGURE 6
Antibacterial activity of ColM and ColM-containing transgenic plant extracts against *E. coli* strains O104:H4, O157:H7, O111:108, NCTC13352, NCTC13919 and ATCC BAA-2452. **(A)** Antimicrobial activity was determined semi-quantitatively on serial dilutions of TSP extracts by soft-agar overlay assay. Error bars indicate standard deviations of biological replicates (n = 3). AU- arbitrary colicin activity units. Transgenic lines: (1) Ls#6.2/T1#1/T2#12; (2) Ls#21/T1#3/T2#16; (3) Ls#16/T1#11; (4) Br#1/T1#12; (5) Br#3/T1#13). **(B)** Expression of recombinant ColM detected by immunoblot with monoclonal ColM antibody in the same transgenic lines. 7.5 µl of TSP extracts were resolved by SDS-PAGE (15% gel).

TABLE 5 Antibacterial activity of colicin M against *E. coli* strains expressed as a minimal inhibitory concentration (MIC).

E. coli strain	MIC [ng/ml]
ATCC BAA-2326 O104:H4	78
ATCC 35150 O157:H7	5000
NCTC13352	19.5
NCTC13919	39
ATCC BAA-2452	78
DH10B	4

field. In addition, lettuce is a very popular crop, which is low in fat, calories and sodium, rich in fiber, iron, folate, and vitamin C and other health-beneficial bioactive compounds (Kim et al., 2016). Another plant in our study, mizuna, is also a fast-growing green leafy vegetable that is eaten raw, is high in phenolic compounds and flavonoids, especially hydroxycinnamic acids, and has high antioxidant activity (Khanam et al., 2012). Mizuna is a traditional and very popular crop in Asia and is increasingly attracting the attention of European and US consumers. Therefore, we developed mizuna plants expressing the ColM gene to impart antibacterial protective functions on a crop that is becoming well-accepted by consumers. In addition, and on a fundamental level, mizuna, in contrast to lettuce, has not been studied as a target for genetic transformation. To our knowledge, we are the first to report not only the successful genetic transformation of mizuna with the *cma* gene, but also the first genetic transformation of this plant species.

According to published data, the transient expression of ColM has been described in the standard host *Nicotiana benthamiana*, as well as in edible plant hosts such as spinach and leafy beets. Purified ColM obtained in plants by the transient expression method had the broadest antimicrobial activity against pathogenic strains of *E. coli* and, in mixtures, supplemented the effectiveness of other colicins (Schulz et al., 2015; Stephan et al., 2017). In addition, transgenic *N. benthamiana* (Hahn-Löbmann et al., 2019) and *N. tabacum* L. plants expressing ColM were developed (Łojewska et al., 2020) and the antibacterial activity of purified ColM obtained from these plants was confirmed against an array of pathogenic strains, including clinical isolates of *E. coli* and *Klebsiella pneumonia*. In the present study, we describe for the first time the antibacterial activity of edible transgenic plants stably expressing recombinant ColM. Our data demonstrate that ColM can be stably expressed in edible plants at a level that provides the desired antibacterial functionality. We also confirmed both the antibacterial activity of transgenic plant extracts and the inheritance of this trait in subsequent generations. Our studies once again confirm that ColM expressed in plants retains full functional activity against *E. coli* pathogenic serotype O104:H4 and O157:H7. Furthermore, extracts of edible plants containing ColM were found to inhibit the growth of multidrug-resistant strains of *E. coli* that produce beta-lactamases and carbapenemases. These results are of practical importance as carbapenems are considered to be antibiotics of last resort and antimicrobial options for the treatment of carbapenem-resistant *Enterobacteriaceae* (CRE) are limited (Sheu et al., 2019). Our results also show that ColM antimicrobial activity is retained for at least three months without loss of activity in heat-dried (up to 40°C) transgenic lettuce and mizuna biomass. According to published data, ColM is a fairly stable protein. It was demonstrated that pure bacteria-derived ColM remain stable for more than 1 year in solution at concentrations above 1 mg/ml (Schaller et al., 1981). Although the inactivation of ColM occurred when the solution was diluted, this process can be effectively slowed down or stopped by various additives to the medium. High stability was also demonstrated for plant-derived purified recombinant

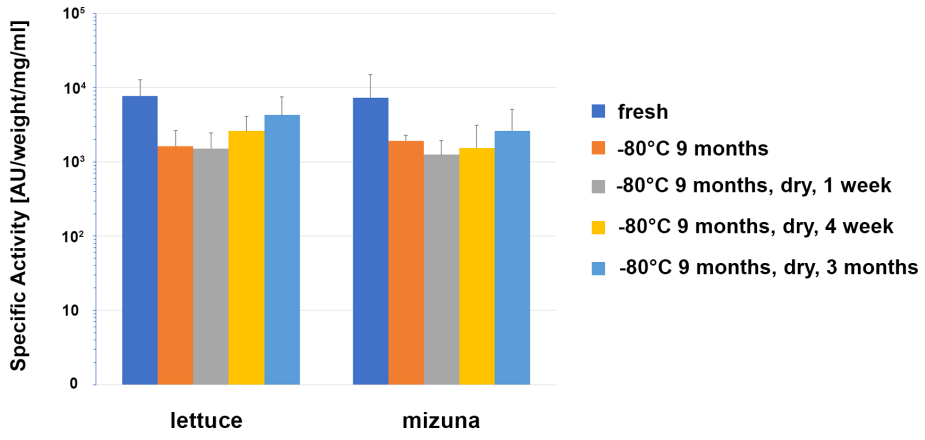

FIGURE 7
Comparison of the antibacterial activity of lettuce and mizuna samples under different storage conditions. Transgenic leaf material was extracted directly after harvest (fresh), after storage for 274 d at -80°C, and after storage for 262 d at -80°C followed by drying for 1 d at 40°C and subsequent storage for 1 week, 4 weeks or 3 months at room temperature. Activity of extracts was determined using soft-agar overlay assay against *E. coli* DH10B. In the graph, mean values with standard deviation of 6 different lettuce plants (Ls#6.2/T1#1/T2#11, Ls#6.2/T1#1/T2#12, Ls#21/T1#3/T2#15, Ls#21/T1#3/T2#16, Ls#16/T1#11, Ls#16/T1#12) or four different mizuna plants (Br#1/T1#11, Br#1/T1#12, Br#3/T1#11, Br#3T1#13) are shown. The concentration was calculated in µg/ml extract and µg/g fresh weight (FW) of plant biomass and as a percentage of TSP and represented as an average value and standard deviation (AV ± SD) of three experiments.

ColM. Recombinant plant-derived ColM remained stable in lyophilized form and in solution stored at 4°C. The solution stored at room temperature was less stable, but ColM was not inactivated for 8 weeks and showed the best stability of all 4 colicins tested (Hahn-Löbmann et al., 2019). However, proteolytic degradation of this bacteriocin is possible in the plant cell. We believe that dried plant biomass retained antimicrobial activity of ColM mostly because of drying procedure which has been applied. Slow drying of entire leaves prevented the decompartmentalization in plant cells thus avoiding massive attack of plant proteases against ColM which could happen, e.g., in case of grinding. In agriculture, dry plant biomass (hay) is known for a good stability of nutritional crude protein. Using a drying procedure for preservation and storage of ColM-containing leaf material was partially inspired by that knowledge. Indeed, this approach appeared to be productive and provided both stable and functional bacteriocine. To our knowledge, this is the first study that demonstrates the antibacterial activity of extracts of edible transgenic plants expressing ColM against various *E. coli* strains, including pathogenic and MDR pathotypes. The use of edible plants expressing ColM as a food or feed additive for preventive purposes is especially poignant due to the magnitude and recurrence of foodborne *E. coli* outbreaks worldwide, the role of leafy vegetables in their transmission, and the continued threat posed by MDR bacteria due to the overuse of antibiotics in agriculture.

Data availability statement

The original contributions presented in the study are included in the article/supplementary material. Further inquiries can be directed to the corresponding author.

Author contributions

NS: Investigation, Writing – original draft. HP: Data curation, Investigation, Writing – original draft. KL: Investigation, Writing – review & editing. YP: Investigation, Writing – review & editing. AG: Conceptualization, Writing – review & editing. MK: Conceptualization, Supervision, Writing – review & editing.

Funding

The author(s) declare financial support was received for the research, authorship, and/or publication of this article. This work was financially supported by National Academy of Sciences of Ukraine: the project 0123U101081 "Synthesis of recombinant pharmaceutical proteins and increasing of content of biologically active natural compounds in plants" and by the National Research Foundation of Ukraine: the project 2020.01/0301 "Plant-based synthesis of recombinant pharmaceutical proteins capable to prevent some infectious diseases of bacterial and viral origin".

Acknowledgments

The authors are grateful to Prof. Dr. Yuri Gleba for the support, inspiration and understanding that have made this paper possible. We thank Doreen Bartels for excellent technical assistance and Dr. Anett Stephan and Dr. Simone Hahn-Löbmann (all Nomad Bioscience GmbH, Halle (Saale), Germany) for fruitful discussions. We thank Dr. Daniel Tusé (DT/Consulting Group, Sacramento, CA, USA) for critical reading of manuscript and valuable comments.

Conflict of interest

Author HP and AG were employed by the company Nomad Bioscience GmbH.

The remaining authors declare that the research was conducted in the absence of any commercial or financial relationships that could be construed as a potential conflict of interest.

Publisher's note

References

Alegbeleye, O. O., Singleton, I., and Sant'Ana, A. S. (2018). Sources and contamination routes of microbial pathogens to fresh produce during field cultivation: A review. *Food Microbiol.* 73, 177–208. doi: 10.1016/j.fm.2018.01.003

Bendandi, M., Marillonnet, S., Kandzia, R., Thieme, F., Nickstadt, A., Herz, S., et al. (2010). Rapid, high-yield production in plants of individualized idiotype vaccines for non-Hodgkin's lymphoma. *Ann. Oncol.* 21 (12), 2420–2427. doi: 10.1093/annonc/mdq256

Benitez-Chao, D. F., Leyn-Buitimea, A., Lerma-Escalera, J. A., and Morones-Ramirez, J. R. (2021). Bacteriocins: an overview of antimicrobial, toxicity, and biosafety assessment by in *vivo* models. *Front. Microbiol.* 12. doi: 10.3389/fmicb.2021.630695

Bertani, L. (1951). Studies on lysogenesis. I. The mode of phage liberation by lysogenic *Escherichia coli*. *J. Bacteriol.* 62, 293–300. doi: 10.1128/jb.62.3.293-300.1951

Callaway, T. R., Stahl, C. H., Edrington, T. S., Genovese, K. J., Lincoln, L. M., Anderson, R. C., et al. (2004). Colicin concentrations inhibit growth of O157:H7 *in vitro*. *J Food Prot* 67, 2603–2607. doi: 10.4315/0362-028X-67.11.2603

Cavera, V. L., Arthur, T. D., Kashtanov, D., and Chikindas, M. L. (2015). Bacteriocins and their position in the next wave of conventional antibiotics. *Int. J. Antimicrob. Agents.* 46, 494–501. doi: 10.1016/j.ijantimicag.2015.07.011

Chérier, D., Patin, D., Blanot, D., Touzé, T., and Barreteau., H. (2021). The biology of colicin M and its orthologs. *Antibiotics* 10, 1109. doi: 10.3390/antibiotics.10091109

Chichester, J. A., Jones, R. M., Green, B. J., Stow, M., Miao, F., Moonsammy, G., et al. (2012). Safety and immunogenicity of a plant-produced recombinant hemagglutinin-based influenza vaccine (HAI-05) derived from A/Indonesia/05/2005 (H5N1) influenza virus: A phase 1 randomized, double-blind, placebo-controlled, dose-escalation study in healthy adults. *Viruses* 4 (11), 3227–3244. doi: 10.3390/v4113227

Cleveland, J., Montville, T. J., Nes, I. F., and Chikindas, M. L. (2001). Bacteriocins: safe, natural antimicrobials for food preservation. *Int. J. Food Microbiol.* 71, 1–20. doi: 10.1016/s0168-1605(01)00560-8

Daniell, H., Singh, N. D., Mason, H., and Streatfield, S. J. (2009). Plant-made vaccine antigens and biopharmaceuticals. *Trends Plant Sci.* 14, 669–679. doi: 10.1016/j.tplants.2009.09.009

Food and Drug Administration. (2021). *FDA Releases Annual Summary Report on Antimicrobials Sold or Distributed in 2020 for Use in Food-Producing Animals*. Available at: https://www.fda.gov/animal-veterinary/cvm-updates/fda-releases-annual-summary-report-antimicrobials-sold-or-distributed-2020-use-food-producing.

Gabrielsen, C., Brede, D. A., Nes, I. F., and Diep, D. B. (2014). Circular bacteriocins: biosynthesis and mode of action. *Appl. Environ. Microbiol.* 80, 6854–6862. doi: 10.1128/AEM.02284-14

Gamborg, O. L., Miller, R. A., and Ojima, K. (1968). Nutrient requirements of suspension cultures of soybean root cells. *Exp. Cell Res.* 50, 151–158. doi: 10.1016/0014-4827(68)90403-5

Ghequire, M. G. K., and De Mot, R. (2017). Turning over a new leaf: bacteriocins going green. *Trends Microbiol.* 26 (1), 1–2. doi: 10.1016/j.tim.2017.11.001

Gleba, Y. Y., Tusé, D., and Giritch, A. (2014). Plant viral vectors for delivery by *Agrobacterium*. *Curr. Top. Microbiol. Immunol.* 375, 155–192. doi: 10.1007/82_2013_352

GRAS Notice (GRN). Available at: https://fda.report/media/93655/GRAS-Notice-000593 (Accessed 29 July 2021).

Hahn-Löbmann, S., Stephan, A., Schulz, S., Schneider, T., Shaverskyi, A., Tusé, D., et al. (2019). Colicins and salmocins – new classes of plant-made non-antibiotic food antibacterials. *Front. Plant Sci.* 10. doi: 10.3389/fpls.2019.00437

Hamabata, T., Sato, T., Takita, E., Matsui, T., Imaoka, T., Nakanishi, N., et al. (2019). Shiga toxin 2eB-transgenic lettuce vaccine is effective in protecting weaned piglets from edema disease caused by Shiga toxin-producing *Escherichia coli* infection. *Anim. Sci. J.* 90 (11), 1460–1467. doi: 10.1111/asj.13292

Irvin, K., Viazis, S., Fields, A., Seelman, S., Blickenstaff, K., Gee, E., et al. (2021). An overview of traceback investigations and three case studies of recent outbreaks of *escherichia coli* O157:H7 infections linked to romaine lettuce. *J. Food Prot.* 84, 1340–1356. doi: 10.4315/JFP-21-112

Khanam, U. K. S., Oba, S., Yanase, E., and Murakami, Y. (2012). Phenolic acids, flavonoids and total antioxidant capacity of selected leafy vegetables. *J. Funct. Foods* 4 (4), 979–987. doi: 10.1016/j.jff.2012.07.006

Kim, M., Moon, Y., Tou, J., Mou, B., and Waterland, N. (2016). Nutritional value, bioactive compounds and health benefits of lettuce (*Lactuca sativa* L.). *J. Food Composition Anal.* 49, 19–34. doi: 10.1016/j.jfca.2016.03.004

Kumariya, R., Garsa, A. K., Rajput, Y. S., Sood, S. K., Akhtar, N., and Patel, S. (2019). Bacteriocins: Classification, synthesis, mechanism of action and resistance development in food spoilage causing bacteria. *Microb. Pathog.* 128, 171–177. doi: 10.1016/j.micpath.2019.01.002

Lakshmi, P. S., Verma, D., Yang, X., Lloyd, B., and Daniell, H. (2013). Low cost tuberculosis vaccine antigens in capsules: expression in chloroplasts, bio-encapsulation, stability and functional evaluation in *vitro*. *PloS One* 8, e54708. doi: 10.1371/journal.pone.0054708

Leroux-Roels, I., Maes, C., Joye, J., Jacobs, B., Jarczowski, F., Diessner, A., et al. (2022). A randomized, double-blind, placebo-controlled, dose-escalating phase I trial to evaluate safety and immunogenicity of a plant-produced, bivalent, recombinant norovirus-like particle vaccine. *Front. Immunol.* 13. doi: 10.3389/fimmu.2022.1021500

Liu, Y. Y., Wang, Y., Walsh, T. R., Yi, L. X., Zhang, R., Spencer, J., et al. (2016). Emergence of plasmid-mediated colistin resistance mechanism MCR-1 in animals and human beings in China: a microbiological and molecular biological study. *Lancet Infect. Dis.* 16, 161–168. doi: 10.1016/S1473-3099(15)00424-7

Łojewska, E., Kowalczyk, T., Olejniczak, S., and Sakowicz, T. (2016). Extraction and purifcation methods in downstream processing of plant-based recombinant proteins. *Protein Expr. Purif.* 120, 110–117. doi: 10.1016/j.pep.2015.12.018

Łojewska, E., Sakowicz, T., Kowalczyk, A., Konieczka, M., Grzegorczyk, J., Sitarek, P., et al. (2020). Production of recombinant colicin M in *Nicotiana tabacum* plants and its antimicrobial activity. *Plant Biotechnol. Rep.* 14, 33–43. doi: 10.1007/s11816-019-00571-y

Low, J. C., McKendrick, I. J., McKechnie, C., Fenlon, D., Naylor, S. W., Currie, C., et al. (2005). Rectal carriage of enterohemorrhagic *Escherichia coli* O157 in slaughtered cattle. *Appl. Environ. Microbiol.* 71, 93–97. doi: 10.1128/AEM.71.1.93-97.2005

Matsui, T., Asao, H., Ki, M., Sawada, K., and Kato, K. (2009). Transgenic lettuce producing a candidate protein for vaccine against edema disease. *Biosci. Biotechnol. Biochem.* 73 (7), 1628–1634. doi: 10.1271/bbb.90129

Matsui, T., Takita, E., Oiwa, S., Yokoyama, A., Kato, K., and Sawada, K. (2021). Lettuce-based production of an oral vaccine against porcine edema disease for the seed lot system. *Plant Biotechnol. (Tokyo)* 38 (2), 239–246. doi: 10.5511/plantbiotechnology.21.0414

McNulty, M. J., Gleba, Y., Tusé, D., Hahn-Löbmann, S., Giritch, A., Nandi, S., et al. (2020). Techno-economic analysis of a plant-based platform for manufacturing antimicrobial proteins for food safety. *Biotechnol. Prog.* 36 (1), e2896. doi: 10.1002/btpr.2896

Munns, K. D., Selinger, L. B., Stanford, K., Guan, L., Callaway, T. R., and McAllister, T. A. (2015). Perspectives on super-shedding of *Escherichia coli* O157:H7 by cattle. *Foodborne Pathog. Dis.* 12, 89–103. doi: 10.1089/fpd.2014.1829

Murashige, T., and Skoog, F. (1962). A revised medium for rapid growth and bioassays with tobacco tissue cultures. *Physiol. Plant* 15, 473–497. doi: 10.1111/j.1399-3054.1962.tb08052

Navarro-Garcia, F. (2014). *Escherichia coli* O104:H4 Pathogenesis: an Enteroaggregative E. coli/Shiga Toxin-Producing *E. coli* Explosive Cocktail of High Virulence. *Microbiol. Spectr.* 2, 6. doi: 10.1128/microbiolspec.EHEC-0008-2013

Paveenkittiporn, W., Kerdsin, A., Chokngam, S., Bunthi, C., Sangkitporn, S., and Gregory, C. J. (2017). Emergence of plasmid-mediated colistin resistance and New Delhi metallo-β-lactamase genes in extensively drug-resistant *Escherichia coli* isolated from a patient in Thailand. *Diagn. Microbiol. Infect. Dis.* 87, 157–159. doi: 10.1016/j.diagmicrobio.2016.11.005

Puligundla, P., and Lim, S. (2022). Biocontrol Approaches against *Escherichia coli* O157:H7 in Foods. *Foods* 11, 5. doi: 10.3390/foods11050756

Schaller, K., Dreher, R., and Braun, V. (1981). Structural and functional properties of colicin M. *J. Bacteriol.* 146 (1), 54–63. doi: 10.1128/jb.146.1.54-63.1981

Schulz, S., Stephan, A., Hahn, S., Bortesi, L., Jarczowski, F., Bettmann, U., et al. (2015). Broad and efficient control of major foodborne pathogenic strains of *Escherichia coli* by mixtures of plant-produced colicins. *Proc. Natl. Acad. Sci. U.S.A.* 112, E5454–E5460. doi: 10.1073/pnas.1513311112

Shcherbak, N., Kishchenko, O., Sakhno, L., Komarnytsky, I., and Kuchuk, M. (2013). *Lox*-dependent gene expression in transgenic plants obtained via *Agrobacterium*-mediated transformation. *Tsitol. Genet.* 47, 21–32. doi: 10.3103/S0095452713030079

Sheu, C. C., Chang, Y. T., Lin, S. Y., Chen, Y. H., and Hsueh, P. R. (2019). Infections caused by carbapenem-resistant Enterobacteriaceae: An update on therapeutic options. *Front. Microbiol.* 10. doi: 10.3389/fmicb.2019.00080

Slayton, R. B., Turabelidze, G., Bennett, S. D., Schwensohn, C. A., Yaffee, A. Q., Khan, F., et al. (2013). Outbreak of Shiga toxin-producing *Escherichia coli* (STEC) O157:H7 associated with romaine lettuce consumption. *PloS One* 8, 2. doi: 10.1371/journal.pone.0055300

Stander, J., Mbewana, S., and Meyers, A. E. (2022). Plant-derived human vaccines: recent developments. *BioDrugs* 36 (5), 573–589. doi: 10.1007/s40259-022-00544-8

Stephan, A., Hahn-Löbmann, S., Rosche, F., Buchholz, M., Giritch, A., and Gleba, Y. (2017). Simple purification of *Nicotiana benthamiana*-Produced recombinant colicins: high-yield recovery of purified proteins with minimum alkaloid content supports the suitability of the host for manufacturing food additives. *Int. J. Mol. Sci.* 19, 95. doi: 10.3390/ijms19010095

Su, J., Zhu, L., Sherman, A., Wang, X., Lin, S., Kamesh, A., et al. (2015). Low cost industrial production of coagulation factor IX bioencapsulated in lettuce cells for oral tolerance induction in hemophilia B. *Biomaterials* 70, 84–93. doi: 10.1016/j.biomaterials

Tietze, E., Dabrowski, P. W., Prager, R., Radonic, A., Fruth, A., Auraß, P., et al. (2015). Comparative genomic analysis of two novel sporadic Shiga toxin-producing *Escherichia coli* O104:H4 strains isolated 2011 in Germany. *PloS One* 10, 4. doi: 10.1371/journal.pone.0122074

Tomás-Callejas, A., Martínez-Hernández, G. B., Artés, F., and Artés-Hernández, F. (2011). Neutral and acidic electrolyzed water as emergent sanitizers for fresh-cut mizuna baby leaves. *Postharvest Biol. Technol.* 59, 298–306. doi: 10.1016/j.postharvbio.2010.09.013

Tusé, D., Ku, N., Bendandi, M., Becerra, C., Collins, R. Jr., Langford, N., et al. (2015). Clinical safety and immunogenicity of tumor-targeted, plant-made id-KLH conjugate vaccines for follicular lymphoma. *Biomed. Res. Int.* 2015, 648143. doi: 10.1155/2015/648143

Urban-Chmiel, R., Marek, A., Stepien-Pysniak, D., Wieczorek, K., Dec, M., Nowaczek, A., et al. (2022). Antibiotic resistance in bacteria - A review. *Antibiotics* 11, 1079. doi: 10.3390/antibiotics11081079

US Center for Disease Control and Prevention. (2020). *Reports of selected E. coli outbreak investigations*. Available at: https://www.cdc.gov/ecoli/outbreaks.html.

Waltenburg, M. A., Schwensohn, C., Madad, A., Seelman, S. L., Peralta, V., Koskeet, S. E., et al. (2021). Two multistate outbreaks of a reoccurring Shiga toxin-producing *Escherichia coli* strain associated with romaine lettuce: USA 2018-2019. *Epidemiol. Infect.* 150, 16. doi: 10.1017/S0950268821002703

Ward, B. J., Makarkov, A., Séguin, A., Pillet, S., Trépanier, S., Dhaliwall, J., et al. (2020). Efficacy, immunogenicity, and safety of a plant-derived, quadrivalent, virus-like particle influenza vaccine in adults (18–64 years) and older adults (≥65 years): two multicentre, randomised phase 3 trials. *Lancet* 396, 1491–1503. doi: 10.1016/S0140-6736(20)32014-6

Wesołowska, A., Ljunggren, M. K., Jedlina, L., Basałaj, K., Legocki, A., Wedrychowicz, H., et al. (2018). A preliminary study of a lettuce-based edible vaccine expressing the cysteine proteinase of *Fasciola hepatica* for fasciolosis control in livestock. *Front. Immunol.* 9. doi: 10.3389/fimmu.2018.02592

Willyard, C. (2017). The drug-resistant bacteria that pose the greatest health threats. *Nature* 543, 15. doi: 10.1038/nature.2017.21550

Xu, S., Campisi, E., Li, J., and Fischetti, V. A. (2021). Decontamination of *Escherichia coli* O157:H7 on fresh Romaine lettuce using a novel bacteriophage lysin. *Int. J. Food Microbiol.* 341, 109068. doi: 10.1016/j.ijfoodmicro.2021.109068

frontiers | Frontiers in Plant Science

TYPE Review
PUBLISHED 15 November 2023
DOI 10.3389/fpls.2023.1252166

OPEN ACCESS

EDITED BY
Ahmad Bazli Ramzi,
National University of Malaysia, Malaysia

REVIEWED BY
Diego Orzaez,
Polytechnic University of Valencia, Spain
Tsan-Yu Chiu,
Beijing Genomics Institute (BGI), China
Johannes Felix Buyel,
University of Natural Resources and Life Sciences, Austria

*CORRESPONDENCE
Ramalingam Sathishkumar
rsathish@buc.edu.in
Ashutosh Sharma
asharma@tec.mx

RECEIVED 03 July 2023
ACCEPTED 17 October 2023
PUBLISHED 15 November 2023

CITATION
Parthiban S, Vijeesh T, Gayathri T, Shanmugaraj B, Sharma A and Sathishkumar R (2023) Artificial intelligence-driven systems engineering for next-generation plant-derived biopharmaceuticals. *Front. Plant Sci.* 14:1252166. doi: 10.3389/fpls.2023.1252166

Artificial intelligence-driven systems engineering for next-generation plant-derived biopharmaceuticals

Subramanian Parthiban[1], Thandarvalli Vijeesh[1], Thashanamoorthi Gayathri[1], Balamurugan Shanmugaraj[1], Ashutosh Sharma[2]* and Ramalingam Sathishkumar[1]*

[1]Plant Genetic Engineering Laboratory, Department of Biotechnology, Bharathiar University, Coimbatore, India, [2]Tecnologico de Monterrey, School of Engineering and Sciences, Centre of Bioengineering, Queretaro, Mexico

Recombinant biopharmaceuticals including antigens, antibodies, hormones, cytokines, single-chain variable fragments, and peptides have been used as vaccines, diagnostics and therapeutics. Plant molecular pharming is a robust platform that uses plants as an expression system to produce simple and complex recombinant biopharmaceuticals on a large scale. Plant system has several advantages over other host systems such as humanized expression, glycosylation, scalability, reduced risk of human or animal pathogenic contaminants, rapid and cost-effective production. Despite many advantages, the expression of recombinant proteins in plant system is hindered by some factors such as non-human post-translational modifications, protein misfolding, conformation changes and instability. Artificial intelligence (AI) plays a vital role in various fields of biotechnology and in the aspect of plant molecular pharming, a significant increase in yield and stability can be achieved with the intervention of AI-based multi-approach to overcome the hindrance factors. Current limitations of plant-based recombinant biopharmaceutical production can be circumvented with the aid of synthetic biology tools and AI algorithms in plant-based glycan engineering for protein folding, stability, viability, catalytic activity and organelle targeting. The AI models, including but not limited to, neural network, support vector machines, linear regression, Gaussian process and regressor ensemble, work by predicting the training and experimental data sets to design and validate the protein structures thereby optimizing properties such as thermostability, catalytic activity, antibody affinity, and protein folding. This review focuses on, integrating systems engineering approaches and AI-based machine learning and deep learning algorithms in protein engineering and host engineering to augment protein production in plant systems to meet the ever-expanding therapeutics market.

KEYWORDS

artificial intelligence, molecular pharming, synthetic biology, deep learning, machine learning

1 Introduction

Plant molecular pharming refers to the recombinant expression of biologics including vaccines, hormones, therapeutics and diagnostic reagents in plant-based systems. The field is gaining attention since the biologics produced from plants are efficient and similar to products from other conventional systems with the advantage of eukaryotic host performing post-translational modifications. Some of these recombinant biologics produced in plant systems are SARS-CoV2 virus-like particle (VLPs), spike antigen, anti-SARS-CoV2 mAb H4 and B38, anti-EBV (Ebola virus) mAb 6D8, 4H2 IgG and IgM (against *Coccidioides*), antimicrobial peptide (AMP) LL-37 and human apolipoprotein A-I_{Milano} (Apo A-I_{Milano}) (Fulton et al., 2015; Holásková et al., 2018; Ali and Kim, 2019; Shanmugaraj et al., 2020; Jugler et al., 2022; Zhao et al., 2023). Various model plant systems have been used as stable or transient heterologous expression hosts for recombinant protein production that include, tobacco (*Nicotiana benthamiana* and *Nicotiana tabacum*), Arabidopsis, tomato, potato, rice, maize, soybean, etc. (Ghag et al., 2021; Lobato Gómez et al., 2021). The plant host systems are useful in many aspects such as cost-effectiveness, multimeric protein assembly, scale-up and safety (minimal/no risk of human pathogen contaminations). Even with the listed advantages, there are few limitations to use plants as expression systems such as lack of humanized *N*-glycosylation post-translational modification which is needed for antibody production and stability of plant-produced proteins are still a concern (Sethi et al., 2021). Recombinant biologics production is dependent on several factors such as vector construction, codon optimization, regulatory components, protein localization and glycosylation (Amack and Antunes, 2020; Jin et al., 2022; Mirzaee et al., 2022; Moon et al., 2022; Zhao et al., 2023).

Systems Engineering in biology can be defined as a holistic approach that analyzes, models, alters, optimizes, and regulates the complex processes of biological systems resulting in desired functions. Artificial Intelligence (AI) refers to the development of machines and systems that use algorithms and statistical models to analyze data, identify patterns and can perform/outperform tasks that demand human intelligence in learning, reasoning, planning, communicating, and problem-solving (Russell, 2010). Machine Learning (ML) is a subset of AI that enables the systems to learn by providing abundant training datasets and is classified into supervised, unsupervised and semi-supervised learning algorithms. Supervised algorithms are the most used of the three since they are developed using labelled datasets from databases with minimum data redundancy, feature extraction, analysis & selection of main traits, prediction methods, and performance evaluation. They provide an excellent prospect for biologists in identifying patterns of gene expression and relevant features, thereby governing the identification through deep understanding of different combinations of the responsible factors (Singh et al., 2016; Silva et al., 2019). Deep Learning (DL) is a network-based supervised learning method with multiple layers of simple modules pooled and arrayed for learning, computing, and mapping a big dataset through each layer. It takes advantage over other AI-based ML algorithms in exploring complex structures of high-dimensional data built from the simplest layers (Lecun et al., 2015). Industry 4.0 revolutionizes traditional practices of manufacturing in industrial settings with the integration of digital technologies, automation, and data exchange, which concourses physical and digital systems leading to increased efficiency, productivity and innovation. Intervention of automation, cyber-physical systems, internet of things (IoT) and big data analytics would prove to be efficient and robust in plant-based biologics production (Dubey et al., 2018; Chen et al., 2020).

AI has been used in recombinant biologics production in host systems such as mammalian cells (CHO and HEK293), yeast (*Saccharomyces cerevisiae* and *Pichia pastoris*) and bacterial (*Escherichia coli* and *Bacillus subtilis*) systems (Van Brempt et al., 2020; Smiatek et al., 2021; Feng et al., 2022a; Li et al., 2022a; Packiam et al., 2022). Application of AI or ML algorithms include protein engineering, protein-protein interaction, stability, localization, solubility, functional motif prediction and catalytic activity which increases the production and functionality of recombinant proteins (Han et al., 2019; Jiang et al., 2021; Feng et al., 2022a; LaFleur et al., 2022; Masson et al., 2022; Kalemati et al., 2023). Till date, AI finds very least or no intervention in plant molecular pharming. In this review, we discuss about the systems biology concepts with the introduction of AI, as shown in Figure 1, in different aspects of recombinant biologics production to increase the stability, functionality and applications of AI-based ML algorithms in engineering systems to overcome the challenges and to enhance the production of next generation plant-based biologics.

2 Advantages of plant expression system

The market size of plant-based biologics was valued at $116.1 million during the year 2021, and with the compound annual growth rate (CAGR) at 4.8%, it is being estimated to reach $182.9 million by the year 2031. Few of the major plant-based production firms include Leaf Expression Systems, Zea Biosciences, Plant Biotechnology Inc., InVitria, Mapp Biopharmaceutical and PlantForm (Allied Market Research, 2023). Very few plant-based recombinant therapeutics have been commercialized following development and many are under clinical trials (He et al., 2021; Lobato Gómez et al., 2021). Elelyso, taliglucerase alfa, produced in carrot cell culture by ProtalixBio Therapeutics was approved by FDA in 2012 to treat Gaucher disease and has been commercialized (Mor, 2015). ZMapp – an antibody cocktail produced in *N. benthamiana* by Leaf Biopharmaceutical (commercialization arm of Mapp Biopharmaceutical) was used to treat Ebola outbreak under emergency use authorization during 2014 in Africa (Qureshi, 2016). Recombinant growth factors were produced in the endosperm of barley grain by ORF Genetics and have been commercialized as skincare products (ORF Genetics, 2023). Covifenz, a plant-based SARS CoV2 VLP vaccine against COVID19, developed by Medicago was authorized by Health Canada during 2022 (Hager et al., 2022).

Protein-based pharmaceutical products are growing rapidly in recent years and most of them are produced in mammalian and

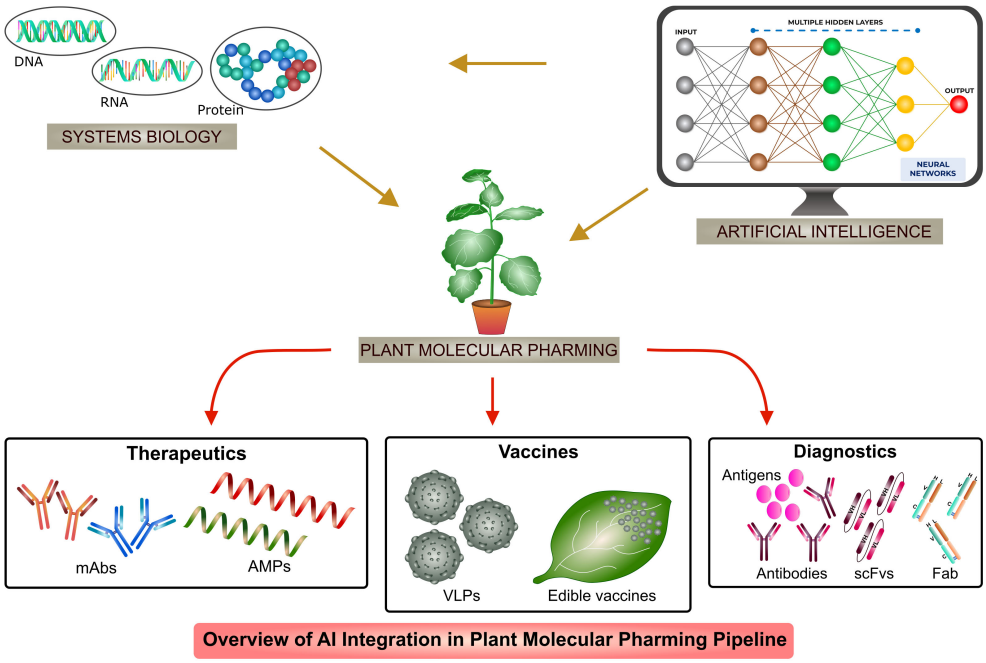

FIGURE 1
Overview of AI integration in plant molecular pharming pipeline.

microbial expression systems. Now-a-days, plant systems have emerged as an alternative platform for large scale production of recombinant proteins as they necessitate no capital-intensive infrastructure, bioreactors, or expensive culture media, but may be quickly scaled in low-cost greenhouses using simple reagents (Chen and Davis, 2016). When compared with prokaryotic and other host systems, plants offer an alternative bioreactor system for recombinant expression due to their glycan profile and cost-effective management system (Schillberg et al., 2019). Apart from the advantages mentioned above, plant systems are human pathogen free, sterile conditions are not required during production and scalable due to open-field cultivation (Buyel, 2019). For all these reasons plant expression system has been established as a prominent bioreactor for the production of therapeutic proteins such as vaccines, therapeutic proteins and growth hormones (Limkul et al., 2016; Moon et al., 2022).

Each expression host has its advantages and limitations. For instance, mammalian cell systems are capable of inherently producing recombinant biologics in humanized form, but it is difficult to maintain cell lines free from human pathogens and contaminants (Sethi et al., 2021). Plant system has many advantages over other systems including rapid (production of recombinant protein starts at day 2-3 post infiltration), cost-effective (produced at a cost of $0.27 for 3 mg dose of recombinant AMP), scale-up (increasing the plant biomass as required and thereby protein yield), purity (up to 99%), safety (production without any contaminant interference and functionally safe in humans) and post-translational modifications (*N*-glycosylation in engineered tobacco plants, which prokaryotic host system lacks). These advantages can be briefed with an example each using *N. benthamiana* transient expression host system. SARS-CoV2 RBD (Receptor binding domain) Fc fusion vaccine candidate was expressed in *N. benthamiana* and was extracted 4 days post infiltration which gave an yield of 25 µg/g FW (Siriwattananon et al., 2021). Alam et al. (2018) were able to produce antiviral compound Griffithsin at 99% purity from tobacco plant. Two mAb isotypes, 4H2 IgG and 4H2 IgM antibodies against *Coccidioides* CTS1 (Valley Fever) antigen were expressed in *N. benthamiana* plants showing homogenous N-glycosylation profile with a dominant GnGn/GnM structure, highly similar to mammals. Techno-economic analysis by McNulty et al. (2020) of *N. benthamiana*-based recombinant protein production reveals that the plant can produce up to 4 g of protein per kg FW (g/kg FW) with the yield up to 300 kg of recombinant protein per year through transient expression.

3 Systems engineering approaches to produce recombinant biopharmaceuticals in plants

Plant-based biologics have emerged as a promising alternative for therapeutics production due to their low-cost and scalable nature. This is critical for meeting the demand for immunizations during pandemics. Production of recombinant therapeutics in plants can be achieved by either stable or transient expression. Stable expression systems are developed by nuclear transformation or chloroplast transformation through *Agrobacterium*-mediated or biolistic gene transfer (Gelvin, 2003; Tien et al., 2019; Bolaños-Martínez et al., 2020; Heenatigala et al., 2020; Kumar and Ling, 2021). Meanwhile, transient expression systems are developed by plant virus-based vectors or agroinfiltration. Stable expression

systems possess advantages including scale-up, low storage costs, glycosylation patterns and reduced cross contamination of animal-borne agents; Transient expression systems are known for their rapid, cost-effective, increased protein accumulation and commercialization potential (Moon et al., 2019). Transient expression of recombinant biopharmaceuticals in plant system is the most preferred mode of production since the system accumulates large quantities of proteins quickly. Different immunogens and therapeutic agents have been produced through transient expression in leaves by agroinfiltration (Iyappan et al., 2018; Page et al., 2019; Rattanapisit et al., 2020).

Proteins reach functional state by proper folding, disulphide bond formation, subunit assembly and post-translational modifications. Prokaryotic host systems pose limitations such as lack of post-translational modifications (glycosylation and sialylation), signal peptide cleavage and pro-peptide processing (Gomord and Faye, 2004). Glycosylation is the most prevalent and diverse type of post-translational modification of proteins shared by all eukaryotic cells. A complex metabolic network and many glycosylation pathways are used during the enzymatic glycosylation of proteins to produce a wide variety of proteoforms (Schjoldager et al., 2020). For instance in humans, N-acetylglucosaminyl transferases IV and V present in Golgi functions in galactosylation, branch elongation and sialic acid capping, which is not found in plants (Strasser, 2022; Strasser, 2023). In order to produce therapeutic proteins of interest in plant with desired glycosylation pattern, β-1,4 galactosyl transferase co-expression and sub-cellular localization to Golgi is preferred (Navarre et al., 2017; Strasser, 2022). Recombinant glycoproteins produced in plants have residues of α1,3-fucose and β1,2-xylose linked to the same core N-glycan. These two sugar residues could be immunogenic since they are absent in human glycoproteins (Margolin et al., 2020a). In Arabidopsis, tobacco, and rice, multiplex CRISPR-Cas9 technology was used to knock out two glycosyl transferases, β1,2-xylosyltransferase and α1,3-fucosyltransferase, in order to humanize glycosylation patterns in plants and produced biopharmaceuticals. The results demonstrate that complete suppression of these two sugar residues was reported in Arabidopsis and tobacco, while the presence of Lewis structure in rice shows that the glycosylation pattern differs between dicots like Arabidopsis and tobacco and monocots like rice (Jansing et al., 2019; Jung et al., 2021). Many therapeutic proteins that are glycosylated need to be sialylated ultimately to fully activate their biological functions, however plants are not capable of N-glycan sialylation, in contrast to mammals. The ability to perform N-glycan sialylation is much sought after in the plant-based biopharmaceutical industry since sialic acids are a frequent terminal alteration on human N-glycans. Plants can be engineered across α2,6-sialylation or α2,3-sialylation pathways that showed active IgG with anti-inflammatory properties and increased pharmacokinetic activity of therapeutics produced in plants (Strasser, 2023). N-glycan sialylation is highly desirable due to its function in extended half-life, stability, solubility, and receptor binding (Bohlender et al., 2020; Chia et al., 2023). A whole mammalian biosynthetic pathway, including the coordinated expression of the genes for (i) biosynthesis, (ii) activation, (iii) transport, and (iv) transfer of Neu5Ac to terminal galactose, has been introduced into *N. benthamiana* in order to achieve *in planta* protein sialylation (Izadi et al., 2023).

Recombinant biologics expressed in plants are designed as fusion proteins to contain an N-terminal or C-terminal tag (His, FLAG, HA, CBM3 etc.) for easy purification and analysis. Immobilized metal-ion affinity chromatography is widely used for purification of hexahistidine tagged proteins (Vafaee and Alizadeh, 2018; Islam et al., 2019; Hanittinan et al., 2020; Islam et al., 2020; Marques et al., 2020; Soni et al., 2022). Other techniques such as one-step cation-exchange chromatography, Protein G-/A-based affinity chromatography, diafiltration (antibody purification) and polyelectrolyte precipitation (removal of plant proteins), hydrophobic interaction chromatography (HIC) followed by hydrophobic charge induction chromatography (HCIC) are employed in recombinant plant protein purification (Fulton et al., 2015; Park et al., 2015; Shi et al., 2019; Miura et al., 2020; Lim et al., 2022; Grandits et al., 2023).

4 AI-based ML algorithms in recombinant protein production

Gene designing and genetic engineering are key tools in molecular pharming, which enable the expression of protein of interest in host system, and development of genetically modified organisms with desirable traits. The design of gene and its expression cassette is the first step in getting desired protein in the plant system (Rozov and Deineko, 2019). Proper designing plays a major role in the production of biologics that includes selection of host system, codon optimization, regulatory components associated with foreign gene, host engineering, mode of expression, and purification of biopharmaceuticals (Webster et al., 2017; Peyret et al., 2019; Belcher et al., 2020; Sainsbury, 2020; Hassan et al., 2021; Vazquez-Vilar et al., 2023). AI-based ML algorithms are proven choice for cost-cutting and efficient designing of product manufacturing in different host systems. Few of the competent network models were built on Convolutional Neural Networks (CNNs), a DL architecture inspired from connectivity patterns of animal visual cortex to identify, locate and differentiate objects in any image (Barré et al., 2017). Different AI-based ML and DL algorithms have been developed to increase the recombinant biopharmaceutical production in the hosts by detecting, analyzing and optimizing the conditions such as screening and candidate selection, vector construction, codon optimization, protein modelling and design, growth condition optimization and protein solubilization and purification. A model architecture of CNN is shown in Figure 2.

4.1 AI in codon optimization

Introduction of native genes into alternate host system causes incompatibility in codon usage bias, sequence repeats, % of GC, negative cis-regulatory elements and Shine-Dalgarno sequence (Tuan-Anh et al., 2017; Constant et al., 2023; Jain et al., 2023).

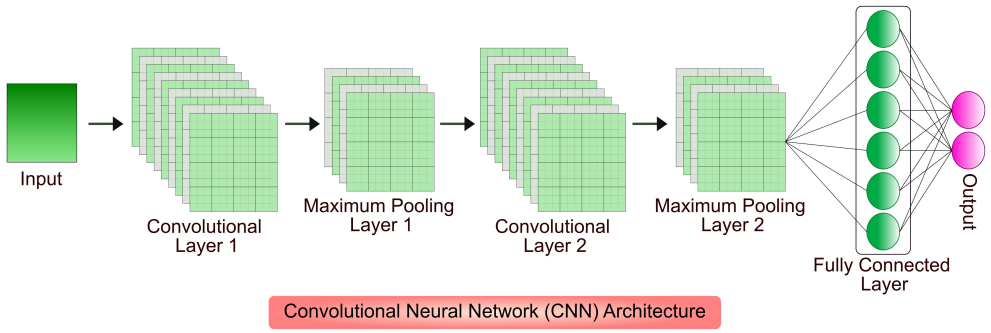

FIGURE 2
An illustration of input characteristics recognition using CNN. The input spatial features pass through multiple convolutional and pooling layers; processed data is received at a fully connected layer. The convolutional layer applies filters to extract features from input, pooling layer downsamples the features in order to reduce computation and fully connected layer makes the final prediction to result the output.

Codon bias affects the expression of transgene in the host plant which result in stopping at disfavored codons, truncation, misincorporation or frameshift. Site directed mutagenesis can resolve these problems by introducing silent mutations in coding region of the transgene and help the host species read transgene codon without any hindrance (Ma et al., 2003). Heterologous expression of recombinant proteins in different hosts needs optimization of coding sequences with synonymous codons as the host systems tend to remove heterologous proteins through proteolysis. Further, codon optimization renders the recombinant protein with structural and functional conformation at increased levels of expression in different host systems (Al-Hawash et al., 2017; Argentinian AntiCovid Consortium, 2020; Ding et al., 2022). The codon optimization percentage is proportional to the level of recombinant transgene expression. The amount of expression of the four variants of the *bar* gene with varying percentages of optimized codons was examined using experimental and *in silico* methods, and it was found that genes with 50–70% of optimized codons were expressed effectively in *N. tabacum* (Agarwal et al., 2019). Beta-defensin from chicken called chicken β Gallinacin-3 has demonstrated broad-spectrum antibacterial action against plant infections. Using DNAWORKS3.0 and the Genscript Rare Codon Analysis Tool, chicken β Gallinacin-3 gene sequences were codon optimized and tested. The results demonstrated constitutive expression in *Medicago sativa* and improved antibacterial activity against *E. coli*, *S. aureus*, and *Salmonella typhi* (Jin et al., 2022). Despite species difference, the codon optimizer program improved translation efficiency in tobacco and lettuce by using codon usage hierarchy of the *psbA* gene (Kwon et al., 2016). Adiponectin, an adipokine and a cell signaling protein, is produced as a secretory protein in *Withania somnifera* hairy root culture. Codon usage data, base composition and codon adaptive index (CAI) of *W. somnifera* were analyzed; the human adiponectin gene sequence was optimized and expressed as secretory product. Optimization of codons increased the expression levels of protein secretion (Dehdashti et al., 2020). The synthesis and expression of therapeutic proteins depend heavily on codon optimization. Effective methods are required to efficiently optimize codons for the generation of recombinant proteins in plants (Webster et al., 2017). Codon usage bias was utilized to optimize nucleotide sequences for host-specific expression in many systems including *E. coli*, Chinese Hamster Ovary (CHO) cells, HEK293, etc (Al-Hawash et al., 2017; Shayesteh et al., 2020; Lu et al., 2021). Till date, no AI tool has been designed to optimize codons for increasing the plant-based recombinant biologics production. The challenges posed by conventional methods include a vast possibility of codon combinations, irrational effects following transcription and translation, protein misfolding and loss of function (Constant et al., 2023).

Neural network (NN) models identify unexplored patterns in the native DNA sequences from the training set, predicts the most valid coding sequences using the test set and optimize DNA sequence for translation. The NN-optimization is found to be more efficient than conventional methods resulting in significantly higher yields of recombinant biologics (Goulet et al., 2023). Many sequence-based ML algorithms using deep neural networks (DNN) extract features from input codon data, predict and evaluate sequence data. Two major parameters that play a crucial role in codon optimization are 1) codon adaptation index (CAI) and 2) tRNA adaptation index (tAI). CAI is the frequency of codon usage in an organism's coding DNA sequence (CDS) and tAI is the measure of intracellular tRNA to translate into proteins and individual codon-anticodon pairing efficiency (Sabi et al., 2017; Tuan-Anh et al., 2017; Fu et al., 2020; Constant et al., 2023; Goulet et al., 2023). A Recurrent Neural Network (RNN) model trained sequence was tested for its efficiency by transient transfection of unoptimized and optimized sequences in CHO (ExpiCHO) cells. The titres of model protein, human programmed death ligand 1 (PD-L1) extracellular domain, were quantitated nine days after transfection. The RNN-optimized sequence was expressed largely (179.5 ± 12.4 μg/mL) than the native sequence (104.5 ± 5.7 μg/mL). The RNN model was used in optimization of mAb and stable integration of mAb CDS in CHO-K1-derived cells. The RNN-optimization of CDS yielded 2030 μg/mL and the unoptimized sequence resulted in an yield of 960 μg/mL (Goulet et al., 2023). Influence of AI in bacterial expression system is more than any other eukaryotic systems and so codon optimization was widely carried out through ML-based models. Tuan-Anh et al. (2017) used

neural network with CAI and GC content for optimizing codons expressing prochymosin, the chymosin-precursor in *E. coli* system. Codon optimization could preferably not just used for increasing heterologous recombinant expression, but also for increasing the protein solubility. MPEPE, a newly developed protein solubility prediction DNN model was built using convolution layers, pooling layers and long-short term memory (LSTM) layers. The architecture was built as embedded matrix, through 'one-hot encoding' technique using integers '1' and '0', to include synonymous codons of individual amino acids. Point mutation in sites was scrutinized through evolutionary analysis without interfering the protein function. The target nucleotides for expression studies were used as inputs in MPEPE for virtual screening and recombinant proteins were expressed in *E. coli* BL21 (DE3) cells with an increased level of soluble protein expression (Ding et al., 2022). Bidirectional LSTM Conditional Random Field (BiLSTM-CRF) model is a codon optimization model built for *E. coli* by H. Fu et al. (2020). The model converts codon optimization to sequence annotation and trains the data of *E. coli* gene set through word-embedding vector. The multivalent *Plasmodium falciparum* vaccine antigen FALVAC-1 and PTP4A3, a prognostic cancer biomarker optimized by BiLSTM-CRF were expressed in *E. coli* BL21 (DE3). The model efficiently optimized the low-expression candidate to higher expression levels, which proved the robustness of the model and the high expression candidate PTP4A3 was expressed in similar levels which proved the stability of algorithm. Jain et al. (2023) designed ICOR (Improving Codon Optimization with RNNs), a DL tool, built on BiLSTM architecture through 'one-hot encoding' method, with a large non-redundant dataset of *E. coli* genomes and upon correlation comparison with the mRNA expression in real-time based on a work by dos Reis et al. (2003), the improvement in expression observed was about 236%. The multilayer network model may be trained for other host systems including model plants (such as *N. benthamiana* or *N. tabacum*) as shown in Figure 3 with complete omics dataset through transfer learning approach to increase the yield. CO-BERTa, a deep contextual language model was trained with GFP (Green Fluorescent Protein) and anti-HER2 VHH CDSs on *Enterobacterales* dataset for functional protein measurement. The mCherry reporter protein which showed 28.7% pairwise identity to GFP and anti-SARS-CoV2 VHH which showed 73.7% pairwise identity to anti-HER2 VHH was chosen to test the model. These proteins differ in their length but share similar structural features, a major feature being β-barrel. ACE (Activity-specific Cell Enrichment) measurement of CO-BERTa codon optimized proteins in SoluPro^{TM} *E. coli* B strain showed highest expression levels than commercial algorithms (except Genewiz, $p<0.05$) (Constant et al., 2023). Further, genome analysis and codon usage patterns of plant host systems through artificial neural networks (ANNs) could significantly increase the expression of recombinant biologics (Doyle et al., 2016).

Quantum computers can be used to optimize codons for high expression of proteins. Quantum Annealing (QA) algorithm uses quantum computers to give high-dimensional combinatorial optimization of codons using Binary Quadratic Model (BQM) built on 'one-hot encoding' technique. mRNA codons of peptide fragments and full length proteins of SARS-CoV2 spike glycoprotein were optimized using Quantum Approximate Optimization Algorithm (QAOA) (Fox et al., 2021).

Currently, there are no ML-based algorithms available for codon optimization of recombinant proteins to express in plants. The algorithms available for other host systems could be adapted, remodelled and designed for plant-based expression hosts since many of the model plants' genome is available publicly.

4.2 AI in protein modelling and design

The recombinant proteins expressed in different systems are influenced majorly by factors including structure, solubility, catalytic activity, protein folding and stability. Vector and gene of interest is designed to overcome the challenges of recombinant protein expression. The components of protein modelling include host and expression vector selection, promoter, selectable marker, fusion tags. ML based algorithms enhance the expression and overcome the challenges in expression of recombinant biologics in multiple expression systems. These algorithms analyses and tests (either nucleotides – CDS/RNA-seq or amino acids) sequences and provides with the fitness of protein variants (Wittmann et al., 2021). Few ML models utilize structure along with sequences of amino acids for modelling of proteins. The RNNs and other neural network models are powerful than other ML models since these could learn from raw data directly without any sequence alignment and heuristic scoring (Deep RNN for Protein Function Prediction from Sequence). While molecular dynamics simulations for an antibody through supercomputers require hours and even days, neural networks such as CNN models take only seconds to get the work done in personal computers (Lai, 2022). Regulatory elements are one of the key components of recombinant protein production and synthetic promoters have been designed using ML models to increase the transcription efficiency. Highly functional Synthetic Promoters with Enhanced Cell-State Specificity (SPECS) were identified from a library of 6107 promoters using multiple ML regression algorithms, from which a generalized linear model with elastic net regularization (GLMNET) was chosen as the efficient model to predict highly active promoters. The spatiotemporal activity of each promoter was analyzed by expression of fluorescent protein in HEK-293T cells (Wu et al., 2019). In the work by Vo ngoc et al. (2020), human PolII core promoter was analyzed to create HARPE (high-throughput analysis of randomized promoter elements). The HARPE training dataset included 200,000 variants of promoter sequences and downstream core promoter region (DPR) models were generated by support vector regression (SVR) algorithm and tested *in vitro* and in HeLa cells. Designing protein includes predicting counterparts, which are involved in structural integrity and stability of proteins (Masson et al., 2022). These include epitope prediction, vaccine designing and remote homology detection, which utilize parts of the protein molecule to increase its activity (Mettu et al., 2016; Moss et al., 2019; Yang et al., 2021b; Koşaloğlu-Yalçın et al., 2022; Routray et al., 2022).

Using DeepLoc, a deep convolutional network Kraus et al. (2017) showed improved performance over traditional approaches

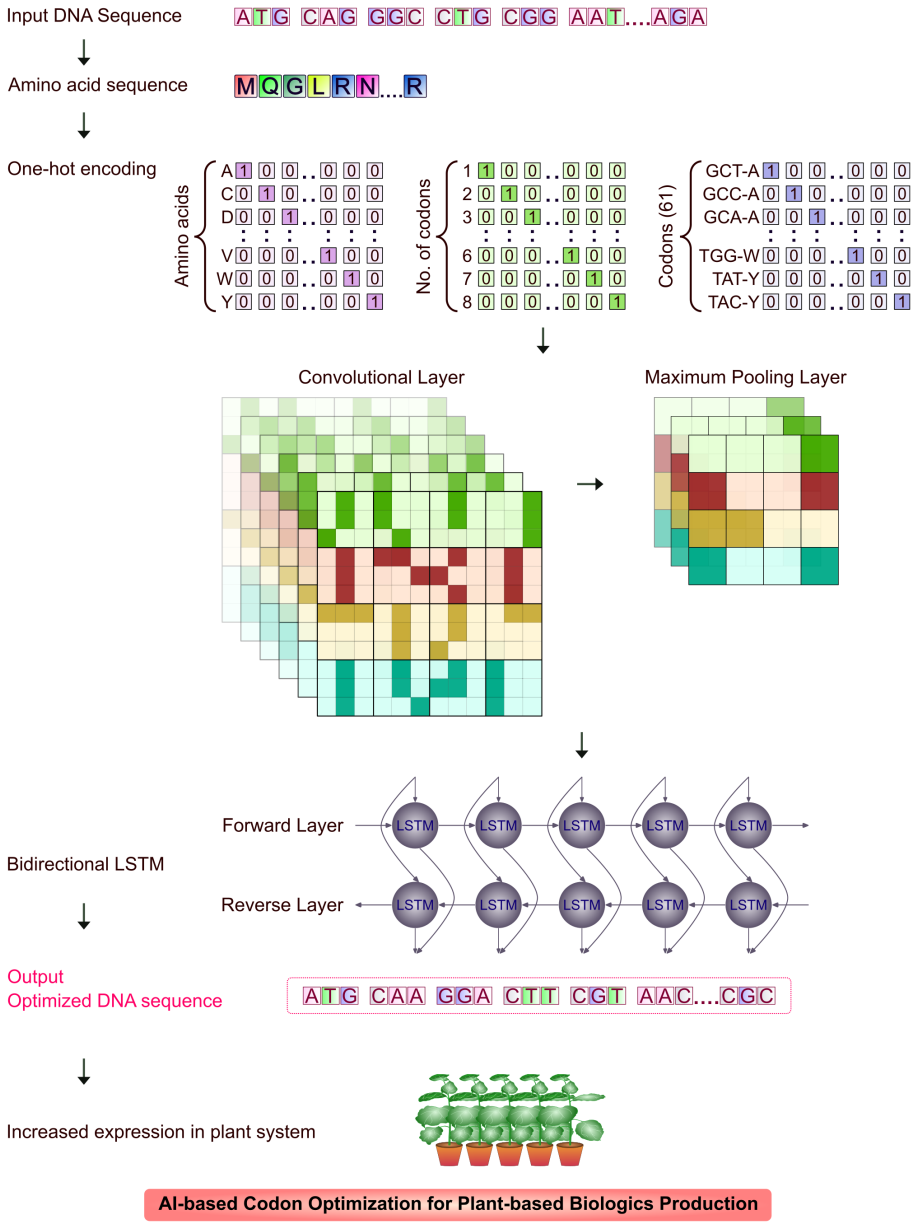

FIGURE 3
An overview of CNN and BiLSTM in codon optimization for plant expression system. Input DNA sequence is translated to amino acid sequence and reverse translated to DNA sequence. The sequence is further tested using CNN for codon optimization metrics prediction for plant expression system and BiLSTM tests with synonymous codons for optimal codon usage for high expression in plant system.

in the automated classification of protein subcellular localization in yeast cells. Organelle targeting and sub-cellular localization increases the recombinant therapeutic protein expression in plants to higher levels. Localization of recombinant proteins in cytosol and different plant organelles such as nucleus, chloroplast, mitochondria and endoplasmic reticulum (ER) of plant tissues such as seeds and leaves are useful in increased accumulation and stability of expressed proteins (Vafaee and Alizadeh, 2018; Arcalis et al., 2019; Bidarigh fard et al., 2019; Islam et al., 2019; Shi et al., 2019; Hanittinan et al., 2020; Islam et al., 2020; Li et al., 2022b; Lim et al., 2022). Signal sequences are added to N-terminus or C-terminus of the biologics to increase the yield and a C-terminal ER retention signal is the most widely used strategy to accumulate higher amount of proteins in recombinant expression. Sahu et al. (2021) developed a tool, Plant-mSubP, based on integrated ML approaches with SVM as the model to predict localization of proteins to single and dual organelle targets.

Analysis of the enriched bococizumab yeast cell libraries along with similar library for antibody affinity was done using an ML model, which enabled the identification of rare variants with co-optimized levels of low self-association and high affinity (Makowski et al., 2022). Similarly, mAbs can be screened and optimized for production in specific host systems that could include plants as well (Feng et al., 2022a; Lai, 2022). Proteins such as toxins which are

difficult to produce in certain hosts can be expressed easily using deep-learning based CNN algorithms (Pan et al., 2020). A wide range of ML algorithms used in various eukaryotic and prokaryotic systems for modelling different proteins is shown in Table 1.

4.3 ML models in engineering strains for recombinant protein production

A large repertoire of omics data is obtained from the host system at different levels of replication (genome), transcription (transcriptome), translation (proteome), and regulation (metabolome). These data can be used to engineer host cells to improve recombinant protein yield (Ramzi et al., 2020; Samoudi et al., 2021). ML algorithms can be implemented in understanding the genome-scale metabolic models (GEMs), which encompasses hundreds of metabolic pathways and thousands of metabolic reactions. ML can be a stand-alone or a complementary approach, in learning regulatory levels of complex pathways in plants such as transcriptional, translational and allosteric regulation. These ML algorithms are shown to exhibit more robustness than statistical tools (Radivojević et al., 2020; Zhang et al., 2020; Strain et al., 2023).

Multilayer Perceptron (MLP), an NN model was used to analyse the human RNA-seq data from ARCHS4 database based on secretory index (SI) and extrapolated to engineer CHO cells (Zaragoza, 2022). In order to predict yeast cell growth Culley et al. (2020) proposed ML–based data integration techniques, combining gene expression profiles that rigorously assess and compare with computationally generated metabolic flux. A total

TABLE 1 AI in protein modelling and design.

Component	Name of the program	Type of ML algorithm	Architecture	Function/ Parameter	Model system/ training dataset	References
mRNA	APARENT (APA REgressionNeT)	CNN	One-hot encoded matrix system with two convolutional layers	• mRNA isoform prediction and polyadenylation within +10 to +35 nt downstream of 6-base central sequence element (CSE) • cleavage site prediction across polyA signal	HEK293	Bogard et al. (2019)
	6-mer Logistic Regression Baseline	Linear logistic regression	One-hot encoded matrix system with 6-mer counts	• mRNA isoform prediction and polyadenylation • cleavage site prediction		
mRNA, gene enhancers and protein	DEN (Deep Exploration Network)	Deep Convolutional Generative Adversarial Networks (DC-GANs)	One-hot encoded matrix Latent Seed Sequence Tensor	• polyadenylation signals conformed to mRNA isoforms and 3' cleavage sites • differential splicing • maximum transcriptional activation of gene enhancers • functional variants of GFP (Green Fluorescent Protein)	HEK293 HeLa MCF7 CHO	Linder et al. (2020)
	APARENT	CNN				
	-	GP regression				
	APA VAE (Variational Autoencoder)	Residual Neural Network (ResNet)				
	KL-bounded DEN	CNN				
Gene interaction and expression	scCapsNet	DNN	Capsule Neural Network	Discovery of gene interactions; closely related in function but presenting differential gene expression pattern in single cell types (based on transcriptome analysis)	scRNA-seq dataset including mouse retinal bipolar (mRBC) cells and human peripheral blood mononuclear cells (hPBMC)	Wang et al. (2020)
Transcription factor	Independent Component Analysis (ICA)	Unsupervised ML	-	Gene expression and transcriptional regulation in *E. coli* through transcriptome analysis	*E. coli* K12 RNA-seq expression profiles	Sastry et al. (2019)
Transcription factor binding	FactorNet	Convolutional RNN	One hot encoded 4-row bit matrix, LSTM	Transcription Factor (TF) cell type specific binding site prediction. (Eg.TF E2F1	DNase-seq, ChIp-seq and RNA-seq data of chromosomes X and	Quang and Xie (2019)

(Continued)

TABLE 1 Continued

Component	Name of the program	Type of ML algorithm	Architecture	Function/ Parameter	Model system/ training dataset	References
				binding to GM12878 and HeLa-S3)	1-22 from ENCODE-DREAM challenge	
Promoters	Hybrid biophysical-ML approach	Ridge regression model	-	• Synthetic promoter designing • Identification of -35 and -10 motifs and optimal spacer length	*E. coli*	LaFleur et al. (2022)
Synthetic promoter	DL model	Deep CNN	Transformer model with BiLSTM	Design regulatory sequences including orthologous promoters	RNA-seq data from *S. cerevisiae* and 10 other Ascomycota species	Vaishnav et al. (2022)
Protein	DeepRHD	DNN	CNN based bidirectional GRU (Gated Recurrent Units)	Remote homology prediction of protein sequences using physico chemical properties and evolutionary information	SCOP1.67 dataset	Routray et al. (2022)
Protein	ProtT5	pLM (protein language models) Logistic Regression	Attention based deep dilated residual networks consisting of convolution layers (ResNet CNN)	Protein (transmembrane beta barrel proteins – OmpX and variants) structure prediction from sequences	High resolution protein 3D structure dataset from ProteinNet12	Weissenow et al. (2022)
Protein	ML model	Linear regression models including glmnet, partial least squares, averaged neural network, SVM with radial basis function kernel, stochastic gradient boosting, boosted generalized linear model, random forest, cubist and naïve Bayes models	Caret package in R	Factors influencing recombinant protein stability including Molecular weight, cysteine residues and N-linked glycosylation	CHO cells expressing human secretome	Masson et al. (2022)
Protein	ASPIRER	DL model	XGBoost and N-terminal sequence-based CNN	Prediction of Non-classical secreted proteins (NCSPs)	Gram positive bacteria NCSPs dataset from UniProt	Wang et al. (2022)
Protein	eUniRep	DL NN	UniRep multiplicative LSTM	Protein, avGFP and TEM-1 β-lactamase, engineering (Low-*N* engineering) using small number of functional variants	*E. coli* DH5α	Biswas et al. (2021)
Protein	UniRep	SVM	RNN	Prediction of recombinant gene expression and protein solubility	*B. subtilis*	Martiny et al. (2021)
		LR				
		Random Forest (RF)				
		ANN				
Protein	ECNet	RNN	BiLSTM, Transformer architecture with TAPE integration	Protein fitness prediction based on evolutionary context, engineered TEM-1 β-lactamase variants showing enhanced ampicillin resistance	*E. coli* DH5α Diverse large-scale deep mutational scanning (DMS) datasets and random mutagenesis datasets	Luo et al. (2021)
Protein	EPSOL	Keras based DL model	Multidimensional Embedding, multi-convolutional-pooling	Protein solubility prediction	Heterologous expressed *E. coli* soluble and insoluble	Wu and Yu (2021)

(Continued)

TABLE 1 Continued

Component	Name of the program	Type of ML algorithm	Architecture	Function/ Parameter	Model system/ training dataset	References
			module and a Multi-layer Perceptron (MLP)		protein dataset compiled by Smialowski et al. (2012)	
Protein	DEEPred	Multi-layered perceptrons (MLPs)	Feed-forward multitask DNN	Sequence/Gene Ontology (GO) based functional definition prediction of proteins	*Pseudomonas aeruginosa* strain reference genome and UniProtKB/Swiss-Prot dataset	Sureyya Rifaioglu et al. (2019)
Protein	ML models	GANs	Generator Neural Network and Discriminator Neural Network	Prediction of Protein solubility	eSol database dataset	Han et al. (2019)
		Logistic regression				
		Decision Tree				
		SVM				
		Naïve Bayes				
		Cforest				
		XGboost				
		ANNs				
Protein	DeepSol	DL model	CNN, non-linear high-dimensional k-mer vector spaces, deep feed-forward neural network (FFNN)	Protein solubility prediction	Heterologous expressed *E. coli* soluble and insoluble protein dataset compiled by Smialowski et al. (2012)	Khurana et al. (2018)
Protein	ML	RNN	BiLSTM, One-hot encoded matrix	Identification and function prediction of protein homologs including iron sequestering proteins, cytochrome P450, serine and cysteine proteases and G-Protein coupled receptors, detection through fluorescence (GFP)	*E. coli*	Liu (2017)
Protein	SPIDER2	Deep learning neural network	Stacked sparse autoencoder	Protein secondary structure, solvent accessible surface area, main chain torsion angle prediction	Non-redundant high resolution protein structures dataset	Yang et al. (2017)
Amyloidogenic proteins	AbsoluRATE	SVM	Sequence-based regression	Aggregation kinetics prediction of amyloidogenic proteins	CPAD 2.0 database dataset	Rawat et al. (2021)
Antibody	DeepAb	Deep residual convolutional network (Deep RCN) with Rosetta-based protocol	RNN, BiLSTM, LSTM	Antibody Fv structure prediction from sequence	Observed Antibody Space (OAS) database, SAbDab database	Ruffolo et al. (2022)
Antibody	DeepH3	Deep residual network	One dimensional and two dimensional convolutions	Prediction of *de novo* CDR H3 loop structures	Rosetta and SAbDab dataset	Ruffolo et al. (2020)
mAbs	solPredict	ESM1b-based Multilayer perceptron (MLP2Layer)	Pretrained protein language model EMS1b embedding	• Rapid, large-scale high throughput screening of mAb sequences (IgG1, IgG2 and IgG4) and quantitative solubility prediction	HEK293/CHO	Feng et al. (2022a)

(Continued)

TABLE 1 Continued

Component	Name of the program	Type of ML algorithm	Architecture	Function/ Parameter	Model system/ training dataset	References
		transfer learning model		eliminating precipitation in Histidine pH 6.0 (H6) buffer system • Eliminates the need for 3D modelling		
mAbs/IgG1	DeepSCM	Scikit-learn	CNN architecture	Molecular dynamics simulation to screen high concentration antibody viscosity prediction	SAbDab and AbYsis database dataset	Lai (2022)
	Keras v2.7.0	-				
Multiepitope vaccine	DeepVacPred	DNN-V	Multi-layer CNN and a 4-layer linear neural network	Designing vaccine subunit containing both T- and B-cell epitopes of Spike glycoprotein against SARS-CoV2	*E. coli* K12	Yang et al. (2021b)
T-cell Epitope	Antigen eXpression based Epitope Likelihood-Function (AXEL-F)/ NetMHCpan 4.1 combination	-	Neural networks	• Expression of source antigen; T cell epitope prediction and peptide presentation to MHC Class I molecule • SARS-CoV2 epitope prediction	IEDB HLA class I ligands dataset; RNA-Seq data of HeLa cells; SARS-CoV2 expression dataset from Finkel et al. (2021)	Koşaloğlu-Yalçın et al. (2022)
T-cell Epitope	-	Epitope likelihood	Aggregate z-score, structure-based processing likelihood	*P. aeruginosa* endotoxin domain III (PE-III) epitope prediction	*P. aeruginosa*	Moss et al. (2019)
T-cell Epitope	-	Epitope likelihood	Aggregate z-score	CD4+ T-cell epitope prediction in bacterial and viral antigens without genotype information through antigen processing constraint modelling	Sequence data from different studies in C57BL/6 mice, HLA-DR4-transgenic mice and humans	Mettu et al. (2016)
Protein localization	MULocDeep	Bayesian optimization & Attention visualization	LSTM	Protein localization in organelles such as nucleus, mitochondria, plastid and thylakoid and extracellular matrix	Mitochondrial proteome data of *A. thaliana* cell cultures, *Solanum tuberosum* tubers, *Vicia faba* roots	Jiang et al. (2021)
Protein localization	Plant-mSubP	SVM	OvR (One-vs.-Rest)	Single- and dual- organelle targeting/subcellular localization of proteins in plants	Plant protein sequence dataset from Uniprot Database	Sahu et al. (2021)
Cytokines and peptides	ProtConv	Transfer learning CNN	LSTM, ResNet and Transformer with TAPE embedding LeNet-5 architecture	Function prediction of proinflammatory cytokines and anticancer peptides	IEDB and CancerPPD database dataset	Sara et al. (2021)
Peptide	FBGAN (Feedback GAN)	GANs	RNN and Feedback loop training architecture	• Generation of synthetic AMPs and α-helical peptide coding genes • Optimization of secondary structure	Uniprot database dataset	Gupta and Zou (2018)
Peptide-MHC Class I binding	CapsNet-MHC	CNN	Capsule Neural Network	Prediction of interaction between allelic variants of MHC and peptides with rare sequence lengths	IEDB dataset	Kalemati et al., (2023)
Peptide-HLA binding	DeepSeqPanII	Pan-specific DNN with attention mechanism	LSTM	Prediction of Peptide-HLA Class II binding	IEDB datasets BD2013 and BD2016	Liu et al. (2022b)

(Continued)

TABLE 1 Continued

Component	Name of the program	Type of ML algorithm	Architecture	Function/ Parameter	Model system/ training dataset	References
MHC Class II Antigen Presentation	NNAlign_MAC	ANN	NNAlign_MA ML framework	• CD4 T cell epitope prediction • MHC class II antigen presentation prediction • Prediction of protein-drug immunogenicity	Single allele and Multiple allele dataset & IEDB dataset	Barra et al. (2020)
Signal Peptide	XGBoost	Regression model	-	Increasing the protein translocation rates to ER by optimizing synthetic signal peptide-protein (mAb/ScFv) complex formation	CHO-K1 cells	O'Neill et al. (2023)
Signal peptide	Sequence-to-sequence model	Attention-based neural network	Transformer model	Signal peptide prediction from Amylase, lipase, protease and xylanase enzymes	*B. subtilis*	Wu et al. (2020)
Signal peptide	SignalP 5.0	DL model	Non-linear PSSMs (position specific scoring matrix), BiLSTM and a conditional random field	Peptide identification (three classes including Sec/SPI, Sec/SPII, Tat/SPI) in prokaryotes	Reference proteomes of *E. coli* K12 and *S. cerevisiae*	Almagro Armenteros et al. (2019)
Toxic motifs	ToxDL	Deep CNN	Bidirectional GRU, one-hot encoded matrix	Toxicity assessment of genetically engineered organisms by highlighting toxic motifs and alteration of toxicity	Toxic/venom protein dataset from Animal Toxin Annotation Project in UniProt	Pan et al. (2020)
	Domain2Vec		Skip-gram model			
NSAID	Ensemble Decision Tree (DT)	Extremely Random Tree (ET)	Multiple base trees with bagging strategy	Non-steroidal anti-inflammatory drug, Oxaprozin, solubility in supercritical CO_2 fluid	Oxaprozin solubility dataset from Khoshmaram et al. (2021)	Alshehri et al. (2022)
		Random Forest (RF)				
		Gradient Boosting	Sequence of base predictors			

of 1,143 *S. cerevisiae* mutants were tested and 27 machine learning methods were analyzed.

ART (Automated Recommendation Tool) and EVOLVE algorithm are ML-based Bayesian ensemble optimization tools used in increasing the production of tryptophan in yeast, *S. cerevisiae*. These ML algorithms were used to design 30 different promoter combinations from the transcriptome dataset, which were used to predict engineered strains to show increased productivity. The engineered strain SP606 was found to possess higher synthesis rate of proxy GFP than other strains designed using ML and library preparation. Also, the engineered yeast strain SP606 was identified to have an increased titre and productivity of tryptophan (Zhang et al., 2020). ART was also trained with concentration dataset of proteins/enzymes involved in heterologous pathway for the production of limonene. New strain design sets of *E. coli* for enhanced production of limonene were provided by ART (Radivojević et al., 2020).

Similarly, supervised learning algorithms have predicted pathway dynamics with the use of multiomics data (proteome and metabolome data) in *E. coli* for enhancing limonene production (Costello and Martin, 2018). In contrast, an unsupervised ML approach termed as HybridFBA, was proposed by Ramos et al. (2022) that combined GEM and metabolic flux balance analysis (FBA) using principle component analysis (PCA) in CHO cells (Strain et al., 2023). Machine Learning Predictions Having Amplified Secretion (MaLPHAS) by Eden Bio Ltd is an ML algorithm that predicted knock out of five genes, out of which Component of Oligomeric Golgi Complex (*cog6*) knockout strain resulted in doubled secretion of recombinant protein in the host *Komagataella phaffii* (*P. pastoris*) compared with the *bgs7* supersecretor strain (Markova et al., 2022).

DCell is a virtual eukaryotic cell composed of 2,526 subsystems embedded as VNNs (visible neural networks), a deep ANN, in hierarchy. The model was built using the hierarchical architecture of subsystems of *S. cerevisiae*. Being trained on several million genotypes, during simulation, DCell generates patterns of molecular activities based on genotype to phenotype relationship (Ma et al., 2018). DCell can identify gene deletions/knockouts using Gene Ontology (GO), which will result in phenotype change (Ma et al., 2018; Kim et al., 2020).

The ML algorithms and tools can be used to introduce or remove genes from a pathway to direct the increased production of humanized recombinant biologics in plant system. Knock-out approach of removing plant-specific glycans [β(1,2)-Xyl and

α(1,3)-Fuc] or knock-in strategy to express human [β(1,4)-Gal]and addition of sialic acid residues in specific host plants result in humanized protein expression. Such mechanisms could be explored and analyzed through ML tools such as ART (Sethi et al., 2021). Also, metabolic flux of host plant systems can be studied to generate stable lines with optimized metabolic pathways for desired post translational modifications of recombinant biologics.

4.4 Automation and AI in plant growth monitoring and biomass production

One of the big attributes of plant molecular pharming for recombinant biologics production, next to host selection and engineering is plant growth and maintenance. Plants are efficient biofactories for the manufacture of recombinant proteins and growth monitoring is a vital aspect when it comes to both laboratory scale and commercial production. Several automation technologies including affordable sensors built on Raspberry Pi, robotics and high-definition cameras work based on image acquisition (Jahnke et al., 2016; Jolles, 2021; Banerjee et al., 2022; Wan et al., 2022). The camera sensors have been deployed to analyze the plant growth patterns, phenotypes such as plant morphology, height, canopy, temperature, leaf biomass, leaf area index, greenness, age and different stresses. Similarly, seed count, shape, size and color, parameters for plant growth such as temperature, photoperiod, grow light color, etc. were studied by robot-assisted systems. A large training dataset of raw images captured in the camera sensors are analyzed through DNN modules and processed for color correction and segmentation for analysis (Jahnke et al., 2016; Ubbens and Stavness, 2017; Tovar et al., 2018; Zheng et al., 2019; Tausen et al., 2020; Bose and Hautop Lund, 2022). The efficient analysis of images are carried out by models based on CNNs that include U-Net, R-CNN and ResNet (Ubbens and Stavness, 2017; Lin et al., 2019; Zheng et al., 2019; Tausen et al., 2020; Bose and Hautop Lund, 2022). The IoT based sensors and programs are not limited to phenotyping the growth and morphology of plants but could detect plant nutrient deficiencies, diseases and soil parameters, thereby reduce the labor intensive maintenance and increase the sustainability (Dhivya et al., 2021; Monteiro et al., 2021; Bose and Hautop Lund, 2022). Plant monitoring and phenotyping using integrated automation and ML approaches is illustrated in Figure 4.

With the wider and large-scale biologics production environment, a large number of sensors in plant monitoring are needed and it becomes highly difficult to build the architecture for plant maintenance. Hence remote sensing using unmanned aerial vehicles (UAVs) is used in place at low altitudes to acquire high-resolution multispectral images of plants grown in agricultural field and greenhouses. The UAV high-throughput phenotyping

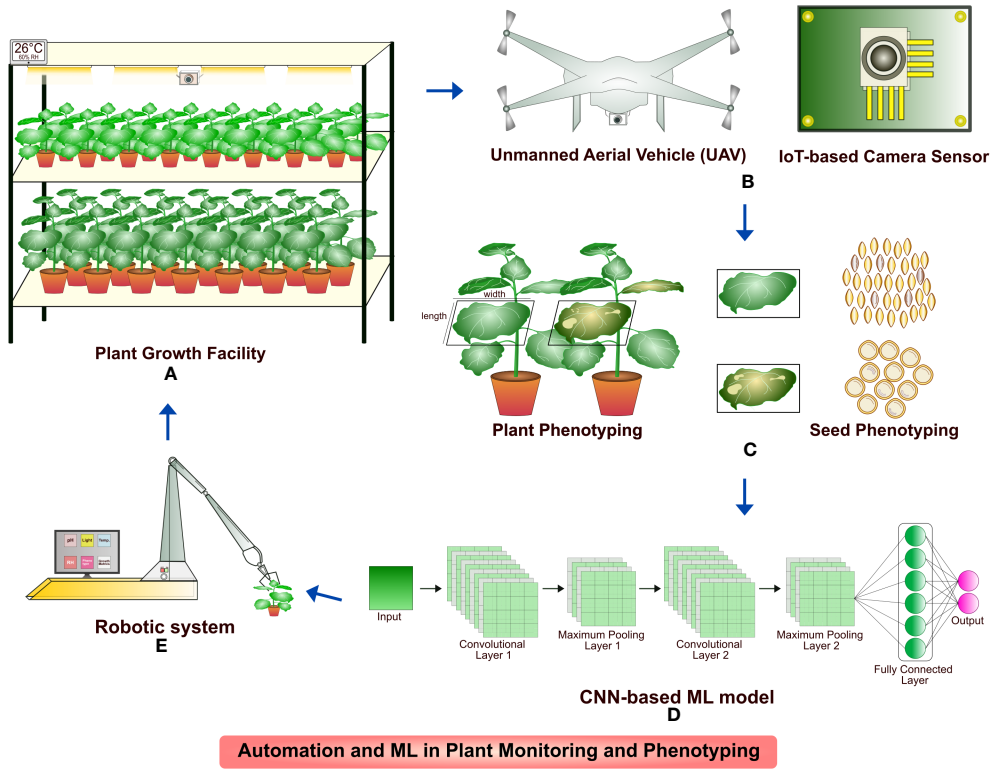

FIGURE 4
An illustration of plant monitoring and phenotyping with the integration of automation and ML approaches. **(A)** and **(B)** *N. benthamiana* plants grown in containment facility monitored continuously by image sensors; UAV deployed for plant monitoring in greenhouse; **(C)** Image acquisition of plant phenotypes such as height, width, leaf greenness, disease identification, seed count, morphology and segregation; **(D)** Phenotyping of plants by CNN-based ML model; **(E)** Robotic system for optimization and maintenance of environmental requirements for plant growth trained by CNN model.

platform, working on support vector machine (SVM) and SVM-derived models, processes the spectral information of optical images for the identification of plant growth, biomass, stress and disease stages (Maimaitijiang et al., 2020; Fu et al., 2021; Yang et al., 2021a; Aslan et al., 2022; Jiang et al., 2022a; Bai et al., 2023a). Several plants used as hosts in production of recombinant biopharmaceuticals such as *Glycine max* (L.) Merr. (soybean), *Triticum aestivum* (wheat), *Hordeum vulgare* (barley), *Oryza sativa* (rice), *Zea mays* (maize), *Arachis hypogaea* L. (peanut), *Arabidopsis thaliana* (Arabidopsis), *Brassica napus* (rapeseed), *Lycopersicon esculentum Mill.* (Tomtato), *Cucumis Linn.* (cucumber), *L. sativa Linn.* (lettuce), *Brassica oleracea linn.* (cabbage), *Raphanus sativus linn.* (turnip), *Apium graveliens Linn.* (celery) and *Spinacia oleracea Linn.* (spinach) and *N. tabacum* (tobacco) can be monitored using the sensors for high product yield (Minervini et al., 2015; Jahnke et al., 2016; Minervini et al., 2017; Ubbens and Stavness, 2017; Zheng et al., 2019; Maimaitijiang et al., 2020; Fu et al., 2021; Sangjan et al., 2021; Sarkar et al., 2021; Yang et al., 2021a; Banerjee et al., 2022; Bai et al., 2023a; Bai et al., 2023b; Sun et al., 2023). A detailed list of automation and AI-based tools used in plant monitoring is listed in Table 2. These technologies are not limited to monitoring the mentioned plants but can be extended to all the plant host systems used in expression of recombinant biologics.

4.5 ML approaches in cell suspension cultures and bioreactors

Plant cell suspension cultures offer a unique platform for the production of recombinant proteins due to their ability to perform post-translational modifications similar to mammalian cells (Gutierrez-valdes et al., 2020). Plant cell suspension cultures are usually prepared from callus tissue in shaker flasks or fermenters to form single cells and small aggregates and growing plant cells in a liquid medium in a controlled environment, such as bioreactor, where various factors like temperature, pH, and ratio of nutrient are to be optimized for cell growth and protein production (Cardon et al., 2019). Several proteins have been produced in bioreactor using cell suspension cultures including ORF8, an accessory protein of SARS-CoV2 in suspension cultured tobacco BY-2 cells (Imamura et al., 2021), rrBChE, rice recombinant butyrylcholinesterase in rice cell suspension culture (Macharoen et al., 2021), LBT-Syn protein in carrot cell suspension culture (Carreño-Campos et al., 2022), taliglucerase (ELELYSO), a recombinant version of human glucocerebrosidase in carrot cell cultures (Mor, 2015) etc.

Large scale production of plant-expressed recombinant proteins can be achieved by growing the transformed plant cell in different bioreactor shapes, however, there are diverse problems to be addressed such as pH of media, minerals, growth regulators, cell density, gaseous atmosphere, agitation system and sterilization conditions (Ruffoni et al., 2010).

Now-a-days AI techniques are increasingly being applied to bioreactors, which are essential tools in bioprocessing for the production of various biological products such as recombinant proteins, vaccines, and biofuels. ML models can identify the optimal operating conditions, such as temperature, pH, dissolved oxygen, and nutrient concentrations, to maximize product yield and quality. By integrating with sensors, data acquisition systems and control algorithms, AI models can analyze data in real time and automatically adjust process parameter accordingly. AI can adapt and adjust process parameters for optimal performance, reducing the need for manual intervention.

Optimizing plant tissue culture media is a complicated and time-consuming process, which is influenced by genotype, mineral nutrients, plant growth regulators, vitamins and other factors. ML approaches such as multilayer perceptron neural network (MLPNN), k-nearest neighbors (KNN) and gene expression programming (GEP) were used for developing prediction models in optimizing plant tissue culture media composition (Hosseini et al., 2022). In another work, three ANN models: CIPnet, CWnet and DCnet were developed to predict the best media composition for callus weight (CW), callus induction percentage (CIP) and days to callus initiation (DC). The performance was satisfactory and showed the R^2 values of 0.95, 0.95 and 0.88 for CIPnet, CW, and DCnet respectively (Munasinghe et al., 2020). The formation of foam in bioreactor is another major issue in pharmaceutical industry and creates operational issues. To address the issue in bioreactor, a CNN-based model was developed for the real-time identification of foam formation (Austerjost et al., 2021). Cell proliferation could be monitored through ML based algorithms. An ML model was trained for monitoring insect cell proliferation and viability percentage upon baculovirus infection in the bioreactor (Altenburg et al., 2023).

ANN based ML algorithm was used to control the micro-aerobic conditions to achieve a satisfactory product yield. Metabolic flux-based control strategy technique (SUPERSYS_MCU) was used to address the issue. To generate a surrogate model in the form of an ANN, the control strategy used simulations of a genome-scale metabolic model. The meta-model provided setpoints to the controller, allowing adjustment of the inlet airflow to control oxygen uptake rate (Zangirolami et al., 2021). Application of ANN models in predicting the system performance of osmotic membrane bioreactors (OMBRs) was investigated and such models developed showed good performance for the prediction of water flux and membrane fouling simulations (Viet and Jang, 2021).

Deep learning techniques in a hybrid semi metric modelling contest, such as deep feed forward neural network with varying depths, the rectified linear unit (ReLU) activation function, dropout regularization of network weights, and stochastic training with the ADAM method were explored (Mestre et al., 2022). Performance of ML algorithms was analyzed to predict n-caproate and n-caprylate productivities in bacteria using 16S rRNA amplicons in a bioreactor. The bioreactor performance was analyzed quantitatively and accurately from the dataset generated from different bioreactors. ML models were trained independently and tested with 16S rRNA amplicon sequencing data to predict n-caproate and n-caprylate productivities. The tests concluded that random forest was the best algorithm producing more consistent results with low error rate and more than 90% accuracy in the prediction of n-caproate and n-caprylate (Liu et al., 2022a). To predict the accuracy of real-time liquid level four ML algorithms, multiple linear regression (MLR), artificial neural network (ANN),

random forest (RF), and support vector machine (SVM) with radial basis kernel were analyzed and found that ANN and RF models performed well (Yu et al., 2022).

4.6 AI in downstream processing

The market demand of biopharmaceutical products is constantly increasing every year and there is an increasing pressure on price reduction for global access to biological drugs. In order to meet the market demand, significant improvement has been carried out in upstream processes, however the productivity in downstream has not increased accordingly (Ötes et al., 2017). The most challenging phase of therapeutic protein production in industries is the downstream processing (DSP) and DSP is accounting for a large portion of the total production costs. The growing demand and developments in upstream processing of therapeutics have burdened the downstream purification processes, due to high cost and insufficient processing capacity (Li et al., 2019). DSP of recombinant therapeutic proteins involves a series of operation such as filtration, followed by capture, purification, and polishing steps mainly done by chromatography (Gaughan, 2016). Chromatography is considered as the workhorse of DSP because it can selectively enrich the target proteins while eliminating impurities and this is achieved by exploiting differences in molecular properties, such as size, charge and hydrophobicity (Bernau et al., 2022). The development of product specific chromatography-based purification techniques is time consuming and expensive because target proteins make up a small portion of the total protein in the initial plant extract. To address this issue, Buyel and Fischer (2014) created a general downstream procedure for the purification of recombinant proteins produced in plants with diverse features. This was done by concentrating on the resin's ability to bind tobacco host cell proteins (HCPs) under various conditions such as pH and conductivity.

TABLE 2 Automation and AI Tools in plant monitoring.

Platform	Automation Technology	Imaging Device	Phenotype/ Parameter	Plant Species	References
UAV remote sensing	Multirotor UAV with CNN architecture	XIMEAMQ022MG-CM Camerawith CMOS sensor and 16 mm lens and Sony NEX-7 Camera	Disease severity at 25m altitude	*O. sativa* (rice)	Bai et al. (2023a)
High throughput UAV remote sensing	DJI Phantom 4 Advanced quadcopter	Drone RGB camera	Accurate plant count, location and size determination to distinguish in paddy field at 7m altitude	*O. sativa*(rice)	Bai et al. (2023b)
RiceNet	Deep Learning Network				
Edge-computing based network monitoring	IoT monitoring with deep learning algorithm-based Edge Image Processing Architecture	Raspberry Pi Camera with 5MP sensor	• Plant growth • Environment and Water quality	-	Wan et al. (2022)
GrowBot	Robotic system with U-Net: CNN	OV5647 CMOS image sensor with Raspberry Pi4	Plant growth based on nutrient deficiency and temperature stress	*Ocimum basilicum* (basil)	Bose and Hautop Lund (2022)
AscTec Navigator 3.4.5	UAV with built-in GPS	AscTec Falcon 8 octocopter (Ascending technologies, Germany) Sony α6000 24.3 MP camera with 20mm f/2.8 lens	• Leaf Area Index at 20m altitude • Leaf/biomass growth • Vegetation indices • Chlorophyll index	*A. hypogaea* L. (peanut)	Sarkar et al. (2021)
WEKA (Waikato Environment for Knowledge Analysis) software v3.8.4	ANN				
WOFOST	UAV imaging integration	-	Leaf area index (LAI), biomass, yield	*T. aestivum* (winter wheat)	Yang et al. (2021a)
Hyperspectral Reflectance	MLP, SVM and RF with remote sensing	UniSpec-DC Spectral Analysis System (PP Systems International Inc., USA)	• Biomass yield • Plant growth and development stages	*G. max* (soybean)	Yoosefzadeh-Najafabadi et al. (2021)
Greenotyper	U-Net: CNNs	RPi3 Model B with RPi Camera module v2.1	• Plant area • Greenness • Overlapping growth patterns	*Trifolium repens* (white clover)	Tausen et al. (2020)
Keras	U-Net based CNN segmentation model	2592 x 1944 x 3 resolution camera (5 MP)	Powdery mildew disease detection	*Cucumis sativus* (cucumber)	Lin et al. (2019)

(Continued)

TABLE 2 Continued

Platform	Automation Technology	Imaging Device	Phenotype/ Parameter	Plant Species	References
CropDeep	RetNet with ResNet50 CNN	IoT cameras, Autonomous Spray robots, Autonomous Picking Robots, Mobicamera and Smartphone camera	• Precision farming • Plant identification, growth and location • Different plant variety monitoring • Fruit and vegetable health status	25 plant varieties including *L. sativa Linn.* (lettuce), *A. graveliens Linn.* (celery), *Cucumis Linn.* (cucumber), *B. oleracea Linn.* (cabbage), *S. oleracea Linn.* (spinach), *L. esculentum Mill.* (tomato), *R. sativus Linn.* (turnip)	Zheng et al. (2019)
Alexnet	CNN-Long-Short Term Memories (LSTM) architecture	Canon EOS 650D	Plant growth pattern of different genotypes	*A. thaliana*	Taghavi Namin et al. (2018)
Persistent Homology based topological methods	DIRT (Digital Imaging of Root Traits) Gaussian kernel density estimator Elliptical Fourier descriptors	-	• Leaf shape, serrations and root architecture • Discrimination between genotypes	*Solanum pennellii* (wild tomato)	Li et al. (2018)
PlantCV	U-Net based CNN	Raspberry Pi Camera	Plant convex hull, width and length	*A. thaliana*	Tovar et al. (2018)
		Nikon COOLPIX L830 Camera	Seed size, shape, count and color	*Chenopodium quinoa* Willd. (Quinoa)	
LeafNet	Caffe framework based Deep Learning CNN	*LeafSnap*, *Flavia* and *Foliage* dataset images using Mobile cameras (iPhones mostly)	Species identification through leaf features like edges and venations	*LeafSnap*, *Flavia* and *Foliage* dataset	Barré et al. (2017)
Deep Plant Phenomics (DPP)	Deep CNN with PlantCV module	Canon PowerShot SD1000 7 MP camera, Model B with Raspberry Pi 5 MP camera module	Leaf size, shape and leaf count	*A. thaliana* *N. tabacum* (tobacco)	Ubbens and Stavness (2017) Minervini et al. (2015)
phenoSeeder	KR 10 scara R600-Z300 robot (KUKA Roboter GmbH, Germany)	Oscar F-810C Camera (Allied-Vision Technologies, GmbH, Germany)	Seed projected area, length, width and color	*B. napus* (rapeseed), *H. vulgare* (barley) and *A. thaliana*	Jahnke et al. (2016)
		Grasshopper GRAS-50S5M-C Camera (Point Grey, Canada) with 35mm lens	Seed volume		
UAV remote sensing SAMPLINGTSPN	UAV and GPML (Gausian Processes for Machine Learning) Toolbox	MikroKopter, Hexa XL with Multispectral Tetracam Camera	Nitrogen level prediction at 30m altitude	*Z. mays* (maize)	Tokekar et al. (2016)
DIRT (Digital Imaging of Root Traits)	-	-	Root angles (top and bottom), stem diameter, width of root system	*Z. mays* (maize)	Das et al. (2015)
GARNICS	Robotic system with ML-based algorithms	Robot head with 4 x Point Grey Grasshopper, 3.45 µm pixels Camera and Schneider KreuznachXenoplan 1.4/ 17-0903 lenses Canon PowerShot SD1000 7 MP camera, Model B with Raspberry Pi 5 MP camera module	• Plant detection and localization • Plant and leaf segmentation • Leaf shade, appearance and difference detection • Leaf counting • Leaf growth tracking • Classification based on mutant and treatment recognition and age regression	*A. thaliana* *N. tabacum* (tobacco)	Minervini et al. (2015)

Recent developments in ML and DL based programs can be utilized to overcome the challenges in downstream processing (Bernau et al., 2022). ML has been applied to chromatography system to monitor real time processing, process optimization, retention time prediction and peak monitoring. In order to predict the chromatographic conditions (i.e., solvents and solvent ratio), three vectorization types such as learned embedding, extended-connectivity fingerprints (ECFP), ECFP encoder+FFNN and three machine learning approaches (FFNN, LSTM and CNN), DNN architectures and a set of hyperparameter values were investigated. The best results were achieved for the prediction of solvents and solvent ratio with ECFP LSTM auto-encoder with FFNN as the supervised machine-learning method with an accuracy of 0.95 for first task and 0.982 for second task respectively (Vaškevičius et al., 2021). Several ML models have been developed so far to address some of the challenges in downstream processing such as XGboost for the prediction of column performance (Jiang et al., 2022b), PeakBot for chromatographic peak prediction (Bueschl et al., 2022), DeepRT for peptide retention time prediction (Ma et al., 2017) and an algorithm to predict the HCPs elution behavior (Buyel et al., 2013).

5 Challenges and current limitations

Plant-based expression systems have several advantages for producing proteins, however, also come with limitations and challenges. Here are few limitations and challenges in plant-based expression systems such as low productivity, post-translational modification, protein stability, biosafety concerns, high costs of downstream processing, regulatory approval, and slow translation to applications (Schillberg et al., 2019; Schillberg and Finnern, 2021; Sethi et al., 2021). Even though the plant expression system is cheaper and more scalable than conventional expression systems, expression yields and appropriate post-translational modifications along the plant secretory pathway remain a challenge for many proteins. For instance, fusion viral glycoproteins often expressed in plants give low yield and may not be properly processed in some cases (Margolin et al., 2020b). In comparison to mammalian systems, plant-based expression systems introduce different glycosylation patterns which could have an effect on the immunogenicity and functionality of proteins. Although difficult, methods for achieving human-like glycosylation patterns in plants are being explored by engineering host systems using CRISPR/Cas9-based technologies. The intellectual property (IP) and regulatory body approval is one of the main hurdles in the adoption of molecular farming compared to commercial microbial and mammalian cell expression systems which have a proven track record, particularly in the field of biopharmaceutical manufacture. As a result, the industry continues to view molecular farming as risky and chooses to depend on its tried-and-true systems in most circumstances (Schillberg and Finnern, 2021). The possible hazards posed by genetically modified (GM) plants or animals, including the effect on biodiversity, ecological interactions, and possibility of unforeseen effects, must be carefully evaluated. There is a risk that the transgenes may unintentionally spread to other organisms through gene flow, such as cross-pollination or horizontal gene transfer. For molecular pharming processes and products to be safe, it is crucial to implement effective containment strategies, risk assessment and mitigation measures. Techniques such as chloroplast expression and transient expression in closed culture systems could circumvent the environmental risk of transgene transmission through pollen (Moon et al., 2019; Feng et al., 2022b).

AI-based tools have been developed and deployed for various microbial expression systems such as *E. coli*, *P. pastoris*, *S. cerevisiae* and mammalian cell expression systems including CHO, HEK293, HeLa and MCF7 (Linder et al., 2020; Van Brempt et al., 2020; Smiatek et al., 2021; Feng et al., 2022a; Li et al., 2022a; Packiam et al., 2022). Plant host system remains an unexplored arena for AI incorporation. Creation and maintenance of AI-based training models is mainly hindered by lack of abundant experimental dataset that include but not limited to genome, transcriptome and metabolome sequences; plant cell culture, plant growth and bioreactor conditions; protein extraction and optimization, purification strategies and relative parameters such as protein localization, structure, stability, catalytic activity and solubility. Such limited training dataset renders the ML approaches overfitting (Feng et al., 2020; van Dijk et al., 2021). Intervention of automation and AI models discussed in Tables 1, 2 to predict the conditions and maintenance for the large-scale production in plants is yet to be established as illustrated in Figure 4. Data integration of multiple parameters discussed in Table 1 is needed for optimal protein expression. Further the generation of training dataset for plant cell culture condition optimization necessitates a large collection of data (van Dijk et al., 2021); and *in vitro* testing of enormous experimental procedures in different test conditions for an individual recombinant protein production in real-time is laborious; time-consuming; requires well-equipped research facility and investment for growth optimization, plant maintenance and downstream processing (Schillberg et al., 2019; Hesami et al., 2020; Sarker, 2021; van Dijk et al., 2021; Packiam et al., 2022). Even with the available omics data of model plants used in recombinant biologics production, expression training datasets are insufficient for AI-based host engineering and host selection, vector and gene designing, protein modelling, solubility and stability prediction as they are not integrated yet (van Dijk et al., 2021). A large number of data for each parameter (more than 10,000 data points if required) is needed to perform as an effective training dataset (Barré et al., 2017; Hesami et al., 2020; LaFleur et al., 2022; Yang et al., 2023). The illustration in Figure 5 highlights the requirement of training datasets available globally that could build a web of AI-based prediction and optimization tools to tackle the challenges and increase the production of highly active next generation biologics. Several algorithms have been under-utilized or unutilized to increase the recombinant protein yield. ML algorithm could predict the signal peptides and increase the ER translocation rates in CHO cells (O'Neill et al., 2023), and yet not used in exploring recombinant biologics production in plants. CNN-based prediction models have been used effectively for increased protein expression in microbial systems (Zrimec et al., 2020) and so far no tool has been adapted for plant-based expression systems.

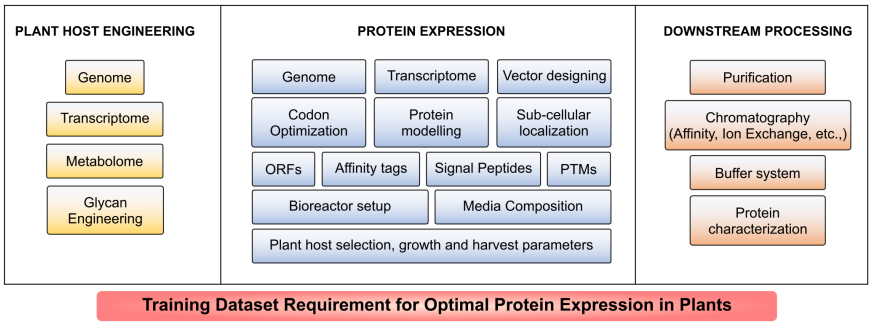

FIGURE 5
Training dataset requirement for optimal protein expression in plants. A large volume of data is required for prediction of optimum conditions at each stage including host engineering, expression and downstream processing for a specific protein to be expressed large-scale in plants.

6 Conclusion and future directions

Plant molecular pharming offers efficient alternate host systems for expression of recombinant biologics. Moreover, the system is robust and cost-effective compared to other hosts. In this review, the concepts of AI in systems engineering for improved production of recombinant biologics were discussed. Several prediction and optimization parameters are known to increase the yield in different expression hosts and integration of machine learning algorithms is new to the plant molecular pharming field. Such plant-based expression parameters include host engineering, growth and maintenance, protein model designing, glycosylation, sialylation, epitope prediction, antibody identification& optimization, regulatory element prediction & optimization and protein stability and activity. Neural network-based ML models when integrated with systems engineering approaches could be advantageous during the manufacture of humanized forms of biologics at various stages of production including seed selection, germination, plant growth parameter optimization, monitoring, recombinant protein modelling, expression, extraction, purification and downstream processing. GEMs and other omics data availability favor the process of designing and optimization of protein production yet more omics (genomics, proteomics, transcriptomics and metabolomics) based studies are needed for complete utilization of ML tools. Transcriptome and metabolome profiles of specific plant hosts in the form of large training data sets need to be fed into neural networks, which then can be used to test the desired function (such as gene knock-out or knock-in). Similarly, parameters of protein production solely based on plant system are to be created as codes using language models and integrated as hierarchical architectures using neural networks. Datasets trained with the discussed parameters using ML models for protein expression in plants could aid in an effective modelling of recombinant biologics and prediction of accurate conditions for protein expression in different plant hosts including but not limited to *N. benthamiana*, *N. tabacum*, *L. sativa* and *O. sativa*. Such ML-based techniques will reduce the time frame and cost of reagents in all the levels of plant-based biologics production rendering functional and active products.

Author contributions

RS proposed the idea of application of AI in plant molecular pharming; SP designed the review manuscript. TG drafted systems biology; SP and TV drafted AI integration concepts and improvised systems biology concepts. RS and BS revised and corrected the manuscript. AS gave expert comments on the technical aspects. All authors contributed to the article and approved the submitted version.

Funding

The authors would like to acknowledge the funding support of University Grants Commission-UK-India Research Initiative (UGC-UKIERI), No.F 184-9/2018(IC), and RashtriyaUchchatar Shiksha Abhiyan (RUSA) 2.0, No. BU/RUSA2.0/BCTRC/2020/BCTRC-CD06, Bharathiar University, India.

Conflict of interest

The authors declare that the research was conducted in the absence of any commercial or financial relationships that could be construed as a potential conflict of interest.

Publisher's note

References

Agarwal, P., Gautam, T., Singh, A. K., and Burma, P. K. (2019). Evaluating the effect of codon optimization on expression of bar gene in transgenic tobacco plants. *J. Plant Biochem. Biotechnol.* 28, 189–202. doi: 10.1007/s13562-019-00506-2

Alam, A., Jiang, L., Kittleson, G. A., Steadman, K. D., Nandi, S., Fuqua, J. L., et al. (2018). Technoeconomic modeling of plant-based griffithsin manufacturing. *Front. Bioeng. Biotechnol.* 6. doi: 10.3389/fbioe.2018.00102

Al-Hawash, A. B., Zhang, X., and Ma, F. (2017). Strategies of codon optimization for high-level heterologous protein expression in microbial expression systems. *Gene Rep.* 9, 46–53. doi: 10.1016/j.genrep.2017.08.006

Ali, S., and Kim, W. C. (2019). A fruitful decade using synthetic promoters in the improvement of transgenic plants. *Front. Plant Sci.* 10. doi: 10.3389/fpls.2019.01433

Allied Market Research. (2023). *Plant-Based Biologics Market by Product Type (Leaf-based, Seed-Based, Fruit-based, Others), by Source (Carrot, Tobacco, Rice, Duckweed, Others), by Target Disease (Gaucher Disease, Fabry Disease, Others): Global Opportunity Analysis and Industry Forecast*. Available at: https://www.alliedmarketresearch.com/plant-based-biologics-market-A74549#:~:text.

Almagro Armenteros, J. J., Tsirigos, K. D., Sønderby, C. K., Petersen, T. N., Winther, O., Brunak, S., et al. (2019). SignalP 5.0 improves signal peptide predictions using deep neural networks. *Nat. Biotechnol.* 37, 420–423. doi: 10.1038/s41587-019-0036-z

Alshehri, S., Alqarni, M., Namazi, N. I., Naguib, I. A., Venkatesan, K., Mosaad, Y. O., et al. (2022). Design of predictive model to optimize the solubility of Oxaprozin as nonsteroidal anti-inflammatory drug. *Sci. Rep.* 12, 1–10. doi: 10.1038/s41598-022-17350-5

Altenburg, J. J., Klaverdijk, M., Cabosart, D., Desmecht, L., Brunekreeft-Terlouw, S. S., Both, J., et al. (2023). Real-time online monitoring of insect cell proliferation and baculovirus infection using digital differential holographic microscopy and machine learning. *Biotechnol. Prog.* 39, e3318. doi: 10.1002/btpr.3318

Amack, S. C., and Antunes, M. S. (2020). CaMV35S promoter – A plant biology and biotechnology workhorse in the era of synthetic biology. *Curr. Plant Biol.* 24, 100179. doi: 10.1016/j.cpb.2020.100179

Arcalis, E., Ibl, V., Hilscher, J., Rademacher, T., Avesani, L., Morandini, F., et al. (2019). Russell-like bodies in plant seeds share common features with prolamin bodies and occur upon recombinant protein production. *Front. Plant Sci.* 10. doi: 10.3389/fpls.2019.00777

Argentinian AntiCovid Consortium. (2020). Structural and functional comparison of SARS-CoV-2-spike receptor binding domain produced in Pichia pastoris and mammalian cells. *Sci. Rep.* 10, 21779. doi: 10.1038/s41598-020-78711-6

Aslan, M. F., Durdu, A., Sabanci, K., and Ropelewska, E. (2022). A comprehensive survey of the recent studies with UAV for precision agriculture in open fields and greenhouses. *Appl. Sci.* 12, 1047. doi: 10.3390/app12031047

Austerjost, J., Söldner, R., Edlund, C., Trygg, J., Pollard, D., and Sjögren, R. (2021). A machine vision approach for bioreactor foam sensing. *SLAS Technol.* 26 (4), 408–414. doi: 10.1177/24726303211008861

Bai, X., Fang, H., He, Y., Zhang, J., Tao, M., Wu, Q., et al. (2023a). Dynamic UAV phenotyping for rice disease resistance analysis based on multisource data. *Plant Phenomics* 5, 1–13. doi: 10.34133/plantphenomics.0019

Bai, X., Liu, P., Cao, Z., Lu, H., Xiong, H., Yang, A., et al. (2023b). Rice plant counting, locating, and sizing method based on high-throughput UAV RGB images. *Plant Phenomics* 5, 1–16. doi: 10.34133/plantphenomics.0020

Banerjee, B. P., Spangenberg, G., and Kant, S. (2022). CBM: an ioT enabled liDAR sensor for in-field crop height and biomass measurements. *Biosensors* 12, 16. doi: 10.3390/bios12010016

Barra, C., Ackaert, C., Reynisson, B., Schockaert, J., Jessen, L. E., Watson, M., et al. (2020). Immunopeptidomic data integration to artificial neural networks enhances protein-drug immunogenicity prediction. *Front. Immunol.* 11. doi: 10.3389/fimmu.2020.01304

Barré, P., Stöver, B. C., Müller, K. F., and Steinhage, V. (2017). LeafNet: A computer vision system for automatic plant species identification. *Ecol. Inform.* 40, 50–56. doi: 10.1016/j.ecoinf.2017.05.005

Belcher, M. S., Vuu, K. M., Zhou, A., Mansoori, N., Agosto Ramos, A., Thompson, M. G., et al. (2020). Design of orthogonal regulatory systems for modulating gene expression in plants. *Nat. Chem. Biol.* 16, 857–865. doi: 10.1038/s41589-020-0547-4

Bernau, C. R., Knödler, M., Emonts, J., Jäpel, R. C., and Buyel, J. F. (2022). The use of predictive models to develop chromatography-based purification processes. *Front. Bioeng. Biotechnol.* 10. doi: 10.3389/fbioe.2022.1009102

Bidarigh fard, A., Dehghan Nayeri, F., and Habibi Anbuhi, M. (2019). Transient expression of etanercept therapeutic protein in tobacco (Nicotiana tabacum L.). *Int. J. Biol. Macromol.* 130, 483–490. doi: 10.1016/j.ijbiomac.2019.02.153

Biswas, S., Khimulya, G., Alley, E. C., Esvelt, K. M., and Church, G. M. (2021). Low-N protein engineering with data-efficient deep learning. *Nat. Methods* 18, 389–396. doi: 10.1038/s41592-021-01100-y

Bogard, N., Linder, J., Rosenberg, A. B., and Seelig, G. (2019). A deep neural network for predicting and engineering alternative polyadenylation. *Cell* 178, 91–106.e23. doi: 10.1016/j.cell.2019.04.046

Bohlender, L. L., Parsons, J., Hoernstein, S. N. W., Rempfer, C., Ruiz-Molina, N., Lorenz, T., et al. (2020). Stable protein sialylation in physcomitrella. *Front. Plant Sci.* 11. doi: 10.3389/fpls.2020.610032

Bolaños-Martínez, O. C., Govea-Alonso, D. O., Cervantes-Torres, J., Hernández, M., Fragoso, G., Sciutto-Conde, E., et al. (2020). Expression of immunogenic poliovirus Sabin type 1 VP proteins in transgenic tobacco. *J. Biotechnol.* 322, 10–20. doi: 10.1016/j.jbiotec.2020.07.007

Bose, R., and Hautop Lund, H. (2022). Convolutional neural network for studying plant nutrient deficiencies. *Proc. Int. Conf. Artif. Life Robot.* 27, 25–29. doi: 10.5954/icarob.2022.is2-2

Bueschl, C., Doppler, M., Varga, E., Seidl, B., Flasch, M., Warth, B., et al. (2022). PeakBot: Machine-learning-based chromatographic peak picking. *Bioinformatics* 38, 3422–3428. doi: 10.1093/bioinformatics/btac344

Buyel, J. F. (2019). Plant molecular farming – Integration and exploitation of side streams to achieve sustainable biomanufacturing. *Front. Plant Sci.* 9. doi: 10.3389/fpls.2018.01893

Buyel, J. F., and Fischer, R. (2014). Generic chromatography-based purification strategies accelerate the development of downstream processes for biopharmaceutical proteins produced in plants. *Biotechnol. J.* 9, 566–577. doi: 10.1002/biot.201300548

Buyel, J. F., Woo, J. A., Cramer, S. M., and Fischer, R. (2013). The use of quantitative structure-activity relationship models to develop optimized processes for the removal of tobacco host cell proteins during biopharmaceutical production. *J. Chromatogr. A* 1322, 18–28. doi: 10.1016/j.chroma.2013.10.076

Cardon, F., Pallisse, R., Bardor, M., Caron, A., Vanier, J., Pierre, J., et al. (2019). Brassica rapa hairy root based expression system leads to the production of highly homogenous and reproducible profiles of recombinant human alpha-L-iduronidase. *Plant Biotechnol. J.* 17 (2), 505–516. doi: 10.1111/pbi.12994

Carreño-Campos, C., Arevalo-Villalobos, J. I., Villarreal, M. L., Ortiz-Caltempa, A., and Rosales-Mendoza, S. (2022). Establishment of the carrot-made LTB-syn antigen cell line in shake flask and airlift bioreactor cultures. *Planta Med.* 88, 1060–1068. doi: 10.1055/a-1677-4135

Chen, Q., and Davis, K. R. (2016). The potential of plants as a system for the development and production of human biologics [version 1; referees: 3 approved]. *F1000Research* 5, 1–8. doi: 10.12688/F1000RESEARCH.8010.1

Chen, Y., Yang, O., Sampat, C., Bhalode, P., Ramachandran, R., and Ierapetritou, M. (2020). Digital twins in pharmaceutical and biopharmaceutical manufacturing. *Processes* 8, 1–33. doi: 10.3390/pr8091088

Chia, S., Tay, S. J., Song, Z., Yang, Y., Walsh, I., and Pang, K. T. (2023). Enhancing pharmacokinetic and pharmacodynamic properties of recombinant therapeutic proteins by manipulation of sialic acid content. *Biomed. Pharmacother.* 163, 114757. doi: 10.1016/j.biopha.2023.114757

Constant, D. A., Gutierrez, J. M., Sastry, A. V., Viazzo, R., Smith, N. R., Hossain, J., et al. (2023). Deep learning-based codon optimization with large-scale synonymous variant datasets enables generalized tunable protein expression. *bioRxiv* 2023, 2.11.528149. doi: 10.1101/2023.02.11.528149

Costello, Z., and Martin, H. G. (2018). A machine learning approach to predict metabolic pathway dynamics from time-series multiomics data. *NPJ Syst. Biol. Appl.* 4, 1–14. doi: 10.1038/s41540-018-0054-3

Culley, C., Vijayakumar, S., Zampieri, G., and Angione, C. (2020). A mechanism-aware and multiomic machine-learning pipeline characterizes yeast cell growth. *Proc. Natl. Acad. Sci.* 117, 18869–18879. doi: 10.1073/pnas.2002959117

Das, A., Schneider, H., Burridge, J., Ascanio, A. K. M., Wojciechowski, T., Topp, C. N., et al. (2015). Digital imaging of root traits (DIRT): A high-throughput computing and collaboration platform for field-based root phenomics. *Plant Methods* 11, 1–12. doi: 10.1186/s13007-015-0093-3

Dehdashti, S. M., Acharjee, S., Nomani, A., and Deka, M. (2020). Production of pharmaceutical active recombinant globular adiponectin as a secretory protein in Withania Somnifera hairy root culture. *J. Biotechnol.* 323, 302–312. doi: 10.1016/j.jbiotec.2020.07.012

Dhivya, S., Priya, S. H., and Sathishkumar, R. (2021). "Opportunities in Agriculture, Biomedicine, and Healthcare," in *Artificial Intelligence Theory, Models, and Applications*. Eds. P. Kaliraj and T. Devi (Boca Raton, FL, Oxon, OX: CRC Press), 121.

Ding, Z., Guan, F., Xu, G., Wang, Y., Yan, Y., Zhang, W., et al. (2022). MPEPE, a predictive approach to improve protein expression in E. coli based on deep learning. *Comput. Struct. Biotechnol. J.* 20, 1142–1153. doi: 10.1016/j.csbj.2022.02.030

dos Reis, M., Wernisch, L., and Savva, R. (2003). Unexpected correlations between gene expression and codon usage bias from microarray data for the whole Escherichia coli K-12 genome. *Nucleic Acids Res.* 31, 6976–6985. doi: 10.1093/nar/gkg897

Doyle, F., Leonardi, A., Endres, L., Tenenbaum, S. A., Dedon, P. C., and Begley, T. J. (2016). Gene- and genome-based analysis of significant codon patterns in yeast, rat and mice genomes with the CUT Codon UTilization tool. *Methods* 107, 98–109. doi: 10.1016/j.ymeth.2016.05.010

Dubey, K. K., Luke, G. A., Knox, C., Kumar, P., Pletschke, B. I., Singh, P. K., et al. (2018). Vaccine and antibody production in plants: Developments and computational tools. *Brief. Funct. Genomics* 17, 295–307. doi: 10.1093/bfgp/ely020

Feng, J., Jiang, M., Shih, J., and Chai, Q. (2022a). Antibody apparent solubility prediction from sequence by transfer learning. *iScience* 25, 105173. doi: 10.1016/j.isci.2022.105173

Feng, Z., Li, X., Fan, B., Zhu, C., and Chen, Z. (2022b). Maximizing the production of recombinant proteins in plants: from transcription to protein stability. *Int. J. Mol. Sci.* 23, 13516. doi: 10.3390/ijms232113516

Feng, L., Zhang, Z., Ma, Y., Du, Q., Williams, P., Drewry, J., et al. (2020). Alfalfa yield prediction using UAV-based hyperspectral imagery and ensemble learning. *Remote Sens.* 12, 2028. doi: 10.3390/rs12122028

Finkel, Y., Mizrahi, O., Nachshon, A., Weingarten-Gabbay, S., Morgenstern, D., Yahalom-Ronen, Y., et al. (2021). The coding capacity of SARS-CoV-2. *Nature* 589, 125–130. doi: 10.1038/s41586-020-2739-1

Fox, D. M., Branson, K. M., and Walker, R. C. (2021). mRNA codon optimization with quantum computers. *PloS One* 16, 1–16. doi: 10.1371/journal.pone.0259101

Fu, H., Liang, Y., Zhong, X., Pan, Z., Huang, L., Zhang, H., et al. (2020). Codon optimization with deep learning to enhance protein expression. *Sci. Rep.* 10, 17617. doi: 10.1038/s41598-020-74091-z

Fu, Y., Yang, G., Song, X., Li, Z., Xu, X., Feng, H., et al. (2021). Improved estimation of winter wheat aboveground biomass using multiscale textures extracted from UAV-based digital images and hyperspectral feature analysis. *Remote Sens.* 13, 1–22. doi: 10.3390/rs13040581

Fulton, A., Lai, H., Chen, Q., and Zhang, C. (2015). Purification of monoclonal antibody against Ebola GP1 protein expressed in Nicotiana benthamiana. *J. Chromatogr. A* 1389, 128–132. doi: 10.1016/j.chroma.2015.02.013

Gaughan, C. L. (2016). The present state of the art in expression, production and characterization of monoclonal antibodies. *Mol. Divers.* 20, 255–270. doi: 10.1007/s11030-015-9625-z

Gelvin, S. B. (2003). Agrobacterium-mediated plant transformation: the biology behind the "gene-jockeying" tool. *Microbiol. Mol. Biol. Rev.* 67, 16–37. doi: 10.1128/MMBR.67.1.16-37.2003

Ghag, S. B., Adki, V. S., Ganapathi, T. R., and Bapat, V. A. (2021). Plant platforms for efficient heterologous protein production. *Biotechnol. Bioprocess Eng.* 26, 546–567. doi: 10.1007/s12257-020-0374-1

Gomord, V., and Faye, L. (2004). Posttranslational modification of therapeutic proteins in plants. *Curr. Opin. Plant Biol.* 7, 171–181. doi: 10.1016/j.pbi.2004.01.015

Goulet, D. R., Yan, Y., Agrawal, P., Waight, A. B., Mak, A. N. S., and Zhu, Y. (2023). Codon optimization using a recurrent neural network. *J. Comput. Biol.* 30, 70–81. doi: 10.1089/cmb.2021.0458

Grandits, M., Grünwald-Gruber, C., Gastine, S., Standing, J. F., Reljic, R., Teh, A. Y.-H., et al. (2023). Improving the efficacy of plant-made anti-HIV monoclonal antibodies for clinical use. *Front. Plant Sci.* 14. doi: 10.3389/fpls.2023.1126470

Gupta, A., and Zou, J. (2018). Feedback GAN (FBGAN) for DNA: a novel feedback-loop architecture for optimizing protein functions. *arXiv Prepr. arXiv* 1804, 1694. doi: 10.48550/arXiv.1804.01694

Gutierrez-valdes, N., Häkkinen, S. T., Lemasson, C., Guillet, M., Ritala, A., and Cardon, F. (2020). Hairy root cultures — A versatile tool with multiple applications. *Front. Plant. Sci.* 11, 1–11. doi: 10.3389/fpls.2020.00033

Hager, K. J., Pérez Marc, G., Gobeil, P., Diaz, R. S., Heizer, G., Llapur, C., et al. (2022). Efficacy and safety of a recombinant plant-based adjuvanted covid-19 vaccine. *N. Engl. J. Med.* 386, 2084–2096. doi: 10.1056/nejmoa2201300

Han, X., Wang, X., and Zhou, K. (2019). Develop machine learning-based regression predictive models for engineering protein solubility. *Bioinformatics* 35, 4640–4646. doi: 10.1093/bioinformatics/btz294

Hanittinan, O., Oo, Y., Chaotham, C., Rattanapisit, K., Shanmugaraj, B., and Phoolcharoen, W. (2020). Expression optimization, purification and in *vitro* characterization of human epidermal growth factor produced in Nicotiana benthamiana. *Biotechnol. Rep.* 28, e00524. doi: 10.1016/j.btre.2020.e00524

Hassan, M. M., Zhang, Y., Yuan, G., De, K., Chen, J. G., Muchero, W., et al. (2021). Construct design for CRISPR/Cas-based genome editing in plants. *Trends Plant Sci.* 26, 1133–1152. doi: 10.1016/j.tplants.2021.06.015

He, W., Baysal, C., Lobato Gómez, M., Huang, X., Alvarez, D., Zhu, C., et al. (2021). Contributions of the international plant science community to the fight against infectious diseases in humans—part 2: Affordable drugs in edible plants for endemic and re-emerging diseases. *Plant Biotechnol. J.* 19, 1921–1936. doi: 10.1111/pbi.13658

Heenatigala, P. P. M., Sun, Z., Yang, J., Zhao, X., and Hou, H. (2020). Expression of lamB vaccine antigen in wolffia globosa (Duck weed) against fish vibriosis. *Front. Immunol.* 11. doi: 10.3389/fimmu.2020.01857

Hesami, M., Naderi, R., Tohidfar, M., and Yoosefzadeh-Najafabadi, M. (2020). Development of support vector machine-based model and comparative analysis with artificial neural network for modeling the plant tissue culture procedures: Effect of plant growth regulators on somatic embryogenesis of chrysanthemum, as a case study. *Plant Methods* 16, 1–15. doi: 10.1186/s13007-020-00655-9

Holásková, E., Galuszka, P., Mičúchová, A., Šebela, M., Öz, M. T., and Frébort, I. (2018). Molecular farming in barley: development of a novel production platform to produce human antimicrobial peptide LL-37. *Biotechnol. J.* 13, 1700628. doi: 10.1002/biot.201700628

Hosseini, M. S., Arab, M. M., Soltani, M., and Eftekhari, M. (2022). Predictive modeling of Persian walnut (Juglans regia L.) in *vitro* proliferation media using machine learning approaches : a comparative study of ANN, KNN and GEP models. *Plant Methods* 18 (1), 1–24. doi: 10.1186/s13007-022-00871-5

Imamura, T., Isozumi, N., Higashimura, Y., Ohki, S., and Mori, M. (2021). Production of ORF8 protein from SARS – CoV – 2 using an inducible virus – mediated expression system in suspension – cultured tobacco BY – 2 cells. *Plant Cell Rep.* 40, 433–436. doi: 10.1007/s00299-020-02654-5

Islam, M. R., Choi, S., Muthamilselvan, T., Shin, K., and Hwang, I. (2020). *In vivo* removal of N-terminal fusion domains from recombinant target proteins produced in nicotiana benthamiana. *Front. Plant Sci.* 11. doi: 10.3389/fpls.2020.00440

Islam, M. R., Kwak, J. W., Lee, J.-s., Hong, S. W., Khan, M. R. I., Lee, Y., et al. (2019). Cost-effective production of tag-less recombinant protein in Nicotiana benthamiana. *Plant Biotechnol. J.* 17, 1094–1105. doi: 10.1111/pbi.13040

Iyappan, G., Shanmugaraj, B. M., Inchakalody, V., Ma, J. K.-C., and Ramalingam, S. (2018). Potential of plant biologics to tackle the epidemic like situations - case studies involving viral and bacterial candidates. *Int. J. Infect. Dis.* 73, 363. doi: 10.1016/j.ijid.2018.04.4236

Izadi, S., Kunnummel, V., Steinkellner, H., Werner, S., and Castilho, A. (2023). Assessment of transient expression strategies to sialylate recombinant proteins in N. benthamiana. *J. Biotechnol.* 365, 48–53. doi: 10.1016/j.jbiotec.2023.02.004

Jahnke, S., Roussel, J., Hombach, T., Kochs, J., Fischbach, A., Huber, G., et al. (2016). phenoSeeder - A robot system for automated handling and phenotyping of individual seeds. *Plant Physiol.* 172, 1358–1370. doi: 10.1104/pp.16.01122

Jain, R., Jain, A., Mauro, E., LeShane, K., and Densmore, D. (2023). ICOR: improving codon optimization with recurrent neural networks. *BMC Bioinf.* 24, 132. doi: 10.1186/s12859-023-05246-8

Jansing, J., Sack, M., Augustine, S. M., Fischer, R., and Bortesi, L. (2019). CRISPR/Cas9-mediated knockout of six glycosyltransferase genes in Nicotiana benthamiana for the production of recombinant proteins lacking β-1,2-xylose and core α-1,3-fucose. *Plant Biotechnol. J.* 17, 350–361. doi: 10.1111/pbi.12981

Jiang, J., Johansen, K., Stanschewski, C. S., Wellman, G., Mousa, M. A. A., Fiene, G. M., et al. (2022a). Phenotyping a diversity panel of quinoa using UAV-retrieved leaf area index, SPAD-based chlorophyll and a random forest approach. *Precis. Agric.* 23, 961–983. doi: 10.1007/s11119-021-09870-3

Jiang, Q., Seth, S., Scharl, T., Schroeder, T., Jungbauer, A., and Dimartino, S. (2022b). Prediction of the performance of pre-packed purification columns through machine learning. *J. Sep. Sci.* 45, 1445–1457. doi: 10.1002/jssc.202100864

Jiang, Y., Wang, D., Yao, Y., Eubel, H., Künzler, P., Møller, I. M., et al. (2021). MULocDeep: A deep-learning framework for protein subcellular and suborganellar localization prediction with residue-level interpretation. *Comput. Struct. Biotechnol. J.* 19, 4825–4839. doi: 10.1016/j.csbj.2021.08.027

Jin, L., Wang, Y., Liu, X., Peng, R., Lin, S., Sun, D., et al. (2022). Codon optimization of chicken β Gallinacin-3 gene results in constitutive expression and enhanced antimicrobial activity in transgenic Medicago sativa L. *Gene* 835, 146656. doi: 10.1016/j.gene.2022.146656

Jolles, J. W. (2021). Broad-scale applications of the Raspberry Pi: A review and guide for biologists. *Methods Ecol. Evol.* 12, 1562–1579. doi: 10.1111/2041-210X.13652

Jugler, C., Grill, F. J., Eidenberger, L., Karr, T. L., Grys, T. E., Steinkellner, H., et al. (2022). Humanization and expression of IgG and IgM antibodies in plants as potential diagnostic reagents for Valley Fever. *Front. Plant Sci.* 13. doi: 10.3389/fpls.2022.925008

Jung, J. W., Shin, J. H., Lee, W. K., Begum, H., Min, C. H., Jang, M. H., et al. (2021). Inactivation of the β (1, 2)-xylosyltransferase and the α (1, 3)-fucosyltransferase gene in rice (Oryza sativa) by multiplex CRISPR/Cas9 strategy. *Plant Cell Rep.* 40, 1025–1035. doi: 10.1007/s00299-021-02667-8

Kalemati, M., Darvishi, S., and Koohi, S. (2023). CapsNet-MHC predicts peptide-MHC class I binding based on capsule neural networks. *Commun. Biol.* 6, 492. doi: 10.1038/s42003-023-04867-2

Khoshmaram, A., Zabihi, S., Pelalak, R., Pishnamazi, M., Marjani, A., and Shirazian, S. (2021). Supercritical process for preparation of nanomedicine: oxaprozin case study. *Chem. Eng. Technol.* 44, 208–212. doi: 10.1002/ceat.202000411

Khurana, S., Rawi, R., Kunji, K., Chuang, G. Y., Bensmail, H., and Mall, R. (2018). DeepSol: A deep learning framework for sequence-based protein solubility prediction. *Bioinformatics* 34, 2605–2613. doi: 10.1093/bioinformatics/bty166

Kim, G. B., Kim, W. J., Kim, H. U., and Lee, S. Y. (2020). Machine learning applications in systems metabolic engineering. *Curr. Opin. Biotechnol.* 64, 1–9. doi: 10.1016/j.copbio.2019.08.010

Koşaloğlu-Yalçın, Z., Lee, J., Greenbaum, J., Schoenberger, S. P., Miller, A., Kim, Y. J., et al. (2022). Combined assessment of MHC binding and antigen abundance improves T cell epitope predictions. *iScience* 25, 103850. doi: 10.1016/j.isci.2022.103850

Kraus, O. Z., Grys, B. T., Ba, J., Chong, Y., Frey, B. J., Boone, C., et al. (2017). Automated analysis of high-content microscopy data with deep learning. *Mol. Syst. Biol.* 13, 1–15. doi: 10.15252/msb.20177551

Kumar, A. U., and Ling, A. P. K. (2021). Gene introduction approaches in chloroplast transformation and its applications. *J. Genet. Eng. Biotechnol.* 19 (1), 1–10. doi: 10.1186/s43141-021-00255-7

Kwon, K. C., Chan, H. T., León, I. R., Williams-Carrier, R., Barkan, A., and Daniell, H. (2016). Codon optimization to enhance expression yields insights into chloroplast translation. *Plant Physiol.* 172, 62–77. doi: 10.1104/pp.16.00981

LaFleur, T. L., Hossain, A., and Salis, H. M. (2022). Automated model-predictive design of synthetic promoters to control transcriptional profiles in bacteria. *Nat. Commun.* 13, 5159. doi: 10.1038/s41467-022-32829-5

Lai, P. K. (2022). DeepSCM: An efficient convolutional neural network surrogate model for the screening of therapeutic antibody viscosity. *Comput. Struct. Biotechnol. J.* 20, 2143–2152. doi: 10.1016/j.csbj.2022.04.035

Lecun, Y., Bengio, Y., and Hinton, G. (2015). Deep learning. *Nature* 521, 436–444. doi: 10.1038/nature14539

Li, F., Chen, Y., Qi, Q., Wang, Y., Yuan, L., Huang, M., et al. (2022a). Improving recombinant protein production by yeast through genome-scale modeling using proteome constraints. *Nat. Commun.* 13, 1–13. doi: 10.1038/s41467-022-30689-7

Li, M., Frank, M. H., Coneva, V., Mio, W., Chitwood, D. H., and Topp, C. N. (2018). The persistent homology mathematical framework provides enhanced genotype-to-phenotype associations for plant morphology. *Plant Physiol.* 177, 1382–1395. doi: 10.1104/pp.18.00104

Li, X., Li, X., Fan, B., Zhu, C., and Chen, Z. (2022b). Specialized endoplasmic reticulum-derived vesicles in plants: Functional diversity, evolution, and biotechnological exploitation. *J. Integr. Plant Biol.* 64, 821–835. doi: 10.1111/jipb.13233

Li, Y., Stern, D., Lin, L., Mills, J., Ou, S., Morrow, M., et al. (2019). Emerging biomaterials for downstream manufacturing of therapeutic proteins. *Acta Biomaterialia* 95, 73–90. doi: 10.1016/j.actbio.2019.03.015

Lim, C. Y., Kim, D. S., Kang, Y., Lee, Y. R., Kim, K., Kim, D. S., et al. (2022). Immune responses to plant-derived recombinant colorectal cancer glycoprotein epCAM-fcK fusion protein in mice. *Biomol. Ther.* 30, 546–552. doi: 10.4062/biomolther.2022.103

Limkul, J., Iizuka, S., Sato, Y., Misaki, R., Ohashi, T., Ohashi, T., et al. (2016). The production of human glucocerebrosidase in glyco-engineered Nicotiana benthamiana plants. *Plant Biotechnol. J.* 14, 1682–1694. doi: 10.1111/pbi.12529

Lin, K., Gong, L., Huang, Y., Liu, C., and Pan, J. (2019). Deep learning-based segmentation and quantification of cucumber powdery mildew using convolutional neural network. *Front. Plant Sci.* 10. doi: 10.3389/fpls.2019.00155

Linder, J., Bogard, N., Rosenberg, A. B., and Seelig, G. (2020). A generative neural network for maximizing fitness and diversity of synthetic DNA and protein sequences. *Cell Syst.* 11, 49–62.e16. doi: 10.1016/j.cels.2020.05.007

Liu, X. (2017). Deep recurrent neural network for protein function prediction from sequence. *arXiv Prepr*. doi: 10.48550/arXiv.1701.08318

Liu, Z., Jin, J., Cui, Y., Xiong, Z., Nasiri, A., Zhao, Y., et al. (2022b). DeepSeqPanII: an interpretable recurrent neural network model with attention mechanism for peptide-HLA class II binding prediction. *IEEE/ACM Trans. Comput. Biol. Bioinforma.* 19, 2188–2196. doi: 10.1109/TCBB.2021.3074927

Liu, B., Sträuber, H., Saraiva, J., Harms, H., Silva, S. G., and Kasmanas, J. C. (2022a). Machine learning-assisted identification of bioindicators predicts medium-chain carboxylate production performance of an anaerobic mixed culture. *Microbiome* 10, 1–21. doi: 10.1186/s40168-021-01219-2

Lobato Gómez, M., Huang, X., Alvarez, D., He, W., Baysal, C., Zhu, C., et al. (2021). Contributions of the international plant science community to the fight against human infectious diseases – part 1: epidemic and pandemic diseases. *Plant Biotechnol. J.* 19, 1901–1920. doi: 10.1111/pbi.13657

Lu, C., Liu, C., Sun, X., Wan, P., Ni, J., Wang, L., et al. (2021). Bioinformatics analysis, codon optimization and expression of ovine pregnancy associated Glycoprotein-7 in HEK293 cells. *Theriogenology* 172, 27–35. doi: 10.1016/j.theriogenology.2021.05.027

Luo, Y., Jiang, G., Yu, T., Liu, Y., Vo, L., Ding, H., et al. (2021). ECNet is an evolutionary context-integrated deep learning framework for protein engineering. *Nat. Commun.* 12, 5743. doi: 10.1038/s41467-021-25976-8

Ma, J. K. C., Drake, P. M. W., and Christou, P. (2003). The production of recombinant pharmaceutical proteins in plants. *Nat. Rev. Genet.* 4, 794–805. doi: 10.1038/nrg1177

Ma, J., Yu, M. K., Fong, S., Ono, K., Sage, E., Demchak, B., et al. (2018). Using deep learning to model the hierarchical structure and function of a cell. *Nat. Methods* 15, 290–298. doi: 10.1038/nmeth.4627

Ma, C., Zhu, Z., Ye, J., Yang, J., Pei, J., Xu, S., et al. (2017). DeepRT: deep learning for peptide retention time prediction in proteomics. *arXiv Prepr*. doi: 10.48550/arXiv.1705.05368

Macharoen, K., Du, M., Jung, S., McDonald, K. A., and Nandi, S. (2021). Production of recombinant butyrylcholinesterase from transgenic rice cell suspension cultures in a pilot-scale bioreactor. *Biotechnol. Bioeng.* 118, 1431–1443. doi: 10.1002/bit.27638

Maimaitijiang, M., Sagan, V., Sidike, P., Daloye, A. M., Erkbol, H., and Fritschi, F. B. (2020). Crop monitoring using satellite/UAV data fusion and machine learning. *Remote Sens.* 12, 1357. doi: 10.3390/RS12091357

Makowski, E. K., Chen, H., Lambert, M., Bennett, E. M., Eschmann, N. S., Zhang, Y., et al. (2022). Reduction of therapeutic antibody self-association using yeast-display selections and machine learning. *MAbs* 14, 2146629. doi: 10.1080/19420862.2022.2146629

Margolin, E., Oh, Y. J., Verbeek, M., Naude, J., Ponndorf, D., Meshcheriakova, Y. A., et al. (2020b). Co-expression of human calreticulin significantly improves the production of HIV gp140 and other viral glycoproteins in plants. *Plant Biotechnol. J.* 18, 2109–2117. doi: 10.1111/pbi.13369

Margolin, E. A., Strasser, R., Chapman, R., Williamson, A.-L., Rybicki, E. P., and Meyers, A. E. (2020a). Engineering the plant secretory pathway for the production of next-generation pharmaceuticals. *Trends Biotechnol.* 38, 1034–1044. doi: 10.1016/j.tibtech.2020.03.004

Markova, E. A., Shaw, R. E., and Reynolds, C. R. (2022). Prediction of strain engineerings that amplify recombinant protein secretion through the machine learning approach MaLPHAS. *Eng. Biol.* 6, 82–90. doi: 10.1049/enb2.12025

Marques, L. É. C., Silva, B. B., Dutra, R. F., Florean, E. O. P. T., Menassa, R., and Guedes, M. I. F. (2020). Transient expression of dengue virus NS1 antigen in nicotiana benthamiana for use as a diagnostic antigen. *Front. Plant Sci.* 10. doi: 10.3389/fpls.2019.01674

Martiny, H. M., Armenteros, J. J. A., Johansen, A. R., Salomon, J., and Nielsen, H. (2021). Deep protein representations enable recombinant protein expression prediction. *Comput. Biol. Chem.* 95, 107596. doi: 10.1016/j.compbiolchem.2021.107596

Masson, H. O., Kuo, C.-C., Malm, M., Lundqvist, M., Sievertsson, Å., Berling, A., et al. (2022). Deciphering the determinants of recombinant protein yield across the human secretome. *bioRxiv* 2022, 12.12.520152. doi: 10.1101/2022.12.12.520152

McNulty, M. J., Gleba, Y., Tusé, D., Hahn-Löbmann, S., Giritch, A., Nandi, S., et al. (2020). Techno-economic analysis of a plant-based platform for manufacturing antimicrobial proteins for food safety. *Biotechnol. Prog.* 36, e2896. doi: 10.1002/btpr.2896

Mestre, M., Ramos, J., Costa, R. S., Striedner, G., and Oliveira, R. (2022). *A general deep hybrid model for bioreactor systems : Combining first principles with deep neural networks*. Amsterdam: Elsevier. Vol. 165. doi: 10.1016/j.compchemeng.2022.107952

Mettu, R. R., Charles, T., and Landry, S. J. (2016). CD4+ T-cell epitope prediction using antigen processing constraints. *J. Immunol. Methods* 432, 72–81. doi: 10.1016/j.jim.2016.02.013

Minervini, M., Fischbach, A., Scharr, H., and Tsaftaris, S. A. (2015). Finely-grained annotated datasets for image-based plant phenotyping. *Pattern Recognit. Lett.* 81, 80–89. doi: 10.1016/j.patrec.2015.10.013

Minervini, M., Giuffrida, M. V., Perata, P., and Tsaftaris, S. A. (2017). Phenotiki: an open software and hardware platform for affordable and easy image-based phenotyping of rosette-shaped plants. *Plant J.* 90, 204–216. doi: 10.1111/tpj.13472

Mirzaee, M., Osmani, Z., Frébortová, J., and Frébort, I. (2022). Recent advances in molecular farming using monocot plants. *Biotechnol. Adv.* 58, 107913. doi: 10.1016/j.bioteChadv.2022.107913

Miura, K., Yoshida, H., Nosaki, S., Kaneko, M. K., and Kato, Y. (2020). RAP tag and PMab-2 antibody: A tagging system for detecting and purifying proteins in plant cells. *Front. Plant Sci.* 11. doi: 10.3389/fpls.2020.510444

Monteiro, A., Santos, S., and Gonçalves, P. (2021). Precision agriculture for crop and livestock farming—Brief review. *Animals* 11, 1–18. doi: 10.3390/ani11082345

Moon, K.-B., Jeon, J.-H., Choi, H., Park, J.-S., Park, S.-J., Lee, H.-J., et al. (2022). Construction of SARS-CoV-2 virus-like particles in plant. *Sci. Rep.* 12, 1005. doi: 10.1038/s41598-022-04883-y

Moon, K., Park, J., Park, Y., Song, I., Lee, H., Cho, H. S., et al. (2019). Development of systems for the production of plant-derived biopharmaceuticals. *Plants* 9, 30. doi: 10.3390/plants9010030

Mor, T. S. (2015). Molecular pharming's foot in the FDA's door: Protalix's trailblazing story. *Biotechnol. Lett.* 37, 2147–2150. doi: 10.1007/s10529-015-1908-z

Moss, D. L., Park, H. W., Mettu, R. R., and Landry, S. J. (2019). Deimmunizing substitutions in Pseudomonas exotoxin domain III perturb antigen processing without eliminating T-cell epitopes. *J. Biol. Chem.* 294, 4667–4681. doi: 10.1074/jbc.RA118.006704

Munasinghe, S. P., Somaratne, S., and Weerakoon, S. R. (2020). Prediction of chemical composition for callus production in Gyrinops walla Gaetner through machine learning. *Inf. Process. Agric.* 7, 511–522. doi: 10.1016/j.inpa.2019.12.001

Navarre, C., Smargiasso, N., Duvivier, L., Nader, J., Far, J., De Pauw, E., et al. (2017). N-Glycosylation of an IgG antibody secreted by Nicotiana tabacum BY-2 cells can be modulated through co-expression of human β-1,4-galactosyltransferase. *Transgenic Res.* 26, 375–384. doi: 10.1007/s11248-017-0013-6

O'Neill, P., Mistry, R. K., Brown, A. J., and James, D. C. (2023). Protein-specific signal peptides for mammalian vector engineering. *bioRxiv*, 532380. doi: 10.1101/2023.03.14.532380

ORF Genetics. (2023). Available at: https://www.orfgenetics.com/.

Ötes, O., Flato, H., Winderl, J., Hubbuch, J., and Capito, F. (2017). Feasibility of using continuous chromatography in downstream processing : Comparison of costs and product quality for a hybrid process vs. a conventional batch process. *J. Biotechnol.* 259, 213–220. doi: 10.1016/j.jbiotec.2017.07.001

Packiam, K. A. R., Ooi, C. W., Li, F., Mei, S., Tey, B. T., Ong, H. F., et al. (2022). PERISCOPE-Opt: Machine learning-based prediction of optimal fermentation conditions and yields of recombinant periplasmic protein expressed in Escherichia coli. *Comput. Struct. Biotechnol. J.* 20, 2909–2920. doi: 10.1016/j.csbj.2022.06.006

Page, M. T., Parry, M. A. J., and Carmo-Silva, E. (2019). A high-throughput transient expression system for rice. *Plant Cell Environ.* 42, 2057–2064. doi: 10.1111/pce.13542

Pan, X., Zuallaert, J., Wang, X., Shen, H. B., Campos, E. P., Marushchak, D. O., et al. (2020). ToxDL: Deep learning using primary structure and domain embeddings for assessing protein toxicity. *Bioinformatics* 36, 5159–5168. doi: 10.1093/bioinformatics/btaa656

Park, S. R., Lim, C. Y., Kim, D. S., and Ko, K. (2015). Optimization of ammonium sulfate concentration for purification of colorectal cancer vaccine candidate recombinant protein GA733-Fck isolated from plants. *Front. Plant Sci.* 6. doi: 10.3389/fpls.2015.01040

Peyret, H., Brown, J. K. M., and Lomonossoff, G. P. (2019). Improving plant transient expression through the rational design of synthetic 5′ and 3′ untranslated regions. *Plant Methods* 15, 1–13. doi: 10.1186/s13007-019-0494-9

Quang, D., and Xie, X. (2019). FactorNet: A deep learning framework for predicting cell type specific transcription factor binding from nucleotide-resolution sequential data. *Methods* 166, 40–47. doi: 10.1016/j.ymeth.2019.03.020

Qureshi, A. I. (2016). "Chapter 11 - Treatment of Ebola Virus Disease: Therapeutic Agents," in *Ebola Virus Disease: From Origin to Outbreak*. Ed. A. Qureshi (London, San Diego, Cambridge, Oxford: Academic Press), 159–166. doi: 10.1016/B978-0-12-804230-4.00011-X

Radivojević, T., Costello, Z., Workman, K., and Garcia Martin, H. (2020). A machine learning Automated Recommendation Tool for synthetic biology. *Nat. Commun.* 11, 1–14. doi: 10.1038/s41467-020-18008-4

Ramos, J. R. C., Oliveira, G. P., Dumas, P., and Oliveira, R. (2022). Genome-scale modeling of Chinese hamster ovary cells by hybrid semi-parametric flux balance analysis. *Bioprocess Biosyst. Eng.* 45, 1889–1904. doi: 10.1007/s00449-022-02795-9

Ramzi, A. B., Baharum, S. N., Bunawan, H., and Scrutton, N. S. (2020). Streamlining natural products biomanufacturing with omics and machine learning driven microbial engineering. *Front. Bioeng. Biotechnol.* 8. doi: 10.3389/fbioe.2020.608918

Rattanapisit, K., Shanmugaraj, B., Manopwisedjaroen, S., Purwono, P. B., Siriwattananon, K., Khorattanakulchai, N., et al. (2020). Rapid production of SARS-CoV-2 receptor binding domain (RBD) and spike specific monoclonal antibody CR3022 in Nicotiana benthamiana. *Sci. Rep.* 10, 17698. doi: 10.1038/s41598-020-74904-1

Rawat, P., Prabakaran, R., Kumar, S., and Gromiha, M. M. (2021). AbsoluRATE: An in-silico method to predict the aggregation kinetics of native proteins. *Biochim. Biophys. Acta - Proteins Proteomics* 1869, 140682. doi: 10.1016/j.bbapap.2021.140682

Routray, M., Vipsita, S., Sundaray, A., and Kulkarni, S. (2022). DeepRHD: An efficient hybrid feature extraction technique for protein remote homology detection using deep learning strategies. *Comput. Biol. Chem.* 100, 107749. doi: 10.1016/j.compbiolchem.2022.107749

Rozov, S. M., and Deineko, E. V. (2019). Strategies for optimizing recombinant protein synthesis in plant cells: classical approaches and new directions. *Mol. Biol.* 53, 157–175. doi: 10.1134/S0026893319020146

Ruffolo, J. A., Guerra, C., Mahajan, S. P., Sulam, J., and Gray, J. J. (2020). Geometric potentials from deep learning improve prediction of CDR H3 loop structures. *Bioinformatics* 36, I268–I275. doi: 10.1093/BIOINFORMATICS/BTAA457

Ruffolo, J. A., Sulam, J., and Gray, J. J. (2022). Antibody structure prediction using interpretable deep learning. *Patterns* 3, 100406. doi: 10.1016/j.patter.2021.100406

Ruffoni, B., Pistelli, L., Bertoli, A., and Pistelli, L. (2010). Plant cell cultures: Bioreactors for industrial production. *Adv. Exp. Med. Biol.* 698, 203–221. doi: 10.1007/978-1-4419-7347-4_15

Russell, S. J. (2010). *Artificial intelligence a modern approach* (New Jersey: Pearson Education, Inc).

Sabi, R., Daniel, R. V., and Tuller, T. (2017). StAIcalc: tRNA adaptation index calculator based on species-specific weights. *Bioinformatics* 33, 589–591. doi: 10.1093/bioinformatics/btw647

Sahu, S. S., Loaiza, C. D., and Kaundal, R. (2021). Plant-mSubP: A computational framework for the prediction of single- And multi-target protein subcellular localization using integrated machine-learning approaches. *AoB Plants* 12, 1–10. doi: 10.1093/AOBPLA/PLZ068

Sainsbury, F. (2020). Innovation in plant-based transient protein expression for infectious disease prevention and preparedness. *Curr. Opin. Biotechnol.* 61, 110–115. doi: 10.1016/j.copbio.2019.11.002

Samoudi, M., Masson, H. O., Kuo, C. C., Robinson, C. M., and Lewis, N. E. (2021). From omics to cellular mechanisms in mammalian cell factory development. *Curr. Opin. Chem. Eng.* 32, 100688. doi: 10.1016/j.coche.2021.100688

Sangjan, W., Carter, A. H., Pumphrey, M. O., Jitkov, V., and Sankaran, S. (2021). Development of a raspberry pi-based sensor system for automated in-field monitoring to support crop breeding programs. *Inventions* 6, 42. doi: 10.3390/inventions6020042

Sara, S. T., Hasan, M. M., Ahmad, A., and Shatabda, S. (2021). Convolutional neural networks with image representation of amino acid sequences for protein function prediction. *Comput. Biol. Chem.* 92, 107494. doi: 10.1016/j.compbiolchem.2021.107494

Sarkar, S., Cazenave, A. B., Oakes, J., McCall, D., Thomason, W., Abbott, L., et al. (2021). Aerial high-throughput phenotyping of peanut leaf area index and lateral growth. *Sci. Rep.* 11, 1–17. doi: 10.1038/s41598-021-00936-w

Sarker, I. H. (2021). Machine learning: algorithms, real-world applications and research directions. *SN Comput. Sci.* 2, 1–21. doi: 10.1007/s42979-021-00592-x

Sastry, A. V., Gao, Y., Szubin, R., Hefner, Y., Xu, S., Kim, D., et al. (2019). The Escherichia coli transcriptome mostly consists of independently regulated modules. *Nat. Commun.* 10, 1–14. doi: 10.1038/s41467-019-13483-w

Schillberg, S., and Finnern, R. (2021). Plant molecular farming for the production of valuable proteins - Critical evaluation of achievements and future challenges. *J. Plant Physiol.* 258–259, 153359. doi: 10.1016/j.jplph.2020.153359

Schillberg, S., Raven, N., Spiegel, H., Rasche, S., and Buntru, M. (2019). Critical analysis of the commercial potential of plants for the production of recombinant proteins. *Front. Plant Sci.* 10. doi: 10.3389/fpls.2019.00720

Schjoldager, K. T., Narimatsu, Y., Joshi, H. J., and Clausen, H. (2020). Global view of human protein glycosylation pathways and functions. *Nat. Rev. Mol. Cell Biol.* 21, 729–749. doi: 10.1038/s41580-020-00294-x

Sethi, L., Kumari, K., and Dey, N. (2021). Engineering of plants for efficient production of therapeutics. *Mol. Biotechnol.* 63, 1125–1137. doi: 10.1007/s12033-021-00381-0

Shanmugaraj, B., Rattanapisit, K., Manopwisedjaroen, S., Thitithanyanont, A., and Phoolcharoen, W. (2020). Monoclonal Antibodies B38 and H4 Produced in Nicotiana benthamiana Neutralize SARS-CoV-2 in *vitro*. *Front. Plant Sci.* 11. doi: 10.3389/fpls.2020.589995

Shayesteh, M., Ghasemi, F., Tabandeh, F., Yakhchali, B., and Shakibaie, M. (2020). Design, construction, and expression of recombinant human interferon beta gene in CHO-s cell line using EBV-based expression system. *Res. Pharm. Sci.* 15, 144–153. doi: 10.4103/1735-5362.283814

Shi, X., Cordero, T., Garrigues, S., Marcos, J. F., Daròs, J. A., and Coca, M. (2019). Efficient production of antifungal proteins in plants using a new transient expression vector derived from tobacco mosaic virus. *Plant Biotechnol. J.* 17, 1069–1080. doi: 10.1111/pbi.13038

Silva, J. C. F., Teixeira, R. M., Silva, F. F., Brommonschenkel, S. H., and Fontes, E. P. B. (2019). Machine learning approaches and their current application in plant molecular biology: A systematic review. *Plant Sci.* 284, 37–47. doi: 10.1016/j.plantsci.2019.03.020

Singh, A., Ganapathysubramanian, B., Singh, A. K., and Sarkar, S. (2016). Machine learning for high-throughput stress phenotyping in plants. *Trends Plant Sci.* 21, 110–124. doi: 10.1016/j.tplants.2015.10.015

Siriwattananon, K., Manopwisedjaroen, S., Shanmugaraj, B., Rattanapisit, K., Phumiamorn, S., Sapsutthipas, S., et al. (2021). Plant-produced receptor-binding domain of SARS-coV-2 elicits potent neutralizing responses in mice and non-human primates. *Front. Plant Sci.* 12. doi: 10.3389/fpls.2021.682953

Smialowski, P., Doose, G., Torkler, P., Kaufmann, S., and Frishman, D. (2012). PROSO II - A new method for protein solubility prediction. *FEBS J.* 279, 2192–2200. doi: 10.1111/j.1742-4658.2012.08603.x

Smiatek, J., Clemens, C., Herrera, L. M., Arnold, S., Knapp, B., Presser, B., et al. (2021). Generic and specific recurrent neural network models: Applications for large and small scale biopharmaceutical upstream processes. *Biotechnol. Rep.* 31, e00640. doi: 10.1016/j.btre.2021.e00640

Soni, A. P., Lee, J., Shin, K., Koiwa, H., and Hwang, I. (2022). Production of recombinant active human TGFβ1 in nicotiana benthamiana. *Front. Plant Sci.* 13. doi: 10.3389/fpls.2022.922694

Strain, B., Morrissey, J., Antonakoudis, A., and Kontoravdi, C. (2023). Genome-scale models as a vehicle for knowledge transfer from microbial to mammalian cell systems. *Comput. Struct. Biotechnol. J.* 21, 1543–1549. doi: 10.1016/j.csbj.2023.02.011

Strasser, R. (2022). Recent developments in deciphering the biological role of plant complex N-glycans. *Front. Plant Sci.* 13. doi: 10.3389/fpls.2022.897549

Strasser, R. (2023). Plant glycoengineering for designing next-generation vaccines and therapeutic proteins. *Biotechnol. Adv.* 67, 108197. doi: 10.1016/j.bioteChadv.2023.108197

Sun, X., Yang, Z., Su, P., Wei, K., Wang, Z., Yang, C., et al. (2023). Non-destructive monitoring of maize LAI by fusing UAV spectral and textural features. *Front. Plant Sci.* 14. doi: 10.3389/fpls.2023.1158837

Sureyya Rifaioglu, A., Doğan, T., Jesus Martin, M., Cetin-Atalay, R., and Atalay, V. (2019). DEEPred: automated protein function prediction with multi-task feed-forward deep neural networks. *Sci. Rep.* 9, 1–16. doi: 10.1038/s41598-019-43708-3

Taghavi Namin, S., Esmaeilzadeh, M., Najafi, M., Brown, T. B., and Borevitz, J. O. (2018). Deep phenotyping: Deep learning for temporal phenotype/genotype classification. *Plant Methods* 14, 1–14. doi: 10.1186/s13007-018-0333-4

Tausen, M., Clausen, M., Moeskjær, S., Shihavuddin, A. S. M., Dahl, A. B., Janss, L., et al. (2020). Greenotyper: image-based plant phenotyping using distributed computing and deep learning. *Front. Plant Sci.* 11. doi: 10.3389/fpls.2020.01181

Tien, N. Q. D., Huy, N. X., and Kim, M. Y. (2019). Improved expression of porcine epidemic diarrhea antigen by fusion with cholera toxin B subunit and chloroplast transformation in Nicotiana tabacum. *Plant Cell. Tissue Organ Cult.* 137, 213–223. doi: 10.1007/s11240-019-01562-1

Tokekar, P., Vander Hook, J., Mulla, D., and Isler, V. (2016). Sensor planning for a symbiotic UAV and UGV system for precision agriculture. *IEEE Trans. Robot.* 32, 1498–1511. doi: 10.1109/TRO.2016.2603528

Tovar, J. C., Hoyer, J. S., Lin, A., Tielking, A., Callen, S. T., Elizabeth Castillo, S., et al. (2018). Raspberry Pi–powered imaging for plant phenotyping. *Appl. Plant Sci.* 6, 1–12. doi: 10.1002/aps3.1031

Tuan-Anh, T., Ly, L. T., Viet, N. Q., and Bao, P. T. (2017). Novel methods to optimize gene and statistic test for evaluation - an application for Escherichia coli. *BMC Bioinf.* 18, 1–10. doi: 10.1186/s12859-017-1517-z

Ubbens, J. R., and Stavness, I. (2017). Deep plant phenomics: A deep learning platform for complex plant phenotyping tasks. *Front. Plant Sci.* 8. doi: 10.3389/fpls.2017.01190

Vafaee, Y., and Alizadeh, H. (2018). Heterologous production of recombinant anti-HIV microbicide griffithsin in transgenic lettuce and tobacco lines. *Plant Cell. Tissue Organ Cult.* 135, 85–97. doi: 10.1007/s11240-018-1445-2

Vaishnav, E. D., de Boer, C. G., Molinet, J., Yassour, M., Fan, L., Adiconis, X., et al. (2022). The evolution, evolvability and engineering of gene regulatory DNA. *Nature* 603, 455–463. doi: 10.1038/s41586-022-04506-6

Van Brempt, M., Clauwaert, J., Mey, F., Stock, M., Maertens, J., Waegeman, W., et al. (2020). Predictive design of sigma factor-specific promoters. *Nat. Commun.* 11, 1–13. doi: 10.1038/s41467-020-19446-w

van Dijk, A. D. J., Kootstra, G., Kruijer, W., and de Ridder, D. (2021). Machine learning in plant science and plant breeding. *iScience* 24, 101890. doi: 10.1016/j.isci.2020.101890

Vaškevičius, M., Kapočiūtė-Dzikienė, J., and Šlepikas, L. (2021). Prediction of chromatography conditions for purification in organic synthesis using deep learning. *Molecules* 26, 2474. doi: 10.3390/molecules26092474

Vazquez-Vilar, M., Selma, S., and Orzaez, D. (2023). The design of synthetic gene circuits in plants: new components, old challenges. *J. Exp. Bot.* 74, 3791–3805. doi: 10.1093/jxb/erad167

Viet, N. D., and Jang, A. (2021). Journal of Environmental Chemical Engineering Development of artificial intelligence-based models for the prediction of filtration performance and membrane fouling in an osmotic membrane bioreactor. *J. Environ. Chem. Eng.* 9, 105337. doi: 10.1016/j.jece.2021.105337

Vo ngoc, L., Huang, C. Y., Cassidy, C. J., Medrano, C., and Kadonaga, J. T. (2020). Identification of the human DPR core promoter element using machine learning. *Nature* 585, 459–463. doi: 10.1038/s41586-020-2689-7

Wan, S., Zhao, K., Lu, Z., Li, J., Lu, T., and Wang, H. (2022). A modularized ioT monitoring system with edge-computing for aquaponics. *Sensors* 22, 9260. doi: 10.3390/s22239260

Wang, X., Li, F., Xu, J., Rong, J., Webb, G. I., Ge, Z., et al. (2022). ASPIRER: A new computational approach for identifying non-classical secreted proteins based on deep learning. *Brief. Bioinform.* 23, 1–12. doi: 10.1093/bib/bbac031

Wang, L., Nie, R., Yu, Z., Xin, R., Zheng, C., Zhang, Z., et al. (2020). An interpretable deep-learning architecture of capsule networks for identifying cell-type gene expression programs from single-cell RNA-sequencing data. *Nat. Mach. Intell.* 2, 693–703. doi: 10.1038/s42256-020-00244-4

Webster, G. R., Teh, A. Y. H., and Ma, J. K. C. (2017). Synthetic gene design—The rationale for codon optimization and implications for molecular pharming in plants. *Biotechnol. Bioeng.* 114, 492–502. doi: 10.1002/bit.26183

Weissenow, K., Heinzinger, M., and Rost, B. (2022). Protein language-model embeddings for fast, accurate, and alignment-free protein structure prediction. *Structure* 30, 1169–1177.e4. doi: 10.1016/j.str.2022.05.001

Wittmann, B. J., Johnston, K. E., Wu, Z., and Arnold, F. H. (2021). Advances in machine learning for directed evolution. *Curr. Opin. Struct. Biol.* 69, 11–18. doi: 10.1016/j.sbi.2021.01.008

Wu, M. R., Nissim, L., Stupp, D., Pery, E., Binder-Nissim, A., Weisinger, K., et al. (2019). A high-throughput screening and computation platform for identifying synthetic promoters with enhanced cell-state specificity (SPECS). *Nat. Commun.* 10, 1–10. doi: 10.1038/s41467-019-10912-8

Wu, Z., Yang, K. K., Liszka, M. J., Lee, A., Batzilla, A., Wernick, D., et al. (2020). Signal peptides generated by attention-based neural networks. *ACS Synth. Biol.* 9, 2154–2161. doi: 10.1021/acssynbio.0c00219

Wu, X., and Yu, L. (2021). EPSOL: sequence-based protein solubility prediction using multidimensional embedding. *Bioinformatics* 37, 4314–4320. doi: 10.1093/bioinformatics/btab463

Yang, Z., Bogdan, P., and Nazarian, S. (2021b). An in silico deep learning approach to multi-epitope vaccine design: a SARS-CoV-2 case study. *Sci. Rep.* 11, 1–21. doi: 10.1038/s41598-021-81749-9

Yang, Y., Heffernan, R., Paliwal, K., Lyons, J., Dehzangi, A., Sharma, A., et al. (2017). Spider2: A package to predict secondary structure, accessible surface area, and main-chain torsional angles by deep neural networks. *Methods Mol. Biol.* 1484, 55–63. doi: 10.1007/978-1-4939-6406-2_6

Yang, H. S., Rhoads, D. D., Sepulveda, J., Zang, C., Chadburn, A., and Wang, F. (2023). Challenges and considerations of developing and implementing machine learning tools for clinical laboratory medicine practice. *Arch. Pathol. Lab. Med.* 147, 826–836. doi: 10.5858/arpa.2021-0635-RA

Yang, T., Zhang, W., Zhou, T., Wu, W., Liu, T., and Sun, C. (2021a). Plant phenomics & precision agriculture simulation of winter wheat growth by the assimilation of unmanned aerial vehicle imagery into the WOFOST model. *PloS One* 16, 1–9. doi: 10.1371/journal.pone.0246874

Yoosefzadeh-Najafabadi, M., Earl, H. J., Tulpan, D., Sulik, J., and Eskandari, M. (2021). Application of machine learning algorithms in plant breeding: predicting yield from hyperspectral reflectance in soybean. *Front. Plant Sci.* 11. doi: 10.3389/fpls.2020.624273

Yu, S. I., Rhee, C., Cho, K. H., and Shin, S. G. (2022). Comparison of different machine learning algorithms to estimate liquid level for bioreactor management. *Environ. Eng. Res.* 28, 220037–220030. doi: 10.4491/eer.2022.037

Zangirolami, T. C., Campani, G., Horta, A. C. L., and Giordano, R. C. (2021). Machine learning applied for metabolic flux - based control of micro - aerated fermentations in bioreactors.. *Biotechnol. Bioeng.* 118, 2076–2091. doi: 10.1002/bit.27721

Zaragoza, J. M. C. (2022). *Data-Driven Cell Engineering of Chinese Hamster Ovary Cells through Machine Learning*. Denmark: Technical University of Denmark.

Zhang, J., Petersen, S. D., Radivojevic, T., Ramirez, A., Pérez-Manríquez, A., Abeliuk, E., et al. (2020). Combining mechanistic and machine learning models for predictive engineering and optimization of tryptophan metabolism. *Nat. Commun.* 11, 4880. doi: 10.1038/s41467-020-17910-1

Zhao, W., Zhou, L. Y., Kong, J., Huang, Z. H., Gao, Y., Zhang, Z. X., et al. (2023). Expression of recombinant human Apolipoprotein A-IMilano in Nicotiana tabacum. *Bioresour. Bioprocess.* 10 (1), 1–14. doi: 10.1186/s40643-023-00623-w

Zheng, Y. Y., Kong, J. L., Jin, X. B., Wang, X. Y., Su, T. L., and Zuo, M. (2019). Cropdeep: The crop vision dataset for deep-learning-based classification and detection in precision agriculture. *Sensors (Switzerland)* 19, 1058. doi: 10.3390/s19051058

Zrimec, J., Börlin, C. S., Buric, F., Muhammad, A. S., Chen, R., Siewers, V., et al. (2020). Deep learning suggests that gene expression is encoded in all parts of a co-evolving interacting gene regulatory structure. *Nat. Commun.* 11, 6141. doi: 10.1038/s41467-020-19921-4

frontiers | Frontiers in Plant Science

TYPE Brief Research Report
PUBLISHED 23 January 2024
DOI 10.3389/fpls.2023.1298880

OPEN ACCESS

EDITED BY
Balamurugan Shanmugaraj,
Chulalongkorn University, Thailand

REVIEWED BY
Muhammad Suleman,
University of Veterinary and Animal Sciences, Pakistan
Jayamurthy P.,
National Institute for Interdisciplinary Science and Technology (CSIR), India

*CORRESPONDENCE
Harish Mani Chandra
mc.harishin@tvu.edu.in

RECEIVED 22 September 2023
ACCEPTED 28 December 2023
PUBLISHED 23 January 2024

CITATION
Mugunthan SP, Venkatesan D, Govindasamy C, Selvaraj D and Mani Chandra H (2024) A preliminary study of the immunogenic response of plant-derived multi-epitopic peptide vaccine candidate of *Mycoplasma gallisepticum* in chickens. *Front. Plant Sci.* 14:1298880. doi: 10.3389/fpls.2023.1298880

A preliminary study of the immunogenic response of plant-derived multi-epitopic peptide vaccine candidate of *Mycoplasma gallisepticum* in chickens

Susithra Priyadarhni Mugunthan[1], Divyadharshini Venkatesan[1], Chandramohan Govindasamy[2], Dhivya Selvaraj[3] and Harish Mani Chandra[1]*

[1]Department of Biotechnology, Thiruvalluvar University, Vellore, Tamil Nadu, India, [2]Department of Community Health Sciences, College of Applied Medical Sciences, King Saud University, Riyadh, Saudi Arabia, [3]Artificial Intelligence Laboratory, School of Computer Information and Communication Engineering, Kunsan National University, Gunsan, Republic of Korea

Mycoplasma gallisepticum (MG) is responsible for chronic respiratory disease in avian species, characterized by symptoms like respiratory rales and coughing. Existing vaccines for MG have limited efficacy and require multiple doses. Certain MG cytoadherence proteins (GapA, CrmA, PlpA, and Hlp3) play a crucial role in the pathogen's respiratory tract colonization and infection. Plant-based proteins and therapeutics have gained attention due to their safety and efficiency. In this study, we designed a 21.4-kDa multi-epitope peptide vaccine (MEPV) using immunogenic segments from cytoadherence proteins. The MEPV's effectiveness was verified through computational simulations. We then cloned the MEPV, introduced it into the plant expression vector pSiM24-eGFP, and expressed it in *Nicotiana benthamiana* leaves. The plant-produced MEPV proved to be immunogenic when administered intramuscularly to chickens. It significantly boosted the production of immunoglobulin Y (IgY)-neutralizing antibodies against cytoadherence protein epitopes in immunized chickens compared to that in the control group. This preliminary investigation demonstrates that the plant-derived MEPV is effective in triggering an immune response in chickens. To establish an efficient poultry health management system and ensure the sustainability of the poultry industry, further research is needed to develop avian vaccines using plant biotechnology.

KEYWORDS

plant made vaccines, *Mycoplasma gallisepticum*, multi-epitope, Avian mycoplasma, plant expression system

1 Introduction

Vaccination against *Mycoplasma gallisepticum* was first recommended by Adler et al. (1960) and used as a control measure for mycoplasmosis in poultry. Currently available vaccines for the control of chronic respiratory disease (CRD) in chickens are either killed whole cells (bacterins) or live attenuated strains. Furthermore, the currently available live attenuated vaccination for this CRD is ineffective in controlling the disease, and there is a risk of virulence re-emergence in *M. gallisepticum*-infected chickens (Ferguson-Noel et al., 2012; Ishfaq et al., 2020). With an increased antimicrobial resistance and abridged antibiotic efficacy to control *M. gallisepticum* (MG) infections, control of CRD is often coupled with novel and effective vaccines and improvement of existing vaccines.

Commercially bacterins/inactivated and live attenuated vaccines have been used in the prevention of *M. gallisepticum* infection. The R strain has reportedly been accessible for many years and has been shown to reduce *M. gallisepticum*-related production loss, egg transmission, and respiratory tract lesions (Ferguson-Noel et al., 2012). Various strains like strain F (CEVAC MG F), strain K (VAXXON® MG Live), strain ts-11 (VAXSAFE MG), strain 6/85, and strain S6 (MG-Bac vaccine) are commercially available globally (Mugunthan et al., 2023). The challenges in current *M. gallisepticum* vaccines are that live vaccines frequently demonstrate pathogenicity and adverse effects, but bacterins are expensive and frequently require repeated doses to boost avian immune systems (Ishfaq et al., 2020).

The majority of contemporary vaccine development tactics are based on single or multiple antigens. A sequence of epitopic (antigenic) peptides make up a multi-epitopic vaccine, which helps prevent infection by eliciting an immune response. A multi-epitopic vaccine should have epitopes that can stimulate the immune system for the production of cytotoxic and helper T lymphocytes as well as B cells against the intended pathogen (Zhang, 2018). Vaccinations based on multi-epitopes have advantages over traditional vaccinations. They take less time to develop and do not involve microbial cultivation. In contrast to live attenuated strains, epitope-based vaccinations reduce the possibility of virulence reversal. Due to their small size, the epitopes can also be perceptively altered and optimized to maximize their efficiency in eliciting stronger immune responses and have increased stability. Since they are highly specialized and stable and do not involve complete microbes, they provide safety. The vaccine candidate can bind numerous human leukocyte antigen (HLA) alleles simultaneously due to the existence of multiple epitopes, ensuring the appropriate immunological response in a diverse population. Multi-epitopic vaccines have been developed for the following poultry disease pathogens: Newcastle disease virus, avian influenza A (H7N9) virus, and *Eimeria* parasite (Sathish et al., 2017; Hasan et al., 2019; Venkatas and Adeleke, 2019; Madlala et al., 2021; Mugunthan and Harish, 2021; Mugunthan and Mani Chandra, 2021). Due to their specificity, epitope-based vaccines are gaining popularity. Although more research and validation are needed, the utilization of recombinant vaccine technology can provide a secure and effective vaccination against MG infections.

Currently, bacterial, yeast, and mammalian expression systems represent the vast majority of the vaccine expression systems used in the development of multi-epitopic vaccines. These traditional vaccine production methods have a number of limitations. For instance, challenges expressing higher eukaryotic proteins, endotoxin buildup, and host contamination with proteases were issues with the bacterial expression method. For the past two decades, apart from the conventional production platforms and technologies used in manufacturing vaccines, drugs, and other biologics by industries and pharmaceutical companies, plant-based production systems have gained attention for vaccine development due to exhilarating prospects and possibility of developing edible vaccines for veterinary diseases, which have the potential to produce safe, effective, stable, and economical prophylactics, vaccines, and medicines for a variety of ailments, including infectious disorders, in large-scale production at a low cost and with no chance of contamination. The most efficient plant host for the production of recombinant proteins is *Nicotiana* spp., which also yields a large amount of biomass in addition to the highest transient concentrations of recombinant proteins (Gray, 1978; Bano et al., 2021; Gómez, et al., 2013). Plant-produced vaccines prioritize demonstrating proof of concept and effectiveness. The recent progress in creating resilient, stable, and temporary plant production systems for vaccine antigens holds implications for veterinary medicine. Moreover, there is the potential for plant-produced vaccines to contribute to the advancement of both animal and potentially human health within the framework of the One Health perspective.

Plant-based vaccines offer several potential benefits, including the ability to achieve high production yields, rapid manufacturing, safety, and cost-effectiveness. Additionally, these vaccines are less likely to be contaminated with uncommon mammalian pathogens (Peyret et al., 2021). Consequently, the idea of using plant-based platforms as an alternative solution to challenges associated with animal-based methods has been under consideration for a while. It is feasible to express viral proteins like the SARS-CoV-2 spike protein within plants, leading to the formation of viruslike particles (Jung et al., 2022). A significant development in this area is Medicago Inc.'s accomplishment of phase 3 clinical trials for a flu vaccine derived from *Nicotiana benthamiana*. This plant-based quadrivalent viruslike particle (QVLP) flu vaccine exhibited efficacy comparable to that of existing vaccines (Ward et al., 2020; Ward et al., 2021). Notably, Medicago's plant-based COVID-19 viruslike particle vaccine (Covifenz®) was granted approval by Health Canada in February 2022, marking it as the first approved plant-based vaccine (Hager et al., 2022). Recently, Lucero et al. (2021) documented that an oral plant-based vaccine for infectious bursal disease elicited a protective immune response in chickens. The utilization of plants as a novel platform for producing protein-based drugs has garnered considerable attention. Epitope-based

vaccines offer several advantages, such as safety, precision, and scalability, but they also face challenges related to the design of effective epitopes, limited immune responses, and potential difficulties in achieving herd immunity.

Hence, in this study we cloned the *M. gallisepticum* multi-epitopic vaccine (MEPV) gene in the pSiM24-eGFP plant expression vector, and by *Agrobacterium*-mediated transient expression, the MEPV protein is expressed in plants. To our knowledge, this is the first study to express an MEPV from *M. gallisepticum* in plants. The protein expression is validated by sodium dodecyl sulfate–polyacrylamide gel electrophoresis (SDS-PAGE) and Western blotting. Furthermore, ELISA confirmed the immunogenic nature of plant-expressed MEPV protein by eliciting antibody response against MEPV.

2 Materials and methods

2.1 Construction of the MEPV plant expression vector

The genetic components of the binary vector pSiM24 are as follows: left and right T-DNA borders, a full-length transcript promoter (M24) of the Mirabilis mosaic virus with duplicated enhancer domains, three multiple cloning sites (Sambrook et al., 1989), a 39rbcsE9 terminator, replication functions for *Escherichia coli* (ColE1) and *Agrobacterium tumefaciens* (pRK2-OriV), and the replicase (bla) (Dey and Maiti, 1999; Haq et al., 1995; Hofgen and Willmitzer, 1988; Sahoo et al., 2013). The MEPV candidate from the epitopic regions of GapA, CrmA, Hlp3, and PlpA was designed (Mugunthan and Harish, 2021). The nucleotide sequence of MEPV was codon optimized and commercially synthesized (Synbio Technologies LLC) with *EcoRI*, *AgeI*, and *XhoI* restriction sites for cloning at the 5′ and 3′ ends, respectively. The MEPV region was ligated into the pSiM24-eGFP vector (Sahoo et al., 2014) using *EcoRI* and *XhoI* restriction sites to construct the plant expression vector pSiM24-eGFP-MEPV (Figure 1A). The ER retention signal peptide (KDEL) was included at the C-terminus of the gene construct.

2.2 Expression of the MEPV candidate in *N. benthamiana* by agroinfiltration

The plant expression vector pSiM24-eGFP-MEPV was transformed into *A. tumefaciens* strain GV3101 cells using the freeze-thaw method (D'Aoust et al., 2008). The recombinant *A. tumefaciens* clones were confirmed by polymerase chain reaction (PCR) using MEPV gene-specific primers. *A. tumefaciens* containing pSiM24-eGFP-MEPV was resuspended with 1× infiltration buffer (10 mM 2-(*N*-morpholino)-etanesulfonic acid (MES), 10 mM $MgSO_4$, at pH 5.5) to get a final OD_{600} of 0.2 prior to agroinfiltration. The *A. tumefaciens* suspension was injected into the adaxial side of 36-day-old *N. benthamiana* leaves. The infiltrated plants were maintained in an optimal 16-h light/8-h dark condition at 28°C and harvested after 1 day to 6 days post infiltration (dpi).

2.3 Extraction and purification of plant-produced MEPV protein

Infiltrated plant and control leaf samples (negative control) (1 g) were homogenized with 500 µl of the extraction buffer [phosphate-buffered saline (PBS) (NaCl 8.00 g, KCl 0.20 g, Na_2HPO_4 1.44 g, KH_2PO_4 0.24 g, H_2O 800 ml, adjust pH to 7.4 with HCl or NaOH) + 0.1% Triton X-100] using a mortar and pestle and stored in ice. The protein content was quantified according to Lowry et al. (1951).

Protein purification (column based) was achieved using the presence of N-terminal His tag in the recombinant MEPV protein. The protein from the highest expression day was used for purification. The purified protein was isolated and quantified according to Lowry et al. (1951).

The purified plant-produced pSiM24-eGFP-MEPV protein was analyzed by using SDS-PAGE and Western blotting. For Western blot analysis, the proteins were separated in SDS-PAGE gel and the gel was equilibrated in transfer buffer and transferred to a nitrocellulose membrane (Pall Life Sciences BioTrace™) using the semidry transfer technique at 0.8 mA/cm^2 and 45 V, for 90 min. Furthermore, the protein was analyzed using a primary antibody (anti-polyhistidine antibody) and a secondary antibody [anti-mouse immunoglobulin G (IgG) antibody conjugated with horseradish peroxidase (HRP)].

2.4 Chicken immunization

The purified plant-produced MEPV proteins at doses of 5 µg, 10 µg, 15 µg, 20 µg, and 25 µg protein were formulated with Freund's complete adjuvant (G-Biosciences) to a total volume of 0.5 ml and injected into a specific pathogen-free (SPF) 21-day-old chicken's pectoral muscle (Evans et al., 2009). PBS containing Freund's adjuvant without the antigen was used as a control. A total volume of 0.5 ml of the vaccine was used for immunization. The blood samples were taken via puncture of the *vena ulnaris* and collected in 2-ml tubes on days 7, 14, 21, 28, 35, 42, and 49 post immunizations. The samples were cooled, and the serum was separated and stored at −20°C until further use.

2.5 Evaluation of antibody response by ELISA

The collected chicken serum was used to quantify the presence of anti-MEPV-specific immunoglobulin Y (IgY) antibodies using ELISA. The purified MEPV protein was diluted in 0.05 M carbonate buffer (pH 9.6) to a final concentration of 0.5 µg/ml, and 100 µl from this dilution was added to each well of an ELISA plate and incubated at 4°C overnight for coating. Next, 100 µl of serum from immunized and control chickens diluted 1:400 in blocking buffer was added to each well and incubated for 30 min at 37°C. The wells were washed, and 100 µl of HRP-conjugated anti-chicken IgY antibodies (Abcam) at a 1:10,000 dilution in PBS was added and incubated at 37°C for 30 min. After incubation, the wells were

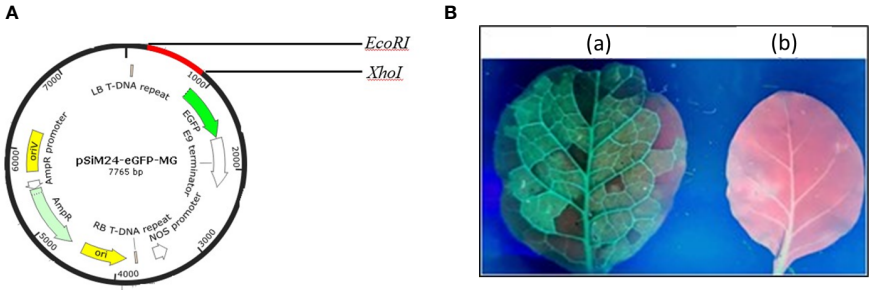

FIGURE 1
(A) Vector map showing the MEPV gene construct (red color) in the pSiM24-eGFP vector. **(B)** Green fluorescent protein (GFP) expression in an *N. benthamiana* leaf seen under a UV illuminator: **(A)** GFP-expressing leaf; **(B)** control.

washed thrice and 100 µl of 3,3′,5,5′-tetramethylbenzidine (TMB) substrate was added and incubated for 15 min. Once the color was developed, 100 µl of 2 M H_2SO_4 was added and the optical density at 450 nm was determined by an ELISA reader (Bio-Rad). All experiments were performed in duplicate, and 1× PBS was used as a control. The antibody titers were compared by GraphPad Prism 9 using Tukey's multiple-comparison test.

2.6 Statistical analysis

GraphPad Prism 9 (GraphPad Software, Inc.) was employed to perform a two-way analysis of variance (ANOVA) and multiple comparisons to determine the statistical significance across groups. Geometric mean titer (GMT) and a 95% confidence interval (CI) were used to depict the results.

3 Results

3.1 Transient expression of MEPV protein in *N. benthamiana*

The codon-optimized MEPV gene was cloned into plant expression vector pSiM24-eGFP. For expression of MEPV protein in plants, *N. benthamiana* plants were infiltrated with *A. tumefaciens* containing pSiM24-eGFP-MEPV. The leaves infiltrated with *A. tumefaciens* containing pSiM24-eGFP-MEPV exhibited substantial phenotypic green fluorescent protein (GFP) expression compared to the leaves infiltrated by *A. tumefaciens* without the plant expression vector (Figure 1B).

3.2 Extraction and purification of plant-produced MEPV protein

The presence of MEPV protein in agroinfiltrated plant leaves was analyzed using 10% SDS-PAGE. The bands were visible at 21.4 kDa, the expected size of MEPV protein. The total protein content was quantified over a period of 7 days (Figure 2A); the highest concentration was observed on day 5.

Plant-produced MEPV protein was extracted and purified by nickel column chromatography, by N-terminal His tag of MEPV protein. The His-tagged fusion proteins were efficiently eluted. In the purified fraction, a prominent single band was observed at 21.4 kDa, which corresponds to the size of MEPV protein (Figures 2B, C). The concentration of the purified protein content of MEPV was 10.32 µg/g fresh weight.

3.3 Immunogenicity in chicken

The titers of total IgY antibodies induced by MEPV in immunized chickens at days 0, 7, 14, 21, 28, 35, 42, and 49 post immunization were measured by ELISA. All chickens immunized with plant-produced MEPV elicited significantly higher antibody titers compared with the control (Figure 3A). Higher levels of specific anti-MEPV IgY antibodies were detected in immunized chickens following immunization after day 7, and the highest was observed 21 days after immunization. Likewise, chickens of all six groups (Groups A, B, C, D, E and F) had nearly similar antibody titers on day 0 post immunization without any significant difference. However, after MEPV immunization, the antibody titer in chickens of Group B to Group F was found to be increased progressively as assessed at 7, 14, and 21 days post immunization and started to gradually decrease at 28, 35, 42, and 49 days post immunization. Significant difference ($p < 0.0001$) in antibody titer was observed between control (Group A) and MEPV-immunized groups (Groups B to F) at all-time points. In Group D (MEPV 15 µg), the serum IgY antibody titers on 14 to 49 days post immunization were comparatively higher when compared with those of other groups (Figure 3B). The plant-produced MEPV was able to elicit immune response in chickens; this was validated by the significant increase in the IgY antibody titer in immunized chickens versus control chickens.

4 Discussion

To manage the losses caused by chronic respiratory disease attributed to *M. gallisepticum*, the widespread reliance on in-feed antibiotics in the poultry industry has presented challenges. These challenges include the emergence of antibiotic-resistant microbes

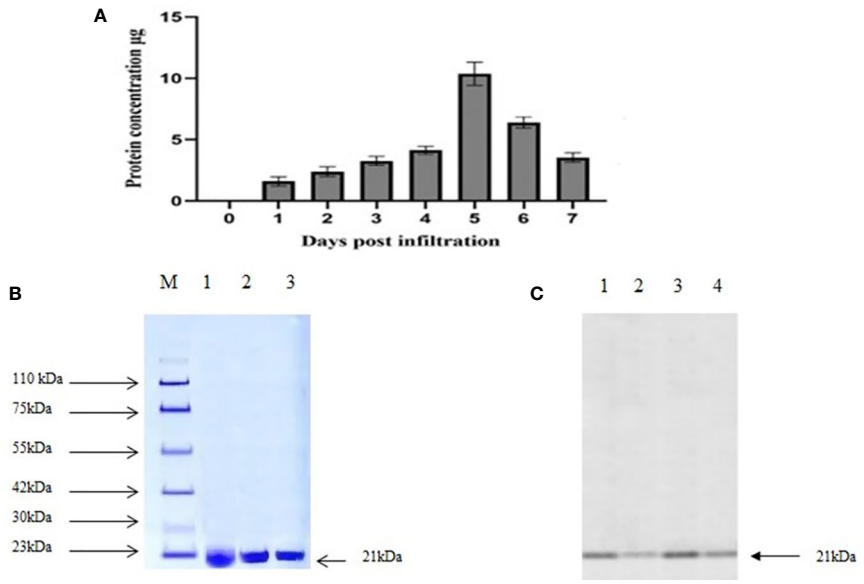

FIGURE 2
(A) Total protein content (µg MEPV/g of fresh weight) concentration. **(B)** SDS analysis of purified protein. M, protein marker; lanes 1 to 3, infiltrated plant leaf sample. **(C)** Western blot analysis of purified protein. Lanes 1 to 4, infiltrated plant leaf sample.

and the presence of antibiotic residues in meat and eggs (Evans and Hafez, 1992). Current *M. gallisepticum* vaccines are ineffective in eradicating the disease and require proper storage and logistics. Consequently, there is a pressing need to develop a vaccine that is effortless and cost-effective to produce, utilizes scalable technology to meet global demand, and provides immunity against *M. gallisepticum* infection.

Plant molecular farming stands out as an alternative technology for expressing heterologous proteins in plants, facilitating the production of antigens and antibodies. Researchers have explored plants as carriers for vaccine antigen expression, demonstrating their potential for effective and affordable recombinant protein production in large quantities (Mason et al., 1996; Fischer et al., 2004). Plant-expressed vaccine antigens have been shown to trigger a protective immune response (Tacket et al., 2000; Komarova et al., 2010; Jacob et al., 2013). In this study, we utilized *Agrobacterium*-mediated transient expression of an *M. gallisepticum* cytoadherence-based MEPV using the pSiM24-eGFP binary vector.

The first ever plant-produced biopharmaceutical licensed by a governmental agency, the Newcastle disease virus (NDV) poultry vaccine by Dow AgroSciences, was developed in tobacco cell suspension cultures [United States Department of Agriculture (USDA)] (Vermij and Waltz, 2006). Although not released to the public, it marked a pivotal moment for plant-based vaccine approval. Numerous studies have reported the expression of immunogenic hemagglutinin-neuraminidase (HN) protein of NDV in plants, eliciting specific immune responses in chickens and mice (Hahn et al., 2007; Gómez et al., 2009; Ma et al., 2020; Shahid et al., 2020; Nurzijah et al., 2022). Similarly, vaccines for infectious bursal disease virus (IBDV) and the poultry parasite *Eimeria* have been expressed in plants, demonstrating the potential for plant-based vaccine production (Richetta et al., 2017; Lucero et al., 2019; Rage et al., 2020).

Research on plant-based vaccine manufacturing for veterinary diseases has gained interest over the past two decades, offering exciting possibilities such as the development of edible vaccines. This could lead to the creation of prophylactics, vaccinations, and medications that are safe, effective, stable, and affordable for various illnesses, including infectious diseases. Edible vaccines can be produced in large quantities at minimal cost, without the need for a cold chain during transit and storage.

Given the global concern over antibiotic resistance, finding an alternative and efficient control for *M. gallisepticum* infection and its associated losses is crucial. Vaccines based on adhesion and phase variation proteins are considered among the most effective options to prevent and control *M. gallisepticum* infection and maintain poultry health, welfare, and production. However, the success or failure of these vaccines depends on factors such as their type, safety, effectiveness, functional mechanisms, and immunogenicity (Mugunthan et al., 2023).

Comparing multi-epitope-based vaccines to traditional immunizations reveals several advantages. They have a shorter development time, do not require microbial cultivation, and can replace multiple wet lab processes. Unlike live attenuated strains, epitope-based vaccines reduce the risk of virulence reversal. The tiny size of epitopes allows for intelligent alteration and optimization to maximize their efficiency and chemical stability. Their high specialization and stability, coupled with not involving full viruses, make them safe. Multi-epitope vaccines can bind numerous HLA alleles simultaneously, ensuring an appropriate immunological response in a diverse population.

The multi-epitope complementary DNA (cDNA) was successfully cloned into the pSiM24-eGFP plant binary vector, confirmed by PCR and restriction digestion, and transformed into *Agrobacterium*. *Agrobacterium* harboring the MEPV gene was transformed into plant leaves for transient expression through

10.3389/fpls.2023.1298880

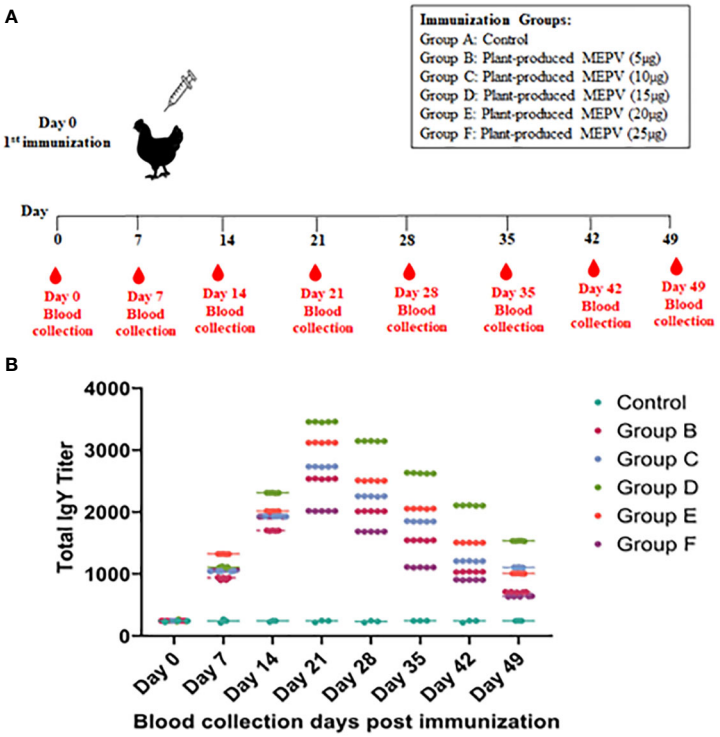

FIGURE 3
Immunization and blood collection schedule in chickens **(A)**. Chickens were divided into six groups, namely, plant-produced MEPV (5 µg), MEPV (10 µg), MEPV (15 µg), MEPV (20 µg), and MEPV (25 µg) vaccine groups (n = 5) and control group (n = 3). Chickens were immunized on day 0 and were bled on days 0, 7, 14, 21, 28, 35, 42, and 49. The response of MEPV-specific IgY titers in immunized animals is presented **(B)**. Data presented as GMT ± 95% CI of the endpoint titer in each group, n = 5 (control, n = 3). Two-way ANOVA and Tukey's test were performed.

agroinfiltration. The expression of the MEPV gene and proteins in agroinfiltrated leaves was confirmed through PCR and SDS-PAGE, respectively. The plant-expressed MEPV protein was purified by nickel His-tag purification, and its size (21.4 kDa) was validated by Western blot analysis. Immunizing chickens with various concentrations of plant-produced MEPV showed a significant increase in antibody titer in Group D (15 µg MEPV) compared to other groups. Higher levels of specific anti-MEPV IgY antibodies were detected in immunized chickens, with the peak observed on day 21 after immunization, consistently across all six groups (Groups A, B, C, D, E, and F). These results suggest that the anti-MEPV IgY antibodies generated could be used to protect chickens against the disease.

The immunogenic property of plant-expressed MEPV was confirmed by ELISA. This study demonstrates that plants can synthesize *M. gallisepticum*-based MEPV antigens. The use of multi-epitopic antigens appears extremely promising in developing vaccine candidates that generate a lasting protective immune response.

5 Conclusion

In conclusion, our study demonstrated that it was feasible to produce MEPV protein in *N. benthamiana* plants using a transient expression system. Furthermore, plant-produced recombinant MEPV protein was shown to be immunogenic in chickens. The vaccine elicited immune responses, suggesting the potential of the plant-produced MEPV as an effective vaccine candidate against CRD caused by *M. gallisepticum*. Collectively, this proof-of-concept study demonstrated that the plant-produced MEPV protein could possibly be further developed as a candidate vaccine.

Data availability statement

The original contributions presented in the study are included in the article/Supplementary Material. Further inquiries can be directed to the corresponding author.

Ethics statement

The animal study was approved by Thiruvalluvar University Ethical Committe. The study was conducted in accordance with the local legislation and institutional requirements.

Author contributions

SPM: Conceptualization, Data curation, Formal analysis, Investigation, Methodology, Writing – original draft. DV: Formal analysis, Investigation, Methodology, Data curation,

Writing – review & editing. CG: Writing – review & editing, Formal analysis, Validation. DS: Formal analysis, Validation, Writing – review & editing. HMC: Investigation, Supervision, Writing – review & editing.

Funding

The author(s) declare financial support was received for the research, authorship, and/or publication of this article. This project was supported by Researchers Supporting Project number (RSPD2024R712), King Saud University, Riyadh, Saudi Arabia.

Acknowledgments

The authors are thankful to Dr. R. Sathishkumar, Department of Biotechnology, Bharathiar University, for his constant support throughout this work.

Conflict of interest

The authors declare that the research was conducted in the absence of any commercial or financial relationships that could be construed as a potential conflict of interest.

Publisher's note

Supplementary material

The Supplementary Material for this article can be found online at: https://www.frontiersin.org/articles/10.3389/fpls.2023.1298880/full#supplementary-material

References

Adler, H. E., McMartin, D., and Shifrine, M. (1960). Immunization against Mycoplasma infections of poultry. *Am. J. veterinary Res.* 21, 482–485.

Bano, N., Patel, P., Chakrabarty, D., and Bag, S. K. (2021). Genome-wide identification, phylogeny, and expression analysis of the bHLH gene family in tobacco (*Nicotiana tabacum*). *Physiol. Mol. Biol. Plants.* 27 (8), 1747–1764. doi: 10.1007/s12298-021-01042-x

D'Aoust, M.-A., Lavoie, P.-O., Couture, M. M.-J., Trépanier, S., Guay, J.-M., Dargis, M., et al. (2008). Influenza virus-like particles produced by transient expression in Nicotiana benthamiana induce a protective immune response against a lethal viral challenge in mice. *Plant Biotechnol. J.* 6, 930–940. doi: 10.1111/j.1467-7652.2008.00384.x

Dey, N., and Maiti, I. B. (1999). Structure and promoter/leader deletion analysis of mirabilis mosaic virus (MMV) full-length transcript promoter in transgenic plants. *Plant Mol. Biol.* 40, 771–782. doi: 10.1023/a:1006285426523

Evans, J. D., Branton, S. L., and Leigh, S. A. (2009). Effect of dosage and vaccination route on transmission of a live attenuated mycoplasma gallisepticum vaccine: A broiler model. *Avian Dis.* 53, 416–420. doi: 10.1637/8621-012309-Reg.1

Evans, R. D., and Hafez, Y. S. (1992). Evaluation of a Mycoplasma gallisepticum strain exhibiting reduced virulence for prevention and control of poultry mycoplasmosis. *Avian Dis.* 36 (2), 197–201.

Ferguson-Noel, N., Cookson, K., Laibinis, V. A., and Kleven, S. H. (2012). The efficacy of three commercial mycoplasma gallisepticum vaccines in laying hens. *Avian Dis.* 56, 272–275. doi: 10.1637/9952-092711-Reg.1

Fischer, R., Stoger, E., Schillberg, S., Christou, P., and Twyman, R. M. (2004). Plant-based production of biopharmaceuticals. *Curr. Opin. Plant Biol.* 7, 152–158. doi: 10.1016/j.pbi.2004.01.007

Gómez, E., Lucero, M. S., ChimenoZoth, S., Carballeda, J. M., Gravisaco, M. J., and Berinstein, A. (2013). Transient expression of VP2 in Nicotiana benthamiana and its use as a plant-based vaccine against Infectious Bursal Disease Virus. *Vaccine* 31, 2623–2627. doi: 10.1016/j.vaccine.2013.03.064

Gómez, E., Zoth, S. C., Asurmendi, S., Vázquez Rovere, C., and Berinstein, A. (2009). Expression of Hemagglutinin-Neuraminidase glycoprotein of Newcastle Disease Virus in agroinfiltrated Nicotiana benthamiana plants. *JBiotechnol* 144, 337–340. doi: 10.1016/j.jbiotec.2009.09.015

Gray, J. C. (1978). Purification and Properties of Monomeric Cytochrome f from Charlock, Sinapis arvensis L. *Eur. J. Biochem.* 82, 133–141. doi: 10.1111/j.1432-1033.1978.tb12004.x

Hager, K. J., Pérez Marc, G., Gobeil, P., Diaz, R. S., Heizer, G., Llapur, C., et al. (2022). Efficacy and safety of a recombinant plant-Based adjuvanted Covid-19 vaccine. *New Engl. J. Med.* 386 (22), 2084–2096. doi: 10.1056/NEJMoa2201300

Hahn, B. S., Jeon, I. S., Jung, Y. J., Kim, J. B., Park, J. S., Ha, S. H., et al. (2007). Expression of hemagglutinin-neuraminidase protein of Newcastle disease virus in transgenic tobacco. *Plant Biotechnol. Rep.* 1, 85–92.

Haq, T. A., Mason, H. S., Clements, J. D., and Arntzen, C. J. (1995). Oral immunization with a recombinant bacterial antigen produced in transgenic plants. *Sci. (New York N.Y.)* 268 (5211), 714–716.

Hasan, M., Ghosh, P. P., Azim, K. F., Mukta, S., Abir, R. A., Nahar, J., et al. (2019). Reverse vaccinology approach to design a novel multi-epitope subunit vaccine against avian influenza A (H7N9) virus. *Microbial Pathogenesis* 130, 19–37. doi: 10.1016/j.micpath.2019.02.023

Hofgen, R., and Willmitzer, L. (1988). Storage of competent cells for Agrobacterium transformation. *Nucl. Acids Res.* 16, 9877–9877. doi: 10.1093/nar/16.20.9877

Ishfaq, M., Hu, W., Khan, M. Z., Ahmad, I., Guo, W., and Li, J. (2020). Current status of vaccine research, development, and challenges of vaccines for Mycoplasma gallisepticum. *Poultry Sci.* 99, 4195–4202. doi: 10.1016/j.psj.2020.06.014

Jacob, S. S., Cherian, S., Sumithra, T. G., Raina, O. K., and Sankar, M. (2013). Edible vaccines against veterinary parasitic diseases—Current status and future prospects. *Vaccine* 31, 1879–1885. doi: 10.1016/j.vaccine.2013.02.022

Jung, J. W., Zahmanova, G., Minkov, I., and Lomonossoff, G. P. (2022). Plant-based expression and characterization of SARS-CoV-2 virus-like particles presenting a native spike protein. *Plant Biotechnol. J.* 20 (7), 1363–1372. doi: 10.1111/pbi.13813

Komarova, T. V., Baschieri, S., Donini, M., Marusic, C., Benvenuto, E., and Dorokhov, Y. L. (2010). Transient expression systems for plant-derived biopharmaceuticals. *Expert Rev. Vaccines* 9, 859–876. doi: 10.1586/erv.10.85

Lowry, O. H., Rosebrough, N. J., Farr, A. L., and Randall, R. J. (1951). Protein measurement with the Folin phenol reagent. *J. biolchemistry* 193 (1), 265–275.

Lucero, M. S., Chimeno Zoth, S., Jaton, J., Gravisaco, M. J., Pinto, S., Richetta, M., et al. (2021). Oral immunization with plant-based vaccine induces a protective response against infectious bursal disease. *Front. Plant Sci.* 12. doi: 10.3389/fpls.2021.741469

Lucero, M. S., Richetta, M., ChimenoZoth, S., Jaton, J., Pinto, S., Canet, Z., et al. (2019). Plant-based vaccine candidate against Infectious bursal disease: An alternative to inactivated vaccines for breeder hens. *Vaccine* 37, 5203–5210. doi: 10.1016/j.vaccine.2019.07.069

Ma, F., Zhang, E., Li, Q., Xu, Q., Ou, J., Yin, H., et al. (2020). A plant-produced recombinant fusion protein-based newcastle disease subunit vaccine and rapid differential diagnosis platform. *Vaccines* 8, 122. doi: 10.3390/vaccines8010122

Madlala, T., Adeleke, V. T., Fatoba, A. J., Okpeku, M., Adeniyi, A. A., and Adeleke, M. A. (2021). Designing multiepitope-based vaccine against Eimeria from immune mapped protein 1 (IMP-1) antigen using immunoinformatic approach. *Sci. Rep.* 11, 18295. doi: 10.1038/s41598-021-97880-6

Mason, H. S., Ball, J. M., Shi, J. J., Jiang, X., Estes, M. K., and Arntzen, C. J. (1996). Expression of Norwalk virus capsid protein in transgenic tobacco and potato and its oral immunogenicity in mice. *Proc. Natl. Acad. Sci. U.S.A.* 93, 5335–5340. doi: 10.1073/pnas.93.11.5335

Mugunthan, S. P., and Harish, M. C. (2021). Multi-epitope-based vaccine designed by targeting cytoadherence proteins of mycoplasma gallisepticum. *ACS Omega* 6, 13742–13755. doi: 10.1021/acsomega.1c01032

Mugunthan, S. P., Kannan, G., Chandra, H. M., and Paital, B. (2023). Infection, Transmission, Pathogenesis and Vaccine Development against Mycoplasma gallisepticum. *Vaccines* 11, 469. doi: 10.3390/vaccines11020469

Mugunthan, S. P., and Mani Chandra, H. (2021). A computational reverse vaccinology approach for the design and development of multi-epitopic vaccine against avian pathogen mycoplasma gallisepticum. *Front. Vet. Sci.* 8. doi: 10.3389/fvets.2021.721061

Nurzijah, I., Elbohy, O. A., Kanyuka, K., Daly, J. M., and Dunham, S. (2022). Development of plant-based vaccines for prevention of avian influenza and newcastle disease in poultry. *Vaccines* 10, 478. doi: 10.3390/vaccines10030478

Peyret, H., Steele, J. F. C., Jung, J. W., Thuenemann, E. C., Meshcheriakova, Y., and Lomonossoff, G. P. (2021). Producing vaccines against enveloped viruses in plants: Making the impossible, difficult. *Vaccines* 9. doi: 10.3390/vaccines9070780

Rage, E., Marusic, C., Lico, C., Baschieri, S., and Donini, M. (2020). Current state-of-the-art in the use of plants for the production of recombinant vaccines against infectious bursal disease virus. Appl. *MicrobiolBiotechnol* 104, 2287–2296. doi: 10.1007/s00253-020-10397-2

Richetta, M., Gómez, E., Lucero, M. S., ChimenoZoth, S., Gravisaco, M. J., Calamante, G., et al. (2017). Comparison of homologous and heterologous prime-boost immunizations combining MVA-vectored and plant-derived VP2 as a strategy against IBDV. *Vaccine* 35, 142–148. doi: 10.1016/j.vaccine.2016.11.029

Sahoo, D. K., Dey, N., and Maiti, I. B. (2014). pSiM24 is a novel versatile gene expression vector for transient assays as well as stable expression of foreign genes in plants. *PLoS One* 9, e98988. doi: 10.1371/journal.pone.0098988

Sahoo, D. K., Stork, J., DeBolt, S., and Maiti, I. B. (2013). Manipulating cellulose biosynthesis by expression of mutant Arabidopsis proM24::CESA3 ixr1-2 gene in transgenic tobacco. *Plant Biotechnol. J.* 11, 362–372. doi: 10.1111/pbi.12024

Sambrook, J., Fritsch, E. F., and Maniatis, T. (1989). *Molecular Cloning: A Laboratory Manual. 2nd ed* (Plainview, N.Y: Cold Spring Harbor Laboratory Press).

Sathish, K., Mohana, S., Bala, M. S., Harini, C., Ponanna, N. M., Srinivasan, V. A., et al. (2017). Subunit vaccine based on plant expressed recombinant Eimeria gametocyte antigen Gam82 elicit protective immune response against chicken coccidiosis. *J. Vaccines* 8, 6–13. doi: 10.1016/j.vaccine.2011.09.117

Shahid, N., Samiullah, T. R., Shakoor, S., Latif, A., Yasmeen, A., Azam, S., et al. (2020). Early stage development of a newcastle disease vaccine candidate in corn. *Front. Vet. Sci.* 7. doi: 10.3389/fvets.2020.00499

Tacket, C. O., Mason, H. S., Losonsky, G., Estes, M. K., Levine, M. M., and Arntzen, C. J. (2000). Human immune responses to a novel norwalk virus vaccine delivered in transgenic potatoes. *J. Infect. Dis.* 182, 302–305. doi: 10.1086/315653

Venkatas, J., and Adeleke, M. A. (2019). A review of Eimeria antigen identification for the development of novel anticoccidial vaccines. *Parasitol. Res.* 118, 1701–1710. doi: 10.1007/s00436-019-06338-2

Vermij, P., and Waltz, E. (2006). News in brief: USDA approves the first plant-based vaccine. *Nat. Biotechnol.* 24, 233–234. doi: 10.1038/nbt0306-233

Ward, B. J., Makarkov, A., Séguin, A., Pillet, S., Trépanier, S., Dhaliwall, J., et al. (2020). Efficacy, immunogenicity, and safety of a plant-derived, quadrivalent, virus-like particle influenza vaccine in adults (18-64 years) and older adults (≥65 years): two multicentre, randomised phase 3 trials. *Lancet (London England)* 396 (10261), 1491–1503. doi: 10.1016/S0140-6736(20)32014-6

Ward, B. J., Séguin, A., Couillard, J., Trépanier, S., and Landry, N. (2021). Phase III: Randomized observer-blind trial to evaluate lot-to-lot consistency of a new plant-derived quadrivalent virus like particle influenza vaccine in adults 18-49 years of age. *Vaccine* 39 (10), 1528–1533. doi: 10.1016/j.vaccine.2021.01.004

Zhang, L. (2018). Multi-epitope vaccines: a promising strategy against tumors and viral infections. *Cell Mol. Immunol.* 15, 182–184. doi: 10.1038/cmi.2017.92

Frontiers in
Plant Science

Cultivates the science of plant biology and its applications

The most cited plant science journal, which advances our understanding of plant biology for sustainable food security, functional ecosystems and human health.

Discover the latest Research Topics

See more →

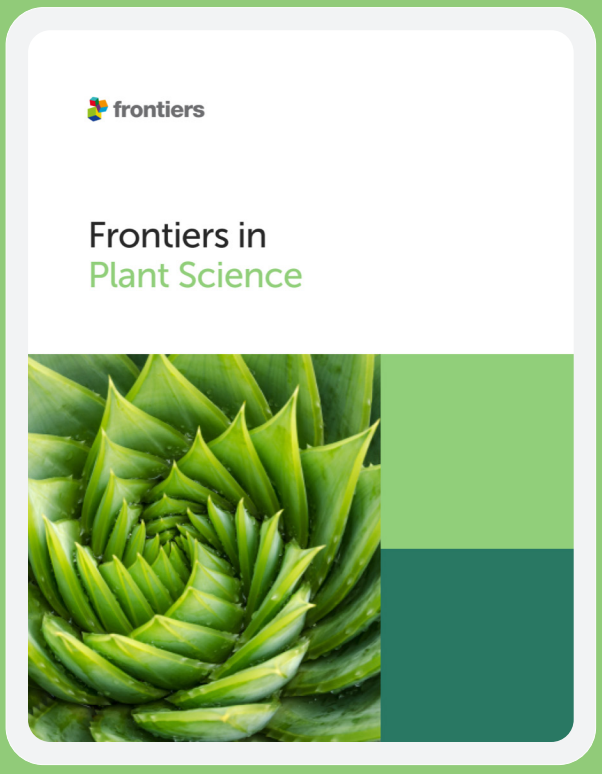

Frontiers

Avenue du Tribunal-Fédéral 34
1005 Lausanne, Switzerland
frontiersin.org

Contact us

+41 (0)21 510 17 00
frontiersin.org/about/contact